EDITORS' SHOWCASE 2021: INSIGHTS IN STEM CELL RESEARCH

EDITED BY: Valerie Kouskoff and Atsushi Asakura
PUBLISHED IN: Frontiers in Cell and Developmental Biology

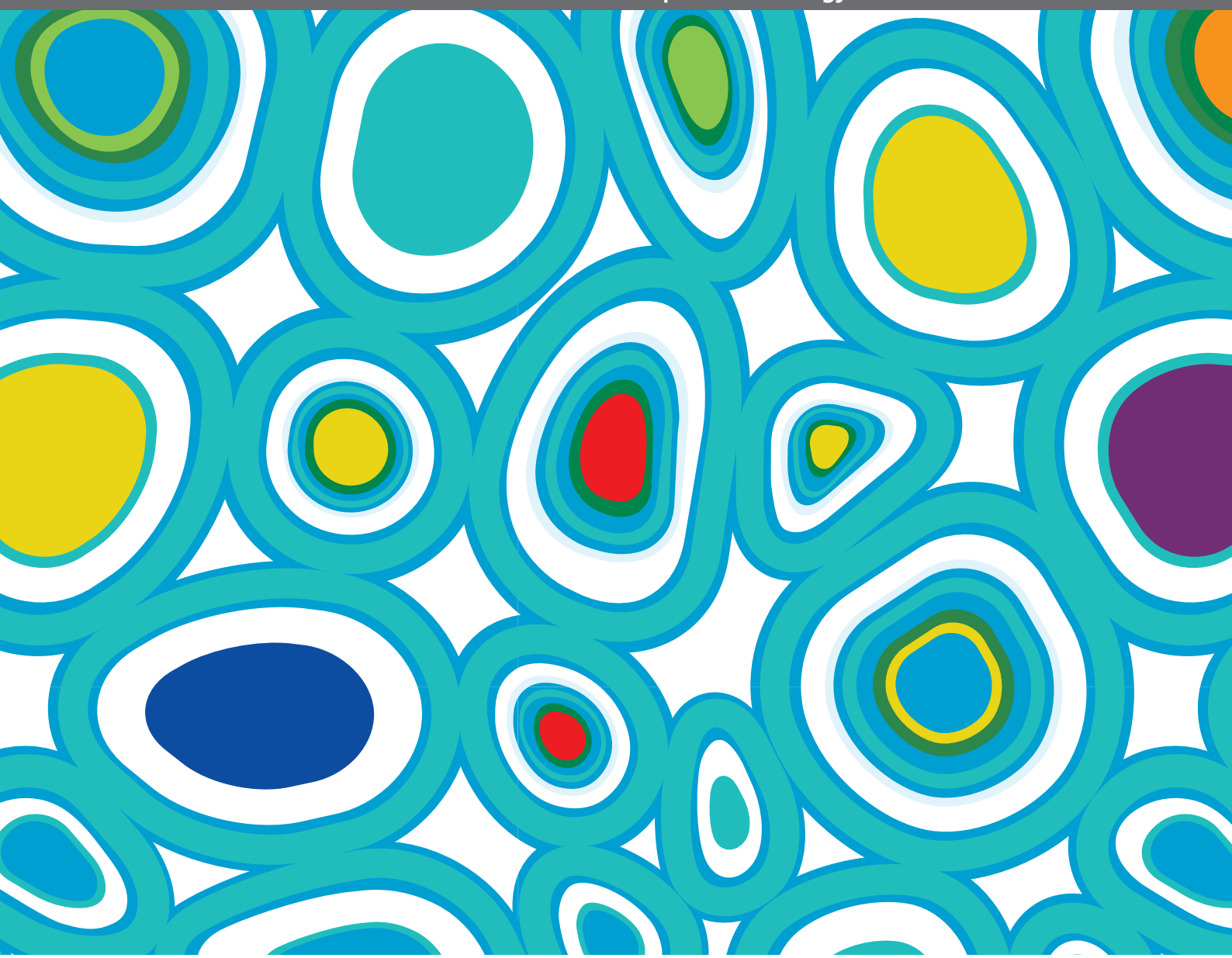

frontiers Research Topics

frontiers

ISSN 1664-8714
ISBN 978-2-83250-044-6
DOI 10.3389/978-2-83250-044-6

About Frontiers

Frontiers is more than just an open-access publisher of scholarly articles: it is a pioneering approach to the world of academia, radically improving the way scholarly research is managed. The grand vision of Frontiers is a world where all people have an equal opportunity to seek, share and generate knowledge. Frontiers provides immediate and permanent online open access to all its publications, but this alone is not enough to realize our grand goals.

Frontiers Journal Series

The Frontiers Journal Series is a multi-tier and interdisciplinary set of open-access, online journals, promising a paradigm shift from the current review, selection and dissemination processes in academic publishing. All Frontiers journals are driven by researchers for researchers; therefore, they constitute a service to the scholarly community. At the same time, the Frontiers Journal Series operates on a revolutionary invention, the tiered publishing system, initially addressing specific communities of scholars, and gradually climbing up to broader public understanding, thus serving the interests of the lay society, too.

Dedication to Quality

Each Frontiers article is a landmark of the highest quality, thanks to genuinely collaborative interactions between authors and review editors, who include some of the world's best academicians. Research must be certified by peers before entering a stream of knowledge that may eventually reach the public - and shape society; therefore, Frontiers only applies the most rigorous and unbiased reviews.
Frontiers revolutionizes research publishing by freely delivering the most outstanding research, evaluated with no bias from both the academic and social point of view. By applying the most advanced information technologies, Frontiers is catapulting scholarly publishing into a new generation.

What are Frontiers Research Topics?

Frontiers Research Topics are very popular trademarks of the Frontiers Journals Series: they are collections of at least ten articles, all centered on a particular subject. With their unique mix of varied contributions from Original Research to Review Articles, Frontiers Research Topics unify the most influential researchers, the latest key findings and historical advances in a hot research area! Find out more on how to host your own Frontiers Research Topic or contribute to one as an author by contacting the Frontiers Editorial Office: frontiersin.org/about/contact

EDITORS' SHOWCASE 2021: INSIGHTS IN STEM CELL RESEARCH

Topic Editors:
Valerie Kouskoff, The University of Manchester, United Kingdom
Atsushi Asakura, University of Minnesota Twin Cities, United States

Citation: Kouskoff, V., Asakura, A., eds. (2022). Editors' Showcase 2021: Insights in Stem Cell Research. Lausanne: Frontiers Media SA. doi: 10.3389/978-2-83250-044-6

Table of Contents

04 ***Systemic Supplementation of Collagen VI by Neonatal Transplantation of iPSC-Derived MSCs Improves Histological Phenotype and Function of Col6-Deficient Model Mice***
Aya Harada, Megumi Goto, Atsuya Kato, Nana Takenaka-Ninagawa, Akito Tanaka, Satoru Noguchi, Makoto Ikeya and Hidetoshi Sakurai

19 ***Potential of Stem Cells and CART as a Potential Polytherapy for Small Cell Lung Cancer***
Evgenii Skurikhin, Olga Pershina, Mariia Zhukova, Darius Widera, Natalia Ermakova, Edgar Pan, Angelina Pakhomova, Sergey Morozov, Aslan Kubatiev and Alexander Dygai

35 ***Differentiation of Human iPS Cells Into Sensory Neurons Exhibits Developmental Stage-Specific Cryopreservation Challenges***
Rui Li, Patrick Walsh, Vincent Truong, Ashley Petersen, James R. Dutton and Allison Hubel

51 ***Circular RNA Expression for Dilated Cardiomyopathy in Hearts and Pluripotent Stem Cell–Derived Cardiomyocytes***
Yiyu Zhang, Guoqing Huang, Zhaohu Yuan, Yonggang Zhang and Rong Chang

60 ***Multiple Gene Transfer and All-In-One Conditional Knockout Systems in Mouse Embryonic Stem Cells for Analysis of Gene Function***
Teruhiko Suzuki, Satoko Takagi and Takahiko Hara

67 ***Regulating Early Biological Events in Human Amniotic Epithelial Stem Cells Using Natural Bioactive Compounds: Extendable Multidirectional Research Avenues***
Farhana Ferdousi and Hiroko Isoda

76 ***The Field of Cell Competition Comes of Age: Semantics and Technological Synergy***
Kieran Maheden, Vivian Weixuan Zhang and Nika Shakiba

84 ***Esrrb Regulates Specific Feed-Forward Loops to Transit From Pluripotency Into Early Stages of Differentiation***
Amin R. Mazloom, Huilei Xu, Jaume Reig-Palou, Ana Vasileva, Angel-Carlos Román, Sonia Mulero-Navarro, Ihor R. Lemischka and Ana Sevilla

97 ***Xenotransplantation of Human Spermatogonia Into Various Mouse Recipient Models***
Dongli Liang, Qi Sun, Zijue Zhu, Chuanyun Wang, Shicheng Ye, Zheng Li and Yuan Wang

110 ***Air Pollution Exposure Induces Vascular Injury and Hampers Endothelial Repair by Altering Progenitor and Stem Cells Functionality***
Alice Costa and Gianandrea Pasquinelli

117 ***Mature Myotubes Generated From Human-Induced Pluripotent Stem Cells Without Forced Gene Expression***
Kei Fujiwara, Risa Yamamoto, Tomoya Kubota, Atsutoshi Tazumi, Tomoka Sabuta, Masanori P. Takahashi and Hidetoshi Sakurai

frontiers in Cell and Developmental Biology

ORIGINAL RESEARCH
published: 23 November 2021
doi: 10.3389/fcell.2021.790341

Systemic Supplementation of Collagen VI by Neonatal Transplantation of iPSC-Derived MSCs Improves Histological Phenotype and Function of Col6-Deficient Model Mice

*Aya Harada[1], Megumi Goto[1], Atsuya Kato[1], Nana Takenaka-Ninagawa[1], Akito Tanaka[1], Satoru Noguchi[2], Makoto Ikeya[1] and Hidetoshi Sakurai[1]**

[1]Department of Clinical Application, Center for iPS Cell Research and Application (CiRA), Kyoto University, Kyoto, Japan, [2]Department of Neuromuscular Research, National Institute of Neuroscience, National Center of Neurology and Psychiatry, Tokyo, Japan

OPEN ACCESS

Edited by:
Atsushi Asakura, University of Minnesota Twin Cities, United States

Reviewed by:
Hiroshi Sakai, Ehime University, Japan
So-ichiro Fukada, Osaka University, Japan

***Correspondence:**
Hidetoshi Sakurai
hsakurai@cira.kyoto-u.ac.jp

Specialty section:
This article was submitted to Stem Cell Research, a section of the journal Frontiers in Cell and Developmental Biology

Received: 06 October 2021
Accepted: 25 October 2021
Published: 23 November 2021

Citation:
Harada A, Goto M, Kato A, Takenaka-Ninagawa N, Tanaka A, Noguchi S, Ikeya M and Sakurai H (2021) Systemic Supplementation of Collagen VI by Neonatal Transplantation of iPSC-Derived MSCs Improves Histological Phenotype and Function of Col6-Deficient Model Mice. Front. Cell Dev. Biol. 9:790341. doi: 10.3389/fcell.2021.790341

Collagen VI is distributed in the interstitium and is secreted mainly by mesenchymal stromal cells (MSCs) in skeletal muscle. Mutations in *COL6A1-3* genes cause a spectrum of COL6-related myopathies. In this study, we performed a systemic transplantation study of human-induced pluripotent stem cell (iPSC)-derived MSCs (iMSCs) into neonatal immunodeficient COL6-related myopathy model (*Col6a1*^{KO}/NSG) mice to validate the therapeutic potential. Engraftment of the donor cells and the resulting rescued collagen VI were observed at the quadriceps and diaphragm after intraperitoneal iMSC transplantation. Transplanted mice showed improvement in pathophysiological characteristics compared with untreated *Col6a1*^{KO}/NSG mice. In detail, higher muscle regeneration in the transplanted mice resulted in increased muscle weight and enlarged myofibers. Eight-week-old mice showed increased muscle force and performed better in the grip and rotarod tests. Overall, these findings support the concept that systemic iMSC transplantation can be a therapeutic option for COL6-related myopathies.

Keywords: iPS cell, mesenchymal stromal cells, COL6-related myopathy, systemic cell transplantation, ullrich congenital muscular dystrophy (UCMD)

INTRODUCTION

Ullrich congenital muscular dystrophy (UCMD), which is regarded as the severe end of COL6-related myopathy, is a life-threatening muscular and connective tissue disorder, characterized by early-onset muscle weakness with multiple joint contractures and distal joint hyperlaxity (Bönnemann, 2011). The onset has been reported to be 12 months on average (Nadeau et al., 2009); nevertheless, multiple joint contractures at birth are evident in early severe cases (Yonekawa and Nishino, 2015). Reduced fetal movement leading to prenatal diagnosis was also identified (Hata et al., 2018). Typically, ambulation can be achieved only for a limited period, and respiratory muscle atrophy and scoliosis cause impaired respiratory function (Yonekawa et al., 2013). Mutations in *COL6A1*, *COL6A2,* and *COL6A3* genes, identified with both recessive and mostly *de novo* dominant

inheritance patterns, have different effects on collagen VI synthesis, assembly, secretion, and function, generating a phenotypically variable spectrum of COL6-related myopathies (Lamandé and Bateman, 2018).

Collagen VI null mice have contributed to our understanding of the pathomechanisms of COL6-related myopathies (Bonaldo et al., 1998; Noguchi et al., 2017). *Col6a1*$^{-/-}$ mice were produced by inserting a neomycin resistance cassette into the second exon of the *Col6a1* gene, which truncated the mRNA transcript. Without α1 (VI) chain, triple helical collagen VI molecules are not expressed in the mutant mice (Bonaldo et al., 1998; Lamandé et al., 1998). On the contrary, *Col6a1*$^{GT/GT}$ mice were generated by knocking in a point mutation in exon 9 in *Col6a1* gene (Noguchi et al., 2017). The resulting miss-splicing after exon 9 causes a marked reduction in normal *Col6a1* mRNA expression and a premature stop codon, resulting in *Col6a1* knockout and the mice having no collagen VI protein in all tissues (Noguchi et al., 2017). Therefore, we refer to *Col6a1*$^{GT/GT}$ mice as *Col6a1*^{KO} mice in this manuscript. Both conventional *Col6a1*$^{-/-}$ mice and *Col6a1*^{KO} mice are phenotypically similar, but *Col6a1*^{KO} mice have a smaller body weight (BW) than WT mice (Bonaldo et al., 1998; Noguchi et al., 2017). Furthermore, although histological phenotypes, such as variations in myofiber size and an increased number of myofibers with central nuclei, are observed in both *Col6a1*-mutated mouse types, a more quantitative analysis is available for *Col6a1*^{KO} mice. Researchers have confirmed that the number of myofibers of very small diameter is increased and the total number of myofibers in the tibialis anterior (TA) muscles starts to be reduced from postnatal day 15 onward, indicating a defect in muscle growth and signaling during development in *Col6a1*^{KO} mice (Noguchi et al., 2017). Since consistent findings were found in muscle biopsies from UCMD patients (Higuchi et al., 2003), *Col6a1*^{KO} mice are considered UCMD model mice. In contrast, the limited quantitative histology data of *Col6a1*$^{-/-}$ mice have made it difficult to define *Col6a1*$^{-/-}$mice as UCMD model mice.

The first clue of a therapeutic approach for COL6-related myopathies came from evidence that mitochondrial dysfunction triggers the apoptosis of myofibers and medication (Irwin et al., 2003; Bernardi and Bonaldo, 2008) and that autophagy is impaired in *Col6a1*$^{-/-}$ mice as well as in UCMD patients (Grumati et al., 2010; Bernardi and Bonaldo, 2013). Cyclosporine A and cyclophilin D both decreased the number of apoptotic events of myofibers by increasing mitochondrial tolerance for depolarized stimulation (Bernardi and Bonaldo, 2008; Tiepolo et al., 2009; Merlini et al., 20112011; Gattazzo et al., 2014), and forced activation of autophagy by a low protein diet benefited the muscle homeostasis of autophagic markers (Castagnaro et al., 2016). Alternatively, allele-specific knockdown strategies demonstrated the restored expression of collagen VI in the fibroblasts of UCMD patients (Bolduc et al., 2014; Noguchi et al., 2014; Marrosu et al., 2017; Bolduc et al., 2019). However, the above approaches are limited to normalizing the autophagic flux, which is not sufficient for improving the muscle function adequately (Merlini et al., 20112011) or unsuitable for long-term use (Castagnaro et al., 2016). Further, gene therapies target only specific mutations and cannot be applied to most patients with different pathogenic variants (Lampe AK et al., 2004). On the contrary, the therapeutic potential of mesenchymal cell transplantation has been recognized since the source of collagen VI in skeletal muscle is interstitial fibroblasts, not myogenic cells (Zou et al., 2008). The local intramuscular injection of adipose-derived mesenchymal stem cells (ADSCs) from neonatal skin resulted in the long-term and continuous secretion of collagen VI in *Col6a1*$^{-/-}$ *Rag1*$^{-/-}$mice, but neither the histological nor functional effects were investigated (Alexeev et al., 2014).

iMSCs are mesenchymal stromal cells (MSCs) derived from human induced pluripotent stem cells (iPSCs) (Fukuta et al., 2014; Matsumoto et al., 2015; Chijimatsu et al., 20172017) and share comparable gene and protein expression levels of collagen VI with primary MSCs from adult skeletal muscles (Takenaka-Ninagawa et al., 2021). When injected locally into the TA muscles of *Col6a1*^{KO}/NSG mice, iMSCs secrete collagen VI for a long time to enhance muscle regeneration at the lesion where collagen VI was restored (Takenaka-Ninagawa et al., 2021). Therefore, we investigated whether systemic iMSC transplantation can potentially restore collagen VI expression throughout the skeletal muscles of the whole body in *Col6a1*^{KO}/NSG mice and ameliorate the pathophysiology. We also expected that neonatal intervention would have a physiological influence on muscle development from an earlier period and produce better effects with a smaller number of donor cells.

Accordingly, this study aimed to prove the therapeutic effects of systemic iMSC transplantation in *Col6a1*^{KO}/NSG mice. We demonstrated that the intraperitoneal (i.p.) injection of iMSCs contributed to the expression of collagen VI among skeletal muscles and increased the size and number of myofibers by upregulating muscle regeneration. The number of abnormal mitochondria in the treated *Col6a1*^{KO}/NSG mice was decreased, suggesting iMSC transplantation may provide some positive environmental changes to *Col6a1*-null muscles. Functional improvements by the transplantation were also achieved.

MATERIALS AND METHODS

Mice

UCMD model mice were generated as previously described (Noguchi et al., 2017). In order to distinguish these mice from conventional *Col6a1*$^{-/-}$ mice, we call them *Col6a1*^{KO} mice. *Col6a1*^{KO} mice were backcrossed to achieve the NSG (NOD acid gamma) background. After establishing the *Col6a1*^{HETERO}/NSG mice line, we crossed the mice again to produce *Col6a1*^{KO}/NSG mice. Because *Col6a1*^{KO}/NSG mice are hard to conceive, the offspring were maintained by *in vitro* fertilization (IVF) with ICR surrogate mothers. We used 3–8 generations of the *Col6a1*^{KO}/NSG strain. The mice were kept under a 12/12 h light-dark cycle with easy and comfortable access to food and water. The pups were weaned at 3 weeks of age. The genotype of the offspring confirmed no contamination of *Col6a1*^{HETERO}/NSG mice. WT/NSG mice (NOD.Cg-*Prkdc* ^{scid} *Il2rg* ^{tm1Wjl}/Szj) were purchased from Charles River Laboratory and kept under the same environment as *Col6a1*^{KO}/NSG mice.

Cells

The differentiation of 201B7 iPSCs to iMSCs via iPSC-derived neural crest cells (iNCCs) was performed as previously published (Fukuta et al., 2014). Luciferase-expressing piggyBac vector (pPV-EF1a-Luc2-iP-A) (Xu et al., 2019) and piggyBac transposase plasmids (pHL-EF1a-hcPBase-A) were introduced into the iNCCs by electroporation with a NEPA21 electroporator (Nepa Gene, Co., Ltd., Chiba, Japan), and the transfected cells were selected with 0.5% puromycin over 7 days. Luciferase-expressing iNCCs were maintained by passaging after 90% confluency or kept frozen in cryopreservation liquid (Bambanker, Nippon Genetics Co., Ltd., CS-02-001) as a stock. The iNCCs were induced to iMSCs just before use. Only passage 5 or 6 iMSCs were used for the transplantation.

Transplantation

Only male pups were used for analysis throughout the study. For neonatal i. p. transplantation, 5×10^6 iMSCs in 20 µl phosphate-buffered saline (PBS) were injected intraperitoneally using a 30G insulin syringe (BD, No. 326668). All the mice analyzed at 8 weeks had a boost i. p. transplantation at 4 weeks, in which 5×10^6 iMSCs in 100 µl PBS were injected using a 23G 1 ml syringe (Terumo, SS-01T2613).

In Vivo Imaging System

Mice were anesthetized with isoflurane, and the luminescence was imaged with an IVIS imaging system (Parkin Elmer) 10 min after the administration of 150 mg/kg d-luciferin substrate (Summit Pharmaceutical International Corporation, XLF-1) in PBS. The luminescence intensity was measured, and the region of interest (ROI) was set to cover all the signals.

RT-PCR

cDNA used for *luciferase* detection was treated as follows. After the removal of DNA contamination with DNase I (Invitrogen, 18068-015), 1 µg mRNA was reverse transcribed with SuperScript III using a random hexamer as instructed (Invitrogen, 18080-051). The PCR products were electrophoresed on a 1% agarose gel for 30 min to detect amplified fragments of luciferase and imaged under a FAS-IV gel imaging device (Nippon Genetics, Co., Ltd.). Positive control samples were dissected from a teratoma that had been formed 8 weeks after the subcutaneous injection of luciferase-integrated iPSCs into the TA muscle of WT/NSG mice. Negative control samples were extracted from the TA muscle of *Col6a1*^{KO}/NSG mice.

Tissue Sectioning

Mice were euthanized by exposure to gradually increasing concentrations of carbon dioxide. Dissected TA and quadriceps were stuck onto the pedestal by tragacanth gum (Wako, 206-02242) on a cork and frozen by dipping into 2-methylbutane (Wako, 166-00615) for 45–60 s at melting point temperature (−156°C). Freshly isolated diaphragms were embedded in OCT compound (Sakura Finetek, 4583, USA) and directly frozen within 2-methylbutane. Frozen muscles were sliced at 12-µm thickness with a Cryostat (Leica, CM1850) and attached to the slide. The sample on the slide was kept at −80°C for the following immunostaining.

Immunohistochemistry

The frozen sample on the slide was fixed in 4% paraformaldehyde for 20 min and washed twice with PBS. After 1-h incubation with Blocking one (Nacalai tesque, 03953-95), the primary antibody in immunoreaction enhancer solution (Can get signal, TOYOBO, NKB-601) was applied to the sample overnight at 4°C. The sample was washed with 0.1% Triton-X in PBS three times for 10 min each. The secondary antibody was applied for 1 h at room temperature, and the sample was washed three times. Images were obtained under a confocal microscope (Zeiss, LSM710). The primary and secondary antibodies used for the immunostaining and the dilution ratios are described in **Supplementary Table S1**.

Cell Apoptosis Assay

TUNEL positive cells were stained with an Apoptag® plus peroxidase *in situ* apoptosis detection kit (Millipore, S7101) following the manufacturer's instructions. After the TUNEL staining, an additional course of immunostaining for MYH3 was performed as described above. The fixation and blocking steps were skipped for the second staining.

Functional Analysis

We planned three different functional tests with the same mice. All tests were conducted within 1 week in the same order: muscle force first, grip test second, and rotarod test third. Non-transplanted and transplanted mice were the siblings of the same surrogate ICR mothers and were randomly selected into either group. They grew up together until weaning at 3 weeks. After weaning, the mice were divided into same-sized cages with five mice each.

Functional Analysis of Maximum Isometric Torque

A custom-made mouse ankle joint motor function analysis system (Bio Research Center, Nagoya, Japan) was used as previously described (Itoh et al., 2017). Briefly, the mice were anesthetized with isoflurane inhalation, and the plantar was attached to the pressure sensor. Two electrodes were attached to the shaved hind limb with viscous electrical conductive gel (CR-S; Sekisui Plastics, Osaka, Japan) in between. One was fixed to the myotendinous junction and the other was fixed 5 mm above it with adhesive tape. Electrical stimulation was applied to the skin surface of the triceps surae muscle using an electric stimulator (SEN-3301; Nihon Kohden, Tokyo, Japan) to induce muscle contraction. Isometric plantarflexion torque was calculated from the pressure applied to the sensor and the distance from the ankle joint to the sensor. The measurement was performed twice for each foot, and the average value was adopted.

Grip Strength Test

All measurements were blindly taken by one experienced examiner (M.G.). After being calmed on the examiner's hand, the mice were placed on wire mesh equipped with a traction meter (no. BS-TM-RM, Brain Science idea, Osaka, Japan) by

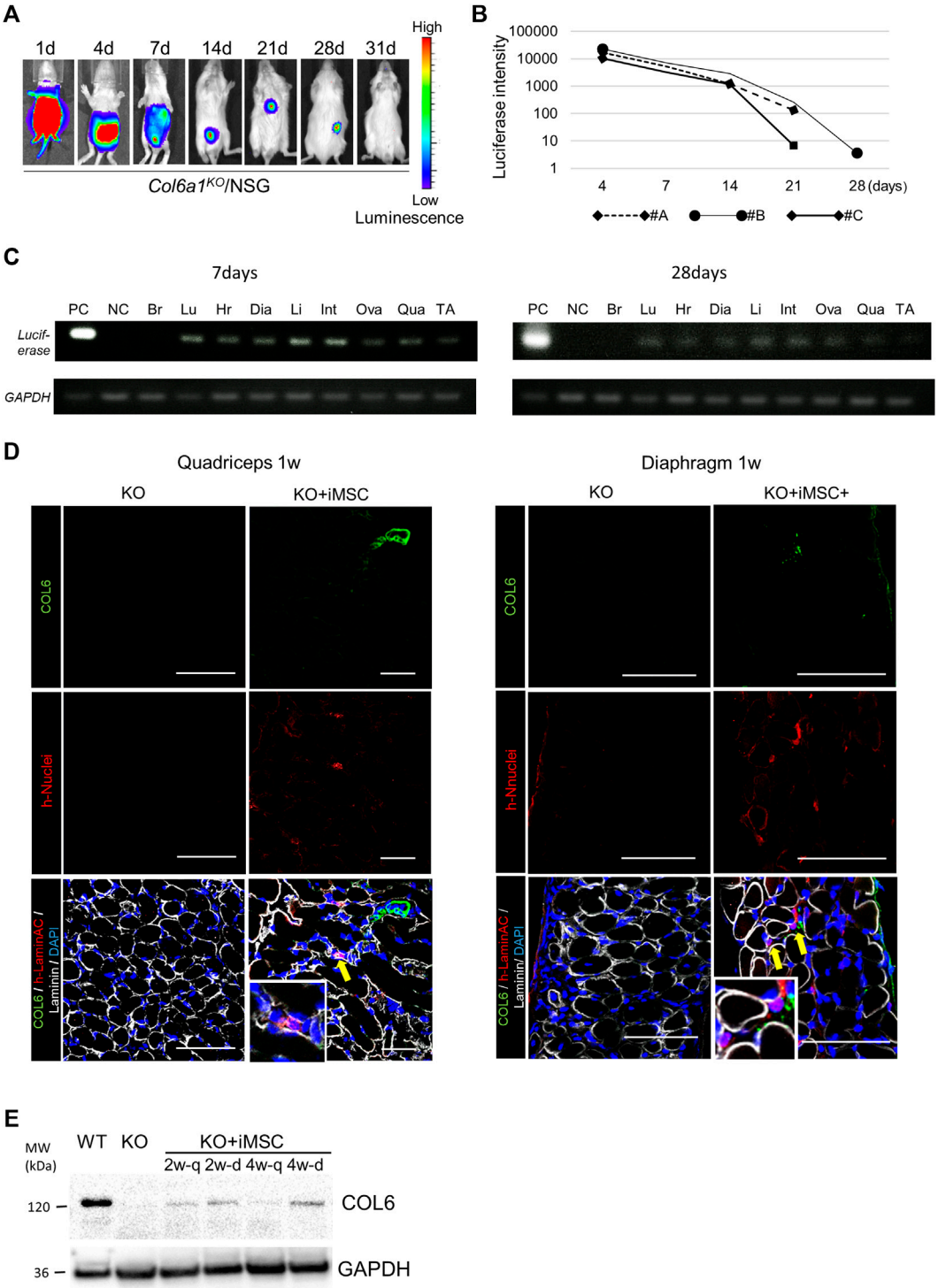

FIGURE 1 | Tracking of donor cells after intraperitoneal transplantation. **(A)** *In vivo* imaging of the donor cells. The signal from the donor cells of #B in **Figure 1B** is shown. The signal disappeared after 4 weeks. **(B)** Time course of the luciferase signal intensity of three mice. **(C)** *Luciferase* detection by PCR 7 days (top) and 28 days (bottom) after the transplantation. 0.8 μg mRNA from each organ was extracted, and the donor cells in each organ were detected by luciferase and GAPDH primers. The signal was detected in the lung (Lu), heart (Hr), diaphragm (Dia), liver (Li), intestine (Int), uterus and ovary (Ova), quadriceps (Qua), and tibialis anterior muscle (TA), but not the brain (Br). The positive control (PC) was extracted from a teratoma dissected 8 weeks after the subcutaneous injection of iPSCs with luciferase integration. NC: negative control. **(D)** Immunofluorescence staining of the quadriceps (left) and diaphragm (right) 7 days after iMSC intraperitoneal transplantation. Donor cells were positive for human-nuclei (yellow arrows). Magnifications of the human-nuclei positive cells are also shown. Scale bars, 50 μm. COL6: collagen VI. **(E)** Western blotting for the detection of collagen VI. Proteins from the quadriceps and diaphragm of *Col6a1*^{KO}/NSG mice 2 and 4 weeks after neonatal transplantation were extracted. PC was a

(*Continued*)

FIGURE 1 | diluted sample (1:10) extracted from the quadriceps of WT/NSG mice at 4 weeks. NC was a sample from the quadriceps of *Col6a1*^{KO}/NSG mice. All blots were derived from the same experiment and processed in parallel.

gripping with all four extremities. The examiner pulled the tail, and the maximum value of the grip strength was measured three times. The average of the three tests was counted as the score of an individual mouse.

Rotarod Test

The test run was performed once a day on a rotarod apparatus (Ugo Basile, Cat No.47600). After 2 runs as mock exams, the duration of the running time was recorded for 3 days. The rotation speed was started at 4 rpm, increased to 50 rpm in 300 s, and kept at 50 rpm for another 300 s. The maximum running time was 600 s. The average of three runs was counted as the score of an individual mouse.

Statistics

Numerical data with three groups were analyzed with a one way-ANOVA followed by the Tukey-Kramer method. The student's t-test was performed between two independent groups. $^{*}p < 0.05$, $^{**}p < 0.01$, and $^{***}p < 0.001$ are labeled in the figures. † was used when p-values were <0.1, indicating that the two groups tended to have a difference, but it was not statistically different.

Study Approval

All animal experiments were performed in accordance with the guidelines of the animal experiment committee and recombinant DNA experiment committee at Kyoto University. The study design was reviewed and accepted by the animal experiment committee in advance of conducting all the experiments (No.17-95-2).

RESULTS

iMSCs Reached Skeletal Muscle and Secreted Collagen VI Locally After Intraperitoneal Injection

First, we confirmed that the donor cells were positive for CD73, CD44, and CD105 and negative for CD45 and HLA-DR (**Supplementary Figure S1A**). The expression of collagen VI was also confirmed (**Supplementary Figure S1B**). Next, we evaluated the potential of human iMSCs to deliver collagen VI to the skeletal muscles in *Col6a1*^{KO}/NSG mice after neonatal i. p. injection. Two days after birth, 5×10^6 luciferase-expressing iMSCs were transplanted to the peritoneal cavity, and their distribution was observed with an IVIS imaging system. The transplanted cells were widely delivered including to the lower and upper extremities after 24 h (**Figure 1A**). The total intensity of the luciferase signal decreased with time but was detectable for 28 days (**Figure 1B**). iMSCs were seen in major organs except for the brain based on *luciferase* transcript expressions at 7 days after the transplantation (**Figure 1C**). Fewer iMSCs were detected at 28 days.

Histological analysis revealed that the iMSCs had reached the interstitial space of the quadriceps and diaphragm 1 week after the transplantation (**Figure 1D**). The expression of restored collagen VI was also confirmed by Western blotting in the quadriceps and diaphragm after 2 weeks (**Figure 1E**). Collagen VI expression in the tissues suggested that iMSCs migrated to the skeletal muscle and secreted collagen VI locally.

To prove that iMSCs can migrate throughout the body via blood vessels, we performed intravenous (i.v.) transplantation from the facial vein 1 day after birth. The transplanted cells distributed to the whole body including the quadriceps and diaphragm, where they secreted collagen VI (**Supplementary Figures S2A,B**). Collagen VI secretion was sustained for more than 28 days in the limb muscles (**Supplementary Figure S2C**). Although the i.v. transplantation had comparable results with the i. p. transplantation, we chose to perform further experiments with i. p. transplantation because i. v. transplantation was technically difficult. Overall, the above findings indicate that transplanted iMSCs can deliver molecules into organs including skeletal muscle, suggesting a potential for treating systemic diseases.

iMSC Transplantation Positively Affected the Phenotype of *Col6a1*^{KO}/NSG Mice

Next, we searched for indicators to evaluate the effects of the transplantation on skeletal muscle. At 4 weeks, there was no positive effect on muscle weight after the transplantation (**Supplementary Figure S3A**), although the engraftment of donor cells and expression of collagen VI in the quadriceps and diaphragm were confirmed (**Supplementary Figure S3B**). A histogram of the diameters of the quadriceps revealed that the myofiber size was smaller in *Col6a1*^{KO}/NSG mice than in wild type (WT)/NSG mice, and its distribution shifted and became larger in the transplanted mice (**Supplementary Figure S3C**). The percentage of small myofibers and large myofibers decreased and increased, respectively (**Supplementary Figure S3D**), and the average size of the myofibers was increased after the transplantation (**Supplementary Figure S3E**). The area of the myofibers tended to increase ($p = 0.064$) (**Supplementary Figures S3F,G**).

When a boost i. p. injection of 5×10^6 iMSCs was added at 4 weeks, the therapeutic effects of the transplantation were more clearly demonstrated at 8 weeks than at 4 weeks. Donor cells after the second i. p. transplantation were dominantly observed in the interstitium, suggesting that the transplanted cells were extravasated from the blood vessels to the quadriceps (**Supplemental Figure S4A**). An IVIS study confirmed similar iMSC dynamics with neonatal transplantation, with the period of

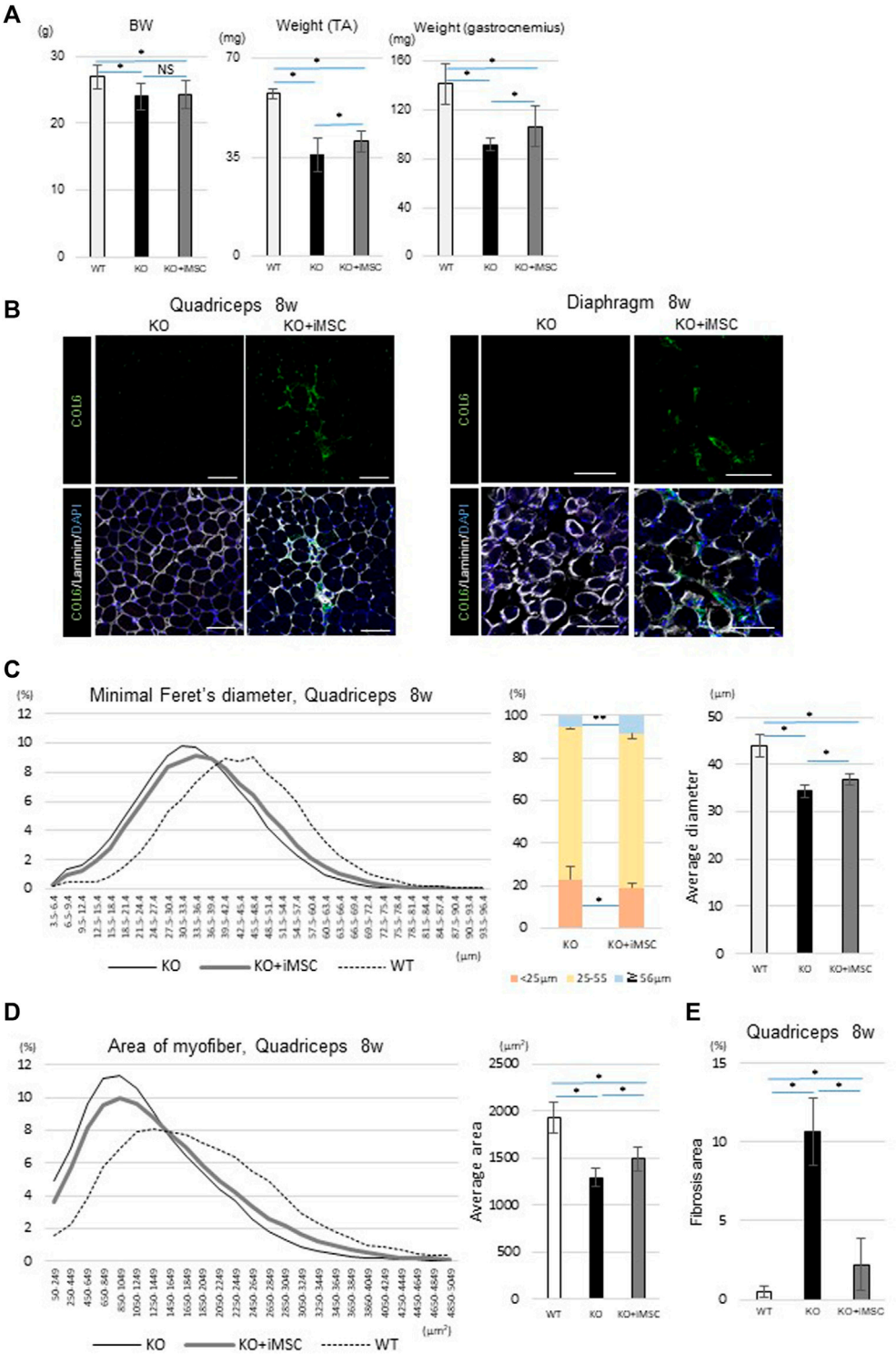

FIGURE 2 | Phenotypes at 8 weeks. **(A)** Body weight (BW) and muscle weight of each group. For BW: WT (n = 15), KO (n = 66), and KO + iMSC (n = 30). For raw weight of the TA (middle) and gastrocnemius muscles (right): WT (n = 6), KO (n = 9), and KO + iMSC (n = 13). (Tukey's test). **(B)** Immunofluorescence staining of the quadriceps (left) and diaphragm (right) in non-transplanted (KO) and transplanted mice (KO + iMSC). The transplanted mice showed collagen VI expression in the interstitial space of the muscles. Scale bars, 50 μm. **(C,D)** Histological analysis of myofibers in the quadriceps. **(C)**: Diameter of the short axis (minimal Feret's diameter). Left: histogram of the diameter; middle: frequency of different diameter groups; right: average diameter. **(D)**: Area of the myofibers. Left: histogram of the myofiber size; right: average size. WT (n = 7), KO (n = 9), and KO + iMSC (n = 13). **(E)** Fibrotic area in the quadriceps calculated by Sirius red staining. WT (n = 4), KO (n = 5), and KO + iMSC (n = 5). (Tukey's test). All error bars indicate ± SD.

the luciferase signal ranging from 2 to 4 weeks (**Supplementary Figure S4B**). Muscle weight at 8 weeks was increased in the transplanted mice compared to the non-transplanted mice, although BW was not significantly changed (**Figure 2A**). Donor cells were much less detected than at 4 weeks, but collagen VI expression had dispersed and remained in the quadriceps and diaphragm of the transplanted mice (**Figure 2B**). Histological analysis of the quadriceps showed the diameter and area of myofibers were increased with the transplantation (**Figures 2C,D**).

Fibrosis in skeletal muscle is abundant in adult *Col6a1*^{KO} mice (Noguchi et al., 2017). On the other hand, one of the concerns of injecting iMSCs is that iMSCs may induce fibrosis depending on their microenvironment because mesenchymal progenitor cells in skeletal muscle can be a source of both fat accumulation and fibrosis in diseased mice (Uezumi et al., 2011). To understand the impact of the iMSC transplantation on fibrosis formation, we performed several studies. Sirius red staining showed that the fibrotic change in the quadriceps was more prominent in non-transplanted *Col6a1*^{KO}/NSG mice than in WT/NSG mice but was ameliorated with the transplantation (**Supplementary Figure S5A**). Quantitative analysis of the fibrotic area also showed suppressed fibrosis in the transplanted mice (**Figure 2E**). The gene expression of *Postn*, a matricellular protein that contributes to fibrosis (Kanaoka et al., 2018), was suppressed in the diaphragm of transplanted mice (**Supplementary Figure S5B**), and reduced Periostin expression in the transplanted mice was confirmed by immunostaining (**Supplementary Figure S5C**).

In sum, iMSC-transplanted mice showed an increased myofiber size at 4 weeks. When the boost transplantation was added at 4 weeks, the muscle weight and myofiber size were increased at 8 weeks without any enhancement of fibrosis.

Quantification of Rescued Collagen VI

The expression of collagen VI was measured by Western blotting and immunofluorescence staining in the quadriceps and diaphragm. The expression level of collagen VI in the Western blotting was detected in all samples at 4 weeks, but undetectable in one of the four samples at 8 weeks (**Supplementary Figure S6A**). The average expression level in the quadriceps sample of the transplanted mice was 0.48% at 4 weeks and 0.24% at 8 weeks that of WT mice at 4 weeks. In the diaphragm, the average percentages were 1.2 and 0.88%, respectively (**Supplementary Figure S6B**).

The collagen VI-rescued area based on immunofluorescence staining was also calculated (**Supplementary Figures S7A, S8A**). The collagen VI expression gradually increased after neonatal transplantation, reaching a peak at around 4–5 weeks, and decreased thereafter in the quadriceps even with boost transplantation at 4 weeks (**Supplementary Figure S7B**). The collagen VI-restored area at 4 weeks in the quadriceps was 5.87%, which is equivalent to 16.3% of the collagen VI positive areas in 4-week-old WT/NSG mice (**Supplementary Figures S7B,C**). The average collagen VI-rescued area at 8 weeks in the quadriceps was 3.45% (equivalent to 11.0% in 8-week-old WT/NSG mice) after neonatal and boost iMSC transplantation at 4 weeks, but 1.03% (equivalent to 3.31% in 8-week-old WT/NSG mice) when only neonatal transplantation was performed (**Supplementary Figures 7B,C**). Boost transplantation at 4 weeks slowed the rate at which collagen VI degraded, but it did not maintain the collagen VI-rescued area at 4 weeks. The donor cells in the quadriceps decreased with time and were rarely detected after 8 weeks (**Supplementary Figure S7d**).

As for the diaphragm, the average collagen VI-rescued area was 5.7% at 4 weeks (equivalent to 22.2% in 4-week-old WT/NSG mice) and 3.6% at 8 weeks (10.4% in 8-week-old WT/NSG mice) (**Supplementary Figures 8B,C**). The number of donor cells in the diaphragm showed a similar pattern as in the quadriceps and decreased with time (**Supplementary Figure S8D**).

Collagen VI expression was barely observed in the quadriceps at 20 weeks following transplantations at the neonatal stage and boost transplantation at 4 weeks (**Supplementary Figure S10A**). The longest period the donor cells could engraft was not confirmed, but some donor cells were detected in the quadriceps at 20 weeks (**Supplementary Figure S9B**). No tumorigenesis was confirmed at 20 weeks in any of the 10 mice that received the two transplantations (neonatal and 4-week boost) (data not shown).

iMSC Transplantation Activated Muscle Regeneration

We then focused on the impact of iMSC transplantation on MYH3+ myofibers. MYH3, an embryonic myosin heavy chain, is the isoform expressed in regenerating fibers after injury or the early stage of muscle development (Schiaffino et al., 2015) and generally detected for 2–3 weeks in newly regenerating myofibers (Jerkovic et al., 1997; Kalhovde et al., 2005). The MYH3 protein expression level gradually decreases and switches to adult-type myosin heavy chain (Li et al., 2013; Yoshimoto et al., 2020). The position change of nuclei is another hallmark of muscle development (Roman and Gomes, 2018). During development, nuclei are spread longitudinally in the center of the myofiber and migrate peripherally toward the end part of the muscle (Roman and Gomes, 2018), which can be observed as a multinuclear myofiber in the section. In a previous study using muscle biopsies from UCMD patients, MYH3 positive regenerating muscle fibers were limited to small diameters (Higuchi et al., 2003), indicating that the impairment of muscle regeneration is one of the phenotypes of UCMD.

At 4 weeks, we observed the area where MYH3+ myofibers were aggregated, which was consistent with the area where collagen VI was expressed in transplanted mice, while MYH3+ myofibers in non-transplanted mice solely existed among mature myofibers (**Figure 3A**). In addition, myofibers weakly positive for MYH3 observed in the transplanted mice grew (**Figure 3A**, arrowheads). Therefore, we analyzed the correlation of the fluorescence intensity and size of MYH3+ myofibers to evaluate the difference in muscle regeneration between transplanted and non-transplanted mice. The number of large, weakly positive MYH3+ myofibers was increased in transplanted mice, whereas smaller, strongly positive MYH3+ myofibers were observed in non-transplanted mice (**Figure 3B**). The number of myofibers with multiple nuclei as well as the ratio of

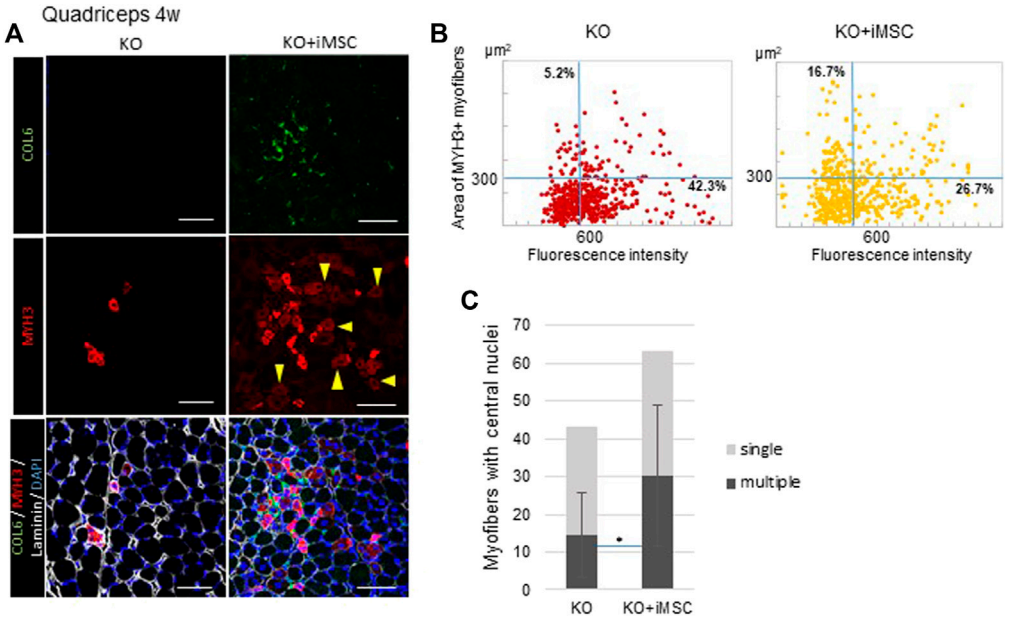

FIGURE 3 | Regenerating myofibers and collagen VI at 4 weeks. **(A)** Immunofluorescence staining of the quadriceps from non-transplanted mice (left) and transplanted mice (right). MYH3+ myofibers were gathered and enlarged around the area where collagen VI was expressed in the transplanted mice. Some MYH3+ myofibers were faint in color (arrowheads), consistent with muscle maturation. Scale bars, 50 μm.**(B)** Correlation plot of the fluorescence intensity and area of MYH3+ myofibers in non-transplanted (left) and transplanted (right) mice. MYH3+ myofibers in the quadriceps of four mice were counted. The percentage in the upper left quadrants, which correspond to more mature MYH3+ myofibers, was increased with iMSC transplantation. **(C)** Number of central nucleated myofibers in the quadriceps. Myofibers with single nuclei (light grey) were not significantly different, but more myofibers with multiple nuclei (dark gray) were observed in the quadriceps in transplanted mice. KO (n = 9) and KO + iMSC (n = 9). (Student's t-test). Error bars indicate ±SD.

multinucleated to single nucleated myofibers were increased in transplanted mice (**Figure 3C**).

Next, in order to reveal the impact of iMSC transplantation on muscle stem (satellite) cells, we counted the number of Pax7+ and MyoD + nuclei in the quadriceps (**Figure 4A**). Pax7 is a marker of satellite cells, and Pax7+MyoD-cells are in the quiescent state (Gnocchi et al., 2009). On the other hand, MyoD is one of the earliest markers of myoblasts (Weintraub, 1993). Pax7+MyoD + cells are active satellite cells during the process of cell division, and MyoD + Pax7-cells are committed myoblasts (Chal and Pourquié, 2017). Muscle regeneration was more active at 4 weeks than at 8 weeks, during which time the total number of positive nuclei for these regeneration markers decreased in both WT/NSG and *Col6a1*^{KO}/NSG mice (**Figure 4B**). A difference in the number of MyoD + Pax7-cells was notable at 8 weeks between non-transplanted and transplanted mice. MyoD + Pax7-cells were upregulated in the non-transplanted mice up to 4 weeks, but thereafter decreased to a level close to WT/NSG mice at 8 weeks. Contrastingly, the count of MyoD + Pax7-cells in the transplanted mice decreased at a slower rate at 8 weeks than in the non-transplanted mice (**Figures 4B,C**). The total number of myofibers in TA muscle increased in transplanted mice as well as in WT/NSG mice, while it was decreased in non-transplanted mice from 4 to 8 weeks (**Figure 4D**).

The dynamics of MYH3+ regenerating myofibers followed the dynamics of MyoD + cells. While MYH3+ myofibers were rarely observed in WT/NSG mice at 4 and 8 weeks, they were scattered in both transplanted and non-transplanted *Col6a1*^{KO}/NSG mice at 4 weeks. However, at 8 weeks, larger MYH3+ myofibers were present in the transplanted mice but rarely detected in the non-transplanted mice (**Figure 4E**). The number of MYH3+ myofibers was not different between the transplanted and non-transplanted mice at 4 weeks, but higher in the transplanted mice at 8 weeks (**Figure 4F**).

In sum, the dynamics of myogenic cells and MYH3+ myofibers indicated that iMSC transplantation retained muscle regenerative capacity over longer periods in *Col6a1*^{KO}/NSG mice.

Effects on Mitochondria Morphology and Apoptosis

Ultrastructural alterations of mitochondria and spontaneous apoptosis are observed in the muscles of *Col6a1*$^{-/-}$ mice (Irwin et al., 2003; Palma et al., 2009) and UCMD patients (Angelin et al., 2007). Mitochondria are involved in the pathogenesis of UCMD, as mitochondrial defects are common findings irrespective of the genetic mutation locus or mode of inheritance, but additional factors are involved in the susceptibility to apoptosis or regeneration (Angelin et al., 2007). Therefore, to elucidate the mechanism of the therapeutic effects of iMSC transplantation, we investigated mitochondria and apoptosis in the muscles of *Col6a1*^{KO}/NSG mice.

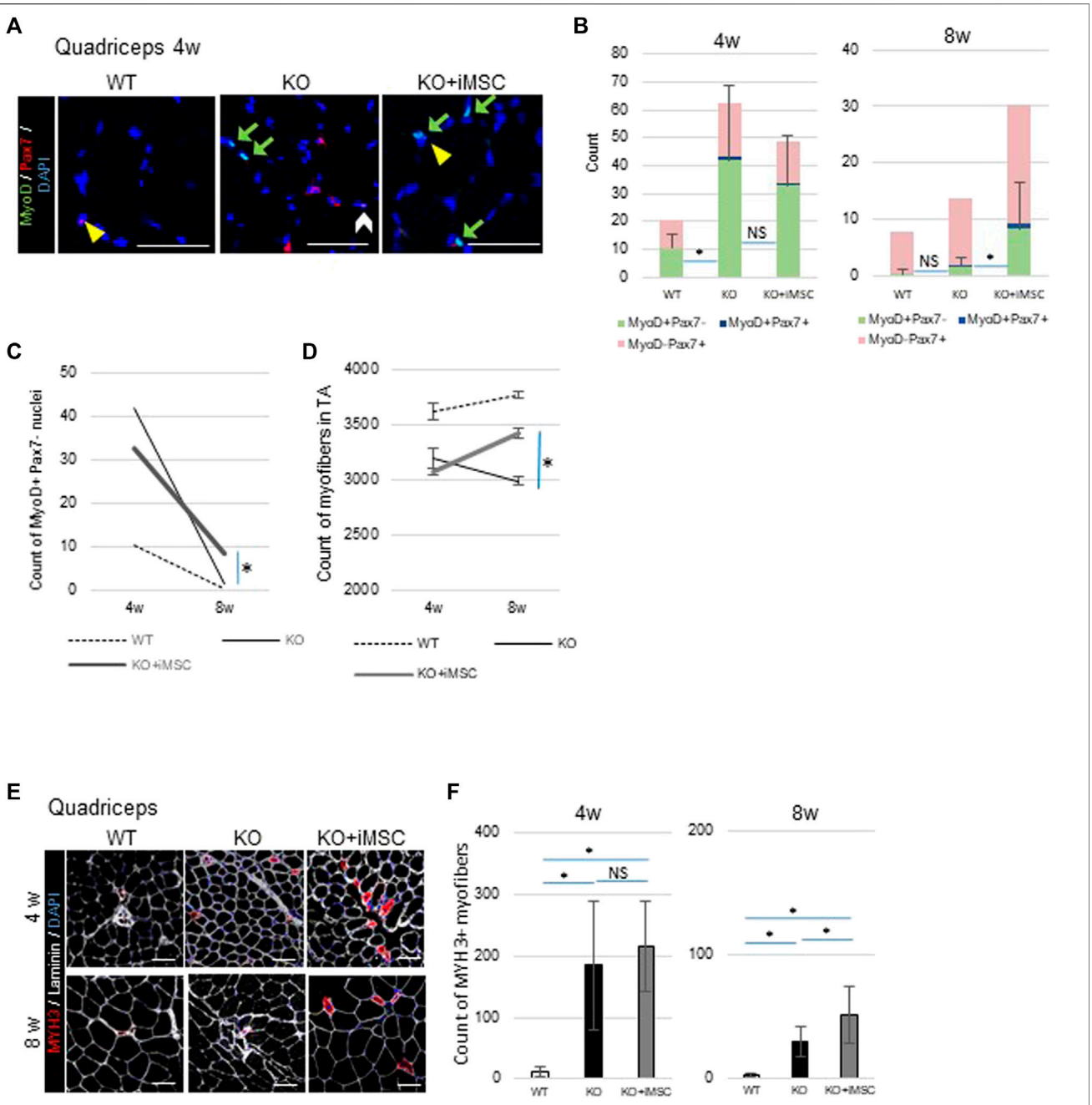

FIGURE 4 | Histological analysis of muscle regeneration. **(A)** Representative images of immunostaining of nuclei with positive regenerative markers. MyoD + cells (green arrows), Pax7+ cells (yellow arrowheads), and MyoD + Pax7+ cells (white arrow) were observed in the quadriceps. Scale bars, 50 μm. **(B)** Quantitative analysis of muscle regeneration capacity at 4 weeks (WT (n = 4), KO (n = 11), and KO + iMSC (n = 11)) and 8 weeks (WT (n = 5), KO (n = 9), and KO + iMSC (n = 13)). The number of nuclei positive for each regenerative marker was counted (Tukey's test). Error bars indicate ±SD. **(C)** Number of Myo + Pax7-nuclei between 4 and 8 weeks. A therapeutic difference was observed in transplanted mice at 8 weeks based on the number of MyoD + nuclei. **(D)** The number of myofibers in TA muscles between 4 and 8 weeks. 4 weeks: WT (n = 5), KO (n = 7), and KO + iMSC (n = 11); 8 weeks: WT (n = 5), KO (n = 8), and KO + iMSC (n = 13). (Student's t-test). Error bars indicate ±SEM. **(E)** Images of MYH3+ myofibers at 4 and 8 weeks. **(F)** The number of MYH3+ myofibers in the quadriceps at 4 weeks (WT (n = 5), KO (n = 7), and KO + iMSC (n = 11)) and at 8 weeks (WT (n = 5), KO (n = 9), and KO + iMSC (n = 12)). (Tukey's test). Error bars indicate ±SD. These results suggested iMSC transplantation positively affected regenerative capacity at 8 weeks.

Regarding the morphology of the mitochondria, multiple abnormal mitochondria were often detected in the quadriceps of *Col6a1*^{KO}/NSG mice (**Figure 5A**), but they were hardly observed in transplanted mice (**Figure 5B**). Moreover, some images of the transplanted mice were consistent with the formation of the autophagosome (**Figure 5B**), which was

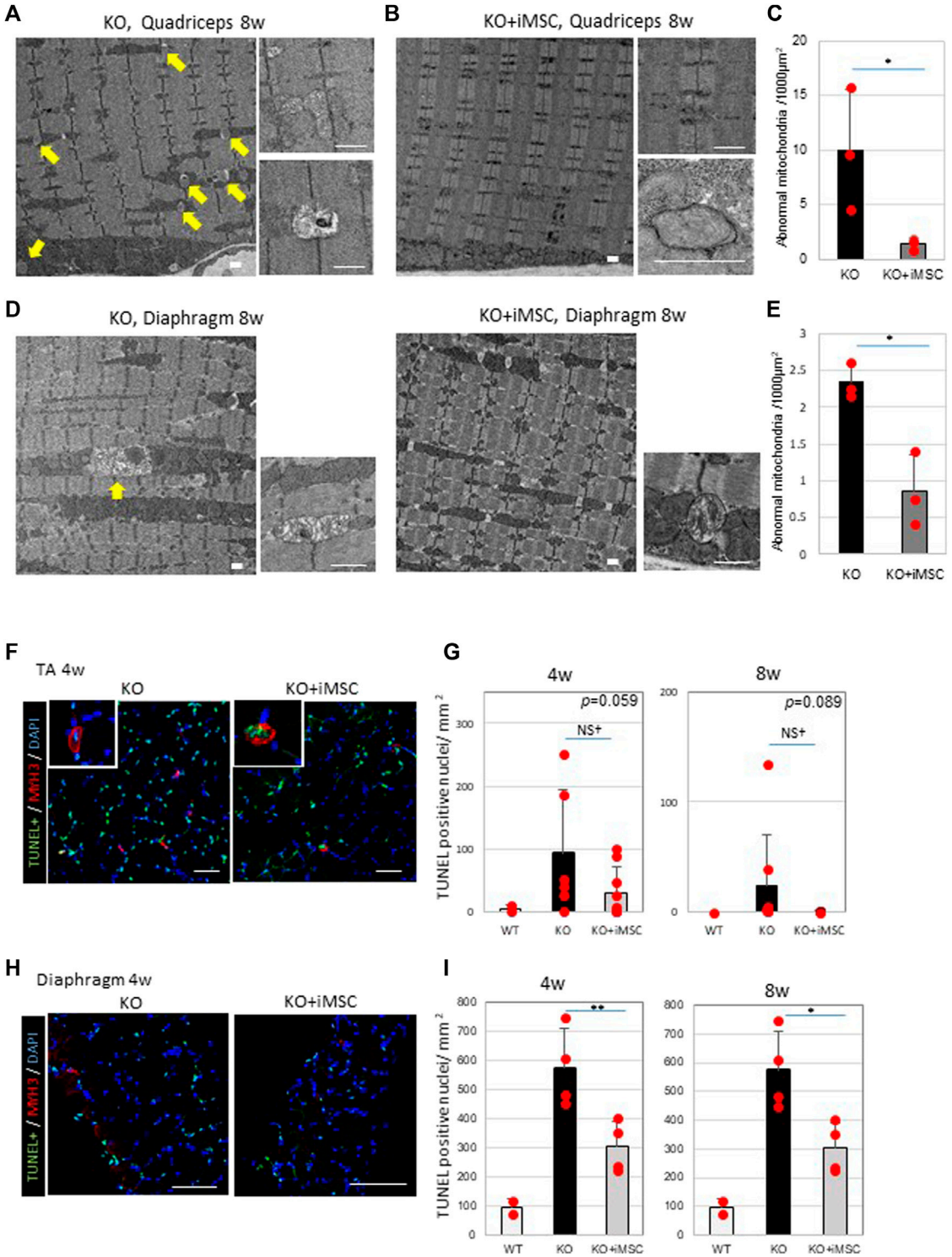

FIGURE 5 | Abnormal mitochondria and apoptosis were decreased in the muscles of iMSC transplanted mice. **(A)** Electron micrographs of the quadriceps of *Col6*^{KO}/NSG mice without transplantation at 8 weeks. Abnormal mitochondria (arrows) are indicated (left). A typical picture of aberrant mitochondria revealed swollen bodies (top right), some of which were rich with protein aggregates (bottom right). Scale bars, 1 μm. **(B)** Electron micrographs of the quadriceps of transplanted KO mice at 8 weeks. Mitochondrial abnormalities were rarely detected (left). Normal mitochondria (top right) and the formation of the autophagosome (bottom right) were also observed. Scale bars, 1 μm. **(C)** Quantification of abnormal mitochondria in the quadriceps at 8 weeks. (Student's *t*-test). **(D)** Electron micrographs of the diaphragms from non-transplanted (left) and transplanted (right) mice at 8 weeks. Abnormal mitochondria were present in non-transplanted mice (arrow), but less so in transplanted mice. Swollen mitochondria were detected in both non-transplanted and transplanted mice (bottom right). Scale bars, 1 μm. **(E)** Quantification of abnormal

(*Continued*)

FIGURE 5 | mitochondria in the diaphragm at 8 weeks. (Student's *t*-test). **(F)** Immunofluorescence staining of the TUNEL assay and MYH3 from TA muscles at 4 weeks. Pictures at the top left are of MYH3+ myofibers whose nuclei were apoptotic, indicating that newly regenerating myofibers were undergoing apoptosis. Scale bars, 50 μm.**(G)** Quantification of apoptotic nuclei in TA muscles at 4 weeks (WT (n = 2), KO (n = 7) and KO + iMSC (*n* = 9)) and 8 weeks (WT (*n* = 2), KO (*n* = 8) and KO + iMSC (*n* = 8)). (Student's *t*-test). **(H)** Immunofluorescence staining of the TUNEL assay and MYH3 from the diaphragm at 4 weeks. Scale bars, 50 μm. **(I)** Quantification of apoptotic nuclei in the diaphragm at 4 weeks (WT (*n* = 2), KO (*n* = 4), and KO + iMSC (*n* = 4)) and 8 weeks (WT (*n* = 2), KO (*n* = 5), and KO + iMSC (*n* = 4)). (Student's *t*-test). All error bars indicate ±SD.

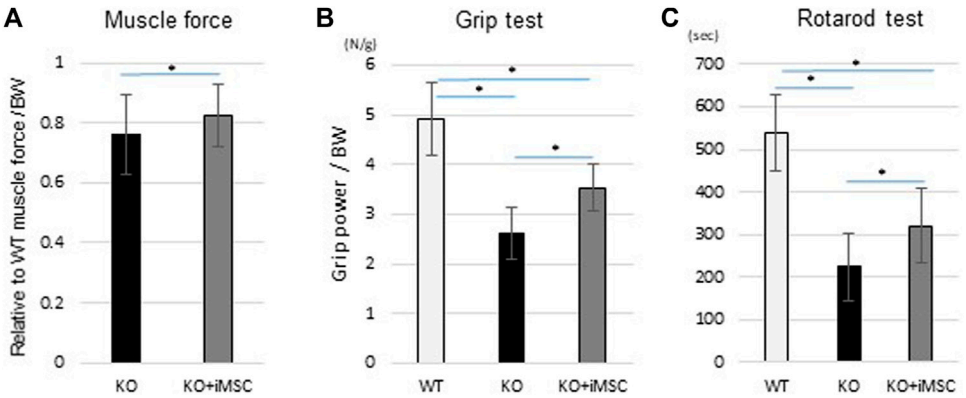

FIGURE 6 | Motor functional tests at 8 weeks. The same mice conducted three different functional tests. KO (*n* = 13) and KO + iMSC (*n* = 14). **(A)** Maximum isometric contraction was measured from both sides of the gastrocnemius under anesthesia. Values are relative to WT mice (*n* = 4) and normalized by body weight. (Student's *t*-test). **(B)** Grip strength with the four limbs was measured three times in each mouse. The average value was used to evaluate improvement in the transplanted mice. (Tukey's test). **(C)** The rotarod test showed tolerance at higher speeds in transplanted mice compared to non-transplanted mice. (Tukey's test). All error bars indicate ±SD.

not the case in non-transplanted mice. The number of abnormal mitochondria was reduced in the quadriceps (**Figure 5C**). Abnormal mitochondria were observed in the diaphragm of both non-transplanted and transplanted mice (**Figure 5D**), but they were fewer in the transplanted group (**Figure 5E**).

Apoptotic nuclei were counted in the TA muscles and diaphragm (**Figures 5F,H**). The number of apoptotic cells tended to be reduced in the TA muscles of transplanted mice (**Figure 5G**), and less apoptosis was identified in the diaphragm of the same group (**Figure 5I**). MYH3+ myofibers were simultaneously stained to evaluate the correlation between apoptosis and regenerating myofibers. Some TUNEL positive nuclei were observed in the MYH3+ myofibers in the TA muscles of both non-transplanted and transplanted mice at 4 weeks (**Figure 5F**), possibly reflecting the specific pathology of UCMD muscles, in which new myofibers during regeneration fail to grow and mature, undergoing apoptosis instead (Paco et al., 2012). On the contrary, TUNEL + MYH3+ myofibers were not detected in the transplanted mice at 8 weeks (data not shown) or at 4 weeks in the diaphragm (**Figure 5H**). Single-stranded DNA-positive nuclei were examined as an alternative marker for apoptosis. A similar distribution of single-stranded DNA positive nuclei was confirmed in the quadriceps and diaphragm of both non-transplanted and transplanted mice (**Supplementary Figure S10**).

These results confirmed abnormal mitochondria and apoptosis in *Col6a1*^{KO}/NSG mice at 4 and 8 weeks and that iMSC transplantation reduced the number of dysmorphic mitochondria and apoptotic cells.

iMSC-Transplanted Mice Were Functionally Improved at 8 weeks

According to a previous report, 14-week-old *Col6a1*^{KO} mice showed functional impairment in grip power, voluntary running, and muscle force (Noguchi et al., 2017). We compared the difference in motor functions in 8-week-old mice to evaluate if the transplantation therapy was functionally beneficial. Care was taken to minimize any environmental factors that might affect the results of the function tests (see Methods). Muscle force was measured with isometric contraction by both sides of the gastrocnemius muscle and was increased with iMSC transplantation (**Figure 6A**). Grip power was improved by 35% with the iMSC transplantation (**Figure 6B**). The average running time in the rotarod test was increased in the transplanted mice compared to the non-transplanted mice (**Figure 6C**). The percentage of mice that completed a 5-min run was 2.6% (1/30) in the non-transplanted group and 9.5% (4/42) in the transplanted group.

DISCUSSION

This study examined the therapeutic effects of systemic iMSC transplantation in UCMD model mice. We demonstrated that

iMSCs act as a vector of collagen VI to skeletal muscles. The rescued collagen VI contributed to the upregulation of muscle regeneration and amelioration of the characteristic pathology of muscles in *Col6a1*^{KO}/NSG mice. Adding the better performance in motor function tests, our findings are preliminary evidence that systemic iMSC transplantation could be a feasible treatment option, especially for neonates or infants with Col6-deficient myopathy.

The muscle regeneration in *Col6a1*^{KO}/NSG mice was enhanced at 4 weeks but decreased at 8 weeks, and iMSC transplantation sustained muscle regeneration. Because our intervention was from the neonatal period, careful interpretation of the results is necessary when considering the effect of the collagen VI replacement, including its effects on muscle growth. Postnatal muscle growth results primarily from individual fiber hypertrophy, and the synthesis of new myotubes from myogenic stem cells contribute only a small part (Gokhin et al., 2008). The fusion of myogenic cells regenerates myofibers once the satellite cell niche is established during the neonatal period (Chal and Pourquié, 2017). Our results suggested that the supplementation of collagen VI promoted mainly muscle hypertrophy up to 4 weeks based on histological analysis, in which the size of the myofibers was increased by transplantation, but the number of myofibers was not. After 4 weeks, the primary effect of collagen VI was to sustain muscle regeneration. A previous study reported that collagen VI is a key component of the satellite niche and that it takes more time to regenerate injured skeletal muscle in *Col6a1*$^{-/-}$ mice than WT mice, though the experiments were performed with older mice (6 months old) (Urciuolo et al., 2013). Our experiments indicated that the collagen VI effects depends on the stage of muscle growth and development. Neonatal transplantation can mimic the physiological condition by supplying collagen VI from the early period of life, which our findings suggest has a positive impact on muscle development. Eventually, the hypertrophy during muscle growth and maintained regeneration led to muscle weight gain and better motor function at 8 weeks. These observations suggest that there is a critical time point for collagen VI supplementation to induce its maximum effects on muscle regeneration.

Notably, we found that the restoration of collagen VI rescued the removal of aberrant mitochondria and possibly suppressed apoptotic events in the transplanted mice. Furthermore, apoptotic cells were rarely observed in the muscle of transplanted mice at 8 weeks. These results are consistent with several previous reports that showed defective mitochondria and ensuing apoptosis in *Col6a1*-null muscles and that pharmacological interventions such as cyclosporine A or other cyclophilin inhibitors, which inhibit the mitochondrial permeability transition pore (PTP), normalized both pathologies, although the mechanism is still not understood (Irwin et al., 2003; Angelin et al., 2007; Merlini et al., 2008; Hicks et al., 2009).

We estimated that the amount of collagen VI rescued by iMSC transplantation was less than 3% total collagen VI in WT/NSG mice. Despite this low level, some pathologies were improved, including mitochondrial morphology, the suppression of cellular apoptosis, and muscle regeneration. We, therefore, speculated that collagen VI might act as a signal transmitter in skeletal muscles in addition to acting as an extracellular matrix. This assumption could explain why low levels of collagen VI could ameliorate the cellular phenotypes. Recently, collagen V has been elucidated as a signal transmitter via the calcitonin receptor in muscle satellite cells (Baghdadi et al., 2018). Although previous studies have shown that integrin β1 and the membrane-spanning proteoglycan NG2 (neuron/glia antigen 2) are receptors for collagen VI (Doane et al., 1998; Tillet et al., 2002; Cattaruzza et al., 2013), it is still unknown whether these molecules are involved in the homeostasis of satellite cells or myofibers.

Notably, the systemic injection used in this study did not cause invasive damage to the muscles. Two previous studies (Alexeev et al., 2014; Takenaka-Ninagawa et al., 2021) that injected adipose-derived MSCs or iMSCs into TA muscles found the muscle may be damaged by the injection, which in turn may affect the regeneration. Furthermore, those studies injected the cells in adult mice, while our injections were done in neonatal mice. The timing of the injections was also different.

Additionally, we performed two transplantations, one at the neonatal stage and the other at 4 weeks, since neither transplantation alone was sufficient for therapeutic effects. Mice who had only the neonatal transplantation did not show a gain in muscle weight at 8 weeks, nor did they show functional improvements. When only one transplantation was performed at 4 weeks, the impact on muscle regeneration was not significant, and there were no changes in the number of MYH3+ myofibers in the quadriceps (data not shown). These results indicate the effectiveness of the boost transplantation and importance of neonatal intervention for the therapeutic effects in our model.

iMSCs are not the only candidate for systemic cell therapy to treat UCMD or other COL6-related myopathies; primary MSCs from other tissues are theoretically applicable, since they too secrete collagen VI. The definitive advantage of using iMSCs, however, is the large number of cells with homogeneous quality that can be prepared for the transplantation. iMSCs have a stable proliferative capacity up to at least 6 passages (Chijimatsu et al., 20172017). Although the risk of oncogenesis remains when using iPSC-derived cells, tumorigenesis was not observed up to 20 weeks in our experiments or 24 weeks when iMSCs were injected intramuscularly (Takenaka-Ninagawa et al., 2021). Our results also indicated that a small number of iMSCs persistently remained in both muscles and non-muscle tissues for longer periods, suggesting longer observation times are required to assess safety. Furthermore, ongoing research around iPSC technology may allow us to apply immunologically favorable cells that are less susceptible to HLA sensitization, such as HLA-homozygous iPSC line stocks (Gourraud et al., 2012; Karagiannis et al., 2019) or the generation of HLA-C-retained/HLA-class II knockout iPSCs (Xu et al., 2019). Considering that repetitive transplantations will be necessary in the clinical setting, it is crucial to have a cell source from the same donor with immunological properties identical to the patient.

The limitation of the study includes the i. p. transplantation, which is not a realistic route for cell transplantation in humans. I.

v. was more efficient than i. p transplantation in terms of delivering the donor cells to the skeletal muscles; therefore, similar or better therapeutic effects can be expected with i. v. transplantation. The current study, however, is a proof of concept that iMSC transplantation can systemically produce small amounts of collagen VI to ameliorate the pathophysiology of *Col6a1*^{KO}/NSG mice. Further confirmation with larger animals will be necessary before clinical application in patients with COL6-related myopathies.

In a broader prospective, the present study demonstrated that iMSCs can supply deficient molecules to target organs, warranting the concept of stem cell therapies for some inherited disorders. The efficacy of stem cell therapies for supplying deficient molecules has been already reported in other congenital diseases such as osteogenesis imperfecta (Guillot et al., 2008; Götherström et al., 2014).

CONCLUSION

We demonstrated the definite therapeutic effects of neonatal iMSC transplantation for immunodeficient UCMD model mice. Because iMSCs were able to migrate to the major organs, the supplementation of collagen VI was realized in skeletal muscles systemically. Accordingly, the histological and functional phenotypes specific to UCMD were ameliorated until at least 8 weeks after the transplantation in mice.

DATA AVAILABILITY STATEMENT

The raw data supporting the conclusion of this article will be made available by the authors, without undue reservation.

ETHICS STATEMENT

The animal study was reviewed and approved by The CiRA animal experiment committee.

AUTHOR CONTRIBUTIONS

AH and HS designed the research. AH conducted the experiments, acquired and analyzed the data, and wrote the manuscript. MG independently conducted the functional tests. AK contributed to the data acquisition, and NT-N helped produce the Col6a1KO/NSG strain. AT performed IVF to maintain the Col6a1KO/NSG strain. SN provided the Col6a1KO mice, and MI differentiated and prepared the iMSCs from iPSCs. HS supervised all the experiments.

FUNDING

This study was supported by Grant-in-Aid for JSPS Fellows (DC1) given to AH (Grant number 18J22274) and by the grant from The Projects for Technical Development, which is a program of the Research Center Network for Realization of Regenerative Medicine, Japan Agency for Medical Research and Development (AMED), to HS (Grant number JP21bm0404044 and JP20bm0404044).

ACKNOWLEDGMENTS

The authors are deeply grateful to Shunsuke Kihara for the confocal microscopy, Denise Zujur and Yoshiko Inada for the FACS analysis, Shuji Kawamura for the electron microscopy, and all lab members for their kind assistance. We also appreciate Peter Karagiannis for critical reading of the manuscript and Misaki Ouchida for the graphic illustration.

SUPPLEMENTARY MATERIAL

The Supplementary Material for this article can be found online at: https://www.frontiersin.org/articles/10.3389/fcell.2021.790341/full#supplementary-material

REFERENCES

Alexeev, V., Arita, M., Donahue, A., Bonaldo, P., Chu, M.-L., and Igoucheva, O. (2014). Human Adipose-Derived Stem Cell Transplantation as a Potential Therapy for Collagen VI-related Congenital Muscular Dystrophy. *Stem Cel Res. Ther.* 5, 21. doi:10.1186/scrt411

Angelin, A., Tiepolo, T., Sabatelli, P., Grumati, P., Bergamin, N., Golfieri, C., et al. (2007). Mitochondrial Dysfunction in the Pathogenesis of Ullrich Congenital Muscular Dystrophy and Prospective Therapy with Cyclosporins. *Pnas* 104, 991–996. doi:10.1073/pnas.0610270104

Baghdadi, M. B., Castel, D., Machado, L., Fukada, S.-i., Birk, D. E., Relaix, F., et al. (2018). Reciprocal Signalling by Notch-Collagen V-CALCR Retains Muscle Stem Cells in Their Niche. *Nature* 557, 714–718. doi:10.1038/s41586-018-0144-9

Bernardi, P., and Bonaldo, P. (2008). Dysfunction of Mitochondria and Sarcoplasmic Reticulum in the Pathogenesis of Collagen VI Muscular Dystrophies. *Ann. N. Y. Acad. Sci.* 1147, 303–311. doi:10.1196/annals.1427.009

Bernardi, P., and Bonaldo, P. (2013). Mitochondrial Dysfunction and Defective Autophagy in the Pathogenesis of Collagen VI Muscular Dystrophies. *Cold Spring Harbor Perspect. Biol.* 5, a011387. doi:10.1101/cshperspect.a011387

Bolduc, V., Foley, A. R., Solomon-Degefa, H., Sarathy, A., Donkervoort, S., Hu, Y., et al. (2019). A Recurrent COL6A1 Pseudoexon Insertion Causes Muscular Dystrophy and Is Effectively Targeted by Splice-Correction Therapies. *JCI insight* 4, e124403. doi:10.1172/jci.insight.124403

Bolduc, V., Zou, Y., Ko, D., and Bönnemann, C. G. (2014). siRNA-Mediated Allele-specific Silencing of a COL6A3 Mutation in a Cellular Model of Dominant Ullrich Muscular Dystrophy. *Mol. Ther. - Nucleic Acids* 3, e147. doi:10.1038/mtna.2013.74

Bonaldo, P., Braghetta, P., Zanetti, M., Piccolo, S., Volpin, D., and Bressan, G. M. (1998). Collagen VI Deficiency Induces Early Onset Myopathy in the Mouse: an Animal Model for Bethlem Myopathy. *Hum. Mol. Genet.* 7, 2135–2140. doi:10.1093/hmg/7.13.2135

Bönnemann, C. G. (2011). The Collagen VI-related Myopathies. *Handb. Clin. Neurol.* 101, 81–96. doi:10.1016/B978-0-08-045031-5.00005-0

Castagnaro, S., Pellegrini, C., Pellegrini, M., Chrisam, M., Sabatelli, P., Toni, S., et al. (2016). Autophagy Activation in COL6 Myopathic Patients by a Low-

Protein-Diet Pilot Trial. *Autophagy* 12, 2484–2495. doi:10.1080/15548627.2016.1231279

Cattaruzza, S., Nicolosi, P. A., Braghetta, P., Pazzaglia, L., Benassi, M. S., Picci, P., et al. (2013). NG2/CSPG4-collagen Type VI Interplays Putatively Involved in the Microenvironmental Control of Tumour Engraftment and Local Expansion. *J. Mol. Cel Biol.* 5, 176–193. doi:10.1093/jmcb/mjt010

Chal, J., and Pourquié, O. (2017). Making Muscle: Skeletal Myogenesis *In Vivo* and *In Vitro*. *Development* 144, 2104–2122. doi:10.1242/dev.151035

Chijimatsu, R., Ikeya, M., Yasui, Y., Ikeda, Y., Ebina, K., Moriguchi, Y., et al. (20172017). Characterization of Mesenchymal Stem Cell-like Cells Derived from Human iPSCs via Neural Crest Development and Their Application for Osteochondral Repair. *Stem Cell Int.* 2017, 1–18. doi:10.1155/2017/1960965

Doane, K. J., Howell, S. J., and Birk, D. E. (1998). Identification and Functional Characterization of Two Type VI Collagen Receptors, Alpha 3 Beta 1 Integrin and NG2, during Avian Corneal Stromal Development. *Invest. Ophthalmol. Vis. Sci.* 39, 263–275.

Fukuta, M., Nakai, Y., Kirino, K., Nakagawa, M., Sekiguchi, K., Nagata, S., et al. (2014). Derivation of Mesenchymal Stromal Cells from Pluripotent Stem Cells through a Neural Crest Lineage Using Small Molecule Compounds with Defined media. *PLoS One* 9, e112291. doi:10.1371/journal.pone.0112291

Gattazzo, F., Molon, S., Morbidoni, V., Braghetta, P., Blaauw, B., Urciuolo, A., et al. (2014). Cyclosporin A Promotes *In Vivo* Myogenic Response in Collagen VI-Deficient Myopathic Mice. *Front. Aging Neurosci.* 6, 244. doi:10.3389/fnagi.2014.00244

Gnocchi, V. F., White, R. B., Ono, Y., Ellis, J. A., and Zammit, P. S. (2009). Further Characterisation of the Molecular Signature of Quiescent and Activated Mouse Muscle Satellite Cells. *PLoS One* 4, e5205. doi:10.1371/journal.pone.0005205

Gokhin, D. S., Ward, S. R., Bremner, S. N., and Lieber, R. L. (2008). Quantitative Analysis of Neonatal Skeletal Muscle Functional Improvement in the Mouse. *J. Exp. Biol.* 211, 837–843. doi:10.1242/jeb.014340

Götherström, C., Westgren, M., Shaw, S. W. S., Åström, E., Biswas, A., Byers, P. H., et al. (2014). Pre- and Postnatal Transplantation of Fetal Mesenchymal Stem Cells in Osteogenesis Imperfecta: a Two-center Experience. *Stem Cell translational Med.* 3, 255–264. doi:10.5966/sctm.2013-0090

Gourraud, P.-A., Gilson, L., Girard, M., and Peschanski, M. (2012). The Role of Human Leukocyte Antigen Matching in the Development of Multiethnic "haplobank" of Induced Pluripotent Stem Cell Lines. *Stem Cells* 30, 180–186. doi:10.1002/stem.772

Grumati, P., Coletto, L., Sabatelli, P., Cescon, M., Angelin, A., Bertaggia, E., et al. (2010). Autophagy Is Defective in Collagen VI Muscular Dystrophies, and its Reactivation Rescues Myofiber Degeneration. *Nat. Med.* 16, 1313–1320. doi:10.1038/nm.2247

Guillot, P. V., Abass, O., Bassett, J. H. D., Shefelbine, S. J., Bou-Gharios, G., Chan, J., et al. (2008). Intrauterine Transplantation of Human Fetal Mesenchymal Stem Cells from First-Trimester Blood Repairs Bone and Reduces Fractures in Osteogenesis Imperfecta Mice. *Blood* 111, 1717–1725. doi:10.1182/blood-2007-08-105809

Hata, T., Kanenishi, K., Mori, N., AboEllail, M. A. M., Hanaoka, U., Koyano, K., et al. (2018). Prediction of Postnatal Developmental Disabilities Using the Antenatal Fetal Neurodevelopmental Test: KANET Assessment. *J. Perinat. Med.* 47, 77–81. doi:10.1515/jpm-2018-0169

Hicks, D., Lampe, A. K., Laval, S. H., Allamand, V., Jimenez-Mallebrera, C., Walter, M. C., et al. (2009). Cyclosporine A Treatment for Ullrich Congenital Muscular Dystrophy: a Cellular Study of Mitochondrial Dysfunction and its rescue. *Brain* 132, 147–155. doi:10.1093/brain/awn289

Higuchi, I., Horikiri, T., Niiyama, T., Suehara, M., Shiraishi, T., Hu, J., et al. (2003). Pathological Characteristics of Skeletal Muscle in Ullrich's Disease with Collagen VI Deficiency. *Neuromuscul. Disord.* 13, 310–316. doi:10.1016/s0960-8966(02)00282-1

Irwin, W. A., Bergamin, N., Sabatelli, P., Reggiani, C., Megighian, A., Merlini, L., et al. (2003). Mitochondrial Dysfunction and Apoptosis in Myopathic Mice with Collagen VI Deficiency. *Nat. Genet.* 35, 367–371. doi:10.1038/ng1270

Itoh, Y., Murakami, T., Mori, T., Agata, N., Kimura, N., Inoue-Miyazu, M., et al. (2017). Training at Non-damaging Intensities Facilitates Recovery from Muscle Atrophy. *Muscle Nerve* 55, 243–253. doi:10.1002/mus.25218

Jerkovic, R., Argentini, C., Serrano-Sanchez, A., Cordonnier, C., and Schiaffino, S. (1997). Early Myosin Switching Induced by Nerve Activity in Regenerating Slow Skeletal Muscle. *Cell Struct. Funct.* 22, 147–153. doi:10.1247/csf.22.147

Kalhovde, J. M., Jerkovic, R., Sefland, I., Cordonnier, C., Calabria, E., Schiaffino, S., et al. (2005). 'Fast' and 'slow' Muscle Fibres in Hindlimb Muscles of Adult Rats Regenerate from Intrinsically Different Satellite Cells. *J. Physiol.* 562, 847–857. doi:10.1113/jphysiol.2004.073684

Kanaoka, M., Yamaguchi, Y., Komitsu, N., Feghali-Bostwick, C. A., Ogawa, M., Arima, K., et al. (2018). Pro-fibrotic Phenotype of Human Skin Fibroblasts Induced by Periostin via Modulating TGF-β Signaling. *J. Dermatol. Sci.* 90, 199–208. doi:10.1016/j.jdermsci.2018.02.001

Karagiannis, P., Takahashi, K., Saito, M., Yoshida, Y., Okita, K., Watanabe, A., et al. (2019). Induced Pluripotent Stem Cells and Their Use in Human Models of Disease and Development. *Physiol. Rev.* 99, 79–114. doi:10.1152/physrev.00039.2017

Lamandé, S. R., and Bateman, J. F. (2018). Collagen VI Disorders: Insights on Form and Function in the Extracellular Matrix and beyond. *Matrix Biol.* 71-72, 348–367. doi:10.1016/j.matbio.2017.12.008

Lamandé, S. R., Bateman, J. F., Hutchison, W., Gardner, R. J. M., Bower, S. P., Byrne, E., et al. (1998). Reduced Collagen VI Causes Bethlem Myopathy: a Heterozygous COL6A1 Nonsense Mutation Results in mRNA Decay and Functional Haploinsufficiency. *Hum. Mol. Genet.* 7, 981–989. doi:10.1093/hmg/7.6.981

Lampe Ak, F. K., and Bushby, K. M. (2004). "Collagen Type VI-Related Disorders," in *GeneReviews® [Internet]*. MP Adam, HH Ardinger, RA Pagon, S. E. Wallace, L. J. H. Bean, G. Mirzaa, et al. (Seattle (WA): University of Washington, Seattle), 1993–2020. Available at: https://www.ncbi.nlm.nih.gov/books/NBK1503/.

Li, C., Gao, H. L., Shimokawa, T., Nabeka, H., Hamada, F., Araki, H., et al. (2013). Prosaposin Expression in the Regenerated Muscles of Mdx and Cardiotoxin-Treated Mice. *Histol. Histopathol.* 28, 875–892. doi:10.14670/hh-28.875

Marrosu, E., Ala, P., Muntoni, F., and Zhou, H. (2017). Gapmer Antisense Oligonucleotides Suppress the Mutant Allele of COL6A3 and Restore Functional Protein in Ullrich Muscular Dystrophy. *Mol. Ther. - Nucleic Acids* 8, 416–427. doi:10.1016/j.omtn.2017.07.006

Matsumoto, Y., Ikeya, M., Hino, K., Horigome, K., Fukuta, M., Watanabe, M., et al. (2015). New Protocol to Optimize iPS Cells for Genome Analysis of Fibrodysplasia Ossificans Progressiva. *Stem Cells* 33, 1730–1742. doi:10.1002/stem.1981

Merlini, L., Angelin, A., Tiepolo, T., Braghetta, P., Sabatelli, P., Zamparelli, A., et al. (2008). Cyclosporin A Corrects Mitochondrial Dysfunction and Muscle Apoptosis in Patients with Collagen VI Myopathies. *Pnas* 105, 5225–5229. doi:10.1073/pnas.0800962105

Merlini, L., Sabatelli, P., Armaroli, A., Gnudi, S., Angelin, A., Grumati, P., et al. (20112011). Cyclosporine A in Ullrich Congenital Muscular Dystrophy: Long-Term Results. *Oxidative Med. Cell Longevity* 2011, 1–10. doi:10.1155/2011/139194

Nadeau, A., Kinali, M., Main, M., Jimenez-Mallebrera, C., Aloysius, A., Clement, E., et al. (2009). Natural History of Ullrich Congenital Muscular Dystrophy. *Neurology* 73, 25–31. doi:10.1212/WNL.0b013e3181aae851

Noguchi, S., Ogawa, M., Kawahara, G., Malicdan, M. C., and Nishino, I. (2014). Allele-specific Gene Silencing of Mutant mRNA Restores Cellular Function in Ullrich Congenital Muscular Dystrophy Fibroblasts. *Mol. Ther. - Nucleic Acids* 3, e171. doi:10.1038/mtna.2014.22

Noguchi, S., Ogawa, M., Malicdan, M. C., Nonaka, I., and Nishino, I. (2017). Muscle Weakness and Fibrosis Due to Cell Autonomous and Non-cell Autonomous Events in Collagen VI Deficient Congenital Muscular Dystrophy. *EBioMedicine* 15, 193–202. doi:10.1016/j.ebiom.2016.12.011

Paco, S., Ferrer, I., Jou, C., Cusí, V., Corbera, J., Torner, F., et al. (2012). Muscle Fiber Atrophy and Regeneration Coexist in Collagen VI-Deficient Human Muscle: Role of Calpain-3 and Nuclear Factor-Kb Signaling. *J. Neuropathol. Exp. Neurol.* 71, 894–906. doi:10.1097/NEN.0b013e31826c6f7b

Palma, E., Tiepolo, T., Angelin, A., Sabatelli, P., Maraldi, N. M., Basso, E., et al. (2009). Genetic Ablation of Cyclophilin D Rescues Mitochondrial Defects and Prevents Muscle Apoptosis in Collagen VI Myopathic Mice. *Hum. Mol. Genet.* 18, 2024–2031. doi:10.1093/hmg/ddp126

Roman, W., and Gomes, E. R. (2018). Nuclear Positioning in Skeletal Muscle. *Semin. Cel Develop. Biol.* 82, 51–56. doi:10.1016/j.semcdb.2017.11.005

Schiaffino, S., Rossi, A. C., Smerdu, V., Leinwand, L. A., and Reggiani, C. (2015). Developmental Myosins: Expression Patterns and Functional Significance. *Skeletal muscle* 5, 22. doi:10.1186/s13395-015-0046-6

Takenaka-Ninagawa, N., Kim, J., Zhao, M., Sato, M., Jonouchi, T., Goto, M., et al. (2021). Collagen-VI Supplementation by Cell Transplantation Improves Muscle Regeneration in Ullrich Congenital Muscular Dystrophy Model Mice. *Stem Cel. Res. Ther.* 12, 446. doi:10.1186/s13287-021-02514-3

Tiepolo, T., Angelin, A., Palma, E., Sabatelli, P., Merlini, L., Nicolosi, L., et al. (2009). The Cyclophilin Inhibitor Debio 025 Normalizes Mitochondrial Function, Muscle Apoptosis and Ultrastructural Defects inCol6a1−/−myopathic Mice. *Br. J. Pharmacol.* 157, 1045–1052. doi:10.1111/j.1476-5381.2009.00316.x

Tillet, E., Gential, B., Garrone, R., and Stallcup, W. B. (2002). NG2 Proteoglycan Mediates ?1 Integrin-independent Cell Adhesion and Spreading on Collagen VI. *J. Cel. Biochem.* 86, 726–736. doi:10.1002/jcb.10268

Uezumi, A., Ito, T., Morikawa, D., Shimizu, N., Yoneda, T., Segawa, M., et al. (2011). Fibrosis and Adipogenesis Originate from a Common Mesenchymal Progenitor in Skeletal Muscle. *J. Cel Sci.* 124, 3654–3664. doi:10.1242/jcs.086629

Urciuolo, A., Quarta, M., Morbidoni, V., Gattazzo, F., Molon, S., Grumati, P., et al. (2013). Collagen VI Regulates Satellite Cell Self-Renewal and Muscle Regeneration. *Nat. Commun.* 4, 1964. doi:10.1038/ncomms2964

Weintraub, H. (1993). The MyoD Family and Myogenesis: Redundancy, Networks, and Thresholds. *Cell* 75, 1241–1244. doi:10.1016/0092-8674(93)90610-3

Xu, H., Wang, B., Ono, M., Kagita, A., Fujii, K., Sasakawa, N., et al. (2019). Targeted Disruption of HLA Genes via CRISPR-Cas9 Generates iPSCs with Enhanced Immune Compatibility. *Cell stem cell* 24, 566–578. e567. doi:10.1016/j.stem.2019.02.005

Yonekawa, T., Komaki, H., Okada, M., Hayashi, Y. K., Nonaka, I., Sugai, K., et al. (2013). Rapidly Progressive Scoliosis and Respiratory Deterioration in Ullrich Congenital Muscular Dystrophy. *J. Neurol. Neurosurg. Psychiatry* 84, 982–988. doi:10.1136/jnnp-2012-304710

Yonekawa, T., and Nishino, I. (2015). Ullrich Congenital Muscular Dystrophy: Clinicopathological Features, Natural History and Pathomechanism(s). *J. Neurol. Neurosurg. Psychiatry* 86, 280–287. doi:10.1136/jnnp-2013-307052

Yoshimoto, Y., Ikemoto-Uezumi, M., Hitachi, K., Fukada, S.-i., and Uezumi, A. (2020). Methods for Accurate Assessment of Myofiber Maturity during Skeletal Muscle Regeneration. *Front. Cel Dev. Biol.* 8, 267. doi:10.3389/fcell.2020.00267

Zou, Y., Zhang, R.-Z., Sabatelli, P., Chu, M.-L., and Bönnemann, C. G. (2008). Muscle Interstitial Fibroblasts Are the Main Source of Collagen VI Synthesis in Skeletal Muscle: Implications for Congenital Muscular Dystrophy Types Ullrich and Bethlem. *J. Neuropathol. Exp. Neurol.* 67, 144–154. doi:10.1097/nen.0b013e3181634ef7

Conflict of Interest: The authors declare that the research was conducted in the absence of any commercial or financial relationships that could be construed as a potential conflict of interest.

Publisher's Note: All claims expressed in this article are solely those of the authors and do not necessarily represent those of their affiliated organizations, or those of the publisher, the editors and the reviewers. Any product that may be evaluated in this article, or claim that may be made by its manufacturer, is not guaranteed or endorsed by the publisher.

frontiers in Cell and Developmental Biology

REVIEW
published: 03 December 2021
doi: 10.3389/fcell.2021.778020

Potential of Stem Cells and CART as a Potential Polytherapy for Small Cell Lung Cancer

Evgenii Skurikhin[1], Olga Pershina[1], Mariia Zhukova[1], Darius Widera[2], Natalia Ermakova[1], Edgar Pan[1], Angelina Pakhomova[1], Sergey Morozov[3], Aslan Kubatiev[3] and Alexander Dygai[1,3]*

[1]Laboratory of Regenerative Pharmacology, Goldberg ED Research Institute of Pharmacology and Regenerative Medicine, Tomsk National Research Medical Centre of the Russian Academy of Sciences, Tomsk, Russia, [2]Stem Cell Biology and Regenerative Medicine Group, School of Pharmacy, University of Reading, Reading, United Kingdom, [3]Institute of General Pathology and Pathophysiology, Moscow, Russia

Despite the increasing urgency of the problem of treating small cell lung cancer (SCLC), information on the causes of its development is fragmentary. There is no complete understanding of the features of antitumor immunity and the role of the microenvironment in the development of SCLC resistance. This impedes the development of new methods for the diagnosis and treatment of SCLC. Lung cancer and chronic obstructive pulmonary disease (COPD) have common pathogenetic factors. COPD is a risk factor for lung cancer including SCLC. Therefore, the search for effective approaches to prevention, diagnosis, and treatment of SCLC in patients with COPD is an urgent task. This review provides information on the etiology and pathogenesis of SCLC, analyses the effectiveness of current treatment options, and critically evaluates the potential of chimeric antigen receptor T cells therapy (CART therapy) in SCLC. Moreover, we discuss potential links between lung cancer and COPD and the role of endothelium in the development of COPD. Finally, we propose a new approach for increasing the efficacy of CART therapy in SCLC.

Keywords: small cell lung cancer, COPD, cancer stem cell, inflammation, CART therapy

OPEN ACCESS

Edited by:
Valerie Kouskoff,
The University of Manchester, United Kingdom

Reviewed by:
Claudia De Vitis,
Sapienza University, Italy
Weiren Luo,
The Second Affiliated Hospital of Southern University of Science and Technology, China

****Correspondence:***
Evgenii Skurikhin
eskurihin@inbox.ru

Specialty section:
This article was submitted to Stem Cell Research, a section of the journal Frontiers in Cell and Developmental Biology

Received: *16 September 2021*
Accepted: *18 November 2021*
Published: *03 December 2021*

Citation:
Skurikhin E, Pershina O, Zhukova M, Widera D, Ermakova N, Pan E, Pakhomova A, Morozov S, Kubatiev A and Dygai A (2021) Potential of Stem Cells and CART as a Potential Polytherapy for Small Cell Lung Cancer. Front. Cell Dev. Biol. 9:778020. doi: 10.3389/fcell.2021.778020

INTRODUCTION

SCLC accounts for 10–15% of all known cases of lung cancer and belongs to the most malignant tumors (Bray et al., 2018; Walcher et al., 2020). SCLC is characterized by its asymptomatic and rapid progression, as well as by early metastasis. The highest incidence of SCLC is recorded in the 40-60 age group. All types of small cell carcinoma have a poor prognosis even in cases when the diagnosis is made at an early stage (Bray et al., 2018; Walcher et al., 2020). In the vast majority of cases, SCLC develops in smokers, with men having a higher incidence. However, lung cancer is also a serious complication in patients with COPD and accounts for approximately 15% of deaths in patients with COPD (Sekine et al., 2012; Denholm et al., 2014).

Abbreviations: CAR, Chimeric antigen receptor; CART therapy, Chimeric antigen receptor T cells therapy; COPD, Chronic obstructive pulmonary disease; CSC, Cancer stem cells; MAB, Monoclonal antibodies; NSCLC, Non-small cell lung cancer; SCLC, Small cell lung cancer.

Standard treatment for diagnosed SCLC is chemotherapy based on platinum preparations with etoposide and radiation therapy (Wang et al., 2019). Patients whose tumor recurs more than 6 months after fist-line chemotherapy are re-treated using the same regimen. Topotecan, with a response rate of 15–20% and an overall survival rate of 1 year in 30% of cases is a second-line treatment for SCLC. The options for subsequent lines of treatment are limited. CART therapy is a promising approach to treating tumors. CART therapy uses antibodies against inhibitory signaling molecules expressed on tumor cells and immune system cells (Dotti et al., 2014). T-cells modified by chimeric antigen receptors have been shown to be effective in patients with hematological malignant neoplasms (Schubert et al., 2016). In addition, safety and applicability of CART therapy has been confirmed for solid tumors. However, there are no reported clinical trials using CART-cells for the treatment of SCLC (Dotti et al., 2014). This is largely due to the high mutational activity of the tumor. Thus, applicability of known therapeutic approaches to SCLC treatment are rather limited, highlighting the urgent need for new treatment methods.

In this review, we analyzed existing reports on diagnosis and treatment of SCLC and propose a novel potential approach to its treatment.

SMALL CELL LUNG CANCER

Epidemiology

Lung cancer is the most common cancer and the leading cause of cancer-related death in both men and women (Bray et al., 2018; Walcher et al., 2020). There are approximately 2.1 million cases of lung cancer and about 1.7 million deaths worldwide each year. Lung cancer claims more lives each year than breast, prostate, and colon cancers combined. In most cases, lung cancer originates from epithelial tissue of the bronchi of various sizes. It can be central, peripheral, or massive, that is, mixed, depending on the origin. WHO identifies two main histological types of lung cancer—non-small cell lung cancer (NSCLC) and small cell lung cancer (SCLC). NSCLC occurs in 85% of all lung cancer cases (Oser et al., 2015; Zamay et al., 2017) and includes squamous cell lung cancer, which originates in the main bronchi (25–30%), adenocarcinoma (40% of cancers) occurring in the small bronchi, and large cell carcinoma (10%) (Lemjabbar-Alaoui et al., 2015). SCLC accounts for 15% of lung cancer cases, and is characterized by an aggressive course. SCLC is believed to be derived from pulmonary neuroendocrine cells (Zamay et al., 2017; Wang et al., 2020). According to the International Association for the Study of Lung Cancer (IASLC), SCLC can be divided into two stages—limited stage and advanced stage. The majority of patients (approximately 70%) with SCLC are diagnosed with advanced stage (Wang et al., 2020). This is at least partly responsible for the poor prognosis.

The overall patients' survival rate with a limited stage of SCLC is from 15 to 20 months and for patients with an advanced stage of SCLC 8–13 months. The 5-year survival rate of patients is 10–13% and 1–2%, respectively (Horn et al., 2016).

Smoking is a major risk factor for developing SCLC. Other risk factors include exposure to asbestos and other carcinogens, such as beryllium, cadmium, silicon dioxide, chlorine compounds, other chemicals, and general air pollution. In addition, hereditary factors play a role if there is a history of lung cancer in close relatives (Wang et al., 2020). In SCLC, several mutations have been found that lead to inactivation of tumor suppressor genes. These include tumor protein 53 (TP53) (75–90%) (Wistuba et al., 2001), retinoblastoma 1(RB1) (60–90%) (Mori et al., 1990; Arriola et al., 2008), and phosphatase and tensin homolog (PTEN) (2–4%) (Kim et al., 1998). Moreover, activation mutations of the oncogenes phosphatidylinositol-4,5-bisphosphate 3-kinase (PIK3CA), epidermal growth factor receptor (EGFR), and v-Ki-ras2 Kirsten rat sarcoma viral oncogene homolog (KRAS) are often found in SCLC (Tatematsu et al., 2008; Shibata et al., 2009). In addition, a change in the expression of the MYC gene family, amplification of the EGFR/BCL2 and a deficiency of the RASSFIA/PTEN/Fhit were observed (Onuki et al., 1999).

Small Cell Lung Cancer Treatment

Until the 1970s, SCLC was not considered an independent nosological unit, and the results of treatment were assessed without taking into account the histological type of lung cancer. Classification of SCLC as a separate disease made it possible to assess the effectiveness of adriamycin-containing treatment regimens, such as CAV ((C)yclophosphamide, (A) driamycin, (V)incristine) (Tashiro et al., 1989; Walcher et al., 2020). In the early 1980s, combinations with nitrosourea derivatives began to be prescribed for patients with SCLC. A little later, etoposide was prescribed as an additional treatment option. In the 1990s, treatment regimens including taxanes and topoisomerase I inhibitors were introduced (Karim and Zekri, 2012).

Currently, there are three main approaches to the treatment of SCLC: surgery, radiation therapy, and chemotherapy. Chemotherapy is central to the treatment of SCLC. Front-line drugs are platinum preparations (cisplatin or carboplatin) in combination with etoposide. With an extensive stage of tumor progression, drugs such as doxorubicin, cyclophosphamide, vincristine, and others are prescribed (European Society for Medical Oncology, 2021; www.esmo.org; www.cancer.gov/types/lung/hp/small-cell-lung-treatment-pdq).

Although patients with SCLC initially respond well to cytotoxic therapy, tumor recurrence occurs in most patients (Giaccone et al., 1987). Patients whose tumor recurs more than 6 months after fist-line chemotherapy should be re-treated using the original treatment regimen. Additionally, topotecan has been introduced into SCLC chemotherapy (Eckardt et al., 2007). Topotecan is characterized by a high response rate (15–20%) and an overall survival rate of 30% within 1 year. Currently, it is a second-line therapy for SCLC.

Most of the clinical observations indicate a low effectiveness of subsequent lines of treatment. With second-line chemotherapy, the 5-year survival rate for patients with SCLC is below 5% (Gaspar et al., 2012; Lallo et al., 2019). In 2013, the National Cancer Institute placed SCLC in the category of resistant tumors

and identified it as a priority for research. However, the situation has not changed dramatically since this recommendation (Lallo et al., 2019; National Cancer Institute, 2021).

The rapid development of drug resistance complicates the treatment of SCLC (Byers and Rudin, 2015). It has been recognized that cells which make up the tumor microenvironment secrete enzymes, anti-inflammatory cytokines, and chemokines causing thereby changes in tumor and immune cells contributing to the escape from immunological surveillance and reduction of the immune response (Lallo et al., 2019). Such mechanisms of tumor activity should be taken into account when developing novel approaches to antitumor therapy.

In the past few years, immunotherapeutic methods have been developed that use or enhance the patient's own immune system to target tumor cells (Sharma and Allison, 2015; Topalian et al., 2015). At the same time, cancer immunotherapy has developed in parallel with the improved understanding of the role of the immune system in tumorigenesis. Among the approaches to stimulate the immune response, vaccines, immunomodulators, and monoclonal antibodies (MAB) can be applied. MABs are directed against checkpoint inhibitor on activated T-cells and/or tumor cells. Thanks to immunotherapy, many patients with advanced lung cancer are in long-term remission and have overall longer survival rates. In this context, the IMPOWER-133 trial showed longer progression-free survival and overall survival in patients treated with etoposide/carboplatin/atezolizumab (Carbone et al., 2017; Horn et al., 2018). Currently, several clinical trials focused on the efficacy and safety of "immune checkpoint inhibitors" in small cell lung cancer patients are being conducted (NCT01331525; NCT02359019; NCT02538666; NCT02481830; NCT02701400; IMPOWER-133; KEYNOTE-028; CheckMate-032) (Yang et al., 2019). However, clinical application of immune checkpoint inhibitors is still associated with limited response rates, severe immune-related adverse events, development of resistance, and more serious exacerbation of cancer progression referred to as hyper-progressive disease (Agrawal, 2019).

CHRONIC OBSTRUCTIVE PULMONARY DISEASE AS A SMALL CELL LUNG CANCER RISK FACTOR

Patients with diseases of the respiratory system (COPD, chronic bronchitis, pulmonary emphysema) have an increased risk of developing lung cancer. Annually, about 1% of patients with COPD develop lung cancer, and the prevalence of COPD in patients with lung cancer is 8–50% (Sekine et al., 2012). Thus, COPD is an independent risk factor for lung cancer (Denholm et al., 2014). Most studies so far investigated the link between COPD and NSCLC. However, there is little data on the association of COPD with the development of SCLC. This is mainly due to the lower prevalence of SCLC compared to NSCLC (Ju et al., 2018).

COPD and lung cancer are different diseases, but they share similar pathogenetic mechanisms, including epithelial-mesenchymal transition, inflammation, oxidative stress, and DNA damage. In COPD, inflammation is found in the airways and airspace and is inherently destructive (Houghton, 2013). In patients with COPD, chronic inflammation is a key feature that positively correlates with disease severity (Hogg et al., 2004) and may be a potential factor in the development of lung cancer in proximal and distant tissues (Parris et al., 2019). Cells such as neutrophils, macrophages, $CD4^+$ and $CD8^+$ lymphocytes are involved in the pathogenesis of COPD and lung cancer (Barnes et al., 2003; Paone et al., 2011; Gomes et al., 2014).

Recent reports point to different specific characteristics of immune cells in lung cancer and COPD. In patients with COPD, alveolar macrophages with the M1 phenotype have been found to polarize to the Th1 phenotype via interferon-γ. This cytotoxic Th1 phenotype is favorable for the tumor microenvironment, but does not occur in solid tumors, where immune cells are predominantly represented by the Th2 phenotype, activated by M2 macrophages (Shaykhiev et al., 2009). Changes in the composition of immune cells may be a useful biomarker in COPD patients with a precancerous condition. It has been shown that an increase in Th1-polarized $CD4^+$ T cells in the lung tissue is associated with the severity of COPD and may be useful in assessing disease progression (Barnes et al., 2003; Paone et al., 2011; Gomes et al., 2014). On the other hand, these inflammatory cells with specific characteristics act as targets and suggest the possibility of targeted therapy for COPD and, separately, precancerous condition and lung cancer.

Co-expression of PD-1, T-cell immunoglobulin, and molecule-3, containing the mucin domain (TIM-3) on $CD8^+$ T-cells, increases with the severity of COPD (Biton et al., 2018). PD-1 blockade is considered as one of the treatment approaches to both reduce the severity of COPD and reduce the likelihood of developing lung cancer. Recent studies have demonstrated an increase in progression-free survival among patients with advanced NSCLC with concomitant COPD receiving anti-PD-1 therapy (Biton et al., 2018; Chalela et al., 2018). The effectiveness of anti-PD-1 therapy among COPD patients is explained by immunological dysregulation leading to increased expression of immune checkpoints among T-cells (Chalela et al., 2018; Mark et al., 2018).

Various approaches to the treatment of lung cancer, including SCLC, have been presented above. The overwhelming majority of treatment options focus on patients with a localized tumor process (limited stage) and a widespread tumor process (advanced stage). This is largely due to the ability to diagnose lung cancer during this period of the development of the disease, including in patients with COPD. Meanwhile, precancerous conditions in patients without and with COPD are practically not covered. This is due to a very fine line of the transition from COPD to SCLC, and due to the lack of approaches to diagnose this process. During the searching for potential biomarkers of the precancerous condition, we turned our attention to such an important pathological process in COPD as systemic endothelial dysfunction (Green and Turner, 2017) with increasing apoptosis of lung endothelial cells (Peinado et al., 2006). An expected result of this is a decrease in alveolar vascularization (Wedzicha et al., 2016). Pulmonary

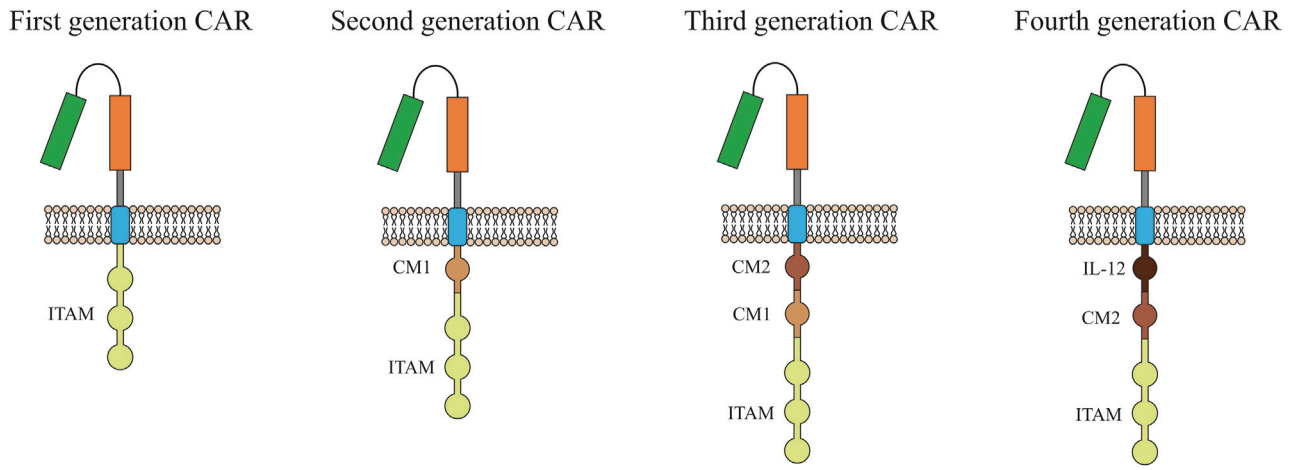

FIGURE 1 | Evolution of chimeric antigen receptor (CAR) from the first generation to the fourth generation. Single chain antibody (CD3ζ or FcεRIγ) links the ITAM at transmembrane region for the first generation. Costimulatory molecule (CM1), such as CD28, has been engineered to the signal transduction region for the second generation. Another costimulatory molecule (CM2) based on the second generation for the third generation has been engineered to the signal transduction region. The interleukin-12 (IL-12) based on the second generation for the fourth generation has been engineered to the signal transduction region. ITAM, Immunoreceptor tyrosine-based activation.

microvascular blood flow and vascular density are already reduced in mild COPD, including in areas of the lungs without overt emphysema (Hueper et al., 2015). In patients with severe COPD, destruction of the microvascular bed is increasing (Hueper et al., 2015). It is known that in patients with pulmonary emphysema, a decrease in the number of endothelial progenitor cells in the blood was noted, and this indicator was the lowest in pan lobular emphysema (Doyle et al., 2017). The results of our own research confirm these data. We propose that damage to the lung endothelium is a factor in the progression of COPD. We can already point out several parameters within the endothelium that can be used as prognostic biomarkers of complications. These include changes of the numbers of endothelial cells, endothelial progenitor cells, pericytes, and smooth muscle cells (Pakhomova et al., 2020). In this regard, angiogenesis can be beneficial for the pulmonary vasculature and alveolar epithelium in pulmonary emphysema and COPD, and thus, presumably, it is possible to prevent the negative development of events: the transition of the disease to a precancerous condition, induction of lung cancer.

T-CELLS IN CART THERAPY

One of the promising methods for eliminating tumor cells may be the use of T-cells with a chimeric antigen receptor (CAR). CARs are modular synthetic receptors with a fragment of a monoclonal antibody designed to selectively bind to specific antigens on the surface of the plasma membrane of tumor cells. The result of the interaction of CAR with a tumor antigen is the activation of T-cell antitumor response (Stern et al., 2020). First generation CARs contained only the CD3ζ, or Fc gamma signaling domains (**Figure 1**). Over time, technology for generating CART cells has improved significantly, which made it possible to add co-stimulating domains such as CD28, 4-1BB, or OX4. Second-generation CARs have been supplemented with one domain while more than two domains can be added to modern CARs (Srivastava and Riddell, 2018).

As noted above, CART cells are designed to recognize specific tumor antigens and eradicate tumor cells. A CD19-specific CART cell therapy has been shown to be effective in B-cell malignancies, including acute lymphoblastic leukemia (ALL), chronic lymphocytic leukemia (CLL), and non-Hodgkin's lymphoma (NHL) (Schubert et al., 2016). However, no definite positive results have been achieved in the treatment of solid tumors with CART cells, in particular, due to the difficulties in the selection of T-cells for the formation of CAR, the selection of a molecular and cellular target, and the recruitment of CART cells. These difficulties and limitations have yet to be overcome.

The therapeutic efficacy of CART anti-cancer therapy largely depends on the choice of T-cell subpopulations and the nature of their modification. In particular, CART cells as the final cell product must have the ability to proliferate in order to obtain a cell mass sufficient for anti-cancer therapy (Wang et al., 2018). In CART therapy, attempt shave been made to use various $CD4^+$ and $CD8^+$ T cells (Golubovskaya and Wu, 2016). It is known that $CD4^+$ T-cells mediate systemic immunity, which is important for long-term tumor elimination (Wang et al., 2018). $CD8^+$ T-cells have the potential not only to recognize, but also to destroy tumor cells (Gascón et al., 2020). Although following CAR modification, cytotoxic $CD8^+$ T-cells mediate the direct eradication of tumor cells, also $CD4^+$ T helper cells (Th cells) have been identified as highly efficient and clinically important T-cells (Stock et al., 2019). Recent studies indicate that $CD4^+$ CART cells have a cytotoxic ability comparable to cytotoxic $CD8^+$ CART cells (Stock et al., 2019), and can increase the proliferation of $CD8^+$ T cells (Yang Y. et al., 2017). Based on data inferred from T cell biology,

trials have been designed and conducted using defined mixtures of CD8 and CD4 T cells to generate CAR products that have demonstrated success in $CD19^+$ leukemias and lymphomas (Gascón et al., 2020).

Cancer immunotherapy can include the use of different subpopulations of memory T-cells and effector T-cells in CART therapy. Subpopulations of $CD4^+$ memory cells (Th1, Th2, Th9, Th17, Th22, Treg, and Tfh) and effector $CD8^+$ cells differ in many parameters including expression of extracellular (CD25, CD45RO, CD45RA, CCR-7, L-selectin or CD62L, etc.) and intracellular markers (FOXP3), epigenetic and genetic factors, and lastly metabolic pathways (catabolism and anabolism). By influencing these parameters, CART therapy can be improved (Golubovskaya and Wu, 2016). It is believed that during immunotherapy, it is important to maintain and/or create a certain ratio between $CD4^+$ Th-cells and cytotoxic $CD8^+$ T-cells. The ratio of $CD4^+$ T-cells/$CD8^+$ T-cells in the cell product can affect the effectiveness of antitumor CART therapy. To resolve this issue, the desired cell subpopulations must be isolated, and CARs need to be separately modified. As a result, it is possible to adjust the ratio of $CD4^+$ T cells/$CD8^+$ T cells in a patient specific manner (Stock et al., 2019). However, this approach complicates the production process.

The differentiation status of T-cells proposed for modification plays a certain role in achieving a positive effect during CART therapy. There is evidence that transfusion of a large number of undifferentiated CART cells has a beneficial effect on treatment (Stock et al., 2019). Undifferentiated CART cells are characterized by high proliferative activity, high viability *in vivo*, and long-term antitumor activity. The therapeutic characteristics of the cell product are influenced not only by the T-cell construct included in the CAR, but also by the culture conditions during the *ex vivo* expansion of the T cells as well. When obtaining the required cell mass of T-cells, cytokines, and pharmacological inhibitors of specific differentiation pathways are used. Currently a standardized and optimal production process for obtaining CART cells has not yet been established. Thus, defined and effective criteria for predicting the response to CART therapy are absent.

Since blood samples are easier to obtain than a lung biopsy, the study of the antigenic profile (immunophenotype) of immune cells circulating in the blood in order to predict the immune response has recently become an increasingly frequent method. Patients with a good response to checkpoint inhibitors usually have fewer T-cells in the peripheral blood compared to patients who do not respond to therapy (Gascón et al., 2020). The initial ratio of T-cell subpopulations, including the content of poorly differentiated cells, in the blood of patients is reflected in the result of CART therapy. In particular, patients with large numbers of circulating tumor cells (CTCs) may have a small number of poorly differentiated T-cells in their blood. As a result, CTCs can be the preferred target for exogenous cytokines compared to CART cells. In such a situation, the cytotoxic activity of T cells against the tumor will be significantly reduced (Gattinoni et al., 2005). Therefore, to provide additional cytokine therapy during CART therapy, it is desirable to select T-cells for CAR modification in patients with a small number of CTCs in the blood.

Generation of CAR in T-cells begins with the collection of unstimulated leukocytes from the blood using leukapheresis. Isolation of the required cell population from the total fraction of lymphocytes is carried out taking into account their functional and structural features. This is based mainly on the assessment of surface markers CD4, CD8, CD25, or CD62L (Levine, 2015). Isolation of the patient's autologous antigen-presenting cells (APCs) for subsequent activation requires additional multi-stage manipulations, which make it difficult to obtain active CART cells in the required period of time. In this regard, alternative approaches have been developed to increase the efficiency. These include the use of beads coated with MABs specific to the CD3 and CD28 antigens (Suhoski et al., 2007). During the activation process, cells are incubated with a viral vector, which is used to deliver RNA encoding a chimeric antigen receptor into T-cells, followed by reverse transcription into DNA and insertion into the patient's T-cell genome. Thereafter, CAR begins to be expressed on the surface of the patient's T-cells (Montini et al., 2009). The final stage of the protocol for the modification of T-cells *in vitro* is obtaining the required amount for administration to the patient (Gattinoni et al., 2005). Part of the cell material is cryopreserved and, if necessary, thawed to confirm its characteristics and to conduct repeated cell therapy (Levine, 2007).

The resistance of tumors to a number of therapeutic agents is well-known. Resistance is based on the functional and structural heterogeneity of the cellular composition of the tumor. It should be noted that it is possible for a tumor to acquire resistance to subsequent therapy with CART cells and to relapse. After a T-cell therapy with CD19-CAR, 70–90% of patients with B-cell malignant neoplasms developed a stable clinical remission. Subsequent clinical trials showed a loss and/or suppression of CD19 antigen expression in 70% of treated patients, which was considered causative for the occurrence of relapses after treatment (Levine, 2007; Maude et al., 2015).

An ideal situation for CART cell therapy is when the target antigen is overexpressed on all or the vast majority of tumor cells and is not expressed on the surface of healthy cells. However, the majority of tumor-associated antigens (TAA) are expressed on the cell membrane of patients with various types of cancer, including NSCLC and SCLC. Many of them are expressed at high levels and by healthy cells. Thus, CART cells might attack healthy tissue, which can lead to serious side effects (Zhong et al., 2020). Importantly, even a slight expression of tumor associated antigens on the surface of healthy cell membranes leads to damage and dysfunction of the lungs, blood system, and gastrointestinal tract and can be life-threatening (Bonifant et al., 2016). Therefore, to reduce the risk of side effects, CART cells should be as selective as possible. One of the options for increasing selectivity is an appropriate choice of the isoform of the target antigen. Expression of one antigen isoform can be observed on tumor cells, and another isoform on healthy cells. Examples for this strategy are CART therapies targeting EGFRvIII and CD44v8-10 (Morgan et al., 2012; Kim and Ryu, 2017). Improving the recognition of the target antigen

by CART cells also allows reducing cellular toxicity to healthy tissues, as well as the incidence of relapses and tumor resistance to CART therapy. These methods are based on the creation of CART cells capable of recognizing several antigens, which significantly increases the specificity and efficiency (Walcher et al., 2020).

Various independent research groups have designed CARs containing two independent domains (Grada et al., 2013; Zah et al., 2016). These CAR T cells work according to the "OR-gate" and can be activated by two antigens and the binding of either antigen induces T-cell activation. One OR-gate strategy utilizes the pooled mixture of two populations of CART cells (CAR pool), each expressing a monospecific CAR. A variation on this theme is to sequentially administer two different CART cell products. Another strategy is the co-expression of two separate CARs in each T cell (dual CAR). Yet another approach uses tandem bispecific CARs (TanCAR) that comprise two scFv domains separated by a linker on one receptor chain, and this strategy was shown to be functionally superior to both the CAR pool and dual-CAR approaches (Hegde et al., 2016; Zah et al., 2020). Under conditions of the developing resistance risk due to a decrease or termination of the expression of the target antigen of the cancer cell, this type of CAR T cell construction can be effective. In particular, CARs targeting two B-cell specific antigens: CD19 and CD22, or CD19 and CD20. These CARs are less sensitive to tumor cell resistance in absence of CD19 (Shah et al., 2019). The disadvantage of this approach is the increased likelihood of a toxic effect in relation to healthy cells and tissues, since with an increase in the number of CAR application points, the number of healthy target cells naturally increases.

Another approach to reduce the toxic effect on healthy cells is to design CAR T cells that work according to the "NOT gate." Here, a T-cell is engineered to have two specific CARs, one of which is activating and the other is inhibitory (iCAR). The principle of this method is when a T-cell expressing both CAR and iCAR meets a cell expressing only the target CAR antigen, it kills the target, but when both CAR and iCAR antigens are encountered on the same cell, negative iCAR regulatory signaling will predominate or attenuate CAR signaling and reduce the activation of T-cells. This approach is possible due to the fact that iCARs have an extracellular domain of antigen recognition, but their intracellular domains, instead of containing activating domains, carry signaling domains from immune inhibitory receptors such as (programmed cell death 1) PD-1 and cytotoxic T-lymphocyte-associated protein 4 (CTLA-4) (Fedorov et al., 2013). The disadvantage of this approach is that it is impossible to separate healthy cells from tumor cells using a single surface marker.

Another method that improves the accuracy of targeting CART cells to tumor cells is an approach to designing CART cells that work according to the "AND" gate, which requires the simultaneous activation of two receptors for the manifestation of an immune response. In this approach, activation of one receptor by a tumor antigen induces the expression of a second CAR, which triggers the destruction of tumor cells. A similar approach is implemented using the synthetic receptor Notch (synNotch) (Roybal et al., 2016b). SynNotch is a synthetic transmembrane receptor, with a cytoplasmic domain that equipped with a transcriptional regulator that is released from the membrane when the ligand interacts with the receptor. Subsequently, it enters the cell nucleus, thereby activating the transcription of target genes (Morsut et al., 2016). In this scenario, synNotch controls the expression of CAR. This CAR triggers T-cell cytotoxicity and shows significant advantages over CAR T cells that have specificity for only one antigen. In preclinical studies, a higher accuracy of the destruction of tumor cells has been shown. Importantly, healthy tissues of animals expressing only one antigen remained unaffected (Roybal et al., 2016a).

Table 1 shows clinical trials with lung cancer as indication (https://clinicaltrials.gov/) registered as of September 2021 (ClinicalTrials, 2021).

In the overwhelming majority of cases, these studies are focused on therapy of NSCLC. Notably, no clinical trials have been conducted involving CART therapy for the treatment of SCLC. Moreover, there are no clinical trials focusing on adoptive T-cell therapy at the 4 phase. We found only an alone clinical trial using CART-cells for the treatment of SCLC (Phase 1, NCT03392064). Chen et al. demonstrated that Delta-like 3-targeted (DLL3) bispecific antibody plus PD-1 inhibition was effective in controlling SCLC growth (Chen et al., 2020). However, investigators have recognized four major distinct subcategories of SCLC using unbiased RNA-sequencing: SCLC-A (it is characterized by transcription factors expressions such as high ASCL1, high DLL3, and protein Schlafen 11 expression), SCLC-P (it is characterized by transcription factors expressions such as high POU2F3 expression), SCLC-N (it is characterized by transcription factors expressions such as high expression of NEUROD1, high expression of somatostatin receptor 2), and SCLC-Y (it is characterized by YAP1 expression) (Sayed and Blais, 2021). Recent studies have also pointed to the presence of an immune-dependent subtype, referred to as SCLC-I with increased immune infiltration (higher antigen presentation + immune cell infiltration) (Rudin et al., 2019; Gay et al., 2021). These subcategories were divided into those with (SCLC-A, SCLC-N) or without (SCLC-P, SCLC-I) neuroendocrine differentiation. Distinct features and therapeutic vulnerabilities were noted in each subcategory. Therefore CART cell therapy targeting only DLL3 presumably may be effective in an only subcategory of SCLC-A.

CANCER STEM CELLS

Molecular Characterization of Cancer Stem Cells

The induction of a tumor can be caused by transformed differentiated cells or transformed somatic stem cells (Hanahan and Weinberg, 2011). Transformation of differentiated cells can occur during tissue regeneration and can be initiated and/or accelerated by infection, chronic inflammation, toxins, radiation, or metabolic disorders (Blackadar, 2016; Basu, 2018). During the transformation process, overexpression of oncogenes and inactivation of tumor suppressors are often observed (Hanahan and Weinberg, 2011). As a result, somatic cells de-differentiate and

TABLE 1 | Clinical trials targeting lung cancer (https://clinicaltrials.gov/) registered as of September 2021.

Condition or disease	Number of clinical trials
Small cell lung cancer	1,063
CART cell	581
Chimeric antigen receptor T-cells	671
CART cell lung cancer	16
CART cell immunotherapy	77
Lung cancer chimeric antigen receptor T-cells	18
CART cell immunotherapy lung cancer	4
CART cell immunotherapy CD133 solid tumors	0
CD133 solid tumors	4
CART cell immunotherapy MUC1	2
PD-L1 antibody small cell lung cancer	8
Small cell lung cancer CART cell immunotherapy	0
Small cell lung cancer CTLA-4	5
Cancer stem cells chimeric antigen receptor-modified T cells	3
Cancer stem cells small cell lung cancer	15
Cell lung cancer epidermal growth factor receptor	284
Small cell lung cancer epidermal growth factor receptor	3
CART mesothelin	19
Cell lung cancer CAR T mesothelin	4
SCLC ICI	1 (Phase 3)
SCLC immunotherapy	42 (34 studies for phase 1, 2; 4 studies for phase 3; no studies for: phase 4)
Small cell lung cancer CART	1 (Phase 1)
Small cell lung cancer CART Mesothelin	0
Cancer stem cells small cell lung cancer CART cell immunotherapy	0

acquire stem character accompanied by uncontrolled growth. Transformation of somatic stem cells or early precursors is caused by a set of genomic changes that allow uncontrolled and niche-independent proliferation (Reya et al., 2001; Li and Neaves, 2006).

In squamous cell carcinomas, the phenotype of cancer cells depends on the source cell and the type of driver mutation responsible for the invasiveness and aggressiveness of the tumor (Yamano et al., 2016; Sánchez-Danés and Blanpain, 2018). Basal stem cells located in the trachea and bronchi are capable of forming heterogeneous spheres. This allows us to consider them as precursors of squamous cell lung cancer (Fukui et al., 2013; Hardavella et al., 2016). It is believed that adenocarcinomas can originate from bronchoalveolar stem cells or pneumocytes of type I and type II (Hardavella et al., 2016). In healthy lungs, these bronchoalveolar stem cells are inactive, but they can begin to actively proliferate and become targets of various factors that cause mutation and transformation (Kim et al., 2005; Hardavella et al., 2016). At an early stage of lung morphogenesis, pulmonary neuroendocrine cells can be identified. In the adult body, after injury from tobacco smoke, oxidative stress, nitrosamines, or burn injury, pulmonary neuroendocrine cell hyperplasia is observed, leading to SCLC, which is a poorly differentiated, high-grade carcinoma (Sutherland et al., 2011; Travis, 2012; Wang et al., 2020).

The drug resistance of SCLC to therapy is associated with tumor heterogeneity. When conducting chemotherapy or radiation therapy, the composition of the tumor changes (Ayob and Ramasamy, 2018; Arnold et al., 2020). In the course of treatment, actively proliferating cancer cells become targets, leading to partial elimination of the tumor (Shibata and Hoque, 2019). At the same time, quiescent cancer stem cells (CSC) survive and may be the main factor in tumor recurrence. Thus, CSCs are potential therapeutic targets, and diagnostic and prognostic markers for SCLC. However, the full potential of these findings has not yet been exploited.

CSC expresses tissue-specific cell surface markers, but none of these markers are exclusive to CSCs. The immunophenotype of CSC may not necessarily be the same for cancer subtypes or even tumors of the same subtype (Klonisch et al., 2008; Rivera et al., 2011). To date, CD133 is the most well documented marker of lung CSC. Lung tumor cells with a high level of CD133 are resistant to chemotherapeutic drugs. Interestingly, expression of CD133 increases even further after the treatment (Sarvi et al., 2014). A high level of expression of CD133 indicates poor outcomes in patients with lung cancer (Rivera et al., 2011; Alamgeer et al., 2013; Huang et al., 2015; Liou, 2019). CD133 is found in a wide range of malignant tumors and characterizes a population of tumor initiating cells in solid breast cancer, as well as in SCLC and NSCLC (Eramo et al., 2008; Tirino et al., 2009). High expression levels of CD133 are also found on undifferentiated cells such as hematopoietic stem cells, endothelial progenitor cells, and neural stem cells (MacDonagh et al., 2017). It was discovered in $CD133^{+}$ SCLC cells, an increased expression of the mitogenic neuropeptide receptors for a gastrin-releasing peptide and arginine-vasopressin (Sarvi et al., 2014). In their study, Zhang Z. et al. found a high degree of stemness, tumorigenicity, and plasticity of NCI-H446 SCLC cells. The markers for these stem cells were CD133, Sall4, Oct4, nestin, neural cell adhesion molecule (NCAM), S100β, vimentin, CD44, and CD105. These cells formed subcutaneous xenograft tumors and orthotopic lung xenograft tumors in BALB/C-nude mice and expressed stem cell markers and the proliferation marker Ki67 (Zhang et al., 2013).

CD44 is another CSC marker and at the same time a cell adhesion molecule usually required for metastasis of $CD133^{+}$ CSC in cancer (Liou, 2019). In addition to CSCs, CD44 is expressed on endothelial and mesenchymal cells (Rivera et al., 2011). Wang P. and colleagues have created a number of lung cancer cell lines from primary tumors. One of the lines was characterized as $CD44^{high}CD90^{+}$ and this set of markers has been proposed for the identification of CSC (Asselin-Labat and Filby, 2012). The high level of expression of CD44, which was found in squamous cell carcinomas, correlated with tumors of a higher malignancy (Roudi et al., 2015). CD44v8-10, also known as CD44R1 and CD44E, is one of the isoforms of CD44v and contains variant exons 13-15 (v8-v10) (Ponta et al., 2003; Zöller, 2011). Clinical studies have shown that CD44v8-10 is

expressed on a variety of human epithelial malignant tumors, including lung tumors and CSC, and its expression correlates with metastasis (Yamaguchi et al., 1995; Yamaguchi et al., 1996; Okamoto et al., 1998; Olsson et al., 2011; Hiraga and Nakamura, 2016).

Another marker often used for the identification of CSC is aldehyde dehydrogenase (ALDH). ALDH is a superfamily of 19 human isoenzymes and is actively expressed on both healthy cells and cancer cells with stem characteristics (Jones et al., 1995; Ginestier et al., 2007; Huang et al., 2009). Overexpression of ALDH1 is usually associated with a poor prognosis in patients with SCLC (Jiang et al., 2009; Okudela et al., 2013; MacDonagh et al., 2017). Analyzing the activity of CD133 and ALDH, Akunuru S. et al. came to the conclusion that separated tumor stem cells ($CD133^{+}$ $ALDH^{high}$) can mutually transform from non-CSC ($CD133^{-}$ or $ALDH^{low}$) (Akunuru et al., 2012). This process is initiated by TGF-β. The transformation of CSC ↔ non-CSC emphasizes the dynamic plasticity of cancer cells (Hiraga and Nakamura, 2016).

In solid tumors, including lung cancer, overexpression of the plasminogen activator urokinase (uPA) and its receptor (urokinase plasminogen activator receptor, uPAR) known as CD87 has been demonstrated. CD87 is actively involved in the migration and regulation of cell adhesion. High expression of CD87 correlates with unfavorable clinical outcome and significantly shorter overall survival in SCLC (Jones et al., 1995; Ginestier et al., 2007). The population of $CD87^{+}$ cells contains a subpopulation of CSC, has the ability to form spheres and possesses an increased potential for initiating tumor growth, as well as a significant resistance to numerous traditional chemotherapeutic agents intended for the treatment of patients with SCLC (Ginestier et al., 2007; Ginestier et al., 2007; Huang et al., 2009; Jiang et al., 2009; Okudela et al., 2013; MacDonagh et al., 2017). The markers CD87 and CD133 were also identified as markers of CSC in SCLC (Jiang et al., 2009).

CD117 (KIT, c-KIT) is a type III receptor tyrosine kinase that is phosphorylated upon binding of its ligand and stem cell factor (SCF), which leads to activation of multiple signal transduction pathways that regulate a number of biological processes, such as apoptosis, differentiation, adhesion, and cell proliferation (Huang et al., 2009; Walcher et al., 2020). SCF and CD117 are overexpressed in lung cancer (Jiang et al., 2009). High expression of SCF and CD117 in lung cancer is closely associated with smoking status, lower survival rates, and chemoresistance (Kubo et al., 2013; Miettinen and Lasota, 2005; Liou, 2019).

The worst overall survival in SCLC was found if high levels of SOX2 expression were detected in CSCs (Donnenberg et al., 2012; Walcher et al., 2020). Overall, expression of the SOX2 protein is associated with aggressive tumors (Saigusa et al., 2009; Levina et al., 2010; Wilbertz et al., 2011; Perumal et al., 2014; Walcher et al., 2020). Upregulation of SOX2 enhances the proliferation of cancer cells and is important for the function of the lung CSC (Wang et al., 2009; Sholl et al., 2010).

Cripto (TDGF1, CRIPTO-1) is a small glycosylphosphatidylinisitol-secreted oncofetal protein that plays an important role in the regulation of stem cell differentiation, embryogenesis, growth and tissue remodeling (Du et al., 2011). When expressed aberrantly, Cripto can stimulate the onset and progression of various types of tumors, including lung cancer (Nakatsugawa et al., 2011). Cripto regulates signaling pathways involved in cell differentiation and development, such as Wnt and Notch (Xiang et al., 2011). Cripto has been shown to interact with a variety of signaling pathways that play a key role in the regulation of normal tissue homeostasis and tumorigenesis. Adult tissues show low levels of Cripto expression, while increased levels of Cripto *in situ* or in the bloodstream are found in many human cancers (Klauzinska et al., 2014; Xu et al., 2017). Resistance to therapy and high oncogenicity of $Cripto^{+}$ cells are associated with the role of Cripto in maintaining the phenotype of CSC and tumor cells (Du et al., 2011; Nagaoka et al., 2013).

B7-H3 (CD276) is a molecule of the B7 family (Mao et al., 2017; Zhang X. et al., 2017). The B7-H3 protein is found in several types of tumor tissues, including NSCLC and prostate cancer. The molecule is expressed by tumor cells and tumor vascular cells, found in clinical samples of human cancer metastases. B7-H3 has been characterized as a co-stimulatory molecule for T-cell activation. The non-immunological activity of B7-H3 is associated with various signaling pathways, interacting with which changes angiogenesis and tumor invasion. B7-H3 is supposed to be used as a target for cancer treatment and as a marker of the evasion of tumor cells from the action of the immune system (Mao et al., 2017; Zhang Q. et al., 2017; Yang et al., 2020).

AXL belongs to the TAM family (Tyro3, AXL, Mer). GAS6 serves as a ligand for AXL with high binding affinity. GAS6/AXL signaling is an important pathway governing the survival, proliferation, migration, and invasion of tumor cells (Zhu et al., 2019). This makes AXL a potential target for cancer treatment. In adults, AXL expression is relatively low (Vajkoczy et al., 2006), but aberrant Gas6/AXL expression has been detected in a number of human malignancies, including breast cancer, chronic lymphocytic leukemia (CLL), lung cancer, pancreatic cancer, glioblastoma, melanoma. This altered expression is associated with disease progression and reduced overall survival. AXL controls cell proliferation through effector molecules in the PI3K/AKT/mTOR, RAS/RAF/MEK/ERK, JAK/STAT, and NF-κB signaling pathways (May et al., 2015) and correlates with stem cell marker genes such as Isl1, Cdc2a, Bglap1, CD44 and ALDH1 (Asiedu et al., 2014). Expression of marker genes increases the oncogenicity of breast cancer stem cells. It is suggested that targeting AXL has great therapeutic potential and may disrupt Wnt/α-catenin and TGFâR signaling and spherical formation, thereby increasing resistance to cancer and its progression (Yen et al., 2017). Given the role of AXL in the development, progression, and drug resistance of cancer, AXL holds great promise as a predictive biomarker and therapeutic target. Several AXL inhibitors have been found to be promising after preclinical studies and are thus in various stages of clinical trials (Tibes et al., 2013; Rodon et al., 2017; Vergote et al., 2017).

TABLE 2 | Markers of lung cancer stem cells.

Marker	Localization, functions
CD133	Member of pentaspan transmembrane glycoproteins, which specifically localizes to cellular protrusions. CD133 is expressed in hematopoietic stem cells, endothelial progenitor cells, glioblastoma, neuronal and glial stem cells, various pediatric brain tumors, as well as in the adult kidney, lung, mammary glands, trachea, salivary glands, uterus, placenta, digestive tract, testes, and some other cell types. CD133 is the most commonly used marker for isolation of CSC population from different tumors, mainly from various gliomas and carcinomas (Eramo et al., 2008; Klonisch et al., 2008; Tirino et al., 2009; Rivera et al., 2011; Alamgeer et al., 2013; Sarvi et al., 2014; Huang et al., 2015; MacDonagh et al., 2017; Liou, 2019).
CD44 CD44v8–10	Cell-adhesion molecule. Expression in normal tissues is low. In addition, CD44 is expressed on endothelial and mesenchymal cells. $CD44^+$ cells showed increased self-renewal ability and increased ability to initiate tumor *in vivo* compared to $CD44^-$ cells (Yamaguchi et al., 1995; Yamaguchi et al., 1996; Okamoto et al., 1998; Ponta et al., 2003; Olsson et al., 2011; Rivera et al., 2011; Zöller, 2011; Asselin-Labat and Filby, 2012; Roudi et al., 2015; Hiraga and Nakamura, 2016; Liou, 2019).
CD87	Participates in cell migration, regulates cell adhesion. High CD87 expression correlates with poor clinical outcome and significantly shorter overall survival in SCLC. $CD87^+$ cell population demonstrated a high spherical ability, an increased tumor initiation potential, and significant resistance to traditional chemotherapeutic agents in SCLC therapy (Romer et al., 2004; Gutova et al., 2007; Almasi et al., 2013; Kubo et al., 2013; Codony-Servat et al., 2016; MacDonagh et al., 2017).
CD117	CD117 (c-KIT) is a type III receptor tyrosine kinase. c-KIT is activated (phosphorylated) by binding of its ligand with stem cell factor (SCF). This leads to activating of signal cascade which activation apoptosis, cell differentiation, proliferation, chemotaxis, and cell adhesion. Overexpression of SCF and CD117 is observed in lung cancer. High SCF expression in lung adenocarcinoma is associated with poor prognosis. Overexpression of CD117 in lung tumors is also associated with poor prognosis, lower survival, and chemoresistance (Romer et al., 2004; Miettinen and Lasota, 2005; Kubo et al., 2013; Liou, 2019; Walcher et al., 2020).
ALDH	High activity of aldehyde dehydrogenase (ALDH) has been found in stem and progenitor cells. High activity and/or overexpression of ALDH can be used as a marker of CSC in various types of cancers, including lung cancer. Overexpression of ALDH1 is associated with a poor prognosis in patients with lung cancer and more severe histological grade and stage of the disease (Jones et al., 1995; Ginestier et al., 2007; Huang et al., 2009; Jiang et al., 2009; Okudela et al., 2013; MacDonagh et al., 2017).
SOX2	There is a relationship between SOX2 expression and SCLC stage and overall survival. SOX2 expression is associated with more aggressive tumors. An increase in SOX2 activity enhances the proliferation of tumor cells. Overexpression of SOX2 is important for lung CSC function (Saigusa et al., 2009; Wang et al., 2009; Levina et al., 2010; Sholl et al., 2010; Wilbertz et al., 2011; Donnenberg et al., 2012; Perumal et al., 2014; Walcher et al., 2020).
CRIPTO-1	There is cell surface glycosylphosphatidylinositol (GPI)-linked glycoprotein which plays an important role in the regulation of stem cell differentiation, embryogenesis, growth and tissue remodeling. Aberrant Cripto expression can stimulate the development and progression of various types of tumors, including lung cancer. Cripto regulates Wnt and Notch signaling pathways. Cripto interacts with a variety of signaling pathways that play a key role in regulating normal tissue homeostasis and tumorigenesis. Cripto expression in adult tissues is low. Tumors show elevated levels of Cripto *in situ* or in the bloodstream. High resistance to chemotherapy and tumorigenicity are associated with Cripto and CSC (Du et al., 2011; Nakatsugawa et al., 2011; Xiang et al., 2011; Nagaoka et al., 2013; Klauzinska et al., 2014; Xu et al., 2017).

Localization and function of molecular markers of Cancer Stem Cells in Lung are summarized in **Table 2**.

Cancer Stem Cells as a Target for Cancer Therapy

The search and development of cancer treatment options focused on inhibiting, damaging and eliminating CSCs has been the focus of research over the past years (Almasi et al., 2013; Walcher et al., 2020). According to Shibata M. and Hoque M.O., the combination of therapy aimed at SSC and traditional non-targeted therapy can lead to a decrease in chemoresistance (Shibata and Hoque, 2019). Approaches to cancer therapy, targeting CSCs, include urokinase plasminogen activator inhibitors as well as stem cell-related pathways such as Wnt and β-catenin (Almasi et al., 2013; Shibata and Hoque, 2019; Walcher et al., 2020). So far, most of these approaches have failed as front-line treatments including immunological approaches, targeting CSC include adoptive cell transfer, targeting checkpoint inhibitors, and antibody-based approaches and vaccination.

As a result of complete and durable responses in individuals who are refractory to standard of care therapy, CAR T cells directed against the CD19 protein have been granted United States Food and Drug Administration (FDA) approval as a therapy for the treatment of pediatric and young adult acute lymphoblastic leukemia and diffuse large B cell lymphoma. Human trials of CAR T cells targeting CD19 or B cell maturation antigen in multiple myeloma have also reported early successes (Long et al., 2018; Schmidts and Maus, 2018). However, a clear and consistently reproducible demonstration of the clinical efficacy of CAR T cells in the setting of solid tumors has not yet been reported. Despite many difficulties, CART cell therapy for solid cancer can be an effective alternative to chemotherapy and radiation therapy (Long et al., 2018; Schmidts and Maus, 2018; Walcher et al., 2020). In experiments on laboratory animals, a monotherapy of solid cancer against directed to $CD133^+$ CTCs showed inhibition of tumor growth in an orthotopic mouse model of glioma (Zhu et al., 2015; Hu et al., 2019). Promising preclinical results have been obtained with combined cell therapy with cytostatic agents (Klapdor et al., 2017). A clinical trial of CD133-targeted

CART cells in patients with breast, brain, liver, pancreas, ovarian, and colorectal cancers has been completed (NCT02541370). In patients with previously treated advanced hepatocellular carcinoma, CART-133 cell therapy demonstrated promising antitumor activity and a manageable safety profile.

Several CAR-based approaches have been developed to target CD44. CAR developments in clinical trials include monoclonal antibodies and antibody conjugates. Early studies with 186 Re-conjugated antibodies against the CD44v6 splicing variant showed positive results (Colnot et al., 2002).

EGFR VIII (epidermal growth factor) is rarely expressed in healthy tissues, making this mutated tumor receptor an attractive target for therapeutic molecules. EGFR overexpression is commonly seen in patients with NSCLC. Molecules that inhibit the activity of EGFR kinase show therapeutic effects. The efficacy of second-generation EGFR-specific T-cells that include the signaling domains CD137 and CD3ζ (CD247) has been reported. The anticancer efficacy of EGFR-positive T-cells against lung carcinoma has been demonstrated *in vitro* as cytotoxicity and secretion of interferon γ (IFN-γ) and IL-2. In a phase I clinical trial, two of 11 patients with refractory NSCLC experienced a partial antitumor response after treatment with second-generation EGFR-specific CART cells (Feng et al., 2017; Yang J. et al., 2017).

Mesothelin is a tumor differentiation antigen that is normally present on the mesothelial cells lining the pleura, peritoneum, and pericardium. Since mesothelin is overexpressed in several cancers and is immunogenic, the protein could be exploited as a tumor marker, unfortunately, it is not a specific antigen for cancer (Colnot et al., 2002; Ginestier et al., 2007; Feng et al., 2017; Klapdor et al., 2017; Hu et al., 2019). However, compared with a low level of expression in normal tissues, mesothelin is overexpressed in about 30% of all cancers, including most epithelioid mesotheliomas; adenocarcinomas of the lungs, stomach, bile ducts, endometrium and pancreas; serous ovarian cancer; squamous cell carcinomas of the head and neck, esophagus, lungs, cervix, and vulva; triple negative breast cancer, desmoplastic small cell tumors and epithelial biphasic synovial sarcomas (Chang et al., 1992; Chang and Pastan, 1996; Yang et al., 2017; Hu et al., 2019; Walcher et al., 2020). Numerous preclinical studies have reported the antitumor efficacy of mesothelin and carcinoembryonic antigen-specific T-cells against antigen-positive tumors such as ovarian and liver cancer. However, there is no direct evidence of antitumor efficacy against primary tumor specimens or lung cancer cell lines. CAR meso T-cells are T-cells, which are transduced with a CAR, composed of anti-mesothelin scFv fused to TCRzeta signaling and co-stimulatory domains. ScFv SS1 is derived from a murine monoclonal antibody and is the most studied. In mice, lentiviral (DNA) CART mesocells, which are injected intratumor or intravenously into mice with pre-established tumors, caused a significant reduction in tumor size or destruction of tumors (Carpenito et al., 2009; O'Hara et al., 2016). Positive results of preclinical studies of the antitumor activity of human mesothelin-specific single-chain antibody variable fragment (P4 scFv) coupled to T cell signaling domains were obtained (Lanitis et al., 2012). Importantly, adoptive transfer of P4 CAR-expressing T cells mediated the regression of large, established tumor in the presence of soluble mesothelin in a xenogenic model of human ovarian cancer. This gives hope for the use of CART mesocells in the treatment of patients with mesothelin-expressing tumors.

FUTURE PERSPECTIVES

SCLC accounts for 10–15% of all known cases of lung cancer and is one of the most malignant and incurable tumors. All types of small cell carcinoma have a poor prognosis even when the diagnosis is made at an early stage. Clinical approaches to treating SCLC (surgery, radiation therapy, and chemotherapy) do not lead to patient recovery. High tumor mutational burden (TMB) and high neoantigens production are the main reasons for the progression of treated lung cancer. Until now, CART lymphocytes have not found their application in the treatment of SCLC. This may be due to the prescription of CART lymphocytes when the tumor mass is formed, whereas CART therapy is a more subtle treatment approach than, for example, radiation therapy and chemotherapy, and is designed to target detection and destruction of tumor cells. Thus, there is an urgent need for new approaches to treating SCLC, or revising the tactics of prescribing existing ones.

It is known that COPD increases the risk of NSCLC. There is much less data on the link between COPD and SCLC (Ju et al., 2018). Thus we focused on a group of COPD patients who develop SCLC (**Figure 2**).

In our opinion, in patients with COPD as a precancerous condition, prevention of SCLC at the stage of transformation of healthy cells into tumor cells seems to be promising. As diagnostic and prognostic markers of lung cancer are associated with COPD, it is proposed to assess the level of neutrophils, cholesterol (Mouronte-Roibás et al., 2019), and alpha1-antitrypsin in peripheral blood (Mouronte-Roibás et al., 2019; Tubío-Pérez et al., 2021). A number of studies indicated the possibility of CSCs using as a diagnostic marker of NSCLC in patients with COPD (Ilie et al., 2014; Marquette et al., 2020). There are few studies examining predictors of SCLC (Huang et al., 2018). In a pilot study, we have demonstrated the need to study different populations of CSCs in breast cancer (Pershina et al., 2021). Similarly, detecting circulating CSCs might by the key to early diagnosis of SCLC.

The first question that arises during the transition to this platform is related to the detection of CTCs (including CSC) in the blood of patients in a precancerous condition. At the stage of precancerous condition, we propose to use already known tumor markers as diagnostic markers of CSC including CD133, CD87, CD44, CD117, ALDH, Sox2, and CRYPTO-1. The need to assess the entire spectrum of antigens is justified by the high heterogeneity of the CSC phenotype in SCLC. Compliance with this requirement puts us on a path towards stratification and personalization from the beginning of the detection of CSCs in blood. Not all tumor antigens are expressed or expressed at the same level in all patients. A number of experts in the field are inclined to believe that when choosing a target marker, attention

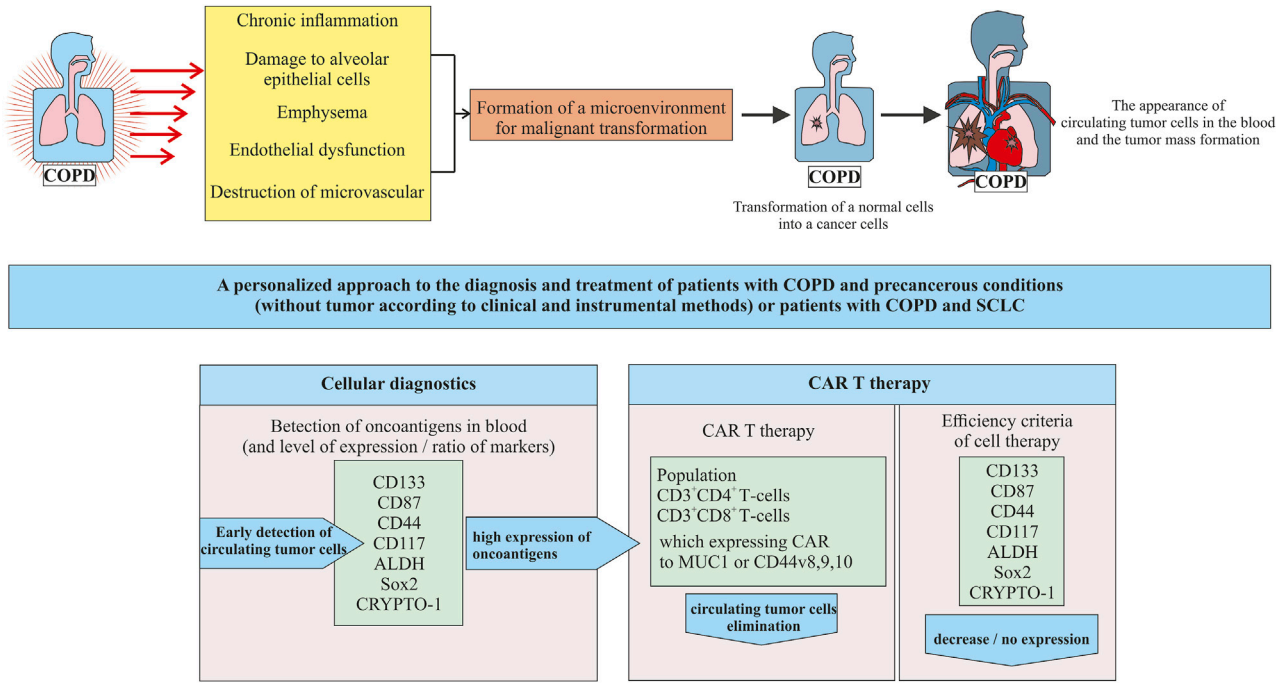

FIGURE 2 | A new approach to cell therapy for patients with COPD in precancerous conditions (tumor mass in the lungs is not yet formed) or patients with COPD and SCLC.

should be paid to antigens with a significant level of expression and to their ratio.

The appearance of one or a group of tumor markers in the blood of patients with a precancerous condition is a signal for CART therapy. To create CARs, populations of $CD3^+CD4^+$ and $CD3^+CD8^+$ blood T cells are proposed. These cells have proven themselves well as the basis for CARs aimed at other conditions. We further propose to use the expressed tumor markers identified in the patient as targets for modified T cells.

Importantly, potentially negative effects of the therapy need to be considered. To reduce the side effects risk of the CART therapy and to increase the selectivity of CART cells in relation to ROS, specific antigens such as EGFRvIII and CD44v8-10 are proposed in addition to the already identified antigens. Creation of CART cells capable of recognizing multiple antigens can significantly increase the effectiveness of CART therapy. A promising approach to the design of CART cells functioning according to the "AND" gate, which requires the simultaneous activation of two receptors for the manifestation of an immune response. With a positive outcome of CART therapy in patients with a precancerous condition, the need for chemotherapy and radiation therapy may disappear. One of the approaches to increase the effectiveness of SCLC treatment is the modulation of immune response and effect on the tumor microenvironment activity.

We propose a new approach for an increase of CART therapy efficiency in SCLC. However, our review and the proposed strategy have some limitations. To assess their applicability to a clinic, the results discussed here need further validation in pre-clinical studies and multi-center clinical studies focused on cohorts with large numbers of patients.

AUTHOR CONTRIBUTIONS

Conceptualization, ES; methodology, OP, MZ, NE, EP, and AP; formal analysis, ES, OP, MZ, NE, EP, and AP; investigation, OP, MZ, NE, EP, and AP; resources, ES; data curation, OP, NE, and AP; writing—original draft preparation, ES and OP; writing—review and editing, ES, DW, and AD; supervision, ES; project administration, ES; funding acquisition, SM, AK, and AD. All authors have read and agreed to the published version of the manuscript. All authors have read and agreed to the published version of the manuscript.

FUNDING

This research was funded by grants from the Ministry of Science and Higher Education Russian Federation, grant number 075-15-2020-773.

REFERENCES

Agrawal, B. (2019). New Therapeutic Targets for Cancer: The Interplay between Immune and Metabolic Checkpoints and Gut Microbiota. *Clin. Transl. Med.* 8, 23. doi:10.1186/s40169-019-0241-x

Akunuru, S., James Zhai, Q., and Zheng, Y. (2012). Non-Small Cell Lung Cancer Stem/Progenitor Cells are Enriched in Multiple Distinct Phenotypic Subpopulations and Exhibit Plasticity. *Cell Death Dis.* 3, e352. doi:10.1038/cddis.2012.93

Alamgeer, M., Ganju, V., Szczepny, A., Russell, P. A., Prodanovic, Z., Kumar, B., et al. (2013). The Prognostic Significance of Aldehyde Dehydrogenase 1A1 (ALDH1A1) and CD133 Expression in Early Stage Non-Small Cell Lung Cancer. *Thorax* 68, 1095–1104. doi:10.1136/thoraxjnl-2012-203021

Almasi, C. E., Drivsholm, L., Pappot, H., Høyer-Hansen, G., and Christensen, I. J. (2013). The Liberated Domain I of Urokinase Plasminogen Activator Receptor - A New Tumour Marker in Small Cell Lung Cancer. *APMIS* 121, 189–196. doi:10.1111/j.1600-0463.2012.02955.x

Arnold, C. R., Mangesius, J., Skvortsova, I.-I., and Ganswindt, U. (2020). The Role of Cancer Stem Cells in Radiation Resistance. *Front. Oncol.* 10, 164. doi:10.3389/fonc.2020.00164

Arriola, E., Cañadas, I., Arumí, M., Rojo, F., Rovira, A., and Albanell, J. (2008). Genetic Changes in Small Cell Lung Carcinoma. *Clin. Transl Oncol.* 10, 189–197. doi:10.1007/s12094-008-0181-1

Asiedu, M. K., Beauchamp-Perez, F. D., Ingle, J. N., Behrens, M. D., Radisky, D. C., and Knutson, K. L. (2014). AXL Induces Epithelial-to-Mesenchymal Transition and Regulates the Function of Breast Cancer Stem Cells. *Oncogene* 33, 1316–1324. doi:10.1038/onc.2013.57

Asselin-Labat, M.-L., and Filby, C. E. (2012). Adult Lung Stem Cells and Their Contribution to Lung Tumourigenesis. *Open Biol.* 2, 120094. doi:10.1098/rsob.120094

Ayob, A. Z., and Ramasamy, T. S. (2018). Cancer Stem Cells as Key Drivers of Tumour Progression. *J. Biomed. Sci.* 25, 20. doi:10.1186/s12929-018-0426-4

Barnes, P. J., Shapiro, S. D., and Pauwels, R. A. (2003). Chronic Obstructive Pulmonary Disease: Molecular and Cellularmechanisms. *Eur. Respir. J.* 22, 672–688. doi:10.1183/09031936.03.00040703

Basu, A. (2018). DNA Damage, Mutagenesis and Cancer. *Int. J. Mol. Sci.* 19, 970. doi:10.3390/ijms19040970

Biton, J., Ouakrim, H., Dechartres, A., Alifano, M., Mansuet-Lupo, A., Si, H., et al. (2018). Impaired Tumor-Infiltrating T Cells in Patients with Chronic Obstructive Pulmonary Disease Impact Lung Cancer Response to PD-1 Blockade. *Am. J. Respir. Crit. Care Med.* 198, 928–940. doi:10.1164/rccm.201706-1110oc

Blackadar, C. B. (2016). Historical Review of the Causes of Cancer. *World J. Clin. Oncol.* 7, 54–86. doi:10.5306/wjco.v7.i1.54

Bonifant, C. L., Jackson, H. J., Brentjens, R. J., and Curran, K. J. (2016). Toxicity and Management in CAR T-Cell Therapy. *Mol. Ther. - Oncolytics* 3, 16011. doi:10.1038/mto.2016.11

Bray, F., Ferlay, J., Soerjomataram, I., Siegel, R. L., Torre, L. A., and Jemal, A. (2018). Global Cancer Statistics 2018: GLOBOCAN Estimates of Incidence and Mortality Worldwide for 36 Cancers in 185 Countries. *CA: A Cancer J. Clin.* 68, 394–424. doi:10.3322/caac.21492

Byers, L. A., and Rudin, C. M. (2015). Small Cell Lung Cancer: Where do we go from Here? *Cancer* 121, 664–672. doi:10.1002/cncr.29098

Carbone, D. P., Reck, M., Paz-Ares, L., Creelan, B., Horn, L., Steins, M., et al. (2017). First-Line Nivolumab in Stage IV or Recurrent Non-Small-Cell Lung Cancer. *N. Engl. J. Med.* 376, 2415–2426. doi:10.1056/nejmoa1613493

Carpenito, C., Milone, M. C., Hassan, R., Simonet, J. C., Lakhal, M., Suhoski, M. M., et al. (2009). Control of Large, Established Tumor Xenografts with Genetically Retargeted Human T Cells Containing CD28 and CD137 Domains. *Proc. Natl. Acad. Sci.* 106, 3360–3365. doi:10.1073/pnas.0813101106

Chalela, R., Gea, J., and Barreiro, E. (2018). Immune Phenotypes in Lung Cancer Patients with COPD: Potential Implications for Immunotherapy. *J. Thorac. Dis.* 10, S2186–S2189. doi:10.21037/jtd.2018.06.143

Chang, K., and Pastan, I. (1996). Molecular Cloning of Mesothelin, a Differentiation Antigen Present on Mesothelium, Mesotheliomas, and Ovarian Cancers. *Proc. Natl. Acad. Sci.* 93, 136–140. doi:10.1073/pnas.93.1.136

Chang, K., Pastan, I., and Willingham, M. C. (1992). Isolation and Characterization of a Monoclonal Antibody, K1, Reactive with Ovarian Cancers and normal Mesothelium. *Int. J. Cancer* 50, 373–381. doi:10.1002/ijc.2910500308

Chen, X., Amar, N., Zhu, Y., Wang, C., Xia, C., Yang, X., et al. (2020). Combined DLL3-Targeted Bispecific Antibody with PD-1 Inhibition is Efficient to Suppress Small Cell Lung Cancer Growth. *J. Immunother. Cancer* 8 (1), e000785. doi:10.1136/jitc-2020-000785

Cheng, Y., Li, H., Liu, Y., Ma, L., Liu, X., Liu, Y., et al. (2015). Distribution and Clinical Significance of CTLA4, PD-1 and PD-L1 in Peripheral Blood of Patients with Small-Cell Lung Cancer. *J. Clin. Oncol.* 33, 7574. doi:10.1200/jco.2015.33.15_suppl.7574

ClinicalTrials (2021). ClinicalTrials.gov. Available at: https://clinicaltrials.gov/ (Accessed September 13, 2021).

Codony-Servat, J., Verlicchi, A., and Rosell, R. (2016). Cancer Stem Cells in Small Cell Lung Cancer. *Transl. Lung Cancer Res.* 5, 16–25. doi:10.3978/j.issn.2218-6751.2016.01.01

Colnot, D. R., Ossenkoppele, G. J., Roos, J. C., Quak, J. J., de Bree, R., Börjesson, P. K., et al. (2002). Reinfusion of Unprocessed, Granulocyte Colony-Stimulating Factor-Stimulated Whole Blood Allows Dose Escalation of 186Relabeled Chimeric Monoclonal Antibody U36 Radioimmunotherapy in a Phase I Dose Escalation Study. *Clin. Cancer Res.* 8, 3401–3406.

Denholm, R., Schüz, J., Straif, K., Stücker, I., Jöckel, K.-H., Brenner, D. R., et al. (2014). Is Previous Respiratory Disease a Risk Factor for Lung Cancer? *Am. J. Respir. Crit. Care Med.* 190, 549–559. doi:10.1164/rccm.201402-0338oc

Donnenberg, A. D., Zimmerlin, L., Landreneau, R. J., Luketich, J. D., and Donnenberg, V. S. (2012). KIT (CD117) Expression in a Subset of Non-Small Cell Lung Carcinoma (NSCLC) Patients. *PLoS One* 7, e52885. doi:10.1371/journal.pone.0052885

Dotti, G., Gottschalk, S., Savoldo, B., and Brenner, M. K. (2014). Design and Development of Therapies Using Chimeric Antigen Receptor-Expressing T Cells. *Immunol. Rev.* 257, 107–126. doi:10.1111/imr.12131

Doyle, M. F., Tracy, R. P., Parikh, M. A., Hoffman, E. A., Shimbo, D., Austin, J. H. M., et al. (2017). Endothelial Progenitor Cells in Chronic Obstructive Pulmonary Disease and Emphysema. *PLoS One* 12, e0173446. doi:10.1371/journal.pone.0173446

Du, L., Yang, Y., Xiao, X., Wang, C., Zhang, X., Wang, L., et al. (2011). Sox2 Nuclear Expression Is Closely Associated with Poor Prognosis in Patients with Histologically Node-Negative Oral Tongue Squamous Cell Carcinoma. *Oral Oncol.* 47, 709–713. doi:10.1016/j.oraloncology.2011.05.017

Eckardt, J. R., von Pawel, J., Pujol, J.-L., Papai, Z., Quoix, E., Ardizzoni, A., et al. (2007). Phase III Study of Oral Compared with Intravenous Topotecan as Second-Line Therapy in Small-Cell Lung Cancer. *J. Clin. Oncol.* 25, 2086–2092. doi:10.1200/jco.2006.08.3998

El Sayed, R., and Blais, N. (2021). Immunotherapy in Extensive-Stage Small Cell Lung Cancer. *Curr. Oncol.* 28 (5), 4093–4108. doi:10.3390/curroncol28050347

Eramo, A., Lotti, F., Sette, G., Pilozzi, E., Biffoni, M., Di Virgilio, A., et al. (2008). Identification and Expansion of the Tumorigenic Lung Cancer Stem Cell Population. *Cell Death Differ* 15, 504–514. doi:10.1038/sj.cdd.4402283

European Society for Medical Oncology (2021). European Society for Medical Oncology. Available at: https://www.esmo.org (Accessed September 13, 2021).

Fedorov, V. D., Themeli, M., and Sadelain, M. (2013). PD-1- and CTLA-4-Based Inhibitory Chimeric Antigen Receptors (iCARs) Divert Off-Target Immunotherapy Responses. *Sci. Transl. Med.* 5, 215ra172. doi:10.1126/scitranslmed.3006597

Feng, K.-c., Guo, Y.-l., Liu, Y., Dai, H.-r., Wang, Y., Lv, H.-y., et al. (2017). Cocktail Treatment with EGFR-specific and CD133-specific Chimeric Antigen Receptor-Modified T Cells in a Patient with Advanced Cholangiocarcinoma. *J. Hematol. Oncol.* 10, 4. doi:10.1186/s13045-016-0378-7

Fukui, T., Shaykhiev, R., Agosto-Perez, F., Mezey, J. G., Downey, R. J., Travis, W. D., et al. (2013). Lung Adenocarcinoma Subtypes Based on Expression of Human Airway Basal Cell Genes. *Eur. Respir. J.* 42, 1332–1344. doi:10.1183/09031936.00144012

Gascón, M., Isla, D., Cruellas, M., Gálvez, E. M., Lastra, R., Ocáriz, M., et al. (2020). Intratumoral Versus Circulating Lymphoid Cells as Predictive Biomarkers in Lung Cancer Patients Treated with Immune Checkpoint Inhibitors: Is the Easiest Path the Best One? *Cells* 9, 1525. doi:10.3390/cells9061525

Gaspar, L. E., McNamara, E. J., Gay, E. G., Putnam, J. B., Crawford, J., Herbst, R. S., et al. (2012). Small-Cell Lung Cancer: Prognostic Factors and Changing

Treatment over 15 Years. *Clin. Lung Cancer* 13, 115–122. doi:10.1016/j.cllc.2011.05.008

Gattinoni, L., Finkelstein, S. E., Klebanoff, C. A., Antony, P. A., Palmer, D. C., Spiess, P. J., et al. (2005). Removal of Homeostatic Cytokine Sinks by Lymphodepletion Enhances the Efficacy of Adoptively Transferred Tumor-specific CD8+ T Cells. *J. Exp. Med.* 202, 907–912. doi:10.1084/jem.20050732

Gay, C. M., Stewart, C. A., Park, E. M., Diao, L., Groves, S. M., Heeke, S., et al. (2021). Patterns of Transcription Factor Programs and Immune Pathway Activation Define Four Major Subtypes of SCLC with Distinct Therapeutic Vulnerabilities. *Cancer Cell* 39, 346–360.e7. doi:10.1016/j.ccell.2020.12.014

Giaccone, G., Ferrati, P., Donadio, M., Testore, F., and Calciati, A. (1987). Reinduction Chemotherapy in Small Cell Lung Cancer. *Eur. J. Cancer Clin. Oncol.* 23, 1697–1699. doi:10.1016/0277-5379(87)90452-4

Ginestier, C., Hur, M. H., Charafe-Jauffret, E., Monville, F., Dutcher, J., Brown, M., et al. (2007). ALDH1 is a Marker of Normal and Malignant Human Mammary Stem Cells and a Predictor of Poor Clinical Outcome. *Cell Stem Cell* 1, 555–567. doi:10.1016/j.stem.2007.08.014

Golubovskaya, V., and Wu, L. (2016). Different Subsets of T Cells, Memory, Effector Functions, and CAR-T Immunotherapy. *Cancers* 8, 36. doi:10.3390/cancers8030036

Gomes, M., Teixeira, A. L., Coelho, A., Araújo, A., and Medeiros, R. (2014). The Role of Inflammation in Lung Cancer. *Adv. Exp. Med. Biol.* 816, 1–23. doi:10.1007/978-3-0348-0837-8_1

Grada, Z., Hegde, M., Byrd, T., Shaffer, D. R., Ghazi, A., Brawley, V. S., et al. (2013). TanCAR: A Novel Bispecific Chimeric Antigen Receptor for Cancer Immunotherapy. *Mol. Ther. Nucleic Acids* 2, e105. doi:10.1038/mtna.2013.32

Green, C. E., and Turner, A. M. (2017). The Role of the Endothelium in Asthma and Chronic Obstructive Pulmonary Disease (COPD). *Respir. Res.* 18, 20. doi:10.1186/s12931-017-0505-1

Gutova, M., Najbauer, J., Gevorgyan, A., Metz, M. Z., Weng, Y., Shih, C.-C., et al. (2007). Identification of uPAR-Positive Chemoresistant Cells in Small Cell Lung Cancer. *PLoS One* 2, e243. doi:10.1371/journal.pone.0000243

Hanahan, D., and Weinberg, R. A. (2011). Hallmarks of Cancer: the Next Generation. *Cell* 144, 646–674. doi:10.1016/j.cell.2011.02.013

Hardavella, G., George, R., and Sethi, T. (2016). Lung Cancer Stem Cells-Characteristics, Phenotype. *Transl. Lung Cancer Res.* 5, 272–279. doi:10.21037/tlcr.2016.02.01

Hegde, M., Mukherjee, M., Grada, Z., Pignata, A., Landi, D., Navai, S. A., et al. (2016). Tandem CAR T Cells Targeting HER2 and IL13Rα2 Mitigate Tumor Antigen Escape. *J. Clin. Invest.* 126, 3036–3052. doi:10.1172/jci83416

Hiraga, T., and Nakamura, H. (2016). Comparable Roles of CD44v8-10 and CD44s in the Development of Bone Metastases in a Mouse Model. *Oncol. Lett.* 12, 2962–2969. doi:10.3892/ol.2016.4985

Hogg, J. C., Chu, F., Utokaparch, S., Woods, R., Elliott, W. M., Buzatu, L., et al. (2004). The Nature of Small-Airway Obstruction in Chronic Obstructive Pulmonary Disease. *N. Engl. J. Med.* 350, 2645–2653. doi:10.1056/nejmoa032158

Horn, L., Mansfield, A. S., Szczęsna, A., Havel, L., Krzakowski, M., Hochmair, M. J., et al. (2018). First-Line Atezolizumab Plus Chemotherapy in Extensive-Stage Small-Cell Lung Cancer. *N. Engl. J. Med.* 379, 2220–2229. doi:10.1056/nejmoa1809064

Horn, L., Reck, M., and Spigel, D. R. (2016). The Future of Immunotherapy in the Treatment of Small Cell Lung Cancer. *Oncologist* 21, 910–921. doi:10.1634/theoncologist.2015-0523

Houghton, A. M. (2013). Mechanistic Links between COPD and Lung Cancer. *Nat. Rev. Cancer* 13, 233–245. doi:10.1038/nrc3477

Hu, B., Zou, Y., Zhang, L., Tang, J., Niedermann, G., Firat, E., et al. (2019). Nucleofection with Plasmid DNA for CRISPR/Cas9-Mediated Inactivation of Programmed Cell Death Protein 1 in CD133-Specific CAR T Cells. *Hum. Gene Ther.* 30, 446–458. doi:10.1089/hum.2017.234

Huang, E. H., Hynes, M. J., Zhang, T., Ginestier, C., Dontu, G., Appelman, H., et al. (2009). Aldehyde Dehydrogenase 1 is a Marker for Normal and Malignant Human Colonic Stem Cells (SC) and Tracks SC Overpopulation During Colon Tumorigenesis. *Cancer Res.* 69, 3382–3389. doi:10.1158/0008-5472.can-08-4418

Huang, L.-S., Yan, H.-Y., Sun, L.-Q. -Z., Xu, Y., Cai, D.-H., Li, X.-H., et al. (2018). Choice of Serum Tumor Markers in Patients with Small Cell Lung Cancer: Progastrin-Releasing Peptide, Neuron-Specific Enolase, and Carcinoembryonic Antigen. *J. Bio-X Res.* 1, 12–17. doi:10.1097/jbr.0000000000000002

Huang, M., Zhu, H., Feng, J., Ni, S., and Huang, J. (2015). High CD133 Expression in the Nucleus and Cytoplasm Predicts Poor Prognosis in Non-small Cell Lung Cancer. *Dis. Markers.* 2015, 986095. doi:10.1155/2015/986095

Hueper, K., Vogel-Claussen, J., Parikh, M. A., Austin, J. H. M., Bluemke, D. A., Carr, J., et al. (2015). Pulmonary Microvascular Blood Flow in Mild Chronic Obstructive Pulmonary Disease and Emphysema. The MESA COPD Study. *Am. J. Respir. Crit. Care Med.* 192, 570–580. doi:10.1164/rccm.201411-2120oc

Ilie, M., Hofman, V., Long-Mira, E., Selva, E., Vignaud, J.-M., Padovani, B., et al. (2014). "Sentinel" Circulating Tumor Cells Allow Early Diagnosis of Lung Cancer in Patients with Chronic Obstructive Pulmonary Disease. *PLoS One* 9, e111597. doi:10.1371/journal.pone.0111597

Jiang, F., Qiu, Q., Khanna, A., Todd, N. W., Deepak, J., Xing, L., et al. (2009). Aldehyde Dehydrogenase 1 is a Tumor Stem Cell-Associated Marker in Lung Cancer. *Mol. Cancer Res.* 7, 330–338. doi:10.1158/1541-7786.mcr-08-0393

Jones, R., Barber, J., Vala, M., Collector, M., Kaufmann, S., Ludeman, S., et al. (1995). Assessment of Aldehyde Dehydrogenase in Viable Cells. *Blood* 85, 2742–2746. doi:10.1182/blood.v85.10.2742.bloodjournal85102742

Ju, S., Lee, H. R., Kim, J.-Y., Kim, H. C., Lee, G.-W., You, J. W., et al. (2018). Impact of Coexistent Chronic Obstructive Pulmonary Disease on the Survival of Patients with Small Cell Lung Cancer Receiving Chemotherapy. *Thorac. Cancer* 9, 1271–1278. doi:10.1111/1759-7714.12832

Karim, S. M., and Zekri, J. (2012). Chemotherapy for Small Cell Lung Cancer: A Comprehensive Review. *Oncol. Rev.* 6, e4. doi:10.4081/oncol.2012.e4

Kim, C. F. B., Jackson, E. L., Woolfenden, A. E., Lawrence, S., Babar, I., Vogel, S., et al. (2005). Identification of Bronchioalveolar Stem Cells in Normal Lung and Lung Cancer. *Cell* 121, 823–835. doi:10.1016/j.cell.2005.03.032

Kim, S. K., Su, L.-K., Oh, Y., Kemp, B. L., Hong, W. K., and Mao, L. (1998). Alterations of PTEN/MMAC1, a Candidate Tumor Suppressor Gene, and its Homologue, PTH2, in Small Cell Lung Cancer Cell Lines. *Oncogene* 16, 89–93. doi:10.1038/sj.onc.1201512

Kim, W.-T., and Ryu, C. J. (2017). Cancer Stem Cell Surface Markers on normal Stem Cells. *BMB Rep.* 50, 285–298. doi:10.5483/bmbrep.2017.50.6.039

Klapdor, R., Wang, S., Hacker, U., Büning, H., Morgan, M., Dörk, T., et al. (2017). Improved Killing of Ovarian Cancer Stem Cells by Combining a Novel Chimeric Antigen Receptor-Based Immunotherapy and Chemotherapy. *Hum. Gene Ther.* 28, 886–896. doi:10.1089/hum.2017.168

Klauzinska, M., Castro, N. P., Rangel, M. C., Spike, B. T., Gray, P. C., Bertolette, D., et al. (2014). The Multifaceted Role of the Embryonic Gene Cripto-1 in Cancer, Stem Cells and Epithelial-Mesenchymal Transition. *Semin. Cancer Biol.* 29, 51–58. doi:10.1016/j.semcancer.2014.08.003

Klonisch, T., Wiechec, E., Hombach-Klonisch, S., Ande, S. R., Wesselborg, S., Schulze-Osthoff, K., et al. (2008). Cancer Stem Cell Markers in Common Cancers - Therapeutic Implications. *Trends Mol. Med.* 14, 450–460. doi:10.1016/j.molmed.2008.08.003

Kubo, T., Takigawa, N., Osawa, M., Harada, D., Ninomiya, T., Ochi, N., et al. (2013). Subpopulation of Small-Cell Lung Cancer Cells Expressing CD133 and CD87 Show Resistance to Chemotherapy. *Cancer Sci.* 104, 78–84. doi:10.1111/cas.12045

Lallo, A., Gulati, S., Schenk, M. W., Khandelwal, G., Berglund, U. W., Pateras, I. S., et al. (2019). *Ex Vivo* culture of Cells Derived from Circulating Tumour Cell Xenograft to Support Small Cell Lung Cancer Research and Experimental Therapeutics. *Br. J. Pharmacol.* 176, 436–450. doi:10.1111/bph.14542

Lanitis, E., Poussin, M., Hagemann, I. S., Coukos, G., Sandaltzopoulos, R., Scholler, N., et al. (2012). Redirected Antitumor Activity of Primary Human Lymphocytes Transduced with a Fully Human Anti-mesothelin Chimeric Receptor. *Mol. Ther.* 20, 633–643. doi:10.1038/mt.2011.256

Lemjabbar-Alaoui, H., Hassan, O. U., Yang, Y.-W., and Buchanan, P. (2015). Lung Cancer: Biology and Treatment Options. *Biochim. Biophys. Acta Rev. Cancer* 1856, 189–210. doi:10.1016/j.bbcan.2015.08.002

Levina, V., Marrangoni, A., Wang, T., Parikh, S., Su, Y., Herberman, R., et al. (2010). Elimination of Human Lung Cancer Stem Cells through Targeting of the Stem Cell Factor-c-Kit Autocrine Signaling Loop. *Cancer Res.* 70, 338–346. doi:10.1158/0008-5472.can-09-1102

Levine, B. L. (2015). Performance-Enhancing Drugs: Design and Production of Redirected Chimeric Antigen Receptor (CAR) T Cells. *Cancer Gene Ther.* 22, 79–84. doi:10.1038/cgt.2015.5

Levine, B. (2007). Personalized Cell-Based Medicine: Activated and Expanded T Cells for Adoptive Immunotherapy. *Bioprocess J.* 6, 14–19. doi:10.12665/j62.levine

Li, L., and Neaves, W. B. (2006). Normal Stem Cells and Cancer Stem Cells: The Niche Matters. *Cancer Res.* 66, 4553–4557. doi:10.1158/0008-5472.can-05-3986

Liou, G.-Y. (2019). CD133 as a Regulator of Cancer Metastasis through the Cancer Stem Cells. *Int. J. Biochem. Cell Biol.* 106, 1–7. doi:10.1016/j.biocel.2018.10.013

Long, K. B., Young, R. M., Boesteanu, A. C., Davis, M. M., Melenhorst, J. J., Lacey, S. F., et al. (2018). CAR T Cell Therapy of Non-hematopoietic Malignancies: Detours on the Road to Clinical Success. *Front. Immunol.* 9, 2740. doi:10.3389/fimmu.2018.02740

MacDonagh, L., Gallagher, M. F., Ffrench, B., Gasch, C., Breen, E., Gray, S. G., et al. (2017). Targeting the Cancer Stem Cell Marker, Aldehyde Dehydrogenase 1, to Circumvent Cisplatin Resistance in NSCLC. *Oncotarget* 8, 72544–72563. doi:10.18632/oncotarget.19881

Mao, Y., Chen, L., Wang, F., Zhu, D., Ge, X., Hua, D., et al. (2017). Cancer Cell-Expressed B7-H3 Regulates the Differentiation of Tumor-Associated Macrophages in Human Colorectal Carcinoma. *Oncol. Lett.* 14, 6177–6183. doi:10.3892/ol.2017.6935

Mark, N. M., Kargl, J., Busch, S. E., Yang, G. H. Y., Metz, H. E., Zhang, H., et al. (2018). Chronic Obstructive Pulmonary Disease Alters Immune Cell Composition and Immune Checkpoint Inhibitor Efficacy in Non-Small Cell Lung Cancer. *Am. J. Respir. Crit. Care Med.* 197, 325–336. doi:10.1164/rccm.201704-0795oc

Marquette, C.-H., Boutros, J., Benzaquen, J., Ferreira, M., Pastre, J., Pison, C., et al. (2020). Circulating Tumour Cells as a Potential Biomarker for Lung Cancer Screening: A Prospective Cohort Study. *Lancet Respir. Med.* 8, 709–716. doi:10.1016/s2213-2600(20)30081-3

Maude, S. L., Teachey, D. T., Porter, D. L., and Grupp, S. A. (2015). CD19-Targeted Chimeric Antigen Receptor T-Cell Therapy for Acute Lymphoblastic Leukemia. *Blood* 125, 4017–4023. doi:10.1182/blood-2014-12-580068

May, C. D., Garnett, J., Ma, X., Landers, S. M., Ingram, D. R., Demicco, E. G., et al. (2015). AXL is a Potential Therapeutic Target in Dedifferentiated and Pleomorphic Liposarcomas. *BMC Cancer* 15, 901. doi:10.1186/s12885-015-1916-3

Miettinen, M., and Lasota, J. (2005). KIT (CD117): A Review on Expression in normal and Neoplastic Tissues, and Mutations and Their Clinicopathologic Correlation. *Appl. Immunohistochem. Mol. Morphol.* 13, 205–220. doi:10.1097/01.pai.0000173054.83414.22

Montini, E., Cesana, D., Schmidt, M., Sanvito, F., Bartholomae, C. C., Ranzani, M., et al. (2009). The Genotoxic Potential of Retroviral Vectors is Strongly Modulated by Vector Design and Integration Site Selection in a Mouse Model of HSC Gene Therapy. *J. Clin. Invest.* 119, 964–975. doi:10.1172/jci37630

Morgan, R. A., Johnson, L. A., Davis, J. L., Zheng, Z., Woolard, K. D., Reap, E. A., et al. (2012). Recognition of Glioma Stem Cells by Genetically Modified T Cells Targeting EGFRvIII and Development of Adoptive Cell Therapy for Glioma. *Hum. Gene Ther.* 23, 1043–1053. doi:10.1089/hum.2012.041

Mori, N., Yokota, J., Akiyama, T., Sameshima, Y., Okamoto, A., Mizoguchi, H., et al. (1990). Variable Mutations of the RB Gene in Small-Cell Lung Carcinoma. *Oncogene* 5, 1713–1717.

Morsut, L., Roybal, K. T., Xiong, X., Gordley, R. M., Coyle, S. M., Thomson, M., et al. (2016). Engineering Customized Cell Sensing and Response Behaviors Using Synthetic Notch Receptors. *Cell* 164, 780–791. doi:10.1016/j.cell.2016.01.012

Mouronte-Roibás, C., Leiro-Fernández, V., Ruano-Raviña, A., Ramos-Hernández, C., Casado-Rey, P., Botana-Rial, M., et al. (2019). Predictive Value of a Series of Inflammatory Markers in COPD for Lung Cancer Diagnosis: A Case-Control Study. *Respir. Res.* 20, 198. doi:10.1186/s12931-019-1155-2

Nagaoka, T., Karasawa, H., Turbyville, T., Rangel, M.-C., Castro, N. P., Gonzales, M., et al. (2013). Cripto-1 Enhances the Canonical Wnt/β-Catenin Signaling Pathway by Binding to LRP5 and LRP6 Co-receptors. *Cell Signal.* 25, 178–189. doi:10.1016/j.cellsig.2012.09.024

Nakatsugawa, M., Takahashi, A., Hirohashi, Y., Torigoe, T., Inoda, S., Murase, M., et al. (2011). SOX2 is Overexpressed in Stem-Like Cells of Human Lung Adenocarcinoma and Augments the Tumorigenicity. *Lab. Invest.* 91, 1796–1804. doi:10.1038/labinvest.2011.140

National Cancer Institute (2021). Small Cell Lung Cancer Treatment (PDQ®)–Health Professional Version. Available at: https://www.cancer.gov/types/lung/hp/small-cell-lung-treatment-pdq (Accessed September 13, 2021).

O'Hara, M., Stashwick, C., Haas, A. R., and Tanyi, J. L. (2016). Mesothelin as a Target for Chimeric Antigen Receptor-Modified T Cells as Anticancer Therapy. *Immunotherapy* 8, 449–460. doi:10.2217/imt.16.4

Okamoto, I., Sasaki, J.-i., Morisaki, T., Saya, H., Miyake, H., Matsumoto, M., et al. (1998). Molecular Detection of Cancer Cells by Competitive Reverse Transcription-Polymerase Chain Reaction Analysis of Specific CD44 Variant RNAs. *J. Natl. Cancer Inst.* 90, 307–315. doi:10.1093/jnci/90.4.307

Okudela, K., Woo, T., Mitsui, H., Suzuki, T., Tajiri, M., Sakuma, Y., et al. (2013). Downregulation of ALDH1A1 Expression in Non-small Cell Lung Carcinomas-its Clinicopathologic and Biological Significance. *Int. J. Clin. Exp. Pathol.* 6, 1–12.

Olsson, E., Honeth, G., Bendahl, P.-O., Saal, L. H., Gruvberger-Saal, S., Ringnér, M., et al. (2011). CD44 Isoforms are Heterogeneously Expressed in Breast Cancer and Correlate with Tumor Subtypes and Cancer Stem Cell Markers. *BMC Cancer* 11, 418. doi:10.1186/1471-2407-11-418

Onuki, N., Wistuba, I. I., Travis, W. D., Virmani, A. K., Yashima, K., Brambilla, E., et al. (1999). Genetic Changes in the Spectrum of Neuroendocrine Lung Tumors. *Cancer* 85, 600–607. doi:10.1002/(sici)1097-0142(19990201)85:3<600:aid-cncr10>3.0.co;2-w

Oser, M. G., Niederst, M. J., Sequist, L. V., and Engelman, J. A. (2015). Transformation from Non-Small-Cell Lung Cancer to Small-Cell Lung Cancer: Molecular Drivers and Cells of Origin. *Lancet Oncol.* 16, e165–e172. doi:10.1016/s1470-2045(14)71180-5

Pakhomova, A. V., Pershina, O. V., Ermakova, N. N., Krupin, V. A., Pan, E. S., Putrova, O. D., et al. (2020). Pericytes and Smooth Muscle Cells Circulating in the Blood as Markers of Impaired Angiogenesis during Combined Metabolic Impairments and Lung Emphysema. *Bull. Exp. Biol. Med.* 168, 334–340. doi:10.1007/s10517-020-04703-1

Paone, G., Conti, V., Vestri, A., Leone, A., Puglisi, G., Benassi, F., et al. (2011). Analysis of Sputum Markers in the Evaluation of Lung Inflammation and Functional Impairment in Symptomatic Smokers and COPD Patients. *Dis. Markers* 31, 91–100. doi:10.1155/2011/139493

Parris, B. A., O'Farrell, H. E., Fong, K. M., and Yang, I. A. (2019). Chronic Obstructive Pulmonary Disease (COPD) and Lung Cancer: Common Pathways for Pathogenesis. *J. Thorac. Dis.* 11, S2155–S2172. doi:10.21037/jtd.2019.10.54

Peinado, V. I., Ramírez, J., Roca, J., Rodriguez-Roisin, R., and Barberà, J. A. (2006). Identification of Vascular Progenitor Cells in Pulmonary Arteries of Patients with Chronic Obstructive Pulmonary Disease. *Am. J. Respir. Cell Mol. Biol.* 34, 257–263. doi:10.1165/rcmb.2005-0255oc

Pershina, O., Ermakova, N., Pakhomova, A., Widera, D., Pan, E., Zhukova, M., et al. (2021). Cancer Stem Cells and Somatic Stem Cells as Potential New Drug Targets, Prognosis Markers, and Therapy Efficacy Predictors in Breast Cancer Treatment. *Biomedicines* 9, 1223. doi:10.3390/biomedicines9091223

Perumal, D., Pillai, S., Nguyen, J., Schaal, C., Coppola, D., and Chellappan, S. P. (2014). Nicotinic Acetylcholine Receptors Induce c-Kit Ligand/Stem Cell Factor and Promote Stemness in an ARRB1/β-arrestin-1 Dependent Manner in NSCLC. *Oncotarget* 5, 10486–10502. doi:10.18632/oncotarget.2395

Ponta, H., Sherman, L., and Herrlich, P. A. (2003). CD44: From Adhesion Molecules to Signalling Regulators. *Nat. Rev. Mol. Cell Biol.* 4, 33–45. doi:10.1038/nrm1004

Reya, T., Morrison, S. J., Clarke, M. F., and Weissman, I. L. (2001). Stem Cells, Cancer, and Cancer Stem Cells. *Nature* 414, 105–111. doi:10.1038/35102167

Rivera, C., Rivera, S., Loriot, Y., Vozenin, M. C., and Deutsch, E. (2011). Lung Cancer Stem Cell: New Insights on Experimental Models and Preclinical Data. *J. Oncol.* 2011, 549181. doi:10.1155/2011/549181

Rodon, J., Postel-Vinay, S., Hollebecque, A., Nuciforo, P., Azaro, A., Cattan, V., et al. (2017). First-in-human Phase I Study of Oral S49076, a Unique MET/AXL/FGFR Inhibitor, in Advanced Solid Tumours. *Eur. J. Cancer* 81, 142–150. doi:10.1016/j.ejca.2017.05.007

Romer, J., Nielsen, B., and Ploug, M. (2004). The Urokinase Receptor as a Potential Target in Cancer Therapy. *Curr. Pharm. Des.* 10, 2359–2376. doi:10.2174/1381612043383962

Roudi, R., Korourian, A., Shariftabrizi, A., and Madjd, Z. (2015). Differential Expression of Cancer Stem Cell Markers ALDH1 and CD133 in Various Lung Cancer Subtypes. *Cancer Invest.* 33, 294–302. doi:10.3109/07357907.2015.1034869

Roybal, K. T., Rupp, L. J., Morsut, L., Walker, W. J., McNally, K. A., Park, J. S., et al. (2016a). Precision Tumor Recognition by T Cells With Combinatorial Antigen-Sensing Circuits. *Cell* 164, 770–779. doi:10.1016/j.cell.2016.01.011

Roybal, K. T., Williams, J. Z., Morsut, L., Rupp, L. J., Kolinko, I., Choe, J. H., et al. (2016b). Engineering T Cells with Customized Therapeutic Response Programs Using Synthetic Notch Receptors. *Cell* 167, 419–432.e16. doi:10.1016/j.cell.2016.09.011

Rudin, C. M., Poirier, J. T., Byers, L. A., Dive, C., Dowlati, A., George, J., et al. (2019). Molecular Subtypes of Small Cell Lung Cancer: A Synthesis of Human and Mouse Model Data. *Nat. Rev. Cancer* 19, 289–297. doi:10.1038/s41568-019-0133-9

Saigusa, S., Tanaka, K., Toiyama, Y., Yokoe, T., Okugawa, Y., Ioue, Y., et al. (2009). Correlation of CD133, OCT4, and SOX2 in Rectal Cancer and Their Association with Distant Recurrence after Chemoradiotherapy. *Ann. Surg. Oncol.* 16, 3488–3498. doi:10.1245/s10434-009-0617-z

Sánchez-Danés, A., and Blanpain, C. (2018). Deciphering the Cells of Origin of Squamous Cell Carcinomas. *Nat. Rev. Cancer* 18, 549–561. doi:10.1038/s41568-018-0024-5

Sarvi, S., Mackinnon, A. C., Avlonitis, N., Bradley, M., Rintoul, R. C., Rassl, D. M., et al. (2014). CD133+ Cancer Stem-Like Cells in Small Cell Lung Cancer are Highly Tumorigenic and Chemoresistant but Sensitive to a Novel Neuropeptide Antagonist. *Cancer Res.* 74, 1554–1565. doi:10.1158/0008-5472.can-13-1541

Schmidts, A., and Maus, M. V. (2018). Making CAR T Cells a Solid Option for Solid Tumors. *Front. Immunol.* 9, 2593. doi:10.3389/fimmu.2018.02593

Schubert, M.-L., Hückelhoven, A., Hoffmann, J.-M., Schmitt, A., Wuchter, P., Sellner, L., et al. (2016). Chimeric Antigen Receptor T Cell Therapy Targeting CD19-Positive Leukemia and Lymphoma in the Context of Stem Cell Transplantation. *Hum. Gene Ther.* 27, 758–771. doi:10.1089/hum.2016.097

Sekine, Y., Katsura, H., Koh, E., Hiroshima, K., and Fujisawa, T. (2012). Early Detection of COPD is Important for Lung Cancer Surveillance. *Eur. Respir. J.* 39, 1230–1240. doi:10.1183/09031936.00126011

Shah, N. N., Zhu, F., Schneider, D., Taylor, C., Krueger, W., Worden, A., et al. (2019). Results of a Phase I Study of Bispecific Anti-CD19, Anti-CD20 Chimeric Antigen Receptor (CAR) Modified T Cells for Relapsed, Refractory, Non-hodgkin Lymphoma. *J. Clin. Oncol.* 37, 2510. doi:10.1200/jco.2019.37.15_suppl.2510

Sharma, P., and Allison, J. P. (2015). The Future of Immune Checkpoint Therapy. *Science* 348, 56–61. doi:10.1126/science.aaa8172

Shaykhiev, R., Krause, A., Salit, J., Strulovici-Barel, Y., Harvey, B.-G., O'Connor, T. P., et al. (2009). Smoking-dependent Reprogramming of Alveolar Macrophage Polarization: Implication for Pathogenesis of Chronic Obstructive Pulmonary Disease. *J. Immunol.* 183, 2867–2883. doi:10.4049/jimmunol.0900473

Shibata, M., and Hoque, M. O. (2019). Targeting Cancer Stem Cells: A Strategy for Effective Eradication of Cancer. *Cancers* 11, 732. doi:10.3390/cancers11050732

Shibata, T., Kokubu, A., Tsuta, K., and Hirohashi, S. (2009). Oncogenic Mutation of PIK3CA in Small Cell Lung Carcinoma: A Potential Therapeutic Target Pathway for Chemotherapy-Resistant Lung Cancer. *Cancer Lett.* 283, 203–211. doi:10.1016/j.canlet.2009.03.038

Sholl, L. M., Barletta, J. A., Yeap, B. Y., Chirieac, L. R., and Hornick, J. L. (2010). Sox2 Protein Expression is an Independent Poor Prognostic Indicator in Stage I Lung Adenocarcinoma. *Am. J. Surg. Pathol.* 34, 1193–1198. doi:10.1097/pas.0b013e3181e5e024

Srivastava, S., and Riddell, S. R. (2018). Chimeric Antigen Receptor T Cell Therapy: Challenges to Bench-to-Bedside Efficacy. *J. Immunol.* 200, 459–468. doi:10.4049/jimmunol.1701155

Stern, L. A., Jonsson, V. D., and Priceman, S. J. (2020). CAR T Cell Therapy Progress and Challenges for Solid Tumors. *Cancer Treat. Res.* 180, 297–326. doi:10.1007/978-3-030-38862-1_11

Stock, S., Schmitt, M., and Sellner, L. (2019). Optimizing Manufacturing Protocols of Chimeric Antigen Receptor T Cells for Improved Anticancer Immunotherapy. *Int. J. Mol. Sci.* 20, 6223. doi:10.3390/ijms20246223

Suhoski, M. M., Golovina, T. N., Aqui, N. A., Tai, V. C., Varela-Rohena, A., Milone, M. C., et al. (2007). Engineering Artificial Antigen-Presenting Cells to Express a Diverse Array of Co-stimulatory Molecules. *Mol. Ther.* 15, 981–988. doi:10.1038/mt.sj.6300134

Sutherland, K. D., Proost, N., Brouns, I., Adriaensen, D., Song, J.-Y., and Berns, A. (2011). Cell of Origin of Small Cell Lung Cancer: Inactivation of Trp53 and Rb1 in Distinct Cell Types of Adult Mouse Lung. *Cancer Cell* 19, 754–764. doi:10.1016/j.ccr.2011.04.019

Tashiro, T., Inaba, M., Kobayashi, T., Sakurai, Y., Maruo, K., Ohnishi, Y., et al. (1989). Responsiveness of Human Lung Cancer/Nude Mouse to Antitumor Agents in a Model Using Clinically Equivalent Doses. *Cancer Chemother. Pharmacol.* 24, 187–192. doi:10.1007/bf00300241

Tatematsu, A., Shimizu, J., Murakami, Y., Horio, Y., Nakamura, S., Hida, T., et al. (2008). Epidermal Growth Factor Receptor Mutations in Small Cell Lung Cancer. *Clin. Cancer Res.* 14, 6092–6096. doi:10.1158/1078-0432.ccr-08-0332

Tibes, R., Fine, G., Choy, G., Redkar, S., Taverna, P., Oganesian, A., et al. (2013). A Phase I, First-In-Human Dose-Escalation Study of Amuvatinib, a Multi-Targeted Tyrosine Kinase Inhibitor, in Patients with Advanced Solid Tumors. *Cancer Chemother. Pharmacol.* 71, 463–471. doi:10.1007/s00280-012-2019-3

Tirino, V., Camerlingo, R., Franco, R., Malanga, D., La Rocca, A., Viglietto, G., et al. (2009). The Role of CD133 in the Identification and Characterisation of Tumour-Initiating Cells in Non-Small-Cell Lung Cancer. *Eur. J. Cardiothoracic Surg.* 36, 446–453. doi:10.1016/j.ejcts.2009.03.063

Topalian, S. L., Drake, C. G., and Pardoll, D. M. (2015). Immune Checkpoint Blockade: A Common Denominator Approach to Cancer Therapy. *Cancer Cell* 27, 450–461. doi:10.1016/j.ccell.2015.03.001

Travis, W. D. (2012). Update on Small Cell Carcinoma and its Differentiation from Squamous Cell Carcinoma and Other Non-small Cell Carcinomas. *Mod. Pathol.* 25, S18–S30. doi:10.1038/modpathol.2011.150

Tubío-Pérez, R. A., Torres-Durán, M., Fernández-Villar, A., and Ruano-Raviña, A. (2021). Alpha-1 Antitrypsin Deficiency and Risk of Lung Cancer: A Systematic Review. *Transl. Oncol.* 14, 100914. doi:10.1016/j.tranon.2020.100914

Vajkoczy, P., Knyazev, P., Kunkel, A., Capelle, H.-H., Behrndt, S., von Tengg-Kobligk, H., et al. (2006). Dominant-Negative Inhibition of the Axl Receptor Tyrosine Kinase Suppresses Brain Tumor Cell Growth and Invasion and Prolongs Survival. *Proc. Natl. Acad. Sci.* 103, 5799–5804. doi:10.1073/pnas.0510923103

Vergote, I. B., Smith, D. C., Berger, R., Kurzrock, R., Vogelzang, N. J., Sella, A., et al. (2017). A Phase 2 Randomised Discontinuation Trial of Cabozantinib in Patients with Ovarian Carcinoma. *Eur. J. Cancer* 83, 229–236. doi:10.1016/j.ejca.2017.06.018

Walcher, L., Kistenmacher, A.-K., Suo, H., Kitte, R., Dluczek, S., Strauß, A., et al. (2020). Cancer Stem Cells-Origins and Biomarkers: Perspectives for Targeted Personalized Therapies. *Front. Immunol.* 11, 1280. doi:10.3389/fimmu.2020.01280

Wang, D., Aguilar, B., Starr, R., Alizadeh, D., Brito, A., Sarkissian, A., et al. (2018). Glioblastoma-Targeted CD4+ CAR T Cells Mediate superior Antitumor Activity. *JCI Insight* 3, e99048. doi:10.1172/jci.insight.99048

Wang, Q., He, W., Lu, C., Wang, Z., Wang, J., Giercksky, K. E., et al. (2009). Oct3/4 and Sox2 are Significantly Associated with an Unfavorable Clinical Outcome in Human Esophageal Squamous Cell Carcinoma. *Anticancer Res.* 29, 1233–1241.

Wang, S., Zimmermann, S., Parikh, K., Mansfield, A. S., and Adjei, A. A. (2019). Current Diagnosis and Management of Small-Cell Lung Cancer. *Mayo Clinic Proc.* 94, 1599–1622. doi:10.1016/j.mayocp.2019.01.034

Wang, Y., Zou, S., Zhao, Z., Liu, P., Ke, C., and Xu, S. (2020). New Insights into Small-Cell Lung Cancer Development and Therapy. *Cell Biol. Int.* 44, 1564–1576. doi:10.1002/cbin.11359

Wedzicha, J., Calverley, P., and Rabe, K. (2016). Roflumilast: A Review of its Use in the Treatment of COPD. *Int. J. Chron. Obstruct. Pulmon. Dis.* 11, 81–90. doi:10.2147/copd.s89849

Wilbertz, T., Wagner, P., Petersen, K., Stiedl, A.-C., Scheble, V. J., Maier, S., et al. (2011). SOX2 Gene Amplification and Protein Overexpression are Associated with Better Outcome in Squamous Cell Lung Cancer. *Mod. Pathol.* 24, 944–953. doi:10.1038/modpathol.2011.49

Wistuba, I. I., Gazdar, A. F., and Minna, J. D. (2001). Molecular Genetics of Small Cell Lung Carcinoma. *Semin. Oncol.* 28, 3–13. doi:10.1053/sonc.2001.25738

Xiang, R., Liao, D., Cheng, T., Zhou, H., Shi, Q., Chuang, T. S., et al. (2011). Downregulation of Transcription Factor SOX2 in Cancer Stem Cells Suppresses Growth and Metastasis of Lung Cancer. *Br. J. Cancer* 104, 1410–1417. doi:10.1038/bjc.2011.94

Xu, C. H., Wang, Y., Qian, L. H., Yu, L. K., Zhang, X. W., and Wang, Q. B. (2017). Serum Cripto-1 is a Novel Biomarker for Non-Small Cell Lung Cancer Diagnosis and Prognosis. *Clin. Respir. J.* 11, 765–771. doi:10.1111/crj.12414

Yamaguchi, A., Saito, M., Goi, T., Iida, A., Takeuchi, K., Hirose, K., et al. (1995). Expression of CD44 Variant Exons 8-10 in Gastric Cancer. *Jpn. J. Cancer Res.* 86, 1166–1171. doi:10.1111/j.1349-7006.1995.tb03310.x

Yamaguchi, A., Urano, T., Goi, T., Saito, M., Takeuchi, K., Hirose, K., et al. (1996). Expression of a CD44 Variant Containing Exons 8 to 10 is a Useful Independent

Factor for the Prediction of Prognosis in Colorectal Cancer Patients. *J. Clin. Oncol.* 14, 1122–1127. doi:10.1200/jco.1996.14.4.1122

Yamano, S., Gi, M., Tago, Y., Doi, K., Okada, S., Hirayama, Y., et al. (2016). Role of deltaNp63 Pos CD 44v Pos Cells in the Development of N-nitroso-tris-chloroethylurea-induced Peripheral-type Mouse Lung Squamous Cell Carcinomas. *Cancer Sci.* 107, 123–132. doi:10.1111/cas.12855

Yang, J. C., Ahn, M. J., Kim, D. W., Ramalingam, S. S., Sequist, L. V., Su, W. C., et al. (2017). Osimertinib in Pretreated T790M-Positive Advanced Non-Small-Cell Lung Cancer: AURA Study Phase II Extension Component. *Am. J. Clin. Oncol.* 35 (12), 1288–1296. doi:10.1200/JCO.2016.70.3223

Yang, S., Wei, W., and Zhao, Q. (2020). B7-H3, a Checkpoint Molecule, as a Target for Cancer Immunotherapy. *Int. J. Biol. Sci.* 16, 1767–1773. doi:10.7150/ijbs.41105

Yang, S., Zhang, Z., and Wang, Q. (2019). Emerging Therapies for Small Cell Lung Cancer. *J. Hematol. Oncol.* 12, 47. doi:10.1186/s13045-019-0736-3

Yang, Y., Kohler, M. E., Chien, C. D., Sauter, C. T., Jacoby, E., Yan, C., et al. (2017). TCR Engagement Negatively Affects CD8 but not CD4 CAR T Cell Expansion and Leukemic Clearance. *Sci. Transl. Med.* 9, eaag1209. doi:10.1126/scitranslmed.aag1209

Yen, S.-Y., Chuang, H.-M., Huang, M.-H., Lin, S.-Z., Chiou, T.-W., and Harn, H.-J. (2017). n-Butylidenephthalide Regulated Tumor Stem Cell Genes EZH2/AXL and Reduced its Migration and Invasion in Glioblastoma. *Int. J. Mol. Sci.* 18, 372. doi:10.3390/ijms18020372

Zah, E., Lin, M.-Y., Silva-Benedict, A., Jensen, M. C., and Chen, Y. Y. (2016). T Cells Expressing CD19/CD20 Bispecific Chimeric Antigen Receptors Prevent Antigen Escape by Malignant B Cells. *Cancer Immunol. Res.* 4, 498–508. doi:10.1158/2326-6066.cir-15-0231

Zah, E., Nam, E., Bhuvan, V., Tran, U., Ji, B. Y., Gosliner, S. B., et al. (2020). Systematically Optimized BCMA/CS1 Bispecific CAR-T Cells Robustly Control Heterogeneous Multiple Myeloma. *Nat. Commun.* 11, 2283. doi:10.1038/s41467-020-16160-5

Zamay, T., Zamay, G., Kolovskaya, O., Zukov, R., Petrova, M., Gargaun, A., et al. (2017). Current and Prospective Protein Biomarkers of Lung Cancer. *Cancers* 9, 155. doi:10.3390/cancers9110155

Zhang, Q., Tian, K., Xu, J., Zhang, H., Li, L., Fu, Q., et al. (2017). Synergistic Effects of Cabozantinib and EGFR-Specific CAR-NK-92 Cells in Renal Cell Carcinoma. *J. Immunol. Res.* 2017, 6915912. doi:10.1155/2017/6915912

Zhang, X., Ji, J., Zhang, G., Fang, C., Jiang, F., Ma, S., et al. (2017). Expression and Significance of B7-H3 and Tie-2 in the Tumor Vasculature of clear Cell Renal Carcinoma. *Onco Targets Ther.* 10, 5417–5424. doi:10.2147/ott.s147041

Zhang, Z., Zhou, Y., Qian, H., Shao, G., Lu, X., Chen, Q., et al. (2013). Stemness and Inducing Differentiation of Small Cell Lung Cancer NCI-H446 Cells. *Cell Death Dis.* 4, e633. doi:10.1038/cddis.2013.152

Zhong, S., Cui, Y., Liu, Q., and Chen, S. (2020). CAR-T Cell Therapy for Lung Cancer: A Promising but Challenging Future. *J. Thorac. Dis.* 12, 4516–4521. doi:10.21037/jtd.2020.03.118

Zhu, C., Wei, Y., and Wei, X. (2019). AXL Receptor Tyrosine Kinase as a Promising Anti-cancer Approach: Functions, Molecular Mechanisms and Clinical Applications. *Mol. Cancer* 18, 153. doi:10.1186/s12943-019-1090-3

Zhu, X., Prasad, S., Gaedicke, S., Hettich, M., Firat, E., and Niedermann, G. (2015). Patient-derived Glioblastoma Stem Cells are Killed by CD133-Specific CAR T Cells but Induce the T Cell Aging Marker CD57. *Oncotarget* 6, 171–184. doi:10.18632/oncotarget.2767

Zöller, M. (2011). CD44: Can a Cancer-Initiating Cell Profit from an Abundantly Expressed Molecule? *Nat. Rev. Cancer* 11, 254–267. doi:10.1038/nrc3023

Conflict of Interest: The authors declare that the research was conducted in the absence of any commercial or financial relationships that could be construed as a potential conflict of interest.

Publisher's Note: All claims expressed in this article are solely those of the authors and do not necessarily represent those of their affiliated organizations, or those of the publisher, the editors and the reviewers. Any product that may be evaluated in this article, or claim that may be made by its manufacturer, is not guaranteed or endorsed by the publisher.

frontiers in Cell and Developmental Biology

ORIGINAL RESEARCH
published: 14 December 2021
doi: 10.3389/fcell.2021.796960

Differentiation of Human iPS Cells Into Sensory Neurons Exhibits Developmental Stage-Specific Cryopreservation Challenges

Rui Li[1], *Patrick Walsh*[2], *Vincent Truong*[2], *Ashley Petersen*[3], *James R. Dutton*[4,5] *and Allison Hubel*[5,6]*

[1]Department of Biomedical Engineering, University of Minnesota, Minneapolis, MN, United States, [2]Anatomic Incorporated, Minneapolis, MN, United States, [3]Division of Biostatistics, University of Minnesota, Minneapolis, MN, United States, [4]Department of Genetics, Cell Biology and Development, University of Minnesota, Minneapolis, MN, United States, [5]Stem Cell Institute, University of Minnesota, Minneapolis, MN, United States, [6]Department of Mechanical Engineering, University of Minnesota, Minneapolis, MN, United States

Differentiation of human induced pluripotent stem cells (hiPSCs) generates cell phenotypes valuable for cell therapy and personalized medicine. Successful translation of these hiPSC-derived therapeutic products will rely upon effective cryopreservation at multiple stages of the manufacturing cycle. From the perspective of cryobiology, we attempted to understand how the challenge of cryopreservation evolves between cell phenotypes along an hiPSC-to-sensory neuron differentiation trajectory. Cells were cultivated at three different stages to represent intermediate, differentiated, and matured cell products. All cell stages remained ≥90% viable in a dimethyl sulfoxide (DMSO)-free formulation but suffered ≥50% loss in DMSO before freezing. Raman spectroscopy revealed higher sensitivity to undercooling in hiPSC-derived neuronal cells with lower membrane fluidity and higher sensitivity to suboptimal cooling rates in stem cell developmental stages with larger cell bodies. Highly viable and functional sensory neurons were obtained following DMSO-free cryopreservation. Our study also demonstrated that dissociating adherent cultures plays an important role in the ability of cells to survive and function after cryopreservation.

Keywords: cryobiology, induced pluripotent stem cell, differentiation, sensory neurons, controlled rate freezing, cryoprotective agents, Raman spectroscopy

OPEN ACCESS

Edited by:
Valerie Kouskoff,
The University of Manchester,
United Kingdom

Reviewed by:
Reyna Hernandez-Benitez,
Salk Institute for Biological Studies,
United States
Yong Fan,
Guangzhou Medical University, China

***Correspondence:**
Allison Hubel
hubel001@umn.edu

Specialty section:
This article was submitted to Stem Cell Research, a section of the journal Frontiers in Cell and Developmental Biology

Received: *18 October 2021*
Accepted: *16 November 2021*
Published: *14 December 2021*

Citation:
Li R, Walsh P, Truong V, Petersen A, Dutton JR and Hubel A (2021) Differentiation of Human iPS Cells Into Sensory Neurons Exhibits Developmental Stage-Specific Cryopreservation Challenges. Front. Cell Dev. Biol. 9:796960. doi: 10.3389/fcell.2021.796960

INTRODUCTION

Human induced pluripotent stem cells (hiPSCs) can be manufactured from a range of somatic cell types and further differentiated into cells valuable for drug discovery (Ko and Gelb, 2014), cell therapy (Yamanaka, 2020), and tissue engineering (Mazzola and Di Pasquale, 2020) applications. However, the generation of hiPSC-derived cells involves complex, protracted, and expensive differentiation protocols that progress through increasingly mature cell stages. There is significant added value in derisking the manufacturing supply chain by being able to efficiently cryopreserve cells at multiple stages along the differentiation trajectory, from the originally isolated somatic tissue through the pluripotent stem cell stage, intermediate progenitor, and differentiated phenotypes, to the terminal mature product. Effective cryopreservation of cells at different

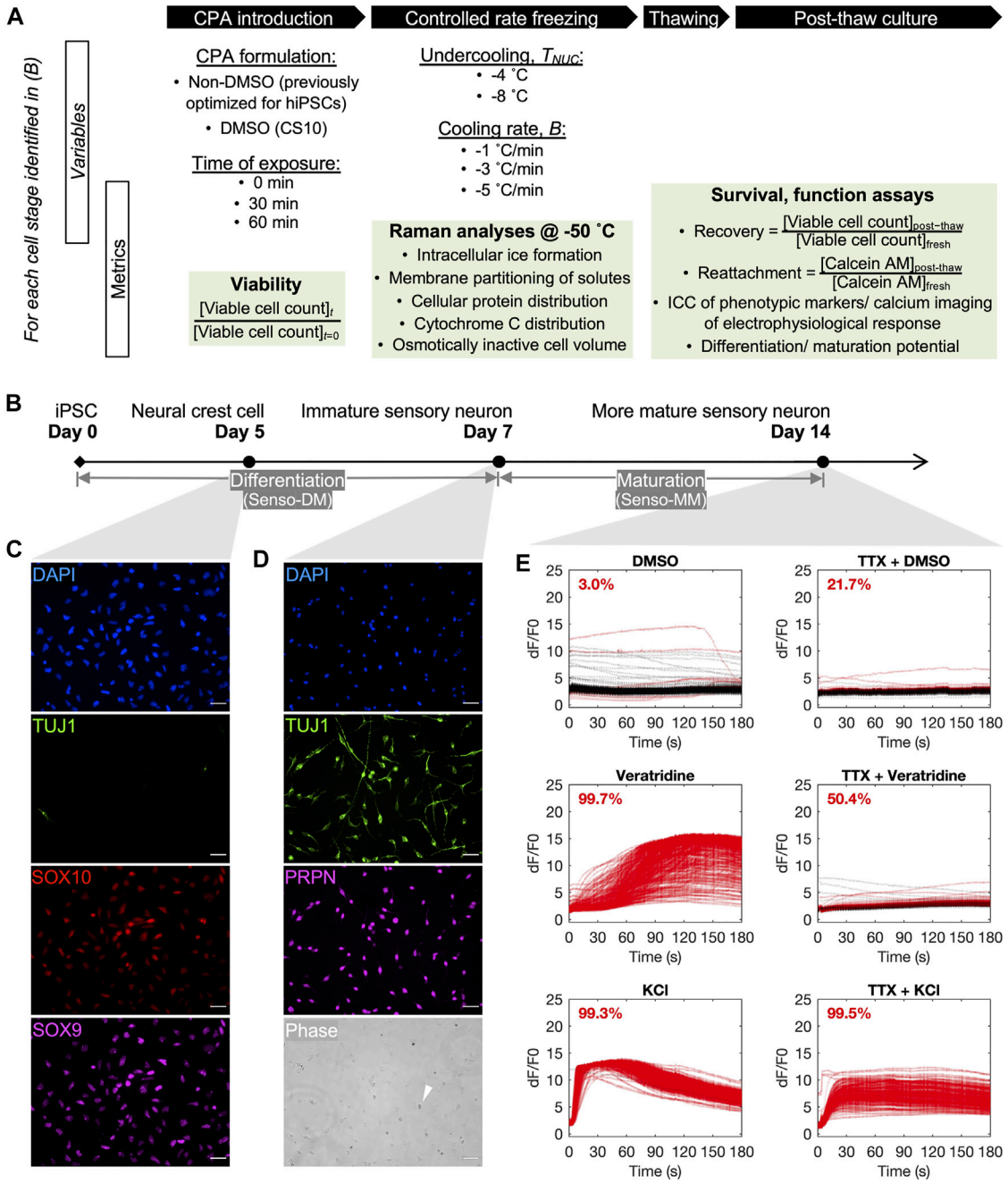

FIGURE 1 | Overview of the cryobiological investigation along a human induced pluripotent stem cell (hiPSC)-to-sensory neuron trajectory. **(A)** Outline of variables and metrics for the analysis, per neuronal cell stage, of cryoprotective agent (CPA) cytotoxicity before freezing, cell response to variation in nucleation temperature (T_{NUC}) and cooling ratio **(B)** during freezing, and cell survival and function after thawing. **(B)** A 14-day differentiation and maturation timeline for cultivating the three developmental stages of neuronal cells of interest for this investigation. **(C)** Immunocytochemistry of day-5 neural crest cells (D5 crest) replated at 100,000 cells/cm^2, 98.4% TUJ1– SOX9 + SOX10 +. Scale bar: 50 µm. **(D)** Phase contrast and immunocytochemistry of day-7 sensory neurons (D7 SN) replated at 50,000 cells/cm^2, 98.8% TUJ1 + PRPN + excluding dead cells by morphology (example indicated by white arrow in phase). Scale bar: 50 µm. **(E)** Calcium imaging of day-14 sensory neurons (D14 mSN), seeded at 50,000 cells/cm^2 on day 7, showing minimal response to dimethyl sulfoxide (DMSO), strong and tetrodotoxin (TTX)-sensitive response to veratridine, and strong response to potassium chloride (KCl). Lines are color-coded red for responder cells and black for nonresponder cells. Proportion of responder cell population indicated per graph.

developmental stages may not only simplify the multistage production of hiPSC-based technologies but also enable off-the-shelf use of the end product.

Researchers in the field of cryobiology have extensively studied the cell and tissue types at the front end of stem cell-based manufacturing process, from starting materials, such as

peripheral blood mononuclear cells (PBMCs) (Nazarpour et al., 2012; Germann et al., 2013; Pi et al., 2020) and fibroblasts (Ragoonanan et al., 2010; Naaldijk et al., 2016) to hiPSCs (Beier et al., 2013; Li et al., 2020) and mesenchymal stromal cells (MSCs) (Hunt, 2011; Pollock et al., 2017). While results of cryopreservation have been reported in some studies of hiPSC-derived cell types (Linville et al., 2020; van den Brink et al., 2020), we lack understanding of scientific principles on formulating cryopreservation media, freezing, thawing, cryoinjury mechanisms for many intermediate and mature cell product phenotypes, whether and how they change from one cell type to another, especially in relation to the expanding variety of cell types in this dynamic field of hiPSC-based manufacturing.

It has been commonly hypothesized among scientists that the more differentiated or more mature the cells are, the more difficult they are to freeze. Cryopreservation practice in the stem cell biology field mirrors this hypothesis, favoring cryopreservation of less differentiated and less mature cell phenotypes along a given differentiation trajectory. Literature describing the cryopreservation of hiPSC-derived cells is predominated by the freezing of intermediate, progenitor-like cell types (McNeish et al., 2010; Nishiyama et al., 2016). The vast majority of academic and industrial use-case literature, in drug screening, for example, completely foregoes cell cryopreservation in favor of continuous cell differentiation and maturation (Egawa et al., 2012; Höing et al., 2012; Burkhardt et al., 2013; Ryan et al., 2013; Yang et al., 2013; Brownjohn et al., 2017; Kondo et al., 2017; Engle et al., 2018; Fujimori et al., 2018). The limited use of cryopreservation is indicative of a knowledge gap that the cutting edge of cryobiological research can begin to address.

In order to effectively cryopreserve cells derived from hiPSCs, it will be important to understand the mechanisms of cell loss when cryopreserving cells along the differentiation and maturation process. As the biological properties of a cell changes as it proceeds along a differentiation trajectory, it will be important to understand how much the cryobiology of that cell changes and whether a given cryopreservation method developed for 1 cell developmental stage can be used for another. These scientific issues will impact the future of hiPSC-based clinical translations.

We present the first systematic evaluation, to our knowledge, of the freezing of discrete differentiation and maturation stages along a cell developmental trajectory, from undifferentiated hiPSC through neural crest cells, immature neurons, to electrophysiologically active sensory neurons, and the influence of stem cell development on the molecular and cellular parameters attributed to cryopreservation success (**Figure 1A**). In this work, the process parameters are defined as cooling rate and ice nucleation temperature. Particularly, different ice nucleation temperatures represent different degrees of undercooling—reaching temperatures below the intrinsic freezing point of the system—a major cause of cryoinjury in cells (John Morris and Acton, 2013). A dimethyl sulfoxide (DMSO)-free cryoprotective agent (CPA) formulation previously optimized for hiPSC cryopreservation and a DMSO-based formulation that is commercially available are compared. Low-temperature Raman spectroscopy is used during freezing to quantify the response of cells at the different developmental stages. An array of standard (e.g., intracellular ice formation) and novel (e.g., membrane partitioning of CPA solutes) Raman metrics are rendered from the label-free, high-resolution hyperspectral images of live cells. A progression of cell-based assays with increasing functional relevance are used after controlled rate freezing and thawing to characterize the post-thaw outcome for cells cryopreserved at the different stages of differentiation and maturation for a given variation of cooling rate and undercooling.

MATERIALS AND METHODS

Induced Pluripotent Stem Cell Culture

The hiPSC line UMN PCBC16iPS (Ye et al., 2013) was maintained using previously published methods between passages 80 and 85. In brief, the cells were cultured as adherent colonies on recombinant human vitronectin (Peprotech) in TeSR-E8 medium (STEMCELL Technologies) and passaged every 4 days as multicellular aggregates using Versene (ThermoFisher Scientific) at a split ratio of 1:16. Cultures were routinely tested for mycoplasma using the MycoAlert PLUS detection kit (Lonza, LT07-701) and karyotyped using G-banding at a 400-band resolution.

Neuronal Differentiation and Maturation

hiPSCs were differentiated into sensory neurons using a commercially available kit (Senso-DM, Anatomic Incorporated 7007) and further matured (Senso-MM, Anatomic Incorporated 7008) per the instructions of the manufacturer. Briefly, hiPSCs were passaged as 3- to 10-cell aggregates using Versene at a split ratio of 1:20 onto Matrix 1. Cultures were exposed to the first of a series of Senso-DM formulations 24 h later, with subsequent formulations applied daily for 1 week in total. The differentiated cells were dissociated and replated onto Matrix 3 and allowed to mature in Senso-MM media for another 7 days with half media exchange every 2 days. Three different stages of neuronal cells were selected for this investigation on the cryobiological change along this hiPSC-derived lineage (**Figure 1B**). They were, respectively, the intermediate SOX9-, SOX10-positive, TUJ1-negative neural crest cells obtained on day 5 of this protocol (also abbreviated as D5 crest in later text, **Figure 1C**), the fully differentiated but immature TUJ1-, PRPH-positive sensory neurons obtained on day 7 (D7 SN, **Figure 1D**), and the electrophysiologically active and more mature sensory neurons on day 14 (D14 mSN, **Figure 1E**). This defined 14-day differentiation and maturation process is referred to simply as the (sensory neuron) differentiation trajectory in later text.

Immunocytochemistry

Cultures were fixed in 3.7% paraformaldehyde (Fisher Scientific) for 10 min, permeabilized in 0.2% Triton X-100 (MilliporeSigma, X100–100 ml) for 10 min, and incubated overnight at 4°C with primary antibodies diluted in a blocking buffer containing 1% bovine serum albumin (Prometheus Protein Biology Products, 25–529) and 0.1% Tween-20 (MilliporeSigma, P7949-100 ml).

The cultures were subsequently washed twice with the blocking buffer and incubated for 2 h with secondary antibodies. DAPI (1: 1,000, ThermoFisher Scientific) was added for 30 min before washing twice in DPBS. Antibodies used include: SOX9 (1: 1,000, MilliporeSigma, AB5535), SOX10 (1:100, R&D Systems, AF2864), TUJ1 (1:500, MilliporeSigma, MAB1637), PRPH (1: 1000, Novus Biologicals, NB300137), Alexa Fluor 488 donkey anti-mouse (1:1,000, Invitrogen A-21202), Alexa Fluor 555 donkey anti-goat (1:1,000, Invitrogen, A-21432), Alexa Fluor 647 donkey anti-rabbit (1:1,000, Invitrogen, A-31573). Negative controls included unstained cultures and positively stained cultures known not to express the antigens of interest. Stained cultures were imaged using a Leica DMI6000B microscope and a DFC365FX camera.

Calcium Imaging

Live D14 mSN cultures were loaded with 2.5 μM Calbryte 520 AM (AAT Bioquest, 20651) and PowerLoad Concentrate (1:100, ThermoFisher Scientific, P10020) for 1 h before imaging. Fluorescent videos of the stained cultures were acquired using a Leica DMI6000B microscope, a DFC365FX camera, and a 10x air objective (NA 0.25, Leica Microsystems) for a duration of 185 s at four frames per second. Varying drug solutions were added to the cultures within the first 10 s of each video. The drugs included veratridine (Tocris, 2918) at a final concentration of 1 μM containing 0.1% DMSO in DPBS, 30 mM potassium chloride (KCl, Millipore Sigma, P5405) containing 0.1% DMSO, 0.1% DMSO as negative control, and 1 μM tetrodotoxin (TTX, Biotium, 00061) intended to block voltage-gated sodium channels.

The image analysis was automated using FIJI. Specifically, individual somata were detected by local maxima-based image segmentation and binary thresholding. Mean intensity was measured over time inside each soma. The intensity profiles were graphed, in terms of $\Delta F/F_0$, where ΔF is the intensity differential compared with background fluorescence (F_0) of the given sample, and the responding cells were quantified using MATLAB. Responders were mathematically defined by the maximum of the first derivative of its fluorescent intensity over time above a constant threshold that was determined by that of the background fluorescence over time.

Cell Viability in Cryoprotective Agents

A solution of non-DMSO cryoprotective agents (CPAs) was formulated using sucrose, glycerol, L-isoleucine, poloxamer 188 (P188), and human serum albumin as previously optimized for the cryopreservation of hiPSC aggregates (Li et al., 2020). A commercially available DMSO-based CPA solution (CryoStor 10, BioLife Solutions) was used in comparison. Neuronal cells were incubated in the CPA solution at room temperature. Viable and nonviable cell counts were based on membrane integrity using 10 μM acridine orange (AO) and 15 μM propidium iodide (PI) and measured at 0, 30, and 60 min.

Membrane Fluidity

hiPSC cultures were dissociated with Versene for 8 or 20 min to obtain a suspension of multicellular aggregates or single cells, respectively. Neuronal cell cultures were dissociated with Accumax (Innovative Cell Technologies) for 10, 45, or 90 min at room temperature on day 5, 7, or 14, respectively. Dissociated cells were washed once and stained with a fluorescent pyrene-decanoic acid (PDA) probe (Membrane Fluidity Kit, Abcam, ab189819) at room temperature for exactly 20 min before washing twice and quantification per the instructions of the manufacturer. Phenol red-free DMEM/F12 was used as the suspension media to minimize extrinsic variability between samples. Relative membrane fluidity was measured by the PDA excimer-to-monomer ratio using a Synergy HTX microplate reader with excitation at 360 nm and emission at 400 and 460 nm (BioTek).

Cell Diameter

Neuronal cells of the different developmental stages were dissociated as described above. Live cells were stained immediately after dissociation using AO and imaged in a hemocytometer (Hausser Scientific) using a Zeiss Axioskop 50 microscope with a 10x air objective (Plan NeoFluar, NA 0.30; Carl Zeiss). The cross-sectional area (A) of each cell was quantified using FIJI via thresholding and boundary recognition. Diameter of the fresh cell (D_{fresh}) was estimated using the following equation.

$$D_{fresh} = 2\sqrt{\frac{A}{\pi}}$$

Low-Temperature Confocal Raman Spectroscopy

Cell samples were prepared in the form of single-cell suspension and frozen at a controlled rate for analysis by Raman spectroscopy following a previously published method (Li et al., 2020; Yu et al., 2021). Specifically, defined cooling rates of −1, −3, and −5°C/min and ice nucleation temperatures of −4°C and −8°C were used as variables of the freezing profile. Data acquisition was performed at −50°C when sample temperature had stabilized for a minimum of 5 min. Raman spectroscopic measurements were made using WITec Confocal Raman Microscope Alpha 300R with UHTS spectrometer and DV401 CCD detector with 600/mm grating, a 532-nm Nd:YAG laser, and a 100x air objective (NA 0.90, Nikon Instruments).

Raman heat maps of different substances of interest were, respectively, rendered pixel-wise by integrating the Raman spectra under the peak at their characteristic wavenumbers (**Supplementary Table S1**). An integration time of 0.2 s was used to scan each 333-nm-by-333-nm pixel. The rendered Raman heat maps were spatially deconvolved using a theoretical point spread function of the instrument prior and quantitatively analyzed using WITec Project FOUR and FIJI, where pixels belonging to the different substances were, respectively, identified by spectral bandpass filtering, thresholding, and boundary recognition. Moran's I calculation of amide I and cytochrome C signals was performed using GeoDa, where spatial dispersion vs. autocorrelation was determined between

−1 and 1 using a spatial weight matrix based on eight nearest neighbors. Similar to fresh cells, cell diameter during freezing was quantified based on the cross-sectional area of the cell as delineated by the amide I and cellular hydrogen bond signals. The effect of freezing on the osmotically inactive cell volume was represented by the diameter of frozen cells normalized to the mean diameter of fresh cells for each given cell stage and freezing condition.

Controlled Rate Freezing and Thawing

Cells of different stages were dissociated as described above and suspended in a collection buffer containing P188 (Li et al., 2020). A twice-concentrated CPA solution previously optimized for hiPSC cryopreservation (Li et al., 2020) was added at equal volume. The mixture was incubated at room temperature for 1 h and subsequently frozen in cryogenic vials (Nunc CryoTubes, ThermoFisher Scientific) using a controlled rate freezer (Kryo 560–16, Planer) following the steps listed below. Similar to Raman experiments, a cooling rate, B, of −1°C/min, −3°C/min, or −5°C/min and ice nucleation temperature, T_{NUC}, of −4°C or −8°C were used (see **Supplementary Figure S1** for the sample cooling profiles).

1. Starting temperature 20°C.
2. −10°C/min to $T_{NUC.}$
3. Hold at T_{NUC} for 15 min to equilibrate sample and chamber temperatures.
4. Induce ice nucleation manually by briefly spraying liquid nitrogen onto vials using a Cryogun (Brymill) for accurate control of the nucleation temperature.
5. B°C/Min to −60°C.
6. −10°C/Min to −100°C.

A sample temperature inside a replicate "dummy" vial was logged for each experiment using the built-in thermocouple of the controlled rate freezer inserted via a bored vial cap. Frozen vials were stored in the liquid phase of liquid nitrogen for 24 h prior to thawing in a 37°C water bath for 2.5 min. Thawed cells were immediately used for post-thaw quantifications.

Post-Thaw Quantification of Cell Survival and Function

Post-thaw cell recovery rate was defined as the percent ratio of viable cell count immediately after thawing and viable cell count immediately before CPA addition prefreeze, based on cell membrane integrity distinguished by AO stain and PI exclusion. Post-thaw cell attachment rate was defined as the percent ratio of adhered, metabolically active cell culture in 24 h after thawing and that of 24 h after passaging fresh cells, where cultures were stained with calcein AM (1:1,000, Corning 354217) at 37°C for 30 min before quantified using Synergy HTX microplate reader with 480-nm excitation and 528-nm emission filters. Post-thaw cell function was measured, respectively, by the ability of cryopreserved D5 crest to continue differentiating to TUJ1-positive, PRPH-positive sensory neurons 48 h later, using immunocytochemistry as described above, of cryopreserved D7 SN to produce calcium response in 7 days, using calcium imaging as described above, and of cryopreserved D14 mSN to retain calcium response in 24 h, all in comparison with fresh cells through the corresponding manipulation with only cryopreservation procedures removed.

Statistics

Independent biological replicates were used with sample size specified in the *Results* section per dataset. Power analysis was performed to ensure sufficient sample size to achieve a power of 0.95. Error bars represent 95% confidence intervals unless otherwise noted. Two-tailed Student's t-tests were performed for two-sample comparisons, unless otherwise noted. ANOVA with Bonferroni correction was performed for comparisons of multiple samples, with the exception of Kruskal–Wallis ANOVA performed for sample populations with non-normal distribution. The null hypothesis was defined as no statistical difference between the parameters (e.g., means) for any pair of groups or between the experimental group and control group. The null hypothesis was rejected, and differences were considered statistically significant for a p-value less than 0.05.

RESULTS

Non-DMSO Solution Composed of Sucrose, Glycerol, L-Isoleucine, P188, and HSA was Superior to DMSO-Based Commercial Solution in Maintaining Neuronal Cell Viability Before Freezing

Cells are cryopreserved in specialized solutions containing cryoprotective agents (CPAs). These solutions are not physiological, and cell losses can result from exposure to these solutions. Different cell types can have different responses to being exposed to the same CPA formulation, and different CPA formulations can have different levels of cytotoxicity for a given cell type. In this study, a non-DMSO CPA solution composed of sucrose, glycerol, L-isoleucine, P188, and HSA and previously developed for hiPSCs (Li et al., 2020) was compared with a DMSO-based solution commercially available and commonly used for hiPSC-derived cells (i.e., CS10) in terms of their ability to maintain the viability of different stages of neuronal cells before freezing. In order to quantify the toxicity of the cryoprotective solutions, viable cell count was tracked, via membrane exclusion fluorescent assay, for 1 h from the introduction of non-DMSO CPA and DMSO solutions before freezing for D5 crest, D7 SN, and D14 mSN, respectively (**Figure 2**).

Compared with the non-DMSO CPA, the DMSO solution resulted in significant cell loss by both loss of membrane integrity and lysis (high cell count with compromised membrane and low total cell count, raw data not shown) for all cell stages within 30 min of exposure. After 1 h of prefreeze incubation in DMSO, all cell stages experienced close to (D5 crest, $p > 0.05$) or greater than (D7 SN and D14 mSN, $p < 0.05$) 50% cell loss. Notably, the cell loss increased over time regardless of cell stage. At both the 30- and 60-min timepoints, it was found with statistical significance ($p < 0.05$) that the farther the cell stage in differentiation and maturation, the lower the cell stability in DMSO.

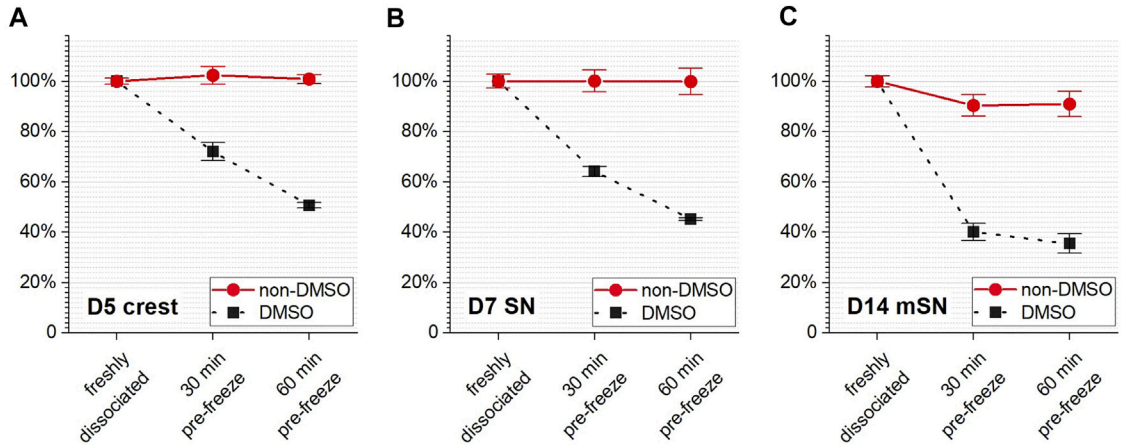

FIGURE 2 | Cell survival rate during CPA incubation prior to cryopreservation as monitored over time of exposure to the non-DMSO CPA solution vs. the DMSO-based solution for **(A)** D5 crest, **(B)** D7 SN, and **(C)** D14 mSN, respectively. Data are represented as mean ± 95% confidence interval. $n = 4$.

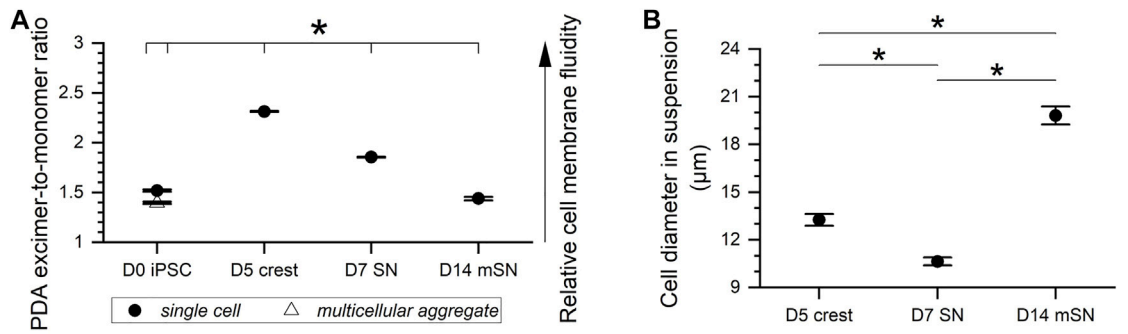

FIGURE 3 | Membrane fluidity and cell size fluctuation along hiPSC derivation to sensory neurons. **(A)** Cell membrane fluidity at different stages of the sensory neuron differentiation and maturation process with all statistically significant pairwise differences. Data are represented as mean ± 95% confidence interval. $n = 9$. *$p < 0.05$. **(B)** Diameter of D5 crest vs. D7 SN vs. D14 mSN dissociated from culture and suspended in growth medium. Data are represented as mean ± 95% confidence interval. Range of n: 60–98. *$p < 0.05$.

In contrast, no significant change in viable cell count ($p > 0.05$) was seen in either D5 crest or D7 SN throughout the 1-h incubation in the non-DMSO solution. While the cell survival rate of D14 mSN decreased from 100% to approximately 90% within the first 30 min of non-DMSO CPA exposure, their viability remained statistically unchanged ($p > 0.05$) for the next 30 min until freezing. Notably, regardless of cell stage, the non-DMSO CPA formulation was significantly superior ($p < 0.05$) to the DMSO-based formulation in stabilizing these neuronal cells and maintaining their viability in the time period prior to the start of freezing.

Membrane Fluidity and Cell Size Fluctuations During Neuronal Cell Differentiation and Maturation Inferred Cell Stage-Dependent Sensitivity to Undercooling and Cooling Rate

As one possible factor influencing the sensitivity of the cells to freezing (Giraud et al., 2000; Blesbois et al., 2005), membrane fluidity was measured for each cell stage, upon dissociation and in suspension, along the 14-day differentiation trajectory (**Figure 3A**). These measurements included hiPSCs in the forms of single cells and multicellular aggregates, D5 crest, D7 SN, and D14 mSN in the form of single cells. Based on PDA excimer-to-monomer ratios, membrane fluidity of the cells underwent significant changes as they became more differentiated and mature. Interestingly, within the 5 days of differentiation from hiPSCs to neural crest cells, the relative membrane fluidity increased by more than 50%. In the next 48 h from neural crest cells to fully differentiated sensory neurons, the change in membrane fluidity inverted direction by decreasing approximately 20%. This decrease continued, at an overall slower rate than earlier, for another week as the neurons matured. PDA assay also showed that hiPSC aggregates had significantly lower membrane fluidity than their single cell counterparts, inversely correlated with the significantly greater sensitivity to undercooling that was found by previous studies (Li et al., 2018, 2020). Notably, the fluctuation

in membrane fluidity along this differentiation trajectory was not unidirectional, increasing during the initial pluripotent-to-progenitor step but decreasing from progenitor through maturation based on the selected discrete cell stages. This fluctuation in membrane fluidity suggests likely fluctuation in the sensitivity of neuronal cells to undercooling, one category of freezing sensitivity in response to a specific parameter of freezing–nucleation temperature.

In addition to membrane fluidity, cell size was considered another potential intrinsic factor influencing cell sensitivity to freezing, specifically cell sensitivity to another parameter of freezing–cooling rate. Larger cells with smaller surface-to-volume ratio may contain more intracellular water during cooling and, thus, higher potential for intracellular ice (Gao and Critser, 2000; Hubel, 2018). The diameter of the cells in suspension was observed to fluctuate significantly from one cell stage to the next along this differentiation trajectory (**Figure 3B**). D7 SN was found with the smallest cell diameter in suspension at 10.6 μm (± 0.2 μm, 95% confidence interval), followed by D5 crest at 13.3 μm (± 0.4 μm), and D14 mSN with the largest cell diameter at 19.8 μm (± 0.6 μm). Changes in soma size have been known in literature to occur during neuronal development (Nixdorf-Bergweiler, 1998; Deshpande et al., 2017). Notably, the fluctuation in cell size was not unidirectional from neuronal differentiation to maturation. However, somata (or cell body) enlargement over the course of neuronal maturation observed in this study was also consistently observed in stem cell biology practices. In subsequent experiments, freezing sensitivity (i.e., undercooling and cooling rate sensitivity) of these neuronal cells was observed using low-temperature Raman spectroscopy and post-thaw cell-based assays to vary by the different stages of development, where correlation between membrane fluidity and cell responses to undercooling and between cell size and cell responses to cooling rate variation was found.

Sensitivity to Undercooling and Mechanisms of Damage Varied by Cell Stage

D5 crest, D7 SN, and D14 mSN were frozen in the non-DMSO or DMSO-based solution under a confocal Raman microscope. The cells were subjected to different degrees of undercooling, where the freezing process was initiated with ice nucleation induced at different temperatures, −4 vs. −8°C, and subsequently cooled at a constant rate of −1°C/min. In each frozen cell, intracellular ice formation, membrane partitioning of solutes, cellular protein distribution, and cytochrome C distribution were quantified (see **Supplementary Figure S2** for definition and illustrative examples of different values of the corresponding metrics). Cryobiological analysis of the frozen cells revealed mechanisms of damage, or the absence thereof, at each cell stage in response to the varied CPA solutions and varied undercooling conditions.

While extracellular ice crystal formation is an element of slow freezing, the formation of intracellular ice crystals of large quantity or size can be a lethal event. In terms of intracellular ice formation (**Figure 4A**), D5 crest showed no statistically significant response to the different ice nucleation temperatures or different CPA formulations. When the non-DMSO CPA was used, D7 SN also showed minimal intracellular ice that was consistent between different ice nucleation temperatures. However, a significantly greater amount of intracellular ice crystals was found in the D7 SN frozen in DMSO, where intracellular ice took up nearly the entirety of cytoplasmic space (abbreviated as chunky intracellular ice from here on) for approximately 30% of the cell population. Moving further along the cell developmental trajectory, when D14 mSN was frozen in the non-DMSO solution, it had significantly more intracellular ice crystals with greater undercooling. When D14 mSN was frozen in the DMSO solution, intracellular ice took a different form, chunky rather than dispersed. As intracellular ice formation has been found to be indicative of sensitivity to undercooling in our earlier studies (Li et al., 2018, 2020), these new results from D5 crest, D7 SN, and D14 mSN suggested not only that undercooling sensitivity varied between the different cell stages but also that the sensitivity of a given cell stage was different in the two CPA formulations.

Cell populations found with substantial quantity of intracellular ice (i.e., five of 10 cells for D7 SN frozen in DMSO; three of 10 cells for D14 mSN frozen in DMSO) were omitted from some of the following analyses (**Figures 4B,C**) due to interference of ice signal and lack of the intracellular Raman signals of interest. As a result, this dataset reveals other mechanisms of damage in cells, while intracellular ice formation was relatively well inhibited. Membrane partitioning of solutes (i.e., non-DMSO CPA or DMSO) describes the steady state of mass transport across the plasma membrane and is mathematically represented as the ratio of the extracellular concentration to the intracellular concentration. While a non-penetrating CPA (e.g., sucrose) is expected to remain out of the cytoplasm, a healthy cell membrane should also be able to partition a penetrating CPA (e.g., glycerol, DMSO), where the intracellular concentration is typically lower than the extracellular concentration of that CPA unless active transport is involved.

In terms of partitioning ratio of the non-DMSO CPA (**Figure 4B**), D5 crest and D7 SN both showed no significant change upon greater undercooling, whereas D14 mSN exhibited significantly weaker membrane partitioning when subjected to lower ice nucleation temperature. One possible explanation for the decrease in partitioning is impaired barrier function of the plasma membrane of the D14 mSN upon undercooling, corresponding to the higher intracellular ice formation of the cells, more punctate protein distribution, and cytochrome C release. Comparing non-DMSO CPA and DMSO, membrane partitioning of DMSO was found to be significantly (up to 2.4-fold) weaker than that of the non-DMSO CPA for the neuronal cell stages investigated. While it cannot indicate or rule out the possibility of membrane impairment by DMSO, the consistent trend across different cell stages clearly showed that cell membranes have a lower barrier effect to DMSO than glycerol and other non-DMSO CPA molecules. As extracellular ice forms and grows with cooling, cells dehydrate, and intracellular solutes become more concentrated. When DMSO was used, the neuronal

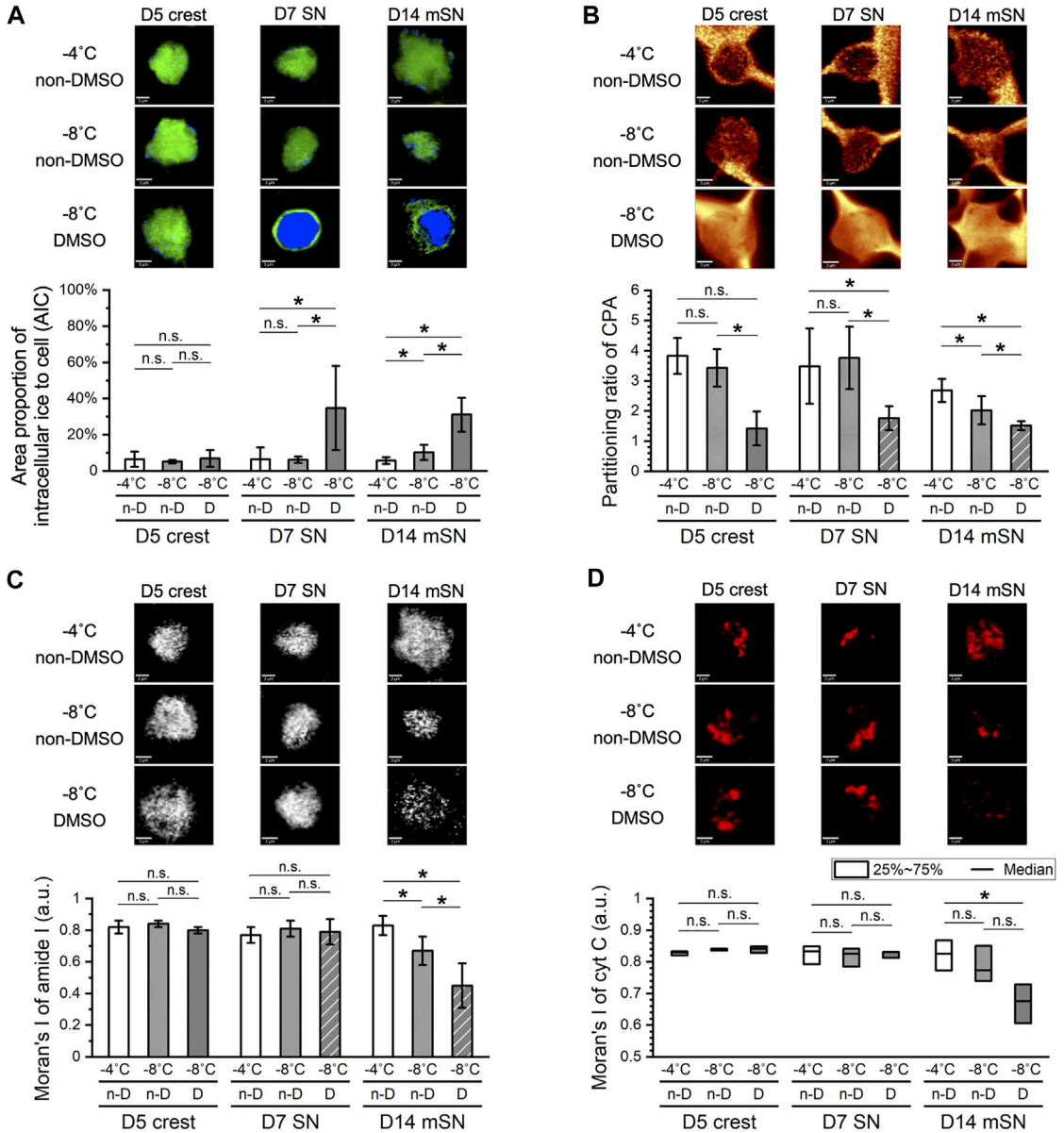

FIGURE 4 | Effects of undercooling on freezing behaviors of D5 crest, D7 SN, and D14 mSN, respectively, as observed by low-temperature Raman spectroscopy, comparing different ice nucleation temperatures between –4°C and –8°C. Data are represented as mean ± 95% confidence interval. n = 10, except for striped columns representing measurements of subset population n = 5 for D7 SN and n = 7 for D14 mSN due to interference of intracellular ice. n-D, non-DMSO; D, DMSO. n.s.: $p > 0.05$; *$p < 0.05$ (see **Supplementary Figure S2** for method illustration of each metric.). **(A)** Intracellular ice formation (blue) significantly increased with greater undercooling only in the case of D7 SN in the DMSO solution and D14 mSN in both non-DMSO and DMSO solutions; no significant change otherwise. **(B)** Membrane partitioning of non-DMSO CPA significantly decreased in D14 mSN subject to greater undercooling, partitioning of DMSO lower than that of non-DMSO CPA across all three cell stages. **(C)** Cellular integrity in terms of spatial autocorrelation of the amide I signal of protein decreased significantly for D14 mSN with greater undercooling and decreased further in the DMSO solution; no significant loss of integrity in D5 crest or D7 SN. **(D)** Significant cytochrome C (cyt C) release was observed for D14 mSN in the DMSO solution but not for any cell stage in the non-DMSO CPA. Kruskal–Wallis ANOVA performed for non-normal distribution of cyt C Moran's I values.

cells were more likely subjected to stresses of high intracellular CPA concentration than when non-DMSO CPA was used.

Moran's I of amide I signal in cells was used to quantify the distribution of cellular proteins. As shown in **Figure 4C**, D14 mSN was the only cell stage among those tested to be affected by the stresses of undercooling and DMSO exposure on a protein level. When chunky intracellular ice was successfully inhibited, D5 crest and D7 SN exhibited consistently high, uniform distribution of proteins during freezing regardless of ice nucleation temperature or CPA formulation, whereas D14 mSN showed more punctate distribution of proteins upon greater undercooling, a sign of cellular disintegration, and became further disintegrated when frozen in the DMSO-based solution. Moran's I of cytochrome C signal in cells measured the

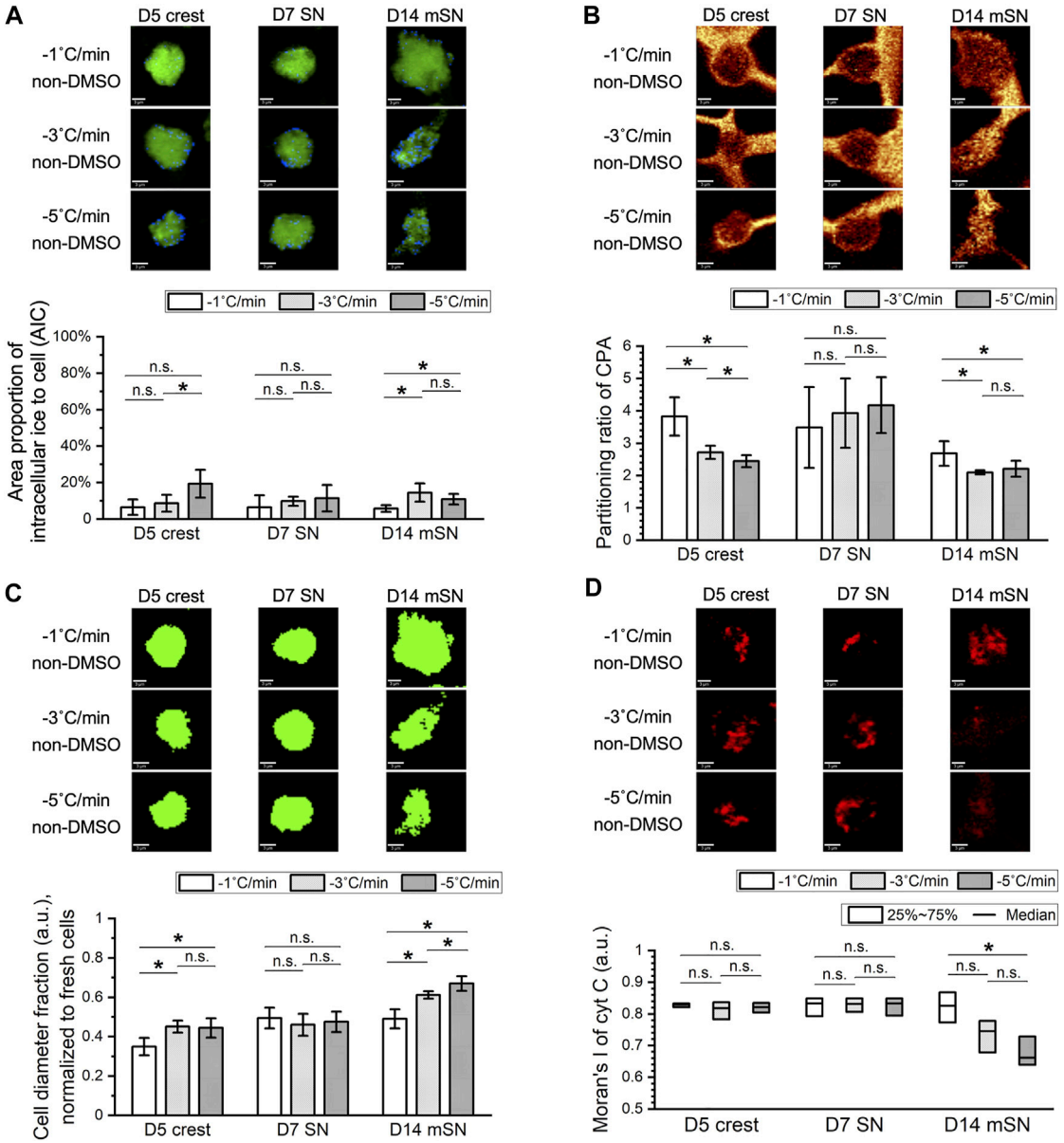

FIGURE 5 | Effects of cooling rate on freezing behaviors of D5 crest, D7 SN, and D14 mSN, as observed by low-temperature Raman spectroscopy, comparing different cooling rates between −1°C/min, −3°C/min, and −5°C/min, respectively. Data are represented as mean ± 95% confidence interval. $n = 10$. n.s.: $p > 0.05$; *$p < 0.05$ (see **Supplementary Figure S2** for method illustration of each metric.) **(A)** Intracellular ice formation (blue) increased with the faster cooling rates in D5 crest and D14 mSN; no significant difference across cooling rates in D7 SN. **(B)** Membrane partitioning of non-DMSO CPA significantly decreased in D5 crest and D14 mSN with the faster cooling rates; no significant difference across cooling rates in D7 SN. **(C)** Loss of cell volume as a result of freezing intensified with the faster cooling rates for D5 crest and D14 mSN; no significant difference across cooling rates in D7 SN. **(D)** Significant cytochrome C (cyt C) release was observed for D14 mSN with the faster cooling rates but not for D5 crest or D7 SN at any of the cooling rates. Kruskal–Wallis ANOVA performed for non-normal distribution of cyt C Moran's I values.

potential of post-thaw mitochondrial apoptosis and necrosis. As shown in **Figure 4D**, D14 mSN was the only cell stage showing cytochrome C release when frozen in DMSO, although the cytochrome C distribution of D14 mSN did not respond significantly to undercooling.

Summarizing these four cryobiological metrics, intracellular ice was the only observed mechanism of freezing damage in the earlier cell stages (i.e., D5 crest, D7 SN), where chunky intracellular ice was particularly prominent in D7 SN frozen in the DMSO solution. Further downstream of this differentiation trajectory, higher undercooling sensitivity manifested in the more mature cell stage (i.e., D14 mSN). For D14 mSN frozen in the non-DMSO CPA, significantly higher quantity of small intracellular ice was found and likely resulted in impaired membrane barrier function, higher intracellular CPA concentration, and consequently partially disintegrated cellular

structure. For D14 mSN frozen in DMSO, besides the damage of chunky intracellular ice, they suffered from cellular disintegration and cytochrome C release. Similar to previously reported observations in hiPSCs (Li et al., 2018, 2020), compared with the DMSO-based formulation, the non-DMSO CPA formulation utilized here reduced damage in cells that were subjected to lower ice nucleation temperature, extrinsically mitigating the cells' sensitivity to undercooling. The overall increase in cell sensitivity to undercooling from a multitude of mechanisms along this sensory neuron differentiation trajectory correlated with the decrease in cell membrane fluidity from D5 crest through D14 mSN (**Figure 3A**), confirming membrane fluidity as a likely factor contributing to the intrinsic sensitivity of the cells to undercooling.

Sensitivity to Cooling Rate Varied Among Cell Stages and Correlated with Cell Size

Parallel to the examination of the effect of undercooling, the effect of different cooling rates on cell behaviors during freezing was also examined. D5 crest, D7 SN, and D14 mSN were subjected to cooling rate that varied between −1°C/min, −3°C/min, and −5°C/min, and their potential mechanisms of damage, or the absence thereof, were analyzed using low-temperature Raman spectroscopy (**Figure 5**). The non-DMSO CPA formulation previously optimized for hiPSCs was used throughout these experiments. Interestingly, D5 crest and D14 mSN both experienced freezing damages that varied by cooling rate, whereas D7 SN consistently exhibited no statistically significant change across the selection of Raman-based cryobiological analyses regardless of the cooling rate.

In terms of intracellular ice formation (**Figure 5A**), with ice nucleation temperature held constant at −4°C, only small rather than chunky intracellular ice was observed. D5 crest maintained minimal levels of intracellular ice with the slower cooling rates (i.e., −1°C/min and −3°C/min) and contained a significantly greater quantity of ice with the fastest cooling rate tested (i.e., −5°C/min). D14 mSN maintained a minimal level of intracellular ice with the slowest cooling rate (i.e., −1°C/min) but had a significant increase in intracellular ice with the faster cooling rates starting at −3°C/min. In terms of membrane partitioning of the non-DMSO CPA (**Figure 5B**), the faster cooling rates (i.e., −3°C/min and −5°C/min) resulted in significantly weaker partitioning in both D5 crest and D14 mSN than the slower cooling rate (i.e., −1°C/min). The weaker partitioning subjected the cells to higher concentrations of intracellular CPA and possibly indicated impairment of the membrane's barrier function.

As extracellular ice grows during cooling, cells are expected to dehydrate and reduce in volume and diameter. As greater dehydration is commonly expected with slower cooling rates, where water takes longer to leave the cell via osmosis and balance the concentration gradient of solutes across the plasma membrane, the reduction of cell diameter as a result of dehydration is expected to be less upon faster cooling rate for a given cell type. Interestingly, when cell diameter was measured during freezing by the distribution of Raman cellular hydrogen bond and amide I signals and normalized to the diameter of the cells before freezing, this inverse correlation between cell diameter fraction and cooling rate was not found for any of the neuronal cells of interest (**Figure 5C**). For D7 SN, no significant difference in cell diameter fraction was observed in response to the cooling rate variations. For D5 crest and D14 mSN, the faster cooling rates (i.e., −3°C/min and −5°C/min) resulted in significantly greater loss of cell diameter than the slower cooling rate (i.e., −1°C/min). Comparing the ratio in spectral intensity of the C–H stretching peak to that of the broad O–H stretching band between the cells frozen at different cooling rates, no distinct difference in the hydration level of the cells was observed (data not shown). Therefore, the correlation between intensified loss of cell diameter and faster cooling rate was likely *not* a direct contradiction to the common expectation described above but suggesting another mechanism of cell damage at play. Combined with more intracellular ice, weaker membrane partitioning, and cytochrome C release observed upon faster cooling, greater loss of cell diameter in the frozen D5 crest and D14 mSN likely indicated loss of cell contents and either necrosis or apoptosis of the cells.

In addition, cytochrome C release was observed in D14 mSN at the faster cooling rates but not in D5 crest (**Figure 5D**). Summarizing the number of mechanisms of freezing damages observed per cell stage and the extent of its response to cooling rate variation, D14 mSN was found to be the most susceptible to fast cooling rates, followed by D5 crest, followed by D7 SN. This trend was consistent with the original cell sizes measured upon dissociation from fresh culture and suspension in the cell growth media (**Figure 3B**). The larger cells (i.e., D14 mSN at ~20 μm in diameter > D5 crest at ~13 μm in diameter) with lower surface-to-volume ratio required slower cooling rate (i.e., −1°C/min) to prevent damages from both intracellular ice formation and dynamic osmotic stresses, whereas the smaller cell (i.e., D7 SN at ~11 μm in diameter) minimized intracellular ice formation, maintained membrane integrity, and prevented disintegration of cellular proteins across the range of cooling rates investigated (i.e., from −1 to −5°C/min). While this correlation between cell size and cooling rate sensitivity, in general, was consistent with what has been demonstrated in literature, the absence of chunky intracellular ice and the analysis of membrane partitioning and cell volumetric loss in the present investigation presented an alternative mechanism of damage in large cells during fast cooling, in contrast with and a supplement to the commonly hypothesized, generalized mechanism that has been based solely on the formation of optically visible (i.e., chunky) intracellular ice crystals.

Successful Cryopreservation Relied on Good Cryoprotection and Compatible Process

The next phase of this investigation involved evaluating the performance of these cryopreserved cells upon vial-based controlled rate freezing in the non-DMSO CPA formulation, with ice nucleation varied between −4°C and −8°C and cooling rate varied between −1°C/min, −3°C/min, and −5°C/min. Post-thaw cell recovery was measured by membrane exclusion

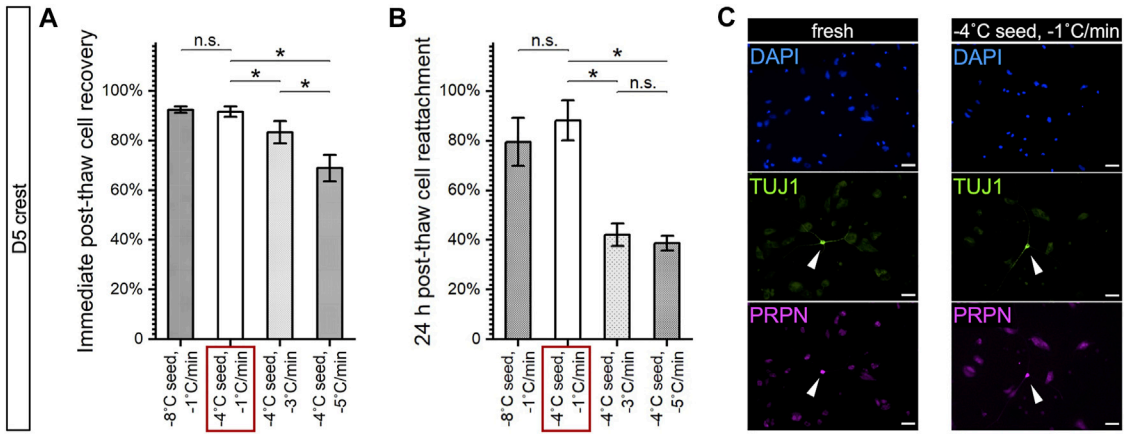

FIGURE 6 | Post-thaw survival and function of cryopreserved D5 crest under varying nucleation temperatures and cooling rates. *$p < 0.05$; n.s.: $p > 0.05$. Red box: best-case parameters tested with the highest recovery and reattachment. **(A)** Post-thaw recovery of D5 crest showing no significant change with greater undercooling but trending significantly lower with faster cooling rate. $n = 4$. **(B)** Post-thaw reattachment of D5 crest showing similar trends as recovery but more distinct cell damage with cooling rates of −3°C/min and −5°C/min. $n = 4$. **(C)** Immunocytochemistry 48 h after re-culture of dissociated (fresh) or cryopreserved (best-case) D5 crest showing <1% TUJ1+, PRPN+ (white arrowheads) neuron differentiation, and a vast majority of resulted cell population with crest-like morphology and low-level, cytoplasmic TUJ1 and PRPN staining. Scale bar: 100 μm.

fluorescent assay to assess membrane integrity. Post-thaw cell reattachment was quantified by measuring the esterase activity of adherent cells. Post-thaw differentiation to sensory neurons was tested for cryopreserved D5 crest to assess their differentiation potential; post-thaw maturation to electrophysiologically active neurons was examined for cryopreserved D7 SN to assess the ability to reach a more mature state; post-thaw electrophysiological response was intended for cryopreserved D14 mSN to assess the ability to retain the level of maturity. The different forms of post-thaw assay progressed in the aforementioned order toward representing the ability of a given cryopreservation method to fulfill the intended utility of the cells.

For D5 crest, both post-thaw recovery (**Figure 6A**) and post-thaw reattachment (**Figure 6B**) demonstrated a lack of cell sensitivity to undercooling and significant cell loss to faster cooling rates. This trend was consistent with the Raman results described earlier, indicating that a cooling rate of −1°C/min or slower was required for D5 crest to prevent loss in membrane integrity or cell adhesion. Despite the successful cryoprotection demonstrated in the combination of −1°C/min cooling and −4°C ice nucleation by post-thaw recovery greater than 90% and post-thaw reattachment of 88%, the cryopreserved D5 crest failed to produce sensory neurons after subsequent days of neuronal induction (**Figure 6C**). However, notably, the fresh control group of D5 crest that was dissociated and replated into culture also lost its ability to differentiate into TUJ1-positive, PRPH-positive neurons. Dissociating the cells on day 5 interrupted the adherent culture and deviated from the originally continuous 7-day differentiation process, which proved to be detrimental to cryopreserving the D5 crest despite the otherwise effective freezing protocol and CPA formulation.

For D7 SN, post-thaw recovery (**Figure 7A**) demonstrated a lack of cell sensitivity to undercooling that was consistent with the Raman results described earlier. However, post-thaw recovery showed a statistically significant difference between different cooling rates that was not revealed by the Raman measurements. In addition, post-thaw reattachment of D7 SN (**Figure 7B**) demonstrated not only cell sensitivity to cooling rate but also to undercooling that was not reflected by the Raman measurements of intracellular ice, membrane partitioning, cellular material integrity or cytochrome C release. The −4°C ice nucleation and −3°C/min cooling were shown as the best combination of controlled rate freezing parameters for D7 SN. Post-thaw functional assay of cryopreserved D7 SN demonstrated a high-confluence, viable post-thaw culture (**Figure 7C**) that successfully produced the more mature neurons with normal electrophysiological responses to the panel of drug molecules (**Figure 7D** and **Supplementary Figure S3**).

For cryopreserved D14 mSN, measurement of immediate post-thaw recovery (**Figure 8A**) appeared to demonstrate a lack of sensitivity to undercooling that was otherwise shown in the earlier Raman results, but it showed a trend of more cell death with faster cooling rate that was consistent with the trend in intracellular ice, membrane impairment, volumetric loss, and cytochrome C release observed by Raman. The 24-h post-thaw reattachment of D14 mSN (**Figure 8B**) also appeared to show a lack of sensitivity to both undercooling and cooling rate variations. However, upon a closer examination of D14 mSN post-thaw using the optimal freezing parameters (i.e., −1°C/min cooling and −4°C ice nucleation) as well as postpassage (**Figure 8C**), we found that both freshly dissociated and cryopreserved cells failed to produce viable culture, rendering 24-h post-thaw reattachment an invalid metric, in this instance, for quantifying the effect of cooling rate or undercooling on the cryopreservation outcome of D14 mSN.

DISCUSSION

In contrast to the abundant methods of primary and stem cell-derived neuronal cell production in literature, a few reports can

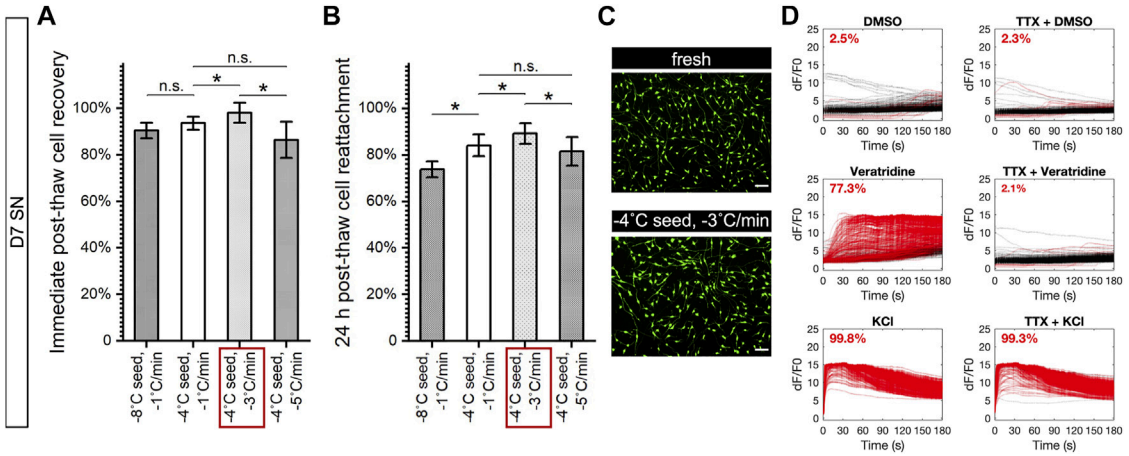

FIGURE 7 | Post-thaw survival and function of cryopreserved D7 SN under varying nucleation temperatures and cooling rates. Data are represented as mean ± 95% confidence interval. *$p < 0.05$; n.s.: $p > 0.05$. Red box: best-case parameters tested with the highest recovery and reattachment. **(A)** Post-thaw recovery of D7 SN showing no significant change with greater undercooling and the best cooling rate at –3°C/min with statistical significance. $n = 4$. **(B)** Post-thaw reattachment of D7 SN showing similar trends as recovery but more distinct cell damage with lower nucleation temperature (–8°C). $n = 4$. **(C)** Calcein AM-stained culture 24 h after replating dissociated (fresh) or cryopreserved (best-case) D7 SN showing high confluence and normal morphology of immature neurons. Scale bar: 100 µm. **(D)** Calcium imaging of post-thaw culture after 7-day maturation of D7 SN cryopreserved with –4°C nucleation and –3°C/min cooling rate, showing little to no response to 0.1% DMSO (negative control), positive response to 1 µM veratridine that was inhibited by TTX, and positive response to 30 mM KCl that was unaffected by TTX. Red line: responder cell; black line: nonresponder cell. Proportion of responder cell population indicated per graph. Range of $n = 417–662$.

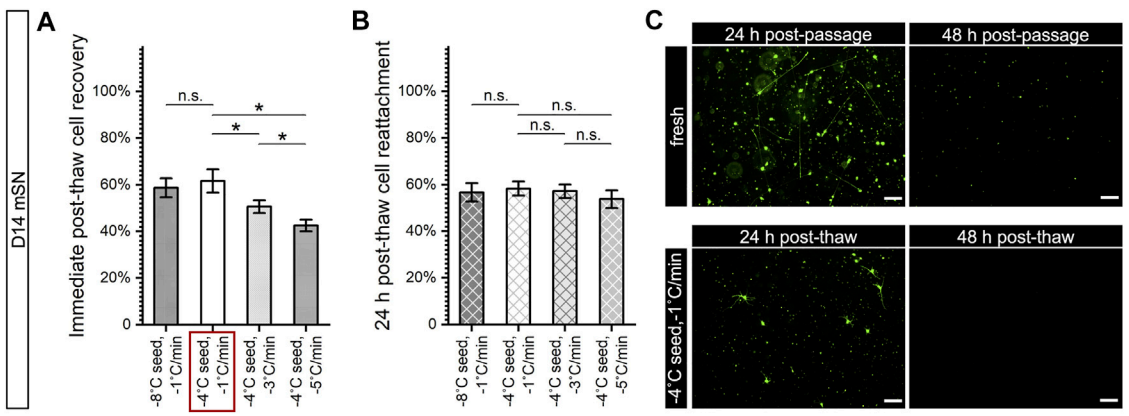

FIGURE 8 | Post-thaw survival and function of cryopreserved D14 mSN under varying nucleation temperatures and cooling rates. Data are represented as mean ± 95% confidence interval. *$p < 0.05$; n.s.: $p > 0.05$. **(A)** Post-thaw recovery of D14 mSN showing no significant change with greater undercooling but trending significantly lower with faster cooling rate. $n = 4$. Red box: best-case parameters tested with the highest recovery. **(B)** Post-thaw reattachment of D14 mSN, normalized to reattachment of dissociated fresh cell control, showing no significant difference between any of the test conditions. $n = 4$. Crossed-out columns denoting insensitive post-thaw assay due to poor outcome of control cells. **(C)** Calcein AM-stained culture 24 and 48 h after replating dissociated (fresh) or cryopreserved (best-case) D14 mSN, showing a vast majority of live (calcein AM positive) cell population nonadherent or with rounded morphology in the first 24 h that was more sparsely distributed in the post-thaw culture, as well as subsequent nearly complete cell loss in both conditions at 48 h. Scale bar: 100 µm.

be found to describe the cryopreservation of these cells. One of these few studies reported the cryopreservation of primary mouse cortical and dopaminergic neurons in DMSO-containing formulations and subsequent phenotypic characterization of the cryopreserved cells at 2 and 4 weeks post-thaw (Pischedda et al., 2018), without survival data obtained in shorter terms post-thaw, which was not directly comparable with results in the present study. Another study reported the cryopreservation of primary mouse motor neurons in DMSO and post-thaw cell recovery rate of 68.8% (Parker et al., 2018). There were two accounts of cryopreserved dopaminergic progenitors and neurons derived from hiPSCs and human embryonic stem cells (hESCs), with the highest reported post-thaw recovery approaching 50% upon 24-h treatment in apoptosis inhibitors (Wakeman et al., 2017; Drummond et al., 2020). In comparison, the present study demonstrated DMSO-free cryopreservation of

neuronal cells, with post-thaw survival of D5 crest measured at 91.6% immediately post-thaw, 88.2% 24 h post-thaw, and of D7 SN measured at 93.6% immediately post-thaw, 84.1% 24 h post-thaw, all of which were significantly higher than 50% ($p < 0.05$) even without the use of apoptosis inhibitor. The methodology and results of this investigation represent a significant addition to the scientific literature related to the cryopreservation of hiPSC-derived sensory neurons and their progenitors. Its outcome may be validated using additional hiPSC lines, alternative neuronal differentiations and other tissue lineages.

Cell Loss Before Freezing and After Thawing Challenges *in Vitro* Neuronal Cell Production

A commonly recognized process bottleneck in the developing supply chain of hiPSC-derived cryopreserved cell therapies has been the temporal restriction on the fill-and-finish step immediately preceding the freezing of cells to minimize cell loss due to DMSO cytotoxicity (Yuan et al., 2014; de Abreu Costa et al., 2017; Pollock et al., 2017; Verheijen et al., 2019). As demonstrated in **Figure 2**, the non-DMSO CPA molecules used in this study (i.e., sucrose, glycerol, isoleucine, P188, HSA) provided a superior alternative to the widely used DMSO in preserving cell viability before freezing. This result supports the transition from DMSO to non-DMSO in order to enable scale-up of the fill-and-finish process in a manufacturing setting, while adhering to a high batch consistency. Compared with DMSO whose cytotoxicity arises from dissolution, epigenetic and genomic alteration, these non-DMSO CPAs, typically with larger molecular weight than DMSO, can cause pre-freeze cell loss predominantly due to osmotic stress upon CPA introduction (Best, 2015; Hornberger et al., 2021; Matsumura et al., 2021). Compared with D5 crest and D7 SN, which exhibited no significant cell loss over the course of prefreeze exposure to the non-DMSO CPA solution ($p > 0.05$), D14 mSN experienced minor (10%) yet significant ($p < 0.05$) decrease in viable cell count during the first 30 min of this process, suggesting that sensitivity to the osmotic stress varied by cell stage with the most mature cells being most sensitive. Prefreeze CPA exposure testing in this study of these neuronal cells in the non-DMSO solution may be expanded in a future study to include longer times of exposure and determine the time limit for a given quality control (QC) range of cell viability.

Membrane Fluidity Informs Undercooling Sensitivity and Cryopreservation Design

Literature in the field of gamete cryobiology has explored and demonstrated the inverse correlation between membrane fluidity and desirable cryopreservation outcome such as motility of recovered spermatozoa (Giraud et al., 2000; Blesbois et al., 2005). In addition, Noutsi et al. (2016) showed the varying extent of fluctuation in membrane fluidity among a selection of cell lines over the course of 4-day static cultures and spontaneous differentiation. These previous studies have required highly specialized spectrofluorometer or two-photon fluorescent microscopy to quantify membrane fluidity for their measurement, both of which are limited by low throughput and adaptability.

We found that membrane fluidity trended lower as differentiation and maturation progressed. The decrease in membrane fluidity was consistent with the increase in undercooling sensitivity of the cells. This result supports the correlation between membrane fluidity and cell freezing damage previously postulated in literature (Giraud et al., 2000; Blesbois et al., 2005) and provides more in-depth evidence specifying the nature of freezing damages as intracellular ice and cell disintegration consequent of extensive undercooling. On one hand, cells like D5 crest with very high membrane fluidity may exhibit little to no sensitivity to changes in ice nucleation temperature. On the other hand, cells like D14 mSN with low membrane fluidity would require a tight control of ice nucleation temperature (e.g., −3 to −7°C) in order to ensure the same level of consistency in their post-thaw cell survival and function.

One may note that despite having relatively higher membrane fluidity than hiPSC aggregates and utilizing the same non-DMSO CPA formulation, D14 mSN responded significantly more poorly to undercooling (**Figures 3** and **6**) than hiPSC aggregates (Li et al., 2020). Membrane fluidity alone may not reflect undercooling sensitivity of a given cell type. Other factors may include intracellular and transmembrane diffusion rates of water and the cell-penetrating CPA molecules (i.e., glycerol) for the given cell sample, as well as membrane partitioning of glycerol and its effect on the molecular interaction between intracellular CPA and water. With greater undercooling, kinetic energy and molecular motion are lower, and upon ice nucleation in the extracellular space, more rigid plasma membrane may not allow water molecules to transport quickly enough from the intracellular space following the sudden increase in the transmembrane concentration differential to avoid intracellular ice formation. Low membrane permeability may decrease the probability of water leaving the intermolecular hydrogen bond network and increase the probability of intracellular ice formation. Dense membrane-cytoskeletal organization may slow down the diffusion of water and CPAs in the cytoplasm and reduce the probability of uniform cryoprotection inside the cell. Shift in the membrane property associated with differentiation or aggregation of hiPSCs may change the partitioning of glycerol as observed by Raman and potentially deviate the local molecular balance from its sweet spot that was seen (Li et al., 2020) to mitigate undercooling stresses for hiPSCs.

It is also important to note that the non-DMSO solution was found to eliminate chunky, lethal intracellular ice formation regardless of the cell stage, whereas the DMSO-based solution was observed to result in significant amounts of such ice crystals when subjected to the same degree of undercooling. As membrane fluidity may drop as cells differentiate and mature, it becomes increasingly important to transition from DMSO, or a single-CPA non-DMSO alternative formulation, to a non-DMSO CPA cocktail like the one used in this study, in order to counter the intrinsic cell vulnerability to undercooling with proper cryoprotection and consequently improve the consistency of cryopreservation outcome and flexibility of CRF in hiPSC-based cell manufacturing.

Cell Size Measurement Informs Cooling Rate Sensitivity and Cooling Rate Selection

It has been hypothesized and demonstrated in cryobiological literature (Gao and Critser, 2000; Hubel, 2018) that the relationship between cooling rate and cryopreservation outcome for a given cell type should resemble an inverted "U," and that the optimal cooling rate of different cell types correlate with their difference in cell size. Within the cooling rate range (−1 to −5°C/min) tested in this study, the optimal cooling rate for D5 crest lay near or below −1°C/min, −3°C/min for D7 SN around, and for D14 mSN also near or below -1°C/min but skewed to a likely slower optimal cooling rate than that of D5 crest. This relativity in optimal cooling rate was consistent with their different cell sizes, where the larger cells (i.e., D14 mSN > D5 crest) require a slower cooling rate (i.e., −1°C/min and potentially lower) to avoid lethal intracellular ice formation.

Interestingly, compared with the nearly 50% drop in post-thaw reattachment of larger cell (D5 crest) along with the increase in cooling rate from −1 to −3°C/min, the decrease in cooling rate from −3 to −1°C/min resulted in less cell loss (i.e., 5% drop in post-thaw reattachment) in the smaller cell (D7 SN). Consistent with what was previously proposed (Gao and Critser, 2000), cooling rate sensitivity is most critical toward large cells with higher than optimal cooling rates. Insulative passive freezing devices and liquid nitrogen-free controlled rate freezers are limited by the typical maximum momentary cooling rate of −2°C/min, where freezing damage by fast cooling may not be a primary concern in their applications. In liquid nitrogen-based controlled rate freezing applications, measuring cell diameter in suspension by light microscopy may be useful to determine whether the cell form of interest requires a slower cooling rate to decrease the probability of freezing damages or relaxes the acceptable range to accommodate deviations toward faster cooling rates or intentional use of accelerated programs.

Dissociation of Adherent Culture Remains a Challenge to Cell Cryopreservation

This investigation revealed a critical challenge to the successful cryopreservation of hiPSC-derived cells. The interruption of culture on day 5 created a barrier to neuronal induction of neural crest cells, and the 90-min Accumax treatment on day 14 failed to produce a viable culture of mature sensory neurons, with or without cryopreservation. Transcriptomic analyses in recent publications (Khan et al., 2016; Adam et al., 2017; Mattei et al., 2020; Miyawaki-Kuwakado et al., 2021) showed that enzymatic dissociation can alter the gene expression of cells in a fashion that is independent of the treatment concentration, duration, and temperature but dependent on the enzyme species. Therefore, in order to successfully cryopreserve intermediate cell stages of an hiPSC differentiation like D5 crest or advanced cell stages of maturation like D14 mSN, it will be critical to optimize the cell dissociation protocol, especially the molecular species if using an enzymatic method, minimizing cell loss, changes in the gene expression, and deviation from the intended cell developmental trajectory.

A recent study demonstrated vitrification of adherent hiPSC-derived neural progenitor cells using the TWIST method with 80% post-thaw recovery. While the methodology of vitrification is limited in scalability, advances as such in improving its sterility and future studies in validating the method for more differentiated, mature cell stages may present practical value toward *in situ* cryopreservation of hiPSC-derived 2D adherent culture at laboratory scale. Furthermore, while slow freezing has been predominantly used for cryopreserving single-cell suspensions, its feasibility for *in situ* cryopreservation of adherent cell sheet was recently demonstrated for readily implantable hiPSC-derived retinal pigment epithelium (Pennington et al., 2021). The 3D spheroid suspension culture of hiPSCs and differentiated cells has recently gained popularity due to its scalability demanded by preclinical and clinical cell production (Chen et al., 2015; Kwok et al., 2018; Takahashi et al., 2018). Cryopreservation of hiPSC-derived cell spheroids may be studied in the future to examine how the effect of cryopreservation on continuity of differentiation varies between different modalities.

DATA AVAILABILITY STATEMENT

The original contributions presented in the study are included in the article/**Supplementary Material**. Further inquiries can be directed to the corresponding author.

AUTHOR CONTRIBUTIONS

RL, JD, and AH conceptualized the article. RL, PW, and VT designed, acquired, analyzed, and interpreted the data, and drafted and wrote the manuscript. RL, PW, VT, AP, JD, and AH revised the manuscript and approved the final version of the manuscript.

FUNDING

This work was supported by the National Institutes of Health (R01EB023880, R01HL154734), National Science Foundation Innovation Corps (1951443), and ERC ATP-Bio (1941543).

ACKNOWLEDGMENTS

The Raman spectroscopy in this work was carried out in the Characterization Facility, University of Minnesota, which receives partial support from the NSF through the MRSEC program. The authors thank their colleague Peter Dosa for providing insightful feedback on the manuscript.

SUPPLEMENTARY MATERIAL

The Supplementary Material for this article can be found online at: https://www.frontiersin.org/articles/10.3389/fcell.2021.796960/full#supplementary-material

REFERENCES

Adam, M., Potter, A. S., and Potter, S. S. (2017). Psychrophilic Proteases Dramatically Reduce Single Cell RNA-Seq Artifacts: A Molecular Atlas of Kidney Development. *Development* 144, 3625–3632. doi:10.1242/dev.151142

Beier, A. F., Schulz, J. C., and Zimmermann, H. (2013). Cryopreservation with a Twist - towards a Sterile, Serum-free Surface-Based Vitrification of hESCs. *Cryobiology* 66, 8–16. doi:10.1016/J.CRYOBIOL.2012.10.001

Best, B. P. (2015). Cryoprotectant Toxicity: Facts, Issues, and Questions. *Rejuvenation Res.* 18, 422–436. doi:10.1089/rej.2014.1656

Blesbois, E., Grasseau, I., and Seigneurin, F. (2005). Membrane Fluidity and the Ability of Domestic Bird Spermatozoa to Survive Cryopreservation. *Reproduction* 129, 371–378. doi:10.1530/rep.1.00454

Brownjohn, P. W., Smith, J., Portelius, E., Serneels, L., Kvartsberg, H., De Strooper, B., et al. (2017). Phenotypic Screening Identifies Modulators of Amyloid Precursor Protein Processing in Human Stem Cell Models of Alzheimer's Disease. *Stem Cel Rep.* 8, 870–882. doi:10.1016/J.STEMCR.2017.02.006

Burkhardt, M. F., Martinez, F. J., Wright, S., Ramos, C., Volfson, D., Mason, M., et al. (2013). A Cellular Model for Sporadic ALS Using Patient-Derived Induced Pluripotent Stem Cells. *Mol. Cell Neurosci.* 56, 355–364. doi:10.1016/J.MCN.2013.07.007

Chen, V. C., Ye, J., Shukla, P., Hua, G., Chen, D., Lin, Z., et al. (2015). Development of a Scalable Suspension Culture for Cardiac Differentiation from Human Pluripotent Stem Cells. *Stem Cel Res.* 15, 365–375. doi:10.1016/J.SCR.2015.08.002

de Abreu Costa, L., Henrique Fernandes Ottoni, M., dos Santos, M., Meireles, A., Gomes de Almeida, V., de Fátima Pereira, W., et al. (2017). Dimethyl Sulfoxide (DMSO) Decreases Cell Proliferation and TNF-α, IFN-γ, and IL-2 Cytokines Production in Cultures of Peripheral Blood Lymphocytes. *Molecules* 22, 1789. doi:10.3390/molecules22111789

Deshpande, A., Yadav, S., Dao, D. Q., Wu, Z.-Y., Hokanson, K. C., Cahill, M. K., et al. (2017). Cellular Phenotypes in Human iPSC-Derived Neurons from a Genetic Model of Autism Spectrum Disorder. *Cel Rep.* 21, 2678–2687. doi:10.1016/j.celrep.2017.11.037

Drummond, N. J., Dolt, K. S., Canham, M. A., Kilbride, P., Morris, G. J., and Kunath, T. (2020). Cryopreservation of Midbrain Dopaminergic Neural Cells Differentiated from Human Embryonic Stem Cells. bioRxiv. doi:10.1101/2020.02.11.944272

Egawa, N., Kitaoka, S., Tsukita, K., Naitoh, M., Takahashi, K., Yamamoto, T., et al. (2012). Drug Screening for ALS Using Patient-specific Induced Pluripotent Stem Cells. *Sci. Transl. Med.* 4, 145ra104. doi:10.1126/scitranslmed.3004052

Engle, S. J., Blaha, L., and Kleiman, R. J. (2018). Best Practices for Translational Disease Modeling Using Human iPSC-Derived Neurons. *Neuron* 100, 783–797. doi:10.1016/j.neuron.2018.10.033

Fujimori, K., Ishikawa, M., Otomo, A., Atsuta, N., Nakamura, R., Akiyama, T., et al. (2018). Modeling Sporadic ALS in iPSC-Derived Motor Neurons Identifies a Potential Therapeutic Agent. *Nat. Med.* 24, 1579–1589. doi:10.1038/s41591-018-0140-5

Gao, D., and Critser, J. K. (2000). Mechanisms of Cryoinjury in Living Cells. *ILAR J.* 41, 187–196. doi:10.1093/ilar.41.4.187

Germann, A., Oh, Y.-J., Schmidt, T., Schön, U., Zimmermann, H., and von Briesen, H. (2013). Temperature Fluctuations during Deep Temperature Cryopreservation Reduce PBMC Recovery, Viability and T-Cell Function. *Cryobiology* 67, 193–200. doi:10.1016/J.CRYOBIOL.2013.06.012

Giraud, M. N., Motta, C., Boucher, D., and Grizard, G. (2000). Membrane Fluidity Predicts the Outcome of Cryopreservation of Human Spermatozoa. *Hum. Reprod.* 15, 2160–2164. doi:10.1093/humrep/15.10.2160

Höing, S., Rudhard, Y., Reinhardt, P., Glatza, M., Stehling, M., Wu, G., et al. (2012). Discovery of Inhibitors of Microglial Neurotoxicity Acting through Multiple Mechanisms Using a Stem-Cell-Based Phenotypic Assay. *Cell Stem Cell* 11, 620–632. doi:10.1016/J.STEM.2012.07.005

Hornberger, K., Li, R., Duarte, A. R. C., and Hubel, A. (2021). Natural Deep Eutectic Systems for Nature-inspired Cryopreservation of Cells. *Aiche J.* 67, e17085. doi:10.1002/aic.17085

Hubel, A. (2018). *Preservation of Cells: A Practical Manual*. Hoboken, NJ, USA: John Wiley & Sons. doi:10.1002/9781118989883Preservation of Cells

Hunt, C. J. (2011). Cryopreservation of Human Stem Cells for Clinical Application: A Review. *Transfus. Med. Hemother* 38, 107–123. doi:10.1159/000326623

John Morris, G., and Acton, E. (2013). Controlled Ice Nucleation in Cryopreservation - A Review. *Cryobiology* 66, 85–92. doi:10.1016/J.CRYOBIOL.2012.11.007

Khan, S. J., Abidi, S. N. F., Tian, Y., Skinner, A., and Smith-Bolton, R. K. (2016). A Rapid, Gentle and Scalable Method for Dissociation and Fluorescent Sorting of Imaginal Disc Cells for mRNA Sequencing. *Fly* 10, 73–80. doi:10.1080/19336934.2016.1173296

Ko, H. C., and Gelb, B. D. (2014). Concise Review: Drug Discovery in the Age of the Induced Pluripotent Stem Cell. *Stem Cell Transl. Med.* 3, 500–509. doi:10.5966/sctm.2013-0162

Kondo, T., Imamura, K., Funayama, M., Tsukita, K., Miyake, M., Ohta, A., et al. (2017). iPSC-Based Compound Screening and *In Vitro* Trials Identify a Synergistic Anti-amyloid β Combination for Alzheimer's Disease. *Cel Rep.* 21, 2304–2312. doi:10.1016/J.CELREP.2017.10.109

Kwok, C. K., Ueda, Y., Kadari, A., Günther, K., Ergün, S., Heron, A., et al. (2018). Scalable Stirred Suspension Culture for the Generation of Billions of Human Induced Pluripotent Stem Cells Using Single-use Bioreactors. *J. Tissue Eng. Regen. Med.* 12, e1076–e1087. doi:10.1002/term.2435

Li, R., Hornberger, K., Dutton, J. R., and Hubel, A. (2020). Cryopreservation of Human iPS Cell Aggregates in a DMSO-free Solution-An Optimization and Comparative Study. *Front. Bioeng. Biotechnol.* 8, 1. doi:10.3389/fbioe.2020.00001

Li, R., Yu, G., Azarin, S. M., and Hubel, A. (2018). Freezing Responses in DMSO-Based Cryopreservation of Human iPS Cells: Aggregates versus Single Cells. *Tissue Eng. C: Methods* 24, 289–299. doi:10.1089/ten.tec.2017.0531

Linville, R. M., DeStefano, J. G., Nerenberg, R. F., Grifno, G. N., Ye, R., Gallagher, E., et al. (2020). Long-Term Cryopreservation Preserves Blood-Brain Barrier Phenotype of iPSC-Derived Brain Microvascular Endothelial Cells and Three-Dimensional Microvessels. *Mol. Pharmaceutics* 17, 3425–3434. doi:10.1021/acs.molpharmaceut.0c00484

Matsumura, K., Hayashi, F., Nagashima, T., Rajan, R., and Hyon, S.-H. (2021). Molecular Mechanisms of Cell Cryopreservation with Polyampholytes Studied by Solid-State NMR. *Commun. Mater.* 2, 15. doi:10.1038/s43246-021-00118-1

Mattei, D., Ivanov, A., van Oostrum, M., Pantelyushin, S., Richetto, J., Mueller, F., et al. (2020). Enzymatic Dissociation Induces Transcriptional and Proteotype Bias in Brain Cell Populations. *Ijms* 21, 7944. doi:10.3390/ijms21217944

Mazzola, M., and Di Pasquale, E. (2020). Toward Cardiac Regeneration: Combination of Pluripotent Stem Cell-Based Therapies and Bioengineering Strategies. *Front. Bioeng. Biotechnol.* 8, 455. doi:10.3389/fbioe.2020.00455

McNeish, J., Roach, M., Hambor, J., Mather, R. J., Weibley, L., Lazzaro, J., et al. (2010). High-throughput Screening in Embryonic Stem Cell-Derived Neurons Identifies Potentiators of α-Amino-3-hydroxyl-5-methyl-4-isoxazolepropionate-type Glutamate Receptors. *J. Biol. Chem.* 285, 17209–17217. doi:10.1074/JBC.M109.098814

Miyawaki-Kuwakado, A., Wu, Q., Harada, A., Tomimatsu, K., Fujii, T., Maehara, K., et al. (2021). Transcriptome Analysis of Gene Expression Changes upon Enzymatic Dissociation in Skeletal Myoblasts. *Genes Cells* 26, 530–540. doi:10.1111/gtc.12870

Naaldijk, Y., Johnson, A. A., Friedrich-Stöckigt, A., and Stolzing, A. (2016). Cryopreservation of Dermal Fibroblasts and Keratinocytes in Hydroxyethyl Starch-Based Cryoprotectants. *BMC Biotechnol.* 16, 85. doi:10.1186/s12896-016-0315-4

Nazarpour, R., Zabihi, E., Alijanpour, E., Abedian, Z., Mehdizadeh, H., and Rahimi, F. (2012). Optimization of Human Peripheral Blood Mononuclear Cells (PBMCs) Cryopreservation. *Int. J. Mol. Cell. Med.* 1, 88–93. Available at: http://www.ncbi.nlm.nih.gov/pubmed/24551763.

Nishiyama, Y., Iwanami, A., Kohyama, J., Itakura, G., Kawabata, S., Sugai, K., et al. (2016). Safe and Efficient Method for Cryopreservation of Human Induced Pluripotent Stem Cell-Derived Neural Stem and Progenitor Cells by a Programmed Freezer with a Magnetic Field. *Neurosci. Res.* 107, 20–29. doi:10.1016/J.NEURES.2015.11.011

Nixdorf-Bergweiler, B. E. (1998). Enlargement of Neuronal Somata in the LMAN Coincides with the Onset of Sensorimotor Learning for Song. *Neurobiol. Learn. Mem.* 69, 258–273. doi:10.1006/NLME.1998.3819

Noutsi, P., Gratton, E., and Chaieb, S. (2016). Assessment of Membrane Fluidity Fluctuations during Cellular Development Reveals Time and Cell Type Specificity. *PLoS One* 11, e0158313. doi:10.1371/journal.pone.0158313

Parker, S. S., Moutal, A., Cai, S., Chandrasekaran, S., Roman, M. R., Koshy, A. A., et al. (2018). High Fidelity Cryopreservation and Recovery of Primary Rodent Cortical Neurons. *eNeuro* 5 (5), 1–12. doi:10.1523/ENEURO.0135-18.2018

Pennington, B. O., Bailey, J. K., Faynus, M. A., Hinman, C., Hee, M. N., Ritts, R., et al. (2021). Xeno-free Cryopreservation of Adherent Retinal Pigmented Epithelium Yields Viable and Functional Cells *In Vitro* and *In Vivo*. *Sci. Rep.* 11, 6286. doi:10.1038/s41598-021-85631-6

Pi, C.-H., Hornberger, K., Dosa, P., and Hubel, A. (2020). Understanding the Freezing Responses of T Cells and Other Subsets of Human Peripheral Blood Mononuclear Cells Using DSMO-free Cryoprotectants. *Cytotherapy* 22, 291–300. doi:10.1016/j.jcyt.2020.01.013

Pischedda, F., Montani, C., Obergasteiger, J., Frapporti, G., Corti, C., Rosato Siri, M., et al. (2018). Cryopreservation of Primary Mouse Neurons: The Benefit of Neurostore Cryoprotective Medium. *Front. Cell. Neurosci.* 12, 81. doi:10.3389/fncel.2018.00081

Pollock, K., Samsonraj, R. M., Dudakovic, A., Thaler, R., Stumbras, A., McKenna, D. H., et al. (2017). Improved Post-Thaw Function and Epigenetic Changes in Mesenchymal Stromal Cells Cryopreserved Using Multicomponent Osmolyte Solutions. *Stem Cell Development* 26, 828–842. doi:10.1089/scd.2016.0347

Ragoonanan, V., Hubel, A., and Aksan, A. (2010). Response of the Cell Membrane-Cytoskeleton Complex to Osmotic and Freeze/thaw Stresses. *Cryobiology* 61, 335–344. doi:10.1016/j.cryobiol.2010.10.160

Ryan, S. D., Dolatabadi, N., Chan, S. F., Zhang, X., Akhtar, M. W., Parker, J., et al. (2013). Isogenic Human iPSC Parkinson's Model Shows Nitrosative Stress-Induced Dysfunction in MEF2-Pgc1α Transcription. *Cell* 155, 1351–1364. doi:10.1016/J.CELL.2013.11.009

Takahashi, Y., Sato, S., Kurashima, Y., Yamamoto, T., Kurokawa, S., Yuki, Y., et al. (2018). A Refined Culture System for Human Induced Pluripotent Stem Cell-Derived Intestinal Epithelial Organoids. *Stem Cel Rep.* 10, 314–328. doi:10.1016/J.STEMCR.2017.11.004

van den Brink, L., Brandão, K. O., Yiangou, L., Mol, M. P. H., Grandela, C., Mummery, C. L., et al. (2020). Cryopreservation of Human Pluripotent Stem Cell-Derived Cardiomyocytes Is Not Detrimental to Their Molecular and Functional Properties. *Stem Cel Res.* 43, 101698. doi:10.1016/j.scr.2019.101698

Verheijen, M., Lienhard, M., Schrooders, Y., Clayton, O., Nudischer, R., Boerno, S., et al. (2019). DMSO Induces Drastic Changes in Human Cellular Processes and Epigenetic Landscape *In Vitro*. *Sci. Rep.* 9, 4641. doi:10.1038/s41598-019-40660-0

Wakeman, D. R., Hiller, B. M., Marmion, D. J., McMahon, C. W., Corbett, G. T., Mangan, K. P., et al. (2017). Cryopreservation Maintains Functionality of Human iPSC Dopamine Neurons and Rescues Parkinsonian Phenotypes *In Vivo*. *Stem Cel. Rep.* 9, 149–161. doi:10.1016/j.stemcr.2017.04.033

Yamanaka, S. (2020). Pluripotent Stem Cell-Based Cell Therapy-Promise and Challenges. *Cell Stem Cell* 27, 523–531. doi:10.1016/j.stem.2020.09.014

Yang, Y. M., Gupta, S. K., Kim, K. J., Powers, B. E., Cerqueira, A., Wainger, B. J., et al. (2013). A Small Molecule Screen in Stem-Cell-Derived Motor Neurons Identifies a Kinase Inhibitor as a Candidate Therapeutic for ALS. *Cell Stem Cell* 12, 713–726. doi:10.1016/J.STEM.2013.04.003

Ye, L., Zhang, S., Greder, L., Dutton, J., Keirstead, S. A., Lepley, M., et al. (2013). Effective Cardiac Myocyte Differentiation of Human Induced Pluripotent Stem Cells Requires VEGF. *PLoS One* 8, e53764. doi:10.1371/journal.pone.0053764

Yu, G., Li, R., and Hubel, A. (2021). "Raman Cryomicroscopic Imaging and Sample Holder for Spectroscopic Subzero Temperature Measurements," in *Methods In Molecular Biology: Cryopreservation And Freeze-Drying Protocols*. Editors W. F. Wolkers and H. Oldenhof (Springer Nature), 351–361. doi:10.1007/978-1-0716-0783-1_14

Yuan, C., Gao, J., Guo, J., Bai, L., Marshall, C., Cai, Z., et al. (2014). Dimethyl Sulfoxide Damages Mitochondrial Integrity and Membrane Potential in Cultured Astrocytes. *PLoS One* 9, e107447. doi:10.1371/journal.pone.0107447

Conflict of Interest: AH has an issued patent # 10314302, and authors RL and AH have an international patent application # PCT/US2020/029847 related to this work and owned by Regents of the University of Minnesota.

The remaining authors declare that the research was conducted in the absence of any commercial or financial relationships that could be construed as a potential conflict of interest.

Publisher's Note: All claims expressed in this article are solely those of the authors and do not necessarily represent those of their affiliated organizations, or those of the publisher, the editors, and the reviewers. Any product that may be evaluated in this article, or claim that may be made by its manufacturer, is not guaranteed or endorsed by the publisher.

frontiers in Cell and Developmental Biology

REVIEW
published: 17 December 2021
doi: 10.3389/fcell.2021.760515

Circular RNA Expression for Dilated Cardiomyopathy in Hearts and Pluripotent Stem Cell–Derived Cardiomyocytes

Yiyu Zhang[1], Guoqing Huang[1], Zhaohu Yuan[2]*, Yonggang Zhang[1] and Rong Chang[1]**

[1]Department of Blood Transfusion, Department of Cardiology, Shenzhen Longhua District Central Hospital, The Affiliated Central Hospital of Shenzhen Longhua District, Guangdong Medical University, Shenzhen, China, [2]Department of Blood Transfusion, Guangzhou First People's Hospital, School of Medicine, South China University of Technology, Guangzhou, China

OPEN ACCESS

Edited by:
Valerie Kouskoff, The University of Manchester, United Kingdom

Reviewed by:
Michel Puceat, Institut National de la Santé et de la Recherche Médicale (INSERM), France
Jing Liu, Tongji University, China

***Correspondence:**
Yiyu Zhang
fengdezhijian2020@126.com
Zhaohu Yuan
eyyuanzhaohu@scut.edu.cn
Rong Chang
qhschangrong@126.com

Specialty section:
This article was submitted to Stem Cell Research, a section of the journal Frontiers in Cell and Developmental Biology

Received: *18 August 2021*
Accepted: *17 November 2021*
Published: *17 December 2021*

Citation:
Zhang Y, Huang G, Yuan Z, Zhang Y and Chang R (2021) Circular RNA Expression for Dilated Cardiomyopathy in Hearts and Pluripotent Stem Cell–Derived Cardiomyocytes. Front. Cell Dev. Biol. 9:760515. doi: 10.3389/fcell.2021.760515

Dilated cardiomyopathy (DCM) is a type of heart disease delimited by enlargement and dilation of one or both of the ventricles along with damaged contractility, which is often accompanied by the left ventricular ejection fraction (LVEF) less than 40%. DCM is progressive and always leads to heart failure. Circular RNAs (circRNAs) are unique species of noncoding RNAs featuring high cell-type specificity and long-lasting conservation, which normally are involved in the regulation of heart failure and DCM recently. So far, a landscape of various single gene or polygene mutations, which can cause complex human cardiac disorders, has been investigated by human-induced pluripotent stem cell (hiPSC) technology. Furthermore, DCM has been modeled as well, providing new perspectives on the disease study at a cellular level. In addition, current genome editing methods can not only repair defects of some genes, but also rescue the disease phenotype in patient-derived iPSCs, even introduce pathological-related mutations into wild-type strains. In this review, we gather up the aspects of the circRNA expression and mechanism in the DCM disease scenario, facilitating understanding in DCM development and pathophysiology in the molecular level. Also, we offer an update on the most relevant scientific progress in iPSC modeling of gene mutation–induced DCM.

Keywords: circular RNAs, heart diseases, arrhythmia, hiPSC disease modeling, dilated cardiomyopathy

INTRODUCTION

Dilated cardiomyopathy (DCM) is genetically and phenotypically heterogenous, accompanied by left ventricular dilatation and dysfunction. It is the most common form of cardiomyopathy in both adults and children in the world. DCM is non-ischemic and progressive, with an increased risk of heart failure (Jefferies and Towbin, 2010). The continuous expansion of the ventricle leads to a decline in left ventricular ejection fraction (LVEF), which in turn leads to abnormalities in the extra myocardial matrix, ventricular arrhythmia, and heart failure. It has been assumed to cause diseases such as viral myocarditis and other rheumatological diseases, while endocrinological disorders might further contribute to occurrence of DCM (Hänselmann et al., 2020; Imanaka-Yoshida, 2020). For example, COVID-19 patients hold higher risk of developing DCM due to continuous immune activation (Komiyama et al., 2020). Importantly, the occurrence of heart failure and arrhythmia determines

patient's poor or good prognosis. Most DCM patients need transplantation to increase the survival rate.

In past several years, the study of circRNAs has opened a new avenue for survey in DCM research (Lei et al., 2018). Increasing evidences show that circRNAs have dynamic changes and tissue specificity in several different cardiovascular diseases, which are derived from DCM (Holdt et al., 2018). While DCM development is progressive, circRNAs can be used as biomarkers for DCM disease diagnosis and therapeutic targets for the single gene mutation in DCM treatment (Lei et al., 2018). Importantly, the study of function of circRNAs offers a valuable resource that can be used to further explore the diagnostic standard and treatment of DCM for tissue specificity genes in heart diseases. Because the development of disease is a long and gradual process, it is convenient to use human cells or tissue disease models as platforms for performing observation and research (Lei et al., 2018).

In this review, we not only discuss the research on mechanisms and roles of circRNAs in DCM but also talk about the hiPSC modeling method for DCM disease investigation with the function and mechanism of circRNAs.

What is DCM?

Heart failure is generally caused by either DCM or ischemic cardiomyopathy (ICM). DCM, a type of cardiomyopathy, is the leading cause of heart transplantation. It occurs most likely in young population with high mortality–morbidity risk, which is attributed to a combination of genetic and acquired triggers. So far, the clinical measure of DCM is mainly based on ejection fraction (EF) and NYHA systematization, without considering the heterogeneity of DCM (Priori et al., 2015; Ponikowski et al., 2016). Overall, nearly 40–50% of DCM patients can relieve from heart failure therapy, with a genetic basis (Merlo et al., 2011; Verdonschot et al., 2018). The clinical symptoms of DCM in children are different from those of adults in some places, such as coarse faces and slightly dilated heart (Carboni et al., 2020). Histological examination of DCM hearts shows evidence of nonspecific changes as well as myocardial hypertrophy and fibrosis (Bakalakos et al., 2018). Biopsy exposes may put patients under unnecessary risk because of idiopathic DCM being nonspecific (Palomer et al., 2018). Familial forms occupy the 40% of cases, but many pathogenic genes are irregular, intergenerational inheritance.

What is DCM-Related Gene?

While studying the role of circRNAs in the development of DCM diseases, we should primarily consider some genes related to the development of DCM disease. It is because most circRNAs are classic noncoding RNA molecules, while only a little of ribosome-associated circRNAs can produce detectable peptides (van Heesch et al., 2019). The function of circRNA has been widely confirmed as an essential role for miRNA sponges to affect mRNA expression to regulate the synthesis of disease-related proteins and/or influence its parental gene expression to produce the protein to affect the biological progress of the disease. Whether and how these circRNAs are relevant to other forms of the mechanism to regulate DCM-related mRNA remains to be studied.

Adverse consequences of DCM generally lead to heart failure, arrhythmias, and sudden cardiac death, and the fundamental reasons are attributed to genetic and environmental factors. In the past few decades, single mutations in genes encoding muscle fibers, cytoskeleton, and channel proteins have been found to be associated with DCM.

TTN truncation variants are the most common cause in DCM patients, accounting for about 20–25% of disease cases, and have the strongest causal effect with DCM3 (Gerull et al., 2002; Herman et al., 2012). The second most common cause is mutation of the LMNA gene, which accounts for about 10% of disease cases. It is worth noting that different gene mutations can cause different phenotypes of DCM, such as arrhythmic DCM (aDCM) and non-arrhythmic DCM (naDCM). In addition, the pathogenic mechanisms of some significant gene mutations which cause DCM are summarized in **Figure 1** (Fatkin et al., 1999; Li et al., 1999; Brauch et al., 2009; Herman et al., 2012). Mutations in RBM20 result in aggressive early release patterns, manifested by progressive dilation and dysfunction of the left ventricle (Hey et al., 2019). It has been found that nearly 80 different gene mutations are closely related to DCM disease, such as CAVIN4 mutations and δ-SG gene mutations.

The Regulationship Between DCM-Related circRNAs and Their Parental Gene

Previous circRNA profiles show 826 back-splice junctions in human left ventricle samples selected from hypertrophic or dilated cardiomyopathy patients, in which 80 junctions come from the titin gene transcript. TTN produces a class of circular RNAs that are dependent on RBM20, which has abundant titin reverse splice junction in introns flanking. These RBM20-dependent TTN circRNAs exclusively come from a region in the TTN transcript. Tijsen et al. found that selective loss of circ-TTN1 in hiPSC-CM leads to structural abnormalities in engineered heart tissues, cell apoptosis, and reduced contractility. Consistent with its SRSF10 binding, the loss of circ-TTN1 leads to abnormal splicing of important cardiomyocyte SRSF10 targets (such as MEF2A and CASQ2). Surprisingly, the loss of circ-TTN1 causes abnormal splicing of TTN itself (Tijsen et al., 2021).

It was compelling that circRNAs produced by titin mostly is involved in the development of heart diseases (Khan et al., 2016). Many circRNAs generated from titin have very complicated exon structures. According to the general situation, TTN circRNA generation comes from alternative splicing, while the more exons are circularized, and the less linearly mRNAs are produced (Ashwal-Fluss et al., 2014; Kelly et al., 2015). Interestingly, there is no TTN I band circRNA expression in the hearts of RBM20 knockout mice and human RBM20 mutation carriers. The corresponding exons are included in a large number of linear TTN transcripts. Meanwhile, this suggests a mechanism in which exons spliced from TTN pre-mRNA can be used as substrates to produce circRNAs (Khan et al., 2016). In addition to this mechanism, hundreds of expression levels of circRNAs are not affected by the host gene expression level, and some host genes

FIGURE 1 | Role of the DCM-related gene.

TABLE 1 | Identification and evaluation of known circRNAs in DCM patient hearts.

CircRNA	Expression in DCM	Study model	Mechanism or potential application
CircRNA (CAMK2D) Khan et al. (2016)	Down	Patient's heart	Their expression is related to RBM20 mRNA levels.
CircRNA (LAMA2) Khan et al. (2016)	Up	Patient's heart	
CircSLC8A1 Siede et al. (2017)	Up	Patient's heart	
CircCHD7 Siede et al. (2017)	Up	Patient's heart	Interact with either the ribosome or Argonaute2 protein complexes.
CircATXN10 Siede et al. (2017)	Up	Patient's heart	
CircDNA6JC Siede et al. (2017)	Down	Patient's heart	
SCAF8_e4:TIAM2_e1 Dong et al. (2020)	Down	Patient's heart	A theoretical basis for future studies of circRNAs in DCM.
SCAF8_e4:TIAM2_e2 Dong et al. (2020)	Down	Patient's heart	
CircFBLN1_5 Dong et al. (2020)	Up	Patient's heart	
CircNLGN1_1 Dong et al. (2020)	Down	Patient's heart	
CircABCC1_9 Dong et al. (2020)	Up	Patient's heart	
CircHERC4_11 Dong et al. (2020)	Down	Patient's heart	
CircTTN_34, 52,70,132 Dong et al. (2020)	Down	Patient's heart	
CircRYR2_71,95 Dong et al. (2020)	Down	Patient's heart	
Has_circ_0067735 Sun et al. (2020)	Down	Child patient's heart	Serve as non-invasive diagnostic biomarkers.
Has_circ_0070186 Sun et al. (2020)	Up	Child patient's heart	
Has_circ_0069972 Sun et al. (2020)	Down	Child patient's heart	
Chr7:8257935–8275635– Lin et al. (2021)	Up	Patient's heart	A theoretical basis for future studies of circRNAs in DCM.
Chr4:187627717–187630999– Lin et al. (2021)	Up	Patient's heart	
Chr1:219352489–219385095+ Lin et al. (2021)	Up	Patient's heart	
Chr5:158204421–158267118– Lin et al. (2021)	Down	Patient's heart	
Chr1:247200894–247202839– Lin et al. (2021)	Down	Patient's heart	
Chr13:35615070–35672542+ Lin et al. (2021)	Down	Patient's heart	

can independently regulate their circRNAs (Siede et al., 2017). The same host gene has different exon splicing, which can produce circRNA variants in different cells (Hu et al., 2019).

circRNAs in the DCM Study

circRNAs in the DCM Patient Heart

After digesting linear RNA with the RNase R, a large number of circular RNAs (circRNAs) are identified by RNA sequencing *via* a high-throughput sequencing platform in DCM patients (**Table 1**).

Dong et al. characterized the circRNA profile landscape of the DCM adult patient's heart and found there are 392 circRNAs consisting of 101 upregulated and 291 downregulated circRNAs ($p < 0.05$ and FC > 2), while most of the dysregulation of circRNAs are downregulated. Notably, circRNAs in DCM are initiated from heart disease–related gene loci, which include the Rt-circRNAs produced from exons of two different neighboring genes, such as Rt-circRNA from SCAF8 and TIAM2, which very likely tend to bind with heart disease–related miRNA. It led to hypothesize that circALMS1_6 could sponge with miR-133, which plays an important role in cardiac remodeling (Dong et al., 2020). Furthermore, along a clinical investigation in identifying the roles of circRNAs in cardiac systolic and diastolic function, Lin et al. constructed the circRNAs–miRNA–mRNA gene regulatory networks including 9,585 circRNAs (231 upregulated and 85 downregulated) and 22,050 mRNAs (617 upregulated and 1125 downregulated). The comprehensive dataset assessed that the downregulated mRNA would inhibit cardiac systolica, and lack of some circRNAs would lead to DCM (Lin et al., 2021).

In addition, Sun et al. carried out a circRNA profile in 25 child patients screening novel non-invasive biomarkers for early

PDCM diagnosis (Sun et al., 2020). A total of 1,156 circRNAs have the differential expression profile in PDCM under condition of fold change >2 and $p < 0.05$, including 257 upregulated and 899 downregulated circRNAs. Has_circ_0067735 and has_circ_0070186 target mRNA CACNA2D2 and IGF1. They are associated with DCM according to KEGG. "Response to wounding," "inflammatory response," and "cytokine secretion" are the most enrichment GO biological processes of PDCM-associated circRNAs (Sun et al., 2020), and this is different from DCM adult patients.

Recent studies show that circRYR2_71 and circRYR2_95 are downregulated in the DCM patient heart (Dong et al., 2020). Ji et al. explored the molecular pathways in miR-31-5p KO mice and cultured cardiomyocytes demonstrating the alleviated myocardial apoptosis *via* quaking and circular RNA Pan3 induced by doxorubicin treatment and QKI gene as a direct target of miR-31-5p (Ji et al., 2020). Research on the RNA-binding protein quaking (Qki) provides more evidences to support the role of the circRNA in dilated cardiomyopathy (Gupta et al., 2018). Qki5 overexpression attenuates dox-induced cardiotoxicity by inhibiting cardiac apoptosis. Special circRNAs back splice and Strn3, Fhod3, and titin have been regulated by Qki5. Importantly, sensitivity of heart cell lines toward DOX toxicity targets inhibition of titin-derived circRNAs (Gupta et al., 2018). This study indicates the important role of the circRNA in DCM in previous doctrine (Khan et al., 2016). Interestingly, van Heesch et al. reported 40 circRNAs, such as the famous CDR1as and circSLC8A1, were found to encode small peptides in the DCM patient hearts (van Heesch et al., 2019). It is worth noting that the parental gene type was determined by the specific function of circRNA itself. To be more specific, according to the healthy heart and DCM heart data, it is found that the parent genes of AUG circRNA are mostly involved in protein modification, such as ubiquitination and poly ubiquitination, while the parent genes of non-AUG circRNA are enriched in structures that bind to RNA (Stagsted et al., 2019).

circRNAs in DCM iPSC-CMs

The study by Siede et al. and Tan et al. provides important evidences for the involvement of circRNAs in the hiPSC-CM model (Siede et al., 2017; Tan et al., 2017). Both hiPSC-CMs and human hearts show thousands of exclusively expressed circRNAs which were conserved (3874 and 6672, respectively). Due to the conservation, it is possible to study these circRNAs in large animal models as well as in human-derived cardiac cells. Both in heart development and stress treatment, dynamically variable of cicRNA expression is existed in the hiPSC-CM model. CircRNAs reverse shear produced from the exon transcript of six protein-coding genes, such as SLC8A1, ARID1A, FNDC3B, CACNA1D, SPHKAP, and ALPK2, which are highly enriched in hiPSC-CMs. In contrast, the expression levels of circAASS, circFIRRE, and circTMEFF1 are notably lower in hiPSC-CMs (Lei et al., 2018). Deep circRNA sequencing of cardiomyocyte development used in β-adrenergic stimulation revealed 4,518 circRNAs, of which the host gene set is enriched with chromatin modifiers and GTPase activity regulators (Siede et al., 2017). In addition to circ-CAMK2D and circ-LAMA2 which have statistical difference, circCACNA1D, circ-RYR2-1, circ-SLC8A1, circ-TNNI3K, circ-TTN1, circ-TTN2, circ-TTN3, circ-TTN4, and circ-TTN5 were found in the DCM patient heart with no significant difference (Khan et al., 2016).

Lei et al. detected some circRNAs, including circSLC8A1, circCACNA1D, circSPHKAP, and circALPK2, highlight their expressions during cardiac differentiation by human-induced pluripotent stem cells (hiPSCs) (Lei et al., 2018). The expression level of these circRNAs increases during cardiac differentiation and among them, circSLC8A1 is the highest level expression during differentiation. According to their high enrichment in hiPSC-derived cardiomyocytes, it led to infer that they have potential to serve as biomarkers of CMs. A previous study revealed differential expression levels of 226 circRNAs during the differentiation of human umbilical cord–derived mesenchymal stem cells into cardiomyocyte-like cells (Ruan et al., 2019). Cardiomyocyte differentiation from hiPSCs is accompanied by changes in gene expression. For example, TnnT2, Mef2c, and Myl7 are clearly upregulated in this differentiation process (Siede et al., 2017). Nkx2.5 and Isl1 are known to be expressed in early stages of cardiac formation. Furthermore, the pluripotent genes or cell type intermediate genes such as TBrachyury, MESP1, POU5F1 (OCT4), Nanog, and KLF4 are downregulated in the process toward cardiomyocyte conversion (Siede et al., 2017). These findings indicate that certain tissue- and stage-specific circRNAs can be used as biomarkers in the process of cardiomyocyte differentiation (Jakobi et al., 2020).

Use of hiPSCs for the Study of circRNAs in DCM

The hiPSC-CM model with the p.S143P LMNA mutation successfully elucidated the mechanisms linking the LMNA alteration and its effect on DCM illness. Progressive arrhythmia or even severe arrhythmia occurs, which is similar to the clinical phenotype of DCM in patients with the p.S143P LMNA mutation, and this often leads to heart failure or sudden deaths. In addition, in the hiPSC-CM model, variability of pulsation rate, handling of abnormal calcium, and augment of sensitivity about pressure are the main causes of disease including atrioventricular conduction defects and ventricular systolic and diastolic dysfunction. Under the treatment of hypoxia stress, the disintegration of the sarcomere structure in myofibrils of hiPSC-CM shows an increasing trend. The construction of this model suggests that whether cells expressing P.S143P LaminA/C or other DCM-related mutants share some common DCM phenotypes and pathogenic characteristics, which is very important for finding suitable drugs for treatment (Shah et al., 2019).

Studies with the gene knock-in animal model and/or hiPSC-CM model would get confidential evidences of the genotype–phenotype correlation, and therefore they offer a powerful tool to interpret the physiological functions of gene mutation–related heart diseases. When establishing a preliminary model of DCM-related circRNA disease, it is necessary to select a circRNA that has a weak effect on the expression of the parental gene, which is helpful to eliminate the interference if the parental gene has a function in the DCM disease

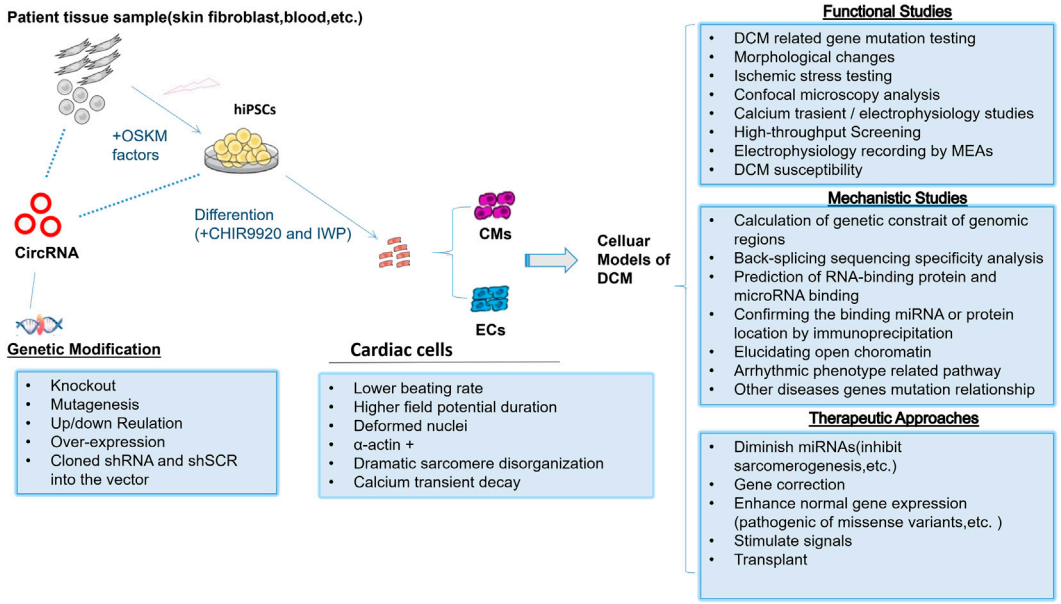

FIGURE 2 | Human pluripotent stem cells as DCM models to study function and mechanism of circRNAs.

progress. Also, it is a good choice to start with some circRNAs related to RBM20 expression as mentioned before. Consequently, studies of molecular mechanisms of circRNAs have just recently begun, so we note that this research in pluripotent stem cell–derived cardiomyocyte about heart diseases is still in its nascent stages, and currently the study mostly focus on its expression situation; only a few research studies explore molecular mechanisms of circRNAs in pluripotent stem cell–derived cardiomyocyte. Recently, Anke et al. successfully constructed the hiPSC-CM model with circular RNA TTN1 deletion (Tijsen et al., 2021). In this study, the most abundant RMB20-dependent circRNA in the human heart was selected, of which parental gene TTN variants are found in 20–30% patients suffering from DCM. The cTTN1 was expressed highly in healthy people but down-regulated in patients with DCM. Therefore, the researcher decided to build a downregulation circRNA model instead of an upregulation one. After inducing the selective loss of cTTN1 in hiPSC-CMs, it was found that the loss of cTTN1 can cause abnormal cardiac tissue structure, apoptosis, and reduced contractility. The cTTN1 mechanisms of action are summarized as follows: 1) The special motif AAAGAACC was found in the back splice junction of cTTN, which has a role in binding the splice regulator SRSF10. 2) The loss of cTTN1 would move most of RBM20 from the nucleus to the cytoplasm, resulting in splicing deletion of the RBM20 and SRSF10 targets. If we want to build the model, we can refer to the figure (**Figure 2**).

Challenges of hiPSC Modeling and Translational Aspects

It seems that hiPSC could provide an unlimited cell source for regenerative medicine in heart transplant and card cytotoxicity experiments. However, several weaknesses, include genomic instability causing chromosomal aberrations, low frequency of iPSCs, wide variation of the quality of iPSC colonies, and hinder iPSC applications even for *in vitro* analysis (Mayshar et al., 2010; Garber, 2015).

Cardiac muscles are composed of cardiomyocytes, extracellular collagenous matrix, vasculature, and *etc.* In addition, cardiomyocytes take only a small part in 25–35% of myocardial tissue (Pinto et al., 2016). For example, iPSC-derived organoids lack enough cell maturation and precise microvascular formation. The procedures of culturing iPSC-CM similarity to ESCs are not complex, but the composition of intrinsic properties of iPSC-derived cardiomyocytes varies under pathological conditions. Therefore, it is a difficult problem to use iPSC-derived cardiomyocytes for modeling heart diseases *in vitro*, although the survival of iPSC-derived cardiomyocytes and the complexity of the model have been used to significantly improve accuracy during the past few years (Breckwoldt et al., 2017; Lemoine et al., 2017; Weinberger et al., 2017; Castro et al., 2019; Meyer et al., 2019).

Uncertainties in cytogenetics and epigenetics make it difficult to directly correlate *in vitro* functional effects and specific genetic variations if using patient-derived iPSCs (Dzilic et al., 2018). In addition, gene variant mutations might be produced and even accumulate during the long time of culturing patient-derived iPSCs (Liu et al., 2014; Yoshihara et al., 2017). Short tandem repeat (STR) analysis is always used for the genetic stability test, and therefore using early passages is necessary.

In the early days, hiPSC-CM treatment was used to fill missing tissue induced by MI. The induced pluripotent stem cells were considered to be superior to human embryonic stem cells (ESCs) for repairing damaged myocardium (Liao et al., 2019). But hESC-VCs could alleviate a severely abnormal heterogeneity of myocardial bioenergetics in hearts (Xiong et al., 2012). Due to the low transplant survival rate and other reasons, trying for over-expression of angiopoietin-1 (Ang-1) or add thymosinβ4 (Tb4)

could improve engraftment and reparative potency of transplanted hiPSC-CMs in a porcine model (Tan et al., 2021; Tao et al., 2021). Finally, pluripotent stem cell (PSC)–derived cardiomyocytes (hiPSC-CMs) were proven to enhance cardiac function by integrating into infarcted hearts in the porcine model of myocardial infarction (Ye et al., 2014).

hiPSCs were believed to be more readily available for cellular transplantation and personalized therapies (Su et al., 2021). The stable CM graft formation in the rodent infarcted hearts after transplanted hiPSC-CMs or hiPSC-CVPCs was an encouraging progress in technology. Overall, the systematic development of human cardiac organoids would accelerate cardiac drug discovery and personalize cardiac treatment in the future. Therefore, iPSC-derived cardiomyocytes should also be linked to animal models or the study of complicated explanted human myocardial tissue in order to obtain actual clinical benefit.

DISCUSSION

Although significant efforts have been made in genetic variants–induced pathophysiological changes for human heart diseases such as DCM, HCM, and various types of long QT syndrome (LQTS), our understanding of circRNA function in heart disease is still very limited. In recent years, high-throughput sequencing detection technologies continue to surmount, which further have improved our knowledge about epigenetic contribution to pathogenesis of heart disease. Increasing evidence supports circRNAs could regulate cardiac hypertrophy, heart failure, and myocardial fibrosis *via* regulation signaling pathways or sponging with some miRNAs. CircRNA mm9_circ_012559, which downregulated, can target with miR-223 to aggravate heart hypertrophy (Wang et al., 2016). CircRNA (HRCR) contains a group of 36 circRNAs which were all upregulated in the heart. HRCR decreases the level of ARC expression and enhances myocardial hypertrophy produced by isoproterenol (ISO) *via* sponging with downregulated MiR-223 (Wang et al., 2016). CircSlc8a1 can adsorb miR-133a which has an important role in cardiac hypertrophy in cardiomyocytes. Therefore, circSlc8a1 knockdown weakens cardiac hypertrophy from excessive pressure (Lim et al., 2019). The overexpression of circRNA_000203 enhances cell size by promoting atrial natriuretic peptide and β-myosin heavy chain expression in neonatal mouse ventricular cardiomyocytes. The upregulated circRNA_000203 in Ang-II–infused mice enhances cardiac hypertrophy and acts with its target siRNA to inhibit hypertrophy in turn (Nishi et al., 2010). However, the exact mechanisms of how these circRNAs affect the progression of DCM remains largely unknown. Some circRNAs are differentially expressed and detected easily in DCM diseases and could play an important role in other heart diseases. For example, circSlc8a1 has also upregulated in myocardial infarction, and it was confirmed as auxiliary diagnostic markers for SCD caused by acute IHD (Tian et al., 2021). This poses a great challenge for identification of DCM-related circRNAs as specific heart disease molecular markers when facing complicated and combined heart disease. More importantly, the ceRNA theory has been the main hypothesis of how circRNAs function as miRNA sponges in heart diseases. However, it is skeptical about whether the physiological expression level of a single circRNA is sufficient to absorb its target miRNAs because miRNA targets including lncRNAs, cirRNAs, mRNAs, and pseudogenes and the efficient regulation are finally determined by the number of common miRNAs and the target binding sites (Le et al., 2017). It is essential for the future study to investigate all the genes composed of the ceRNA network for a better understanding of DCM, especially mostly miRNAs-specific expression only in a certain disease. At last, the detection method of the circRNA has been upgraded from the first- and second-generation sequencing technologies to nanopore third-generation sequencing technologies, but most of the research studies about circRNAs on DCM disease are based on the first- and second-generation sequencing technology. Many circRNAs with full length> 500 nt and specific variable shear excision events cannot be detected by the first- and next-generation sequencing, which may lead to missed detection of some circRNAs that play an important role in the occurrence and development of DCM disease (Rahimi et al., 2021).

As mentioned previously, most of circRNA studies are conducted in mouse models, failing to mimic the *in vivo* patients. Therefore, hiPSC from patients with various heart diseases should be used as a more relevant physiological model. However, it is worthy of noting that using hiPSC as a disease model faces some challenges as follows: In a hiPSC-CM model, cLQTS2 and Kv11.1 activators could restore normal heart signaling, but at the same time there may be a hazard of overcorrection that reduces itself being pro-arrhythmic (Perry et al., 2020). HiPSC-CM do not express other components that make up the protein of cardiomyocytes, including key Ca2+ processing components and contractile elements, despite it could remedy arrhythmic Ca2+ transients and alleviates declined Ca2+ transport in a DCM model; this leads to limited observations (Stroik et al., 2020). But the advantage is always obvious too. The *in vitro* phenotype of hiPSC-CM of asymptomatic and symptomatic individuals with LQT2 differs in the level of CM aggregation; an increase in arrhythmia is observed in symptomatic hiPSC-CM, which makes it convenient for us to use hiPSC-CM to observe the different phenotypes of mutation carriers with different clinical phenotypes (Shah et al., 2020).

The latest research about using hiPSCs for the study of circRNAs in DCM declares that if there is no RBM20 mutation detected when the phenotype resembles the phenotype of DCM with arrhythmias as observed in RBM20 mutation carriers, it is necessary to consider variants in the I-band region (Tijsen et al., 2021) because hindering formation or function of these TTN circular RNAs which stem from the I-band region also may have the DCM clinical phenotype. This will bring some new perspectives to gene-targeted therapy, for example, some gene mutation or deletion diseases that are only judged from clinical symptoms. When the targeted gene therapy is ineffective according to clinical symptoms which are reduced by DCM-related gene mutations or deletion, factors caused by non-coding RNA disorders such as circRNA could be considered. The current research has always emphasized on downregulated circRNAs in DCM patients and

hiPSCs-CM. However, whether the upregulated circRNAs in the DCM patient's heart and hiPSCs-CM have a similar mechanism or a different mechanism could only be further studied.

The short hairpin RNA (shRNA) and antisense oligonucleotide (ASO) have been considered to target mRNAs in the hiPSC-CM model to ameliorate phenotypes of disease. Importantly, Shah, D. gave an outstanding article about these two methods of silencing as therapeutic treatment for MYH7 gene mutation cardiomyopathy. In addition, they found shRNA silencing way may prove to be more efficacious toward ASO silencing in the treatment of the human HCM model (Dainis et al., 2020).

To sum up, there are several examples of human DCM diseases related to titin gene and LMNA gene which have been successfully modeled by linking the homologous cells in 3D fabricated tissue culture models. circRNAs are potential candidates as biomarkers for the diagnosis of DCM. Moreover, most circRNAs have sequence conservation between mammals, providing favorable conditions for the study in cells or animal disease models. hiPSC provides a much facile and accessible way to obtain human cells, while the new differentiation method can cultivate a large number of different classes of cardiomyocytes. Our review provides a new perspective of iPSC-derived atrial cardiomyocytes for exploring the role of circRNAs in the pathophysiology of DCM and offers a platform for evaluating potential treatment methods.

AUTHOR CONTRIBUTIONS

YZ, GH, ZY, YZ, and RC wrote the original draft. YZ and RC supervised this work. All authors have read and agreed to the published version of the manuscript.

FUNDING

This research was funded by the National Natural Science Foundation of China (81801474), the Science and Technology Fund of Shenzhen (JCYJ20180306172502097), and Shenzhen Longhua District Science and Technology Innovation Bureau Project (2020033).

REFERENCES

Ashwal-Fluss, R., Meyer, M., Pamudurti, N. R., Ivanov, A., Bartok, O., Hanan, M., et al. (2014). circRNA Biogenesis Competes with Pre-mRNA Splicing. *Mol. Cel* 56, 55–66. doi:10.1016/j.molcel.2014.08.019

Bakalakos, A., Ritsatos, K., and Anastasakis, A. (2018). Current Perspectives on the Diagnosis and Management of Dilated Cardiomyopathy Beyond Heart Failure: A Cardiomyopathy Clinic Doctor's Point of View. *Hellenic J. Cardiol.* 59, 254–261. doi:10.1016/j.hjc.2018.05.008

Brauch, K. M., Karst, M. L., Herron, K. J., De Andrade, M., Pellikka, P. A., Rodeheffer, R. J., et al. (2009). Mutations in Ribonucleic Acid Binding Protein Gene Cause Familial Dilated Cardiomyopathy. *J. Am. Coll. Cardiol.* 54, 930–941. doi:10.1016/j.jacc.2009.05.038

Breckwoldt, K., Letuffe-Brenière, D., Mannhardt, I., Schulze, T., Ulmer, B., Werner, T., et al. (2017). Differentiation of Cardiomyocytes and Generation of Human Engineered Heart Tissue. *Nat. Protoc.* 12, 1177–1197. doi:10.1038/nprot.2017.033

Carboni, E., Carboni, E., Sestito, S., Lucente, M., Morrone, A., Zampini, L., et al. (2020). Dilated Cardiomyopathy in Mucolipidosis Type 2. *J. Biol. Regul. Homeost Agents* 34, 71–77.

Castro, L., Geertz, B., Reinsch, M., Aksehirlioglu, B., Hansen, A., Eschenhagen, T., et al. (2019). Implantation of hiPSC-Derived Cardiac-Muscle Patches after Myocardial Injury in a Guinea Pig Model. *JoVE* 18, 145. doi:10.3791/58810

Dainis, A., Zaleta-Rivera, K., Ribeiro, A., Chang, A. C. H., Shang, C., Lan, F., et al. (2020). Silencing of MYH7 Ameliorates Disease Phenotypes in Human iPSC-Cardiomyocytes. *Physiol. Genomics* 52, 293–303. doi:10.1152/physiolgenomics.00021.2020

Dong, K., He, X., Su, H., Fulton, D. J. R., and Zhou, J. (2020). Genomic Analysis of Circular RNAs in Heart. *BMC Med. Genomics* 13, 167. doi:10.1186/s12920-020-00817-7

Dzilic, E., Lahm, H., Dreßen, M., Deutsch, M.-A., Lange, R., Wu, S. M., et al. (2018). Genome Editing Redefines Precision Medicine in the Cardiovascular Field. *Stem Cell Int.* 2018, 1–11. doi:10.1155/2018/4136473

Fatkin, D., Macrae, C., Sasaki, T., Wolff, M. R., Porcu, M., Frenneaux, M., et al. (1999). Missense Mutations in the Rod Domain of the Lamin A/C Gene as Causes of Dilated Cardiomyopathy and Conduction-System Disease. *N. Engl. J. Med.* 341, 1715–1724. doi:10.1056/NEJM199912023412302

Garber, K. (2015). RIKEN Suspends First Clinical Trial Involving Induced Pluripotent Stem Cells. *Nat. Biotechnol.* 33, 890–891. doi:10.1038/nbt0915-890

Gerull, B., Gramlich, M., Atherton, J., Mcnabb, M., Trombitás, K., Sasse-Klaassen, S., et al. (2002). Mutations of TTN, Encoding the Giant Muscle Filament Titin, Cause Familial Dilated Cardiomyopathy. *Nat. Genet.* 30, 201–204. doi:10.1038/ng815

Gupta, S. K., Garg, A., Bär, C., Chatterjee, S., Foinquinos, A., Milting, H., et al. (2018). Quaking Inhibits Doxorubicin-Mediated Cardiotoxicity Through Regulation of Cardiac Circular RNA Expression. *Circ. Res.* 122, 246–254. doi:10.1161/CIRCRESAHA.117.311335

Hänselmann, A., Veltmann, C., Bauersachs, J., and Berliner, D. (2020). Dilated Cardiomyopathies and Non-compaction Cardiomyopathy. *Herz* 45, 212–220. doi:10.1007/s00059-020-04903-5

Herman, D. S., Lam, L., Taylor, M. R. G., Wang, L., Teekakirikul, P., Christodoulou, D., et al. (2012). Truncations of Titin Causing Dilated Cardiomyopathy. *N. Engl. J. Med.* 366, 619–628. doi:10.1056/NEJMoa1110186

Hey, T. M., Rasmussen, T. B., Madsen, T., Aagaard, M. M., Harbo, M., Mølgaard, H., et al. (2019). Pathogenic RBM20-Variants Are Associated with a Severe Disease Expression in Male Patients with Dilated Cardiomyopathy. *Circ. Heart Fail.* 12, e005700. doi:10.1126/science.aaa545810.1161/CIRCHEARTFAILURE.118.005700

Holdt, L. M., Kohlmaier, A., and Teupser, D. (2018). Molecular Functions and Specific Roles of circRNAs in the Cardiovascular System. *Non-coding RNA Res.* 3, 75–98. doi:10.1016/j.ncrna.2018.05.002

Hu, X., Chen, L., Wu, S., Xu, K., Jiang, W., Qin, M., et al. (2019). Integrative Analysis Reveals Key Circular RNA in Atrial Fibrillation. *Front. Genet.* 10, 108. doi:10.3389/fgene.2019.00108

Imanaka-Yoshida, K. (2020). Inflammation in Myocardial Disease: From Myocarditis to Dilated Cardiomyopathy. *Pathol. Int.* 70, 1–11. doi:10.1111/pin.12868

Jakobi, T., Siede, D., Eschenbach, J., Heumüller, A. W., Busch, M., Nietsch, R., et al. (2020). Deep Characterization of Circular RNAs from Human Cardiovascular Cell Models and Cardiac Tissue. *Cells* 9, 1616. doi:10.3390/cells9071616

Jefferies, J. L., and Towbin, J. A. (2010). Dilated Cardiomyopathy. *The Lancet* 375, 752–762. doi:10.3390/cells806059410.1016/s0140-6736(09)62023-7

Ji, X., Ding, W., Xu, T., Zheng, X., Zhang, J., Liu, M., et al. (2020). MicroRNA-31-5p Attenuates Doxorubicin-Induced Cardiotoxicity via Quaking and Circular RNA Pan3. *J. Mol. Cell Cardiol.* 140, 56–67. doi:10.1016/j.yjmcc.2020.02.009

Kelly, S., Greenman, C., Cook, P. R., and Papantonis, A. (2015). Exon Skipping Is Correlated with Exon Circularization. *J. Mol. Biol.* 427, 2414–2417. doi:10.1016/j.jmb.2015.02.018

Khan, M. A. F., Reckman, Y. J., Aufiero, S., Van Den Hoogenhof, M. M. G., Van Der Made, I., Beqqali, A., et al. (2016). RBM20 Regulates Circular RNA

Production from the Titin Gene. *Circ. Res.* 119, 996–1003. doi:10.1161/circresaha10.1161/circresaha.116.309568

Komiyama, M., Hasegawa, K., and Matsumori, A. (2020). Dilated Cardiomyopathy Risk in Patients with Coronavirus Disease 2019: How to Identify and Characterise it Early? *Eur. Cardiol.* 15, e49. doi:10.15420/ecr.2020.17

Le, T. D., Zhang, J., Liu, L., and Li, J. (2017). Computational Methods for Identifying miRNA Sponge Interactions. *Brief Bioinform* 18, 577–590. doi:10.1093/bib/bbw042

Lei, W., Feng, T., Fang, X., Yu, Y., Yang, J., Zhao, Z.-A., et al. (2018). Signature of Circular RNAs in Human Induced Pluripotent Stem Cells and Derived Cardiomyocytes. *Stem Cel Res Ther* 9, 56. doi:10.1186/s13287-018-0793-5

Lemoine, M. D., Mannhardt, I., Breckwoldt, K., Prondzynski, M., Flenner, F., Ulmer, B., et al. (2017). Human iPSC-Derived Cardiomyocytes Cultured in 3D Engineered Heart Tissue Show Physiological Upstroke Velocity and Sodium Current Density. *Sci. Rep.* 7, 5464. doi:10.1038/s41598-017-05600-w

Li, D., Tapscoft, T., Gonzalez, O., Burch, P. E., Quiñones, M. A., Zoghbi, W. A., et al. (1999). Desmin Mutation Responsible for Idiopathic Dilated Cardiomyopathy. *Circulation* 100, 461–464. doi:10.1161/01.cir.100.5.461

Liao, S., Zhang, Y., Ting, S., Zhen, Z., Luo, F., Zhu, Z., et al. (2019). Potent Immunomodulation and Angiogenic Effects of Mesenchymal Stem Cells Versus Cardiomyocytes Derived from Pluripotent Stem Cells for Treatment of Heart Failure. *Stem Cel Res Ther* 10, 78. doi:10.1186/s13287-019-1183-3

Lim, T. B., Aliwarga, E., Luu, T. D. A., Li, Y. P., Ng, S. L., Annadoray, L., et al. (2019). Targeting the Highly Abundant Circular RNA circSlc8a1 in Cardiomyocytes Attenuates Pressure Overload Induced Hypertrophy. *Cardiovasc. Res.* 115, 1998–2007. doi:10.1093/cvr/cvz130

Lin, Z., Zhao, Y., Dai, F., Su, E., Li, F., and Yan, Y. (2021). Analysis of Changes in Circular RNA Expression and Construction of ceRNA Networks in Human Dilated Cardiomyopathy. *J. Cel Mol Med* 25, 2572–2583. doi:10.1111/jcmm.16251

Liu, P., Kaplan, A., Yuan, B., Hanna, J. H., Lupski, J. R., and Reiner, O. (2014). Passage Number Is a Major Contributor to Genomic Structural Variations in Mouse iPSCs. *Stem Cells* 32, 2657–2667. doi:10.1002/stem.1779

Mayshar, Y., Ben-David, U., Lavon, N., Biancotti, J.-C., Yakir, B., Clark, A. T., et al. (2010). Identification and Classification of Chromosomal Aberrations in Human Induced Pluripotent Stem Cells. *Cell Stem Cell* 7, 521–531. doi:10.1016/j.stem.2010.07.017

Merlo, M., Pyxaras, S. A., Pinamonti, B., Barbati, G., Di Lenarda, A., and Sinagra, G. (2011). Prevalence and Prognostic Significance of Left Ventricular Reverse Remodeling in Dilated Cardiomyopathy Receiving Tailored Medical Treatment. *J. Am. Coll. Cardiol.* 57, 1468–1476. doi:10.1016/j.jacc.2010.11.030

Meyer, T., Tiburcy, M., and Zimmermann, W.-H. (2019). Cardiac Macrotissues-On-A-Plate Models for Phenotypic Drug Screens. *Adv. Drug Deliv. Rev.* 140, 93–100. doi:10.1016/j.addr.2019.03.002

Nishi, H., Ono, K., Iwanaga, Y., Horie, T., Nagao, K., Takemura, G., et al. (2010). MicroRNA-15b Modulates Cellular ATP Levels and Degenerates Mitochondria via Arl2 in Neonatal Rat Cardiac Myocytes. *J. Biol. Chem.* 285, 4920–4930. doi:10.1074/jbc.M109.082610

Palomer, X., Pizarro-Delgado, J., and Vázquez-Carrera, M. (2018). Emerging Actors in Diabetic Cardiomyopathy: Heartbreaker Biomarkers or Therapeutic Targets? *Trends Pharmacol. Sci.* 39, 452–467. doi:10.1016/j.tips.2018.02.010

Perry, M. D., Ng, C.-A., Mangala, M. M., Ng, T. Y. M., Hines, A. D., Liang, W., et al. (2020). Pharmacological Activation of IKr in Models of Long QT Type 2 Risks Overcorrection of Repolarization. *Cardiovasc. Res.* 116, 1434–1445. doi:10.1093/cvr/cvz247

Pinto, A. R., Ilinykh, A., Ivey, M. J., Kuwabara, J. T., D'Antoni, M. L., Debuque, R., et al. (2016). Revisiting Cardiac Cellular Composition. *Circ. Res.* 118, 400–409. doi:10.1161/CIRCRESAHA.115.307778

Ponikowski, P., Voors, A. A., Anker, S. D., Bueno, H., Cleland, J. G. F., Coats, A. J. S., et al. (2016). 2016 ESC Guidelines for the Diagnosis and Treatment of Acute and Chronic Heart Failure. *Eur. Heart J.* 37, 2129–2200. doi:10.1093/eurheartj/ehw128

Priori, S. G., Blomström-Lundqvist, C., Mazzanti, A., Blom, N., Borggrefe, M., Camm, J., et al. (2015). 2015 ESC Guidelines for the Management of Patients with Ventricular Arrhythmias and the Prevention of Sudden Cardiac Death. *Eur. Heart J.* 36, 2793–2867. doi:10.1093/europace/euv31910.1093/eurheartj/ehv316

Rahimi, K., Venø, M. T., Dupont, D. M., and Kjems, J. (2021). Nanopore Sequencing of Brain-Derived Full-Length circRNAs Reveals circRNA-specific Exon Usage, Intron Retention and Microexons. *Nat. Commun.* 12, 4825. doi:10.1038/s41467-021-24975-z

Ruan, Z. B., Chen, G. C., Zhang, R., and Zhu, L. (2019). Circular RNA Expression Profiles During the Differentiation of Human Umbilical Cord-Derived Mesenchymal Stem Cells into Cardiomyocyte-like Cells. *J. Cel Physiol* 234, 16412–16423. doi:10.1002/jcp.28310

Shah, D., Prajapati, C., Penttinen, K., Cherian, R. M., Koivumäki, J. T., Alexanova, A., et al. (2020). hiPSC-Derived Cardiomyocyte Model of LQT2 Syndrome Derived from Asymptomatic and Symptomatic Mutation Carriers Reproduces Clinical Differences in Aggregates but Not in Single Cells. *Cells* 9, 1153. doi:10.3390/cells9051153

Shah, D., Virtanen, L., Prajapati, C., Kiamehr, M., Gullmets, J., West, G., et al. (2019). Modeling of LMNA-Related Dilated Cardiomyopathy Using Human Induced Pluripotent Stem Cells. *Cells* 8, 594. doi:10.3390/cells8060594

Siede, D., Rapti, K., Gorska, A. A., Katus, H. A., Altmüller, J., Boeckel, J. N., et al. (2017). Identification of Circular RNAs with Host Gene-independent Expression in Human Model Systems for Cardiac Differentiation and Disease. *J. Mol. Cell Cardiol.* 109, 48–56. doi:10.1016/j.yjmcc.2017.06.015

Stagsted, L. V., Nielsen, K. M., Daugaard, I., and Hansen, T. B. (2019). Noncoding AUG circRNAs Constitute an Abundant and Conserved Subclass of Circles. *Life Sci. Alliance* 2, e201900398. doi:10.26508/lsa.201900398

Stroik, D. R., Ceholski, D. K., Bidwell, P. A., Mleczko, J., Thanel, P. F., Kamdar, F., et al. (2020). Viral Expression of a SERCA2a-Activating PLB Mutant Improves Calcium Cycling and Synchronicity in Dilated Cardiomyopathic hiPSC-CMs. *J. Mol. Cell Cardiol.* 138, 59–65. doi:10.1016/j.yjmcc.2019.11.147

Su, L., Kong, X., Loo, S. J., Gao, Y., Kovalik, J.-P., Su, X., et al. (2021). Diabetic Endothelial Cells Differentiated from Patient iPSCs Show Dysregulated Glycine Homeostasis and Senescence Associated Phenotypes. *Front. Cel Dev. Biol.* 9, 667252. doi:10.3389/fcell.2021.667252

Sun, W., Han, B., Cai, D., Wang, J., Jiang, D., and Jia, H. (2020). Differential Expression Profiles and Functional Prediction of Circular RNAs in Pediatric Dilated Cardiomyopathy. *Front. Mol. Biosci.* 7, 600170. doi:10.3389/fmolb.2020.600170

Tan, S. H., Loo, S. J., Gao, Y., Tao, Z. H., Su, L. P., Wang, C. X., et al. (2021). Thymosin β4 Increases Cardiac Cell Proliferation, Cell Engraftment, and the Reparative Potency of Human Induced-Pluripotent Stem Cell-Derived Cardiomyocytes in a Porcine Model of Acute Myocardial Infarction. *Theranostics* 11, 7879–7895. doi:10.7150/thno.56757

Tan, W. L. W., Lim, B. T. S., Anene-Nzelu, C. G. O., Ackers-Johnson, M., Dashi, A., See, K., et al. (2017). A Landscape of Circular RNA Expression in the Human Heart. *Cardiovasc. Res.* 113, cvw250–309. doi:10.1093/cvr/cvw250

Tao, Z., Loo, S., Su, L., Tan, S., Tee, G., Gan, S. U., et al. (2021). Angiopoietin-1 Enhanced Myocyte Mitosis, Engraftment, and the Reparability of hiPSC-CMs for Treatment of Myocardial Infarction. *Cardiovasc. Res.* 117, 1578–1591. doi:10.1093/cvr/cvaa215

Tian, M., Xue, J., Dai, C., Jiang, E., Zhu, B., and Pang, H. (2021). CircSLC8A1 and circNFIX Can Be Used as Auxiliary Diagnostic Markers for Sudden Cardiac Death Caused by Acute Ischemic Heart Disease. *Sci. Rep.* 11, 4695. doi:10.1038/s41598-021-84056-5

Tijsen, A. J., Cócera Ortega, L., Reckman, Y. J., Zhang, X., Van Der Made, I., Aufiero, S., et al. (2021). Titin Circular RNAs Create a Back-Splice Motif Essential for SRSF10 Splicing. *Circulation* 143, 1502–1512. doi:10.1161/CIRCULATIONAHA.120.050455

Van Heesch, S., Witte, F., Schneider-Lunitz, V., Schulz, J. F., Adami, E., Faber, A. B., et al. (2019). The Translational Landscape of the Human Heart. *Cell* 178, 242–260. doi:10.1016/j.cell.2019.05.010

Verdonschot, J. A. J., Hazebroek, M. R., Wang, P., Sanders-Van Wijk, S., Merken, J. J., Adriaansen, Y. A., et al. (2018). Clinical Phenotype and Genotype Associations with Improvement in Left Ventricular Function in Dilated Cardiomyopathy. *Circ. Heart Fail.* 11, e005220. doi:10.1161/CIRCHEARTFAILURE.118.005220

Wang, K., Long, B., Liu, F., Wang, J.-X., Liu, C.-Y., Zhao, B., et al. (2016). A Circular RNA Protects the Heart from Pathological Hypertrophy and Heart Failure by Targeting miR-223. *Eur. Heart J.* 37, 2602–2611. doi:10.1093/eurheartj/ehv713

Weinberger, F., Mannhardt, I., and Eschenhagen, T. (2017). Engineering Cardiac Muscle Tissue. *Circ. Res.* 120, 1487–1500. doi:10.1161/CIRCRESAHA.117.310738

Xiong, Q., Ye, L., Zhang, P., Lepley, M., Swingen, C., Zhang, L., et al. (2012). Bioenergetic and Functional Consequences of Cellular Therapy. *Circ. Res.* 111, 455–468. doi:10.1161/CIRCRESAHA.112.269894

Ye, L., Chang, Y.-H., Xiong, Q., Zhang, P., Zhang, L., Somasundaram, P., et al. (2014). Cardiac Repair in a Porcine Model of Acute Myocardial Infarction with Human Induced Pluripotent Stem Cell-Derived Cardiovascular Cells. *Cell Stem Cell* 15, 750–761. doi:10.1016/j.stem.2014.11.009

Yoshihara, M., Hayashizaki, Y., and Murakawa, Y. (2017). Genomic Instability of iPSCs: Challenges towards Their Clinical Applications. *Stem Cel Rev Rep* 13, 7–16. doi:10.1007/s12015-016-9680-6

Conflict of Interest: The authors declare that the research was conducted in the absence of any commercial or financial relationships that could be construed as a potential conflict of interest.

Publisher's Note: All claims expressed in this article are solely those of the authors and do not necessarily represent those of their affiliated organizations, or those of the publisher, the editors, and the reviewers. Any product that may be evaluated in this article, or claim that may be made by its manufacturer, is not guaranteed or endorsed by the publisher.

frontiers in Cell and Developmental Biology

MINI REVIEW
published: 28 March 2022
doi: 10.3389/fcell.2022.870629

Multiple Gene Transfer and All-In-One Conditional Knockout Systems in Mouse Embryonic Stem Cells for Analysis of Gene Function

Teruhiko Suzuki[1], *Satoko Takagi*[1,2] *and Takahiko Hara*[1,2,3]*

[1]Stem Cell Project, Tokyo Metropolitan Institute of Medical Science, Tokyo, Japan, [2]Graduate School of Medical and Dental Sciences, Tokyo Medical and Dental University, Tokyo, Japan, [3]Graduate School of Science, Department of Biological Science, Tokyo Metropolitan University, Tokyo, Japan

Mouse embryonic stem cells (ESCs) are powerful tools for functional analysis of stem cell-related genes; however, complex gene manipulations, such as locus-targeted introduction of multiple genes and conditional gene knockout conditional knockout, are technically difficult. Here, we review recent advances in technologies aimed at generating cKO clones in ESCs, including two new methods developed in our laboratory: the simultaneous or sequential integration of multiple genes system for introducing an unlimited number of gene cassettes into a specific chromosomal locus using reciprocal recombinases; and the all-in-one cKO system, which enables introduction of an EGFP reporter expression cassette and FLAG-tagged gene of interest under an endogenous promoter. In addition, methods developed in other laboratories, including conventional approaches to establishment of cKO cell clones, inducible Cas9-mediated cKO generation, and cKO assisted by reporter construct, invertible gene-trap cassette, and conditional protein degradation. Finally, we discuss the advantages of each approach, as well as the remaining issues and challenges.

Keywords: embryonic stem cells, gene targeting, conditional knockout, homologous recombination, gene function

OPEN ACCESS

Edited by:
Valerie Kouskoff,
The University of Manchester, United Kingdom

Reviewed by:
Dingpei Long,
Southwest University, China
Dagmar Wirth,
Helmholtz Association of German Research Centers (HZ), Germany

***Correspondence:**
Takahiko Hara
hara-tk@igakuken.or.jp

Specialty section:
This article was submitted to Stem Cell Research, a section of the journal Frontiers in Cell and Developmental Biology

Received: *07 February 2022*
Accepted: *15 March 2022*
Published: *28 March 2022*

Citation:
Suzuki T, Takagi S and Hara T (2022) Multiple Gene Transfer and All-In-One Conditional Knockout Systems in Mouse Embryonic Stem Cells for Analysis of Gene Function. Front. Cell Dev. Biol. 10:870629. doi: 10.3389/fcell.2022.870629

INTRODUCTION

Gene knockout (KO) technology has made a substantial contribution to knowledge of gene function. KO mice and KO cells prepared from them are frequently used for analysis of gene function in mammalian cells; however, generation of KO mice requires extended periods of time and cumbersome processes, including isolation of gene-targeted mouse embryonic stem cell (ESC) clones, production of chimera mice carrying the KO ESCs, establishment of germline-transmitted heterozygous mice, and cross-breeding of the heterozygous mice. Preparation of genetically disrupted cells is an alternative approach for analysis of gene function *in vivo*; however, it is also challenging, due to the technical difficulties involved in gene targeting. Recent developments in genome editing technologies have addressed these issues and greatly accelerated the molecular analysis of gene function (Gaj et al., 2013; Gupta and Musunuru 2014). CRISPR/Cas9 is the most popular genome editing system because of its high efficiency and easy design/implementation. CRISPR/Cas9 generates a double strand break (DSB) at the target site, which is repaired by the error-prone non-homologous end joining (NHEJ) process, resulting in the introduction of insertion/deletion mutations and consequent target gene disruption. CRISPR/Cas9-induced gene disruption is

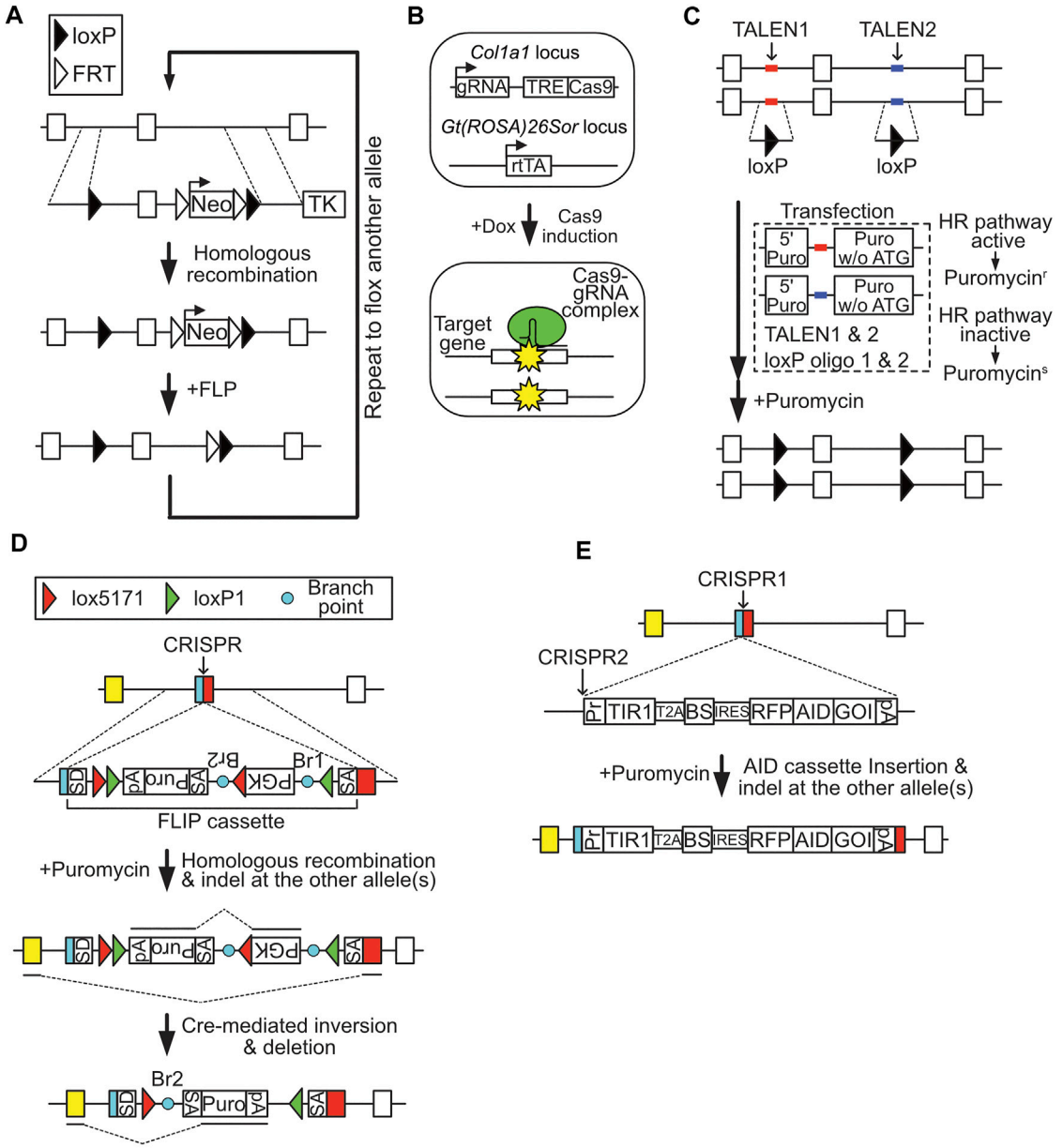

FIGURE 1 | Methods for producing conditional knockout (cKO) cells. **(A)** Conventional cKO method. Filled triangle, loxP site; empty triangle, FRT site. **(B)** Inducible Cas9-mediated cKO method. **(C)** Reporter construct-assisted cKO method. **(D)** cKO using a FLIP cassette. SD, splicing donor sequence; SA, splicing acceptor sequence; Br, branch point; green triangle, loxP1 site; red triangle, lox5171 site; pA, polyadenylation signal. **(E)** cKO using the AID system.

relatively efficient in mammalian cells and has greatly reduced the time and cost required for molecular analysis of gene function. Nevertheless, simple mutagenesis by genome editing technology is not suitable for analysis of lethal genes, which are essential for cell growth, survival, or maintenance of the undifferentiated status of stem cells. Gene knockdown with short interference RNA (siRNA or shRNA) is often applied in these cases; however, these knockdown systems often do not completely suppress target gene expression, which can lead to inconclusive results.

The conditional knockout (cKO) approach, first reported by Gu et al. (1994), is a useful way to study genes difficult to investigate using other approaches. cKO cells are usually generated using recombinases, such as Cre and FLP, in combination with their respective recognition sequences, loxP and FRT. The coding exon(s) of the target gene is/are flanked by these recognition sequences, and their corresponding recombinases are conditionally expressed to induce gene KO in specific cells. Definitive experimental results are expected, as the genetic disruption induces complete elimination of target gene expression. While cKO cells can represent an ideal option, their construction requires targeting of all alleles in each cell. Therefore, few cell lines are suitable for establishing cKO clones,

since most are hyperploid and exhibit low homologous recombination efficiency. To overcome these challenges, various cKO methods have been developed with the aid of genome editing technology. In this review, we provide an overview of recent advances in the development of cKO strategies, particularly the all-in-one cKO system, as well as their advantages and issues that need to be addressed.

CKO CELL ESTABLISHMENT USING A CONVENTIONAL STRATEGY

Mouse ESCs are useful for preparing cKO cells, since ESCs have a normal karyotype and relatively high homologous recombination rates compared with conventional cell lines. The functions of various genes involved in stemness, cell growth, and survival have been clarified using cKO ESCs (Dejosez et al., 2008; Dovey et al., 2010; Lu et al., 2014). The conventional procedure for preparation of cKO ESCs involves introduction of a targeting vector containing positive-selection marker genes (e.g., a neomycin resistance gene) flanked by FRT sites, a negative-selection marker (e.g., herpes simplex virus-derived thymidine kinase), and a coding exon (or exons) of the target gene, flanked by loxP sites, into ESCs (**Figure 1A**). Targeted ESC clones can be isolated by positive-negative selection with 5–10% efficiency (Johnson et al., 1989). After isolation of a targeted clone, the positive-selection marker gene is removed by transient expression of FLP to retain normal expression of the target gene. These targeting processes are then repeated for the other allele. Therefore, a total of four cloning steps are required to establish cKO ESC clones. Due to this time-consuming process, establishment of cKO cells has not been a popular choice for analysis of gene function, despite its numerous advantages. Moreover, prolonged culture of ESCs for repeated cloning may compromise their undifferentiated characteristics. To avoid this concern, one could breed ESC-derived heterozygous mice, although this procedure requires much longer time.

INDUCIBLE CAS9-MEDIATED CKO

Dow et al. (2015) reported a cKO system based on CRISPR/Cas9-induced gene disruption (**Figure 1B**). To enable conditional knockout of the target gene, a guide RNA expression cassette and doxycycline (Dox)-inducible Cas9 cassette were inserted to the safe harbor locus (genetically reliable locus), *Col1a1*, of ESCs stably expressing reverse tetracycline transactivator (rtTA). Using this system, approximately 70% of cells displayed biallelic frame-shift mutation of the target gene in a Dox-dependent manner. Moreover, this technique can induce simultaneous conditional knockout of two target genes with 40–50% efficiency. CRISPR/Cas9-mediated cKO is also applicable in mice. This system greatly reduces the time and labor required to generate cKO ESCs, as well as mice, since it allows one-step preparation of cKO cells. Nevertheless, cells with in-frame mutations, which may behave as normal cells, cannot be eliminated due to the principles underlying this system, which relies on NHEJ-dependent mutagenesis.

REPORTER CONSTRUCT-ASSISTED CKO

DNA DSBs at the targeting site greatly enhance rates of homologous recombination (Donoho et al., 1998). Based on this mechanism, several genome editing technology-assisted methods have been developed for efficient cKO cell cloning. Flemr and Bühler introduced two homozygous loxP sites simultaneously *via* transfection of single-strand oligo-DNA, composed of a loxP sequence and 40 bp homology arms, TAL effector nucleases (TALENs) designed to target the site of interest, and a recombination reporter construct, which contained a 5′ puromycin-resistance gene fragment and a TALENs target sequence, followed by a full-length puromycin-resistance gene without a start codon (**Figure 1C**) (Flemr and Bühler 2015). If homologous recombination mechanisms are active in the transfected cells, TALENs-induced DSB of the reporter construct results in generation of an intact puromycin-resistance gene *via* homologous recombination. Using this method, these researchers successfully generated cKO ESCs by targeting two loxP oligo-DNA molecules on both alleles in a single step; however, this approach still requires extensive screening to obtain correct clones, due to the low efficiency (approximately 4%) of targeting of all four sites. Use of CRISPR/Cas9 instead of TALENs may improve the efficiency.

CKO *VIA* INVERTIBLE GENE-TRAP CASSETTE

Andersson-Rolf et al. used the Cre-regulated invertible gene-trap cassette (FLIP cassette), which relates to the gene trap tool originally developed by Melchner's laboratory for preparing cKO cells (Schnütgen et al., 2005). The FLIP cassette contains a puromycin expression unit, flanked by loxP1 and lox5171 sites, in the middle of an artificial intron sequence (**Figure 1D**) (Andersson-Rolf et al., 2017). To produce cKO cells, the FLIP cassette is inserted into a coding exon of a target gene *via* homologous recombination, with the assistance of CRISPR/Cas9 designed for the target site. The resulting targeted clones can be cKO cells, as CRISPR/Cas9 both assists in targeting the FLIP cassette and destroys untargeted allele(s) of the target gene *via* NHEJ-dependent mutagenesis. Transient expression of Cre in the targeted clone induces inversion of the FLIP cassette and knocks out the target gene by switching the splicing donor/acceptor structure of the artificial intron. The authors produced *Ctnnb1* cKO ESC clones using this method, and verified the loss of ESC dome-like morphology on introduction of Cre. The CRISPR/Cas9 vector designed in the coding exon introduces the FLIP cassette in one allele, while it could also disrupt the other allele of the gene. This smart system is applicable in both ESCs and aneuploid cells, as homologous recombination of the FLIP cassette in one allele is sufficient to generate cKO cells. Nevertheless, the system still requires

relatively extensive screening, since the efficiency is around 6% (4 FLIP/- clones out of 64 isolated clones in the case of ESC screening for *Ctnnb1* cKO cells). Further, gene expression from the targeted allele appears to be compromised, probably due to the selection marker unit inserted in the artificial intron of the FLIP cassette.

CKO *VIA* CONDITIONAL PROTEIN DEGRADATION

Conditional induction of target protein degradation is another method for generating cKO cells (**Figure 1E**). Several techniques for conditional depletion of target proteins have been developed using mutant FKBP, Halo-tag, and auxin-inducible degron (AID) as tag-sequences, and the small chemical compounds, Shld1, HyT13, and auxin [indole-3-acetic acid (IAA)], as regulators of degradation (Banaszynski et al., 2006; Nishimura et al., 2009; Neklesa et al., 2011). Among these approaches, the AID system is the most well-validated, and uses an *Oryza sativa*-derived TIR1 protein, which forms an E3 ubiquitin ligase complex that can induce regulated and rapid degradation of proteins fused with a 7 kDa degron tag derived from *Arabidopsis thaliana* IAA17, in a manner dependent on the small chemical compound, auxin. Thus, introduction of an AID-tag into a target gene in TIR1-expressing cells enables cKO of the target gene.

A recent report described one-step generation of degron-based cKO cells using an improved AID system, which employs mutated TIR1 and an auxin-derivative, 5-Adamantyl-IAA (5-Ad-IAA), to enhance sensitivity (Nishimura et al., 2020). cKO cells are prepared by disrupting the target gene with CRISPR/Cas9 and inserting a vector encoding the mutated TIR1 and AID-tagged target gene cDNA, connected with an internal ribosome entry sequence (IRES), into the DSB site. The targeting efficiency was approximately 75% when this system was used for conditionally knocking out a single allele gene *CENP-H*, which locates on the Z chromosome in DT40 cells. This system is superior to the conditional genetics in terms of reversibility and fast kinetics. Therefore it is suitable for analysis of genes that require rapid depletion, such as cell cycle-related genes. A drawback of this approach is that expression of the target gene is controlled by the IRES sequence; thus target gene expression in the cKO cells does not reflect endogenous gene expression. This is also applicable to the genes in which regulatory elements in introns are eliminated. Another concern is that depletion of the target protein could be incomplete, due to the principles underpinning the system (Ng et al., 2019).

THE ALL-IN-ONE CKO METHOD

The recent study reported a novel cKO method, the all-in-one cKO method, which allows one-step and highly efficient cKO and simultaneous target gene modifications, including epitope tagging and reporter gene knockout/in, *via* CRISPR/Cas9-assisted homologous recombination of the all-in-one cassette in a coding exon of the target gene (**Figure 2A**) (Suzuki et al., 2021). The all-in-one cassette encodes an FRT-flanked promoter-less *EGFP* gene, followed by a P2A peptide sequence, a FLAG-tag sequence, and the coding sequence of the target gene, upstream of the CRISPR/Cas9 target site. Since the EGFP cassette does not contain a promoter, sorting of EGFP-positive cells enables efficient isolation of cKO mESC clones at a frequency of up to 80%. Moreover, targeting of the all-in-one cassette in the presence of the DNA-PK inhibitor, M3814, which enhances homologous recombination, followed by EGFP sorting, resulted in almost 100% cKO efficiency, even in the recombination-non-proficient human fibrosarcoma cell line, HT1080 (Riesenberg et al., 2019). Given this high efficiency, homozygous targeted cKO clones could be easily isolated, even from HT1080 cells. Target gene expression can be monitored *via* EGFP expression in cKO cells, and protein expression can be detected using an anti-FLAG antibody; this feature greatly improves the detection sensitivity of target proteins by western blotting or immunocytochemistry, and is useful for conducting chromatin immunoprecipitation (ChIP) and crosslinking immunoprecipitation (CLIP) assays, as well as for affinity purification of binding proteins for mass spectrometric analysis.

In addition, to enable instant and strictly regulated induction of KO cells from cKO cells, a TetFE ESC line was established. TetFE ESCs have an rtTA expression cassette and a tetracycline response element-regulated FLPERT2 expression cassette in the Gt (ROSA) 26Sor locus to maintain stable expression of transgenes. A simultaneous or sequential integration of multiple gene loading vectors (SIM) system and modified SIM system were employed to introduce those genes (**Figure 2B**). The SIM system was originally developed for efficient sequential introduction of unlimited number of gene loading vectors (GLVs) or simultaneous introduction of multiple GLVs into human/mouse artificial chromosomes (HAC/MAC) (Suzuki et al., 2014; Uno et al., 2018; Suzuki et al., 2020). Both the SIM system and the modified SIM system uses gene-loading modules called SIM cassettes, which contain recognition sequences for Bxb1 and/or φC31 recombinases/integrases, to combine a maximum of three GLVs. While the SIM system utilizes the Cre/loxP reaction for integration of the combined GLVs to the gene-loading site of HAC/MAC, the modified SIM system employs CRISPR/Cas9 for integration to a safe harbor locus *via* NHEJ-dependent knock-in (**Figure 2B**). Co-transfection of the GLVs and recombinases/integrases expression vectors to 3×10^5 target cells was sufficient for obtaining correctly recombined cell clones (Suzuki et al., 2014). It is important to know that human and mouse genomes contain pseudo-attP sequences, which are recognized by φC31 integrase (Thyagarajan et al., 2001). Therefore, validation of GLV integration to an intended site is essential for utilizing the modified SIM system. TetFE ESCs stably express rtTA and conditionally express FLP with an ERT2 domain (FLPERT2), which enables 4-hydroxytamoxifen (4-OHT)-dependent nuclear localization in a Dox-dependent manner. Therefore, KO cells can be easily induced *via* addition of Dox and 4-OHT. This dual regulation system completely prevents spontaneous KO induction caused by leaky activity of FLPERT2 and background expression of Dox-regulated genes. This drug-inducible feature is also advantageous for large-scale preparation of KO cells.

Application of the all-in-one cKO system in conjunction with the TetFE ESCs has been demonstrated in functional analysis of

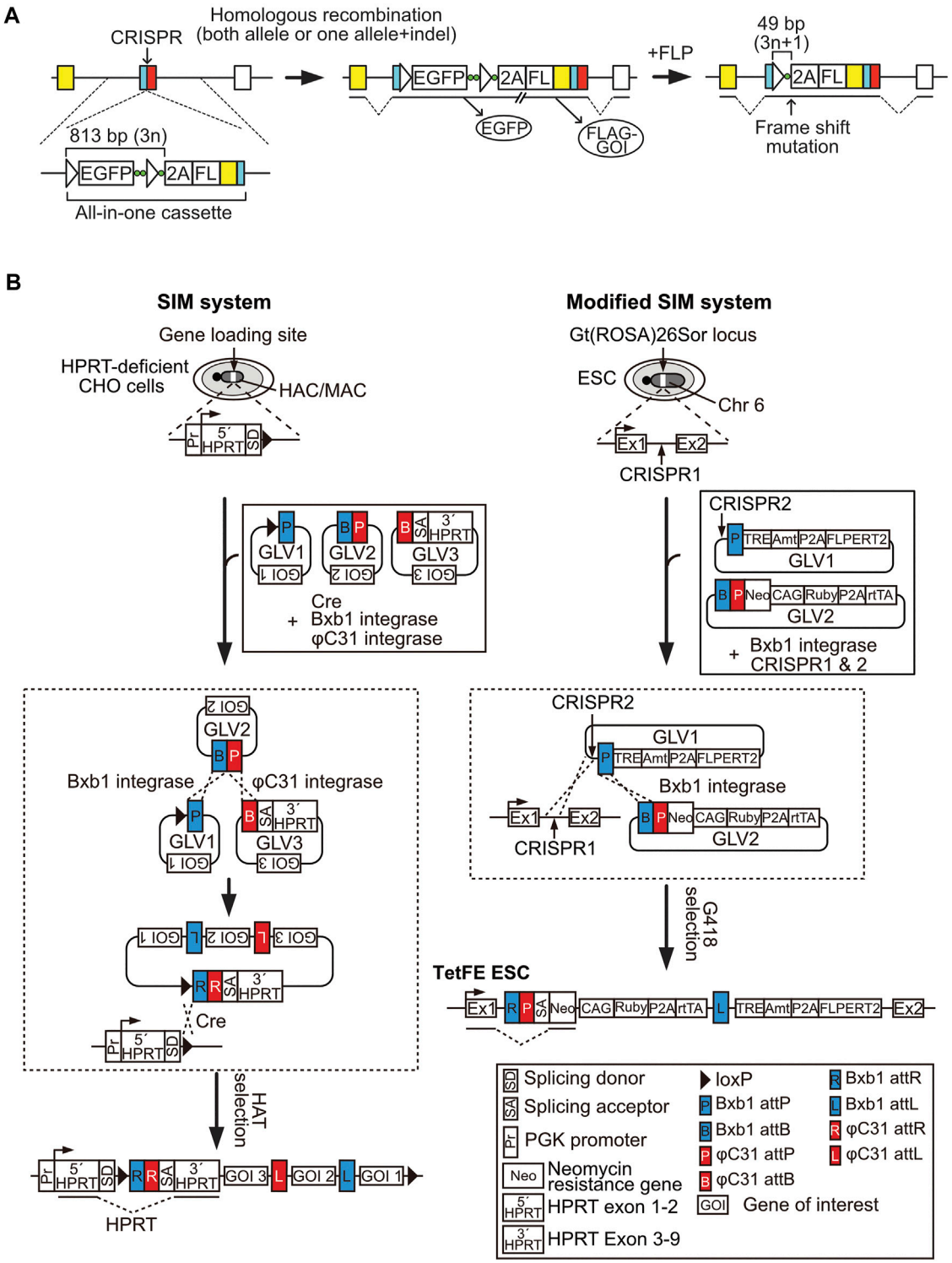

FIGURE 2 | The simultaneous or sequential integration of multiple genes (SIM) system and all-in-one conditional knockout (cKO) methods. **(A)** All-in-one cKO method. Green circle, nucleotides used to induce a frame-shift mutation; empty triangle, FRT site; FL, 3 × FLAG-tag sequence. **(B)** Schematic representation of the SIM system and the modified SIM system. The SIM system and the modified SIM system enable simultaneous loading of multiple gene loading vectors (GLVs) into a human artificial chromosome/mouse artificial chromosome vector and a safe harbor locus, respectively. The procedure to generate TetFE ESCs is shown as an example for loading multiple GLVs via the modified SIM system.

the RNA helicase, DDX1, in ESCs. DEAD box RNA-helicases contain characteristic Asp-Glu-Ala-Asp (DEAD) box motifs that are involved in various RNA metabolism processes, including translation, pre-tRNA splicing, and ribosomal biogenesis (Linder and Jankowsky 2011). DDX1 is a DEAD box RNA helicase suggested to be involved in viral replication, tRNA synthesis, and miRNA processing (Fang et al., 2004; Han et al., 2014; Popow et al., 2014). Further, loss of *Ddx1* stalls mouse development at the 2 to 4 cell stage, possibly due to mis-regulation of DDX1-bound mRNA, which is crucial for 1 to 4 cell stage embryo development (Hildebrandt et al., 2019); however, the precise molecular mechanisms underlying these functions have not been fully elucidated. To clarify these molecular functions, we prepared *Ddx1* cKO TetFE ESCs and found that loss of *Ddx1* resulted in a severe growth defect. Furthermore, the number of TUNEL-positive apoptotic cells was significantly increased in $Ddx1^{-/-}$ ESCs. Accordingly, expression of p53, the master-regulator of cell growth and survival, was upregulated in $Ddx1^{-/-}$ ESCs. These results indicated that loss of *Ddx1* activated the p53-signaling pathway. Further analysis revealed that loss of DDX1 led to an rRNA processing defect, resulting in p53 activation *via* a ribosome stress pathway. Consistent with these findings, the apoptotic phenotype of $Ddx1^{-/-}$ ESCs was rescued by disruption of the *p53* gene. These molecular analyses illustrate the practical utility of the all-in-one cKO method, while most recently developed cKO methods have only been used for proof-of-principle experiments. The disadvantage of the all-in-one cKO method is that it is only applicable for genes whose promoters can drive detectable levels of EGFP expression. Further improvements will be essential to allow application of the method for genes with low expression levels.

DISCUSSION

The recent development of new strategies has greatly reduced the time and labor required for preparation of cKO cells. To encourage wider use of these cKO methods in the academic community, further improvements may be needed. While methods developed to date allow generation of cKO cells in a single step, most still require relatively large-scale screening to isolate a clone due to low cKO efficiencies of approximately 5%. Moreover, some CRISPR/Cas9-assisted methods rely on disruption of untargeted alleles (**Figures 1D,E**), which could restrict the utility of the cKO cells, since cKO cells obtained by this method express lower levels of the target gene than the parental cells, as the target gene is only expressed from the targeted allele. To overcome these limitations, improvements in targeting rate are required for efficient preparation of homozygous targeted cKO clones. Application of homologous recombination-enhancing drugs/genes may improve efficiency, as demonstrated in the all-in-one cKO method. Further, production of homozygous targeted cKO clones in aneuploid cell lines should further broaden the utility of these approaches. The procedure for KO induction of cKO cells is also a potential hurdle to general application of these methods. Since stable expression of recombinases is potentially toxic to cells, transient recombinase expression is appropriate for KO induction. Drug-inducible recombinase expression systems would also be convenient, and are used in several methods. The Dox-inducible, 4-OHT-regulated system applied in the all-in-one cKO method may be optimal for strict regulation of KO induction, as it avoids background induction of KO cells, due to leaky expression/activity of KO inducers.

Conditional knockout of multiple genes can be useful for analysis of signaling pathways or functions of redundant genes. Although simultaneous cKO of two genes was demonstrated using the inducible Cas9-mediated cKO system, the double KO efficiency was 40–50%, which is insufficient to allow molecular function analysis in most cases. Moreover, the system cannot induce KO of each gene separately. Production of cKO cell lines by applying multiple-recombinases and their recognition sequences *via* the efficient methods reviewed here could resolve these issues.

AUTHOR CONTRIBUTIONS

TS and TH designed the study and wrote the manuscript. ST assisted the construction of figures.

FUNDING

This work was supported in part by the Japan Society for the Promotion of Science (JSPS) KAKENHI (grant numbers JP18K06047 (TS) and JP23390256 (TH)) and by Core Research for Evolutionary Science and Technology (CREST) program of the Japanese Science and Technology Agency (JST) (JPMJCR18S4 to TS).

ACKNOWLEDGMENTS

We would like to thank laboratory members for supporting this study.

REFERENCES

Andersson-Rolf, A., Mustata, R. C., Merenda, A., Kim, J., Perera, S., Grego, T., et al. (2017). One-step Generation of Conditional and Reversible Gene Knockouts. *Nat. Methods* 14 (3), 287–289. doi:10.1038/nmeth.4156

Banaszynski, L. A., Chen, L.-c., Maynard-Smith, L. A., Ooi, A. G. L., and Wandless, T. J. (2006). A Rapid, Reversible, and Tunable Method to Regulate Protein Function in Living Cells Using Synthetic Small Molecules. *Cell* 126, 995–1004. doi:10.1016/j.cell.2006.07.025

Dejosez, M., Krumenacker, J. S., Zitur, L. J., Passeri, M., Chu, L. F., Songyang, Z., et al. (2008). Ronin Is Essential for Embryogenesis and the Pluripotency of Mouse Embryonic Stem Cells. *Cell* 133(7), 1162–1174. doi:10.1016/j.cell.2008.05.047

Donoho, G., Jasin, M., and Berg, P. (1998). Analysis of Gene Targeting and Intrachromosomal Homologous Recombination Stimulated by Genomic

Double-Strand Breaks in Mouse Embryonic Stem Cells. *Mol. Cel Biol.* 18, 4070–4078. doi:10.1128/mcb.18.7.4070

Dovey, O. M., Foster, C. T., and Cowley, S. M. (2010). Histone Deacetylase 1 (HDAC1), but Not HDAC2, Controls Embryonic Stem Cell Differentiation. *Proc. Natl. Acad. Sci. U.S.A.* 107:8242–8247. doi:10.1073/pnas.1000478107

Dow, L. E., Fisher, J., O'Rourke, K. P., Muley, A., Kastenhuber, E. R., Livshits, G., et al. (2015). Inducible *In Vivo* Genome Editing with CRISPR-Cas9. *Nat. Biotechnol.* 33, 390–394. doi:10.1038/nbt.3155

Fang, J., Kubota, S., Yang, B., Zhou, N., Zhang, H., Godbout, R., et al. (2004). A DEAD Box Protein Facilitates HIV-1 Replication as a Cellular Co-factor of Rev. *Virology* 330, 471–480. doi:10.1016/j.virol.2004.09.039

Flemr, M., and Bühler, M. (2015). Single-Step Generation of Conditional Knockout Mouse Embryonic Stem Cells. *Cel Rep.* 12, 709–716. doi:10.1016/j.celrep.2015.06.051

Gaj, T., Gersbach, C. A., and Barbas, C. F. (2013). ZFN, TALEN, and CRISPR/Cas-based Methods for Genome Engineering. *Trends Biotechnol.* 31, 397–405. doi:10.1016/j.tibtech.2013.04.004

Gu, H., Marth, J. D., Orban, P. C., Mossmann, H., and Rajewsky, K. (1994). Deletion of a DNA Polymerase β Gene Segment in T Cells Using Cell Type-specific Gene Targeting. *Science*. 265, 103–106. doi:10.1126/science.8016642

Gupta, R. M., and Musunuru, K. (2014). Expanding the Genetic Editing Tool Kit: ZFNs, TALENs, and CRISPR-Cas9. *J. Clin. Invest.* 124, 4154–4161. doi:10.1172/jci72992

Han, C., Liu, Y., Wan, G., Choi, H. J., Zhao, L., Ivan, C., et al. (2014). The RNA-Binding Protein DDX1 Promotes Primary microRNA Maturation and Inhibits Ovarian Tumor Progression. *Cell Rep* 8 (8), 1447–1460. doi:10.1016/j.celrep.2014.07.058

Hildebrandt, M. R., Wang, Y., Li, L., Yasmin, L., Glubrecht, D. D., and Godbout, R. (2019). Cytoplasmic Aggregation of DDX1 in Developing Embryos: Early Embryonic Lethality Associated with Ddx1 Knockout. *Dev. Biol. Jul.* 455(2), 1234–1236. doi:10.1016/j.ydbio.2019.07.014

Johnson, R. S., Sheng, M., Greenberg, M. E., Kolodner, R. D., Papaioannou, V. E., and Spiegelman, B. M. (1989). Targeting of Nonexpressed Genes in Embryonic Stem Cells via Homologous Recombination. *Science*. 245, 1234–1236. doi:10.1126/science.2506639

Linder, P., and Jankowsky, E. (2011). From Unwinding to Clamping - the DEAD Box RNA Helicase Family. *Nat. Rev. Mol. Cel Biol.* 12, 505–516. doi:10.1038/nrm3154

Lu, Y., Liang, F.-X., and Wang, X. (2014). A Synthetic Biology Approach Identifies the Mammalian UPR RNA Ligase RtcB. *Mol. Cel.* 55, 758–770. doi:10.1016/j.molcel.2014.06.032

Neklesa, T. K., Tae, H. S., Schneekloth, A. R., Stulberg, M. J., Corson, T. W., Sundberg, T. B., et al. (2011). Small-molecule Hydrophobic Tagging-Induced Degradation of HaloTag Fusion Proteins. *Nat. Chem. Biol.* 7, 538–543. doi:10.1038/nchembio.597

Ng, L. Y., Ma, H. T., Liu, J. C. Y., Huang, X., Lee, N., and Poon, R. Y. C. (2019). Conditional Gene Inactivation by Combining Tetracycline-Mediated Transcriptional Repression and Auxin-Inducible Degron-Mediated Degradation. *Cell Cycle.* 18(2), 238–248. doi:10.1080/15384101.2018.1563395

Nishimura, K., Yamada, R., Hagihara, S., Iwasaki, R., Uchida, N., Kamura, T., et al. (2020). A Super-sensitive Auxin-Inducible Degron System with an Engineered Auxin-TIR1 Pair. *Nucleic Acids Res.* 48 (18), e108. doi:10.1093/nar/gkaa748

Nishimura, K., Fukagawa, T., Takisawa, H., Kakimoto, T., and Kanemaki, M. (2009). An Auxin-Based Degron System for the Rapid Depletion of Proteins in Nonplant Cells. *Nat. Methods* 6, 917–922. doi:10.1038/nmeth.1401

Popow, J., Jurkin, J., Schleiffer, A., and Martinez, J. (2014). Analysis of Orthologous Groups Reveals Archease and DDX1 as tRNA Splicing Factors. *Nature* 511, 104–107. doi:10.1038/nature13284

Riesenberg, S., Chintalapati, M., Macak, D., Kanis, P., Maricic, T., and Pääbo, S. (2019). Simultaneous Precise Editing of Multiple Genes in Human Cells. *Nucleic Acids Res.* 47 (19), e116. doi:10.1093/nar/gkz669

Schnütgen, F., De-Zolt, S., Van Sloun, P., Hollatz, M., Floss, T., Hansen, J., et al. (2005). Genomewide Production of Multipurpose Alleles for the Functional Analysis of the Mouse Genome. *Proc. Natl. Acad. Sci. U S A.* 102, 7221–7226. doi:10.1073/pnas.0502273102

Suzuki, T., Katada, E., Mizuoka, Y., Takagi, S., Kazuki, Y., Oshimura, M., et al. (2021). A Novel All-In-One Conditional Knockout System Uncovered an Essential Role of DDX1 in Ribosomal RNA Processing. *Nucleic Acids Res. 04* 49 (7), e40. doi:10.1093/nar/gkaa1296

Suzuki, T., Kazuki, Y., Hara, T., and Oshimura, M. (2020). Current Advances in Microcell-Mediated Chromosome Transfer Technology and its Applications. *Exp. Cel Res.*, 390, 111915. doi:10.1016/j.yexcr.2020.111915

Suzuki, T., Kazuki, Y., Oshimura, M., and Hara, T. (2014). A Novel System for Simultaneous or Sequential Integration of Multiple Gene-Loading Vectors into a Defined Site of a Human Artificial Chromosome. *PLoS One* 9, e110404. doi:10.1371/journal.pone.0110404

Thyagarajan, B., Olivares, E. C., Hollis, R. P., Ginsburg, D. S., and Calos, M. P. (2001). Site-Specific Genomic Integration in Mammalian Cells Mediated by Phage φC31 Integrase. *Mol. Cel Biol.* 21, 3926–3934. doi:10.1128/mcb.21.12.3926-3934.2001

Uno, N., Fujimoto, T., Komoto, S., Kurosawa, G., Sawa, M., Suzuki, T., et al. (2018). A Luciferase Complementation Assay System Using Transferable Mouse Artificial Chromosomes to Monitor Protein-Protein Interactions Mediated by G Protein-Coupled Receptors. *Cytotechnology* 70, 1499–1508. doi:10.1007/s10616-018-0231-7

Conflict of Interest: The authors declare that the research was conducted in the absence of any commercial or financial relationships that could be construed as a potential conflict of interest.

Publisher's Note: All claims expressed in this article are solely those of the authors and do not necessarily represent those of their affiliated organizations or those of the publisher, the editors, and the reviewers. Any product that may be evaluated in this article, or claim that may be made by its manufacturer, is not guaranteed or endorsed by the publisher.

frontiers | Frontiers in Cell and Developmental Biology

PERSPECTIVE
published: 01 April 2022
doi: 10.3389/fcell.2022.865810

Regulating Early Biological Events in Human Amniotic Epithelial Stem Cells Using Natural Bioactive Compounds: Extendable Multidirectional Research Avenues

Farhana Ferdousi[1,2,3] *and Hiroko Isoda*[1,2,3,4]*

[1]Alliance for Research on the Mediterranean and North Africa (ARENA), University of Tsukuba, Tsukuba, Japan, [2]Faculty of Life and Environmental Sciences, University of Tsukuba, Tsukuba, Japan, [3]AIST-University of Tsukuba Open Innovation Laboratory for Food and Medicinal Resource Engineering (FoodMed-OIL), AIST, University of Tsukuba, Tsukuba, Japan, [4]R&D Center for Tailor-made QOL, University of Tsukuba, Tsukuba, Japan

Stem cells isolated from perinatal tissue sources possess tremendous potential for biomedical and clinical applications. On the other hand, emerging data have demonstrated that bioactive natural compounds regulate numerous cellular and biochemical functions in stem cells and promote cell migration, proliferation, and attachment, resulting in maintaining stem cell proliferation or inducing controlled differentiation. In our previous studies, we have reported for the first time that various natural compounds could induce targeted differentiation of hAESCs in a lineage-specific manner by modulating early biological and molecular events and enhance the therapeutic potential of hAESCs through modulating molecular signaling. In this perspective, we will discuss the advantages of using naturally occurring active compounds in hAESCs and their potential implications for biological research and clinical applications.

Keywords: human amniotic epithelial cells, natural compound, differentiation inducer, drug screening, cell priming, functional foods, biobank

OPEN ACCESS

Edited by:
Valerie Kouskoff,
The University of Manchester, United Kingdom

Reviewed by:
Toshio Miki,
Nihon University, Japan
Angela Di Baldassarre,
University of Studies G. d'Annunzio Chieti and Pescara, Italy

***Correspondence:**
Hiroko Isoda
isoda.hiroko.ga@u.tsukuba.ac.jp

Specialty section:
This article was submitted to Stem Cell Research, a section of the journal Frontiers in Cell and Developmental Biology

Received: *30 January 2022*
Accepted: *07 March 2022*
Published: *01 April 2022*

Citation:
Ferdousi F and Isoda H (2022) Regulating Early Biological Events in Human Amniotic Epithelial Stem Cells Using Natural Bioactive Compounds: Extendable Multidirectional Research Avenues. Front. Cell Dev. Biol. 10:865810. doi: 10.3389/fcell.2022.865810

INTRODUCTION

The term placenta is considered as an exploitable source of a number of pluripotent stem cells including, human amniotic epithelial stem cells (hAESCs), human amniotic mesenchymal stromal cells (hAMSCs), and human umbilical cord mesenchymal stromal cells (hUMSCs) (Miki and Strom, 2006; Ilancheran et al., 2007; Toda et al., 2007; Hu et al., 2009; Antoniadou and David, 2016; De Coppi and Atala, 2019). As derived from the biological waste product placenta, these perinatal stem cells are readily available, have an abundant supply, require no invasive harvesting procedures as well as have minimal ethical constraints. However, hAESCs possess unique biological characteristics compared to other perinatal pluripotent cells because of their developmental origin from the epiblast at around eight days after fertilization (Miki et al., 2005). They are derived from the innermost single layer of epithelial cells of the amnion that contacts the amniotic fluid directly. Isolated hAESCs express octamer-binding transcription factor-4 (OCT-4), a key transcription factor that maintain pluripotency and self-renewal in embryonic stem cells (ESCs) and induced pluripotent stem cells (iPSCs). hAESCs also express other pluripotent stem cell markers, such as Nanog homeobox

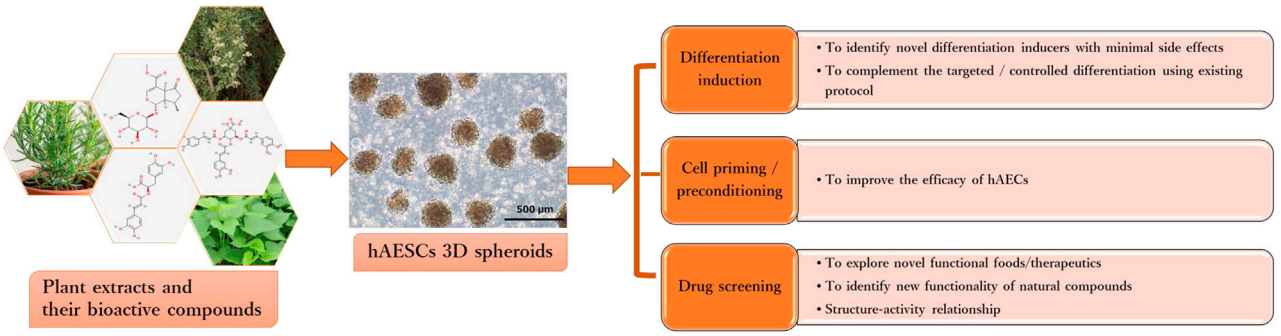

GRAPHICAL ABSTRACT |

TABLE 1 | Biological functions of natural compounds in hAESCs.

Compound	Methodology	Differentiation direction	Biological functions (Enriched Gene Ontology and KEGG pathway)	References
Cyanidin 3-glucoside	Whole genome transcriptome analysis on day 7 cell treatment	Towards adipocyte differentiation	Inhibits cell cycle-related gene expression and induces positive regulation of fibroblast growth factor receptor signaling pathway (GO:0045743), response to muscle activity (GO:0014850)	Takahashi et al. (2021)
Ethanol extract of *Aurantiochytrium*-derived squalene	Whole genome transcriptome analysis on day 7 cell treatment	Towards neuronal differentiation	Induces positive regulation of neuron differentiation (GO:0045666), positive regulation of MAPK cascade (GO:0043410), fibroblast growth factor receptor signaling pathway (GO:0008543), regulation of lipid biosynthetic process (GO: 0046890), cellular response to oxidative process	Ferdousi et al. (2021)
Isorhamnetin	Whole genome transcriptome analysis on day 10 cell treatment, functional analysis	Towards hepatic-lineage specific differentiation	Positive regulation of canonical Wnt signaling pathway (GO:0090263) and TGFb receptor signaling pathway (GO:0007179), cell-matrix adhesion (GO:0007160), extracellular matrix organization (GO:0030198)	Uchida et al. (2020)
Rosmarinic acid	Whole genome transcriptome analysis on day 7 cell treatment	Towards neuronal differentiation	neurogenesis (GO: 0022008), and neuron differentiation (GO: 0030182), Chemical synaptic transmission (GO:0007268)	Ferdousi et al. (2019)
3,4,5-tri-O-caffeoylquinic acid (TCQA)	Whole genome transcriptome analysis on day 7 cell treatment	Towards neuronal and pigment cell differentiation	pigment cell differentiation (GO: 0050931), neurogenesis (GO: 0022008), MAPK cascade, downregulates the expressions of inflammatory cytokines, inhibits cell cycle progression	Bejaoui et al. (2021)
Verbenalin	Whole genome transcriptome analysis on day 7 cell treatment, functional analysis	—	positive regulation of dendrite development (GO: 1900006), negative regulation of type 2 immune response (GO: 0002829), ErbB and MAPK signaling pathways	Ferdousi et al. (2020)
Lycopene	Combination treatment with lycopene and hAESCs in AD rat model	—	Ameliorates Aβ-induced neuroinflammation *in vivo*	Xu et al. (2021)

(NANOG), SRY-Box transcription factor 2 (SOX2), stage-specific embryonic antigen (SSEA)3 and SSEA4, and tumor rejection antigen (TRA)1-60 and TRA 1-80 (Miki et al., 2005; Miki et al., 2010; Murphy et al., 2010; Gaggi et al., 2020). hAESCs lack telomerase activity and have short telomeres, which limit their proliferation efficiency (Gaggi et al., 2020). However, because of their limited proliferation capacity, hAESCs do not pose the risk of tumor or teratoma formation like ESCs (Miki et al., 2005). Moreover, under appropriate differentiation protocol, hAESCs can be differentiated into cells from all three germ layers, such as cells from the endodermal origin-liver, pancreas and lung epithelium, neural cells from the ectodermal origin, and bone and fat cells from mesodermal origin (Sakuragawa et al., 1996; Cai et al., 2005; Miki et al., 2005; Pan et al., 2006; Toda et al., 2007; Miki et al., 2010; Niknejad et al., 2010; Serra et al., 2018; Furuya et al., 2019). Notably, hAESCs have distinct expression profiles of human leukocyte antigens (HLAs). hAESCs show low expression of classical HLA-I: HLA-A, B, and C and no expression of HLA-II: HLA-DP, DQ, and DR, which

contribute to immune recognition and rejection of PSCs after transplantation. hAESCs also express non-classical HLA-I: HLA-E, F, and G, specifically HLA-G, which have inhibitory effects on immune cells (Akle et al., 1981; Li et al., 2005). Thus, hAESCs are regarded as a promising source of stem cells in biological research and regenerative medicine.

On the other hand, natural resource-derived biologically active compounds, such as polyphenols, flavonoids, tannins, terpenoids, and fatty acids, have long been investigated for promoting cell division, and differentiation of pluripotent and adult stem cells (PSCs) under standard culture conditions (Udalamaththa et al., 2016; Udagama and Udalamaththa, 2018). Effects of plant extracts and their bioactive compounds on the proliferation and differentiation of mesenchymal stem cells (MSCs) have been extensively studied (Kornicka et al., 2017; Saud et al., 2019; Maeda, 2020). However, in spite of the fact that hAESCs were discovered nearly two decades ago, only a few studies have attempted to investigate the effects of natural compounds in hAESCs. As part of our continual effort to explore the bioactivities and functionalities of natural compounds of plant origin, we have been investigating their effects on modulating the early biological events in hAESCs (Ferdousi et al., 2019; Aonuma et al., 2020; Ferdousi et al., 2020; Uchida et al., 2020; Bejaoui et al., 2021; Ferdousi et al., 2021; Takahashi et al., 2021). In this perspective, we will discuss the multidirectional research opportunities through integrating natural bioactive compounds with the existing hAESCs research platforms.

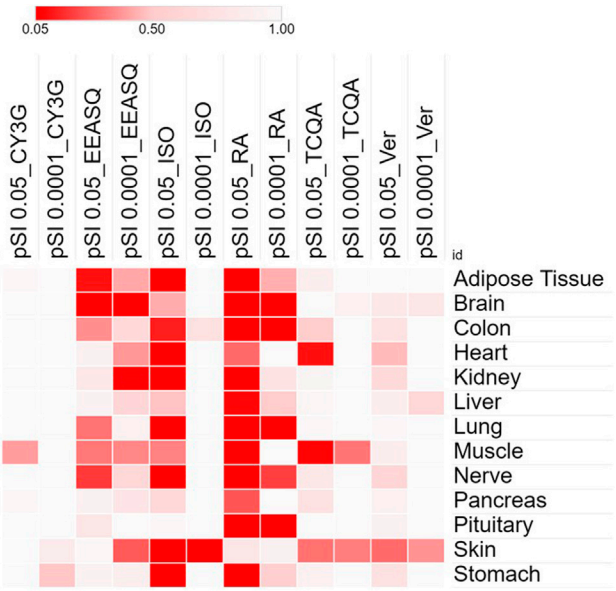

FIGURE 1 | Heat map showing the significance and specificity of the tissue expressions by the differentially expressed genes of different compounds in hAESCs. Cells were treated with compounds for 7–10 days and RNAs were isolated from the control and treated hAESCs for microarray experiments using the Affymetrix's GeneAtlas® System (Affymetrix Inc., Santa Clara, CA, USA, human genome array strips; HG-U219). Genes with a linear fold change >1.1 (verbenalin), 1.2 (RA, TCQA and EEASQ), and 2 (ISO, CY3G) and a p-value < 0.05 (one-way between-subjects ANOVA) were considered as differentially expressed genes. Enrichment analysis was conducted using the Tissue Specific Expression Analysis (TSEA) tool (http://genetics.wustl.edu/jdlab/tsea//). Heat map was generated on Morpheus tool (https://software.broadinstitute.org/morpheus//). Significance of tissue enrichment were identified by Fisher's Exact test. pSI, Specificity Index thresholds; pSI 0.05, significantly enriched all transcripts; pSI 0.0001, most specific subset of significantly enriched transcripts; CY3G, cyanidin 3-glucoside; EEASQ, ethanol extract of Aurantiochytrium-derived squalene; ISO, isorhamnetin; RA, rosmarinic acid; TCQA, 3,4,5-tri-O-caffeoylquinic acid; Ver, verbenalin.

NATURAL COMPOUND-TREATED HAESCS: POTENTIAL RESEARCH OPPORTUNITIES

Natural Bioactive Compounds as Promising Differentiation Inducers of hAESCs

As hAESCs are derived from the pluripotent epiblast, these cells exert a high level of differentiation plasticity. A series of studies demonstrated successful induction of hAESCs into hepatocyte-like cells (Marongiu et al., 2011; Maymó et al., 2018; Furuya et al., 2019), hepatic sinusoidal endothelial cells (Serra et al., 2018), insulin-producing pancreatic β cells (Szukiewicz et al., 2010) through a combined approach using growth factors, cytokines, extracellular matrix proteins, or cocultured with mouse hepatocytes. Similarly, following treatment with noggin, serum, basic fibroblast growth factor (bFGF), and retinoic acid, hAESCs are able to differentiate into neural cells (Ishii et al., 1999; Okawa et al., 2001; Niknejad et al., 2010). Additionally, proper culture condition also induces mesodermal-lineage cells, including adipocytes, osteocytes, chondrocytes, and cardiomyocytes (Miki and Strom, 2006; Fang et al., 2012). Therefore, hAESCs provide an excellent cell source for cell therapy and regenerative medicine. However, hAESCs consist of a heterogeneous cell population according to different stem cell markers profiling (Centurione et al., 2018), which hinders the large-scale clinical transformation of hAESCs.

Additionally, the recombinant growth factors, synthetic and semi-biological cytokines, and proteins used for maintaining proliferation and inducing differentiation of stem cells, are reported to have toxic effects and possible risk of rejection. Also, these reagents are rapidly degradable and are required to replace continuously, making the whole procedure highly expensive, hence limiting their use in therapeutic tissue engineering (Marion and Mao, 2006; Raghavan et al., 2013). In this regard, exploring new biological approaches to facilitate hAESCs differentiation potential is highly needed.

In recent years, a new research stream has been developing to use naturally occurring bioactive compounds as stimulants of stem cells because of their high availability, low toxicity, and minimum side effects. Certain phytochemicals have been extensively studied for adult stem cell proliferation and inhibition of cancer cell proliferation (Udalamaththa et al., 2016). Those plant-derived pharmacologically active substances are reported to increase the rate of cell division and differentiation through modulating complex signal pathways and to facilitate tissue regeneration and immunomodulation. However, in hAESCs, the effects of natural compounds have not been

explored widely. In our previous studies, we have reported for the first time that several natural compounds could regulate early biological events in hAESCs suitable for controlled differentiation of hAESCs. A caffeic acid ester, rosmarinic acid (RA), showed the potential of enhanced neural cell differentiation in hAESCs through downregulating the gene expressions related to canonical WNT pathway, BMP/TGF-b pathway, and notch signaling pathway (Ferdousi et al., 2019). RA also upregulated the expression of nemo like kinase (*NLK*), the positive effector of non-canonical WNT pathway. A caffeoylquinic acid derivative, 3,4,5-Tri-O-Caffeoylquinic acid (TCQA), enhanced the expressions of catenin beta 1 (*CTNNB1*), bone morphogenetic protein 5 (*BMP5*), versican (*VCAN*), melanocortin 1 receptor (*MC1R*), and dermokine (*DMKN*) in hAESCs, which are known to be involved in neural and pigment cell differentiation (Bejaoui et al., 2021). A flavonol aglycone isorhamnetin could induce the expression of several hepatic progenitor markers, like delta-like non-canonical Notch ligand 1 (*DLK1*), epithelial cell adhesion molecule (*EPCAM*), and albumin (*ALB*). Isorhamnetin-treated hAESCs also showed several mature hepatocyte functions, including ICG uptake, glycogen storage, and urea production, and weak hepatic cytochrome P450 (CYP) enzyme activity (Uchida et al., 2020). An anthocyanin, cyanidin 3-glucoside (CY3G), upregulated the expression of meteorin like glial cell differentiation regulator (*METRNL*) in hAESCs, which is an adipomyokine with pleiotropic activities in adipose tissue (Takahashi et al., 2021). These findings in hAESCs are supported by previous studies on these compounds in different *in vitro* and *in vivo* settings. For example, RA has been reported to exert neuroprotective effects in neuroinflammatory and neurodegenerative diseases (Takeda et al., 2002; Ito et al., 2008; Sasaki et al., 2013; Kondo et al., 2015; Makhathini et al., 2018), which has been attributed to RA's capacity to induce neural differentiation and neurotransmitter release. Similarly, TCQA has been reported to improve cognitive function in aging model mice through inducing adult neurogenesis (Sasaki et al., 2019a). TCQA has also been reported to promote hair regrowth and pigmentation *in vitro* and *in vivo* (Bejaoui et al., 2019; 2020). Isorhamnetin has been widely reported to alleviate hepatic fibrosis in a number of *in vivo* models (Lee et al., 2008; Ganbold et al., 2019; Liu et al., 2019), while CY3G is known for its anti-obesity and anti-diabetic effects through modulating adipocyte differentiation (Matsukawa et al., 2015; Olivas-Aguirre et al., 2016; Saulite et al., 2019). In **Figure 1**, we have shown the enriched cell types by differentially expressed genes in different compound-treated hAESCs. Detailed experimental and analysis procedures are available in our previously published paper (Ferdousi et al., 2019). In the future, establishing the optimal hAESCs culture procedure by utilizing appropriate preconditioning with natural compounds is worth further investigation.

Natural Bioactive Compounds to Enhance Therapeutic Potential of hAESCs

The distinct immunomodulatory properties of hAESC make it the most promising candidate for cell-based therapy (Miki, 2011). Specifically, hAESCs have very low immunogenicity, thus are suitable for allotransplantation. Indeed, mounting studies have revealed the beneficial outcomes of hAESCs-based therapy for wound healing (Zhao et al., 2018; Zheng et al., 2018), skin graft (Li et al., 2012), injury repair (Kamiya et al., 2005; Parmar et al., 2006; Bai et al., 2020), pulmonary and liver fibrosis (Manuelpillai et al., 2012; Tan et al., 2014; Miki, 2016; Tan et al., 2017; Cargnoni et al., 2018), and importantly in neurological diseases (Di Germanio et al., 2016; Sanluis-Verdes et al., 2017), including spinal cord injury (Gao et al., 2014), Parkinson's disease (Yang et al., 2010), Alzheimer's disease (AD) (Xue et al., 2012; Kim et al., 2020), and multiple sclerosis (McDonald et al., 2011; Liu et al., 2012). However, successful clinical outcomes of hAESC transplantation depend on its immunomodulating functions. A previous study showed that expansion of hAESCs in serum-free culture media leads to significantly different expressions of stem cell markers, increased differentiation capacity and immunosuppression (Yang et al., 2018). Another study reported that prolonged exposure of hAESCs to the inflammatory cytokines, namely interleukin (IL)-1β and interferon (INF)-γ, resulted in enhanced secretion of immunomodulatory molecules (Kolanko et al., 2019). However, while current studies focus on the safety and efficacy of translating hAESC-based therapy into clinical practices, using natural compounds for priming approaches to improve the therapeutic efficacy of hAESCs has not been explored.

Our previous studies showed that treatment with natural compounds increases anti-inflammatory potential of hAESCs (Bejaoui et al., 2021; Ferdousi et al., 2021; Takahashi et al., 2021). We have also reported that isorhamnetin may have the potential to improve anti-fibrotic effects of hAESCs (Aonuma et al., 2020). Additionally, we showed that an iridoid glucoside verbenalin may enhance therapeutic potential of hAESCs for AD through targeting multiple pathologies simultaneously, including lysosomal dysfunction, pathological angiogenesis, neurometabolic aging, pathological protein aggregation, and circadian rhythms (Ferdousi et al., 2020). A recent interesting study reported that a combination of oral administration of lycopene, a carotenoid hydrocarbon found in bright red fruits and vegetables, and hAESCs transplantation could significantly ameliorate cognitive function in an *in vivo* AD model compared to a single treatment of lycopene and hAESC (Xu et al., 2021). Additionally, combination treatment of lycopene and hAESC also improved immunosuppressive activities in chroid plexus of AD rats. In **Table 1**, biological functions of different compounds in hAESCs are listed. We envision the emerging combination of naturally occurring compounds and hAESCs will offer additional opportunities for successful clinical translation of hAESC.

hAESCs as a Drug Screening Tool for Natural Compounds

Human PSCs, including both ESCs and iPSCs, have been used extensively as physiologically relevant *in vitro* human models in high-throughput drug screening, from target identification to preclinical compound evaluation. Stem cell-based methods

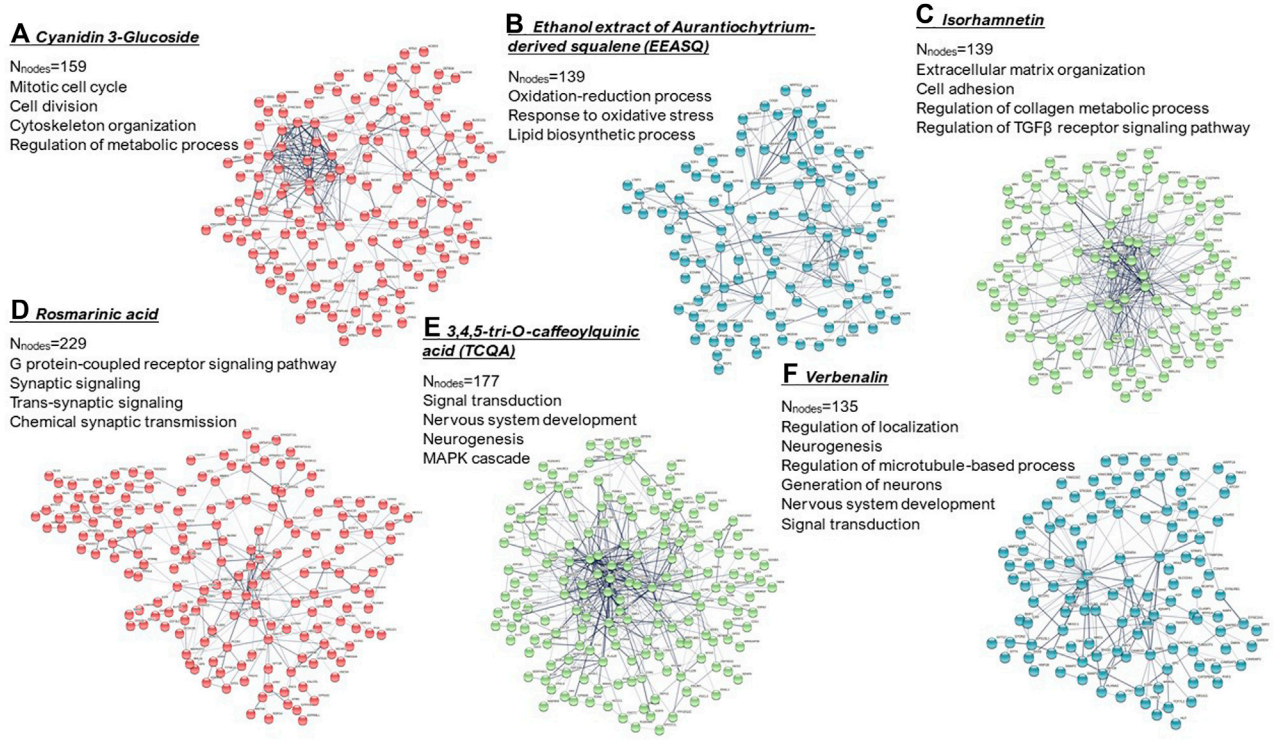

FIGURE 2 | k-means clustering and PPI network of the differentially expressed genes (computed using STRING; https://string-db.org/). Significantly enriched gene ontologies (biological processes) in each network are presented. N_{nodes} = number of nodes. **(A)** Cyanidin 3-glucoside; **(B)** ethanol extract of Aurantiochytrium-derived squalene (EEASQ); **(C)** Isorhamnetin; **(D)** Rosmarinic acid; **(E)** 3,4,5-tri-O-caffeoylquinic acid (TCQA); **(F)** Verbenalin. Cells were treated with compounds for 7–10 days and RNAs were isolated from the control and treated hAESCs for microarray experiments using the Affymetrix's GeneAtlas® System (Affymetrix Inc., Santa Clara, CA, USA, human genome array strips; HG-U219). Genes with a linear fold change >1.1 (verbenalin), 1.2 (RA, TCQA and EEASQ), and 2 (ISO, CY3G) and a p-value < 0.05 (one-way between-subjects ANOVA) were considered as differentially expressed genes.

reduce the timelines and attrition rate of new therapeutics (McNeish, 2004; Ebert and Svendsen, 2010; Laustriat et al., 2010; Grskovic et al., 2011; Rubin and Haston, 2011; Engle and Puppala, 2013). However, limited cell resources, invasive extraction procedures, expensive cell reprogramming and maintenance procedures, and ethical constraints are the main challenges for the large-scale use of ESCs and iPSCs for drug screening and toxicity testing.

On the other hand, a huge number of small molecules derived from or based on natural compounds become available for drug screening and biological investigations each year. However, despite substantial technological advances, the rate of new medicine discovery is exceptionally low. Indeed, drug discovery is greatly hampered by the gap between the validation of the compound and its successful clinical application. The unpredictability of the currently used *in vitro* cellular models, where the crucial elements of drug-biology interaction are lost, and the complexity of the *in vivo* microenvironment are behind the translational inefficiency of new target compounds.

In this regard, hAESCs and other perinatal stem cells, which are derived from biological waste products, may offer promising cell sources in drug screening and toxicity testing efforts. In **Figure 2**, we have shown important biological functions of different natural compounds observed in hAESCs (please refer to **Supplementary Figure** file for details). In hAESCs, isorhamnetin showed anti-fibrotic potential, which was then validated in the cardiac fibrosis *in vivo* model (Aonuma et al., 2020). The observed neuroprotective potential of microalgae-derived squalene (Ferdousi et al., 2021) has also been validated in aging model mice (Sasaki et al., 2019b; Sasaki et al., 2020). Similarly, the chemical synaptic transmission activity of RA was observed in depression model mice (Sasaki et al., 2013; Kondo et al., 2015), and the neurogenesis-regulating effect of TCQA was confirmed in aging mice (Sasaki et al., 2019a). Our observations strongly suggest that hAESCs would provide a promising platform to perform initial functionality screening of natural compounds.

DISCUSSION

Biologically active compounds have been incorporated into stem cell research to maintain stem cell proliferation or to facilitate controlled differentiation into more defined tissues (Udalamaththa et al., 2016; Udagama and Udalamaththa, 2018; Saud et al., 2019). Our previous studies have suggested the potential of natural compounds in optimizing the

microenvironment and regulating the early biological events to induce directed differentiation of hAESCs. Although hAESCs have already been studied extensively for their therapeutic potential (Toda et al., 2007), we anticipate that the emerging combination of natural compounds and hAESCs would lead to a stable molecular signature, enhanced proliferation capacity, and improved therapeutic efficacy.

One of the major challenges in hAESCs research is the heterogeneity in primary amnion-derived epithelial cell populations based on their cell surface profiling (Centurione et al., 2018; Ghamari et al., 2020). For example, studies showed that NANOG is expressed in only 1–3% of hAESCs, about 50% of term hAESCs express SSEA-4, and co-expression of SSEA-4, TRA1-60, and TRA1-81 is found in 4% of amniotic epithelial cells (Miki et al., 2005; Miki and Strom, 2006; Miki et al., 2007; Bryzek et al., 2013). Additionally, hAESCs derived from different areas of amniotic membrane exhibited different pluripotent surface markers expression and proliferative ability (Centurione et al., 2018). However, several studies have proposed better controllable approaches for generating hAESCs homogeneous enough for biological and clinical application (Miki et al., 2010; Murphy et al., 2010; Zhou et al., 2013; Gramignoli et al., 2016; Gottipamula and Sridhar, 2018; Yang et al., 2018). Another study showed that expansion of hAESCs in 3D culture system and subsequent isolation from the adherent subpopulations may enhance the stemness properties of hAESCs (Furuya et al., 2019).

From one human term amniotic membrane, nearly 200 million hAESCs can be harvested, allowing sufficient cell supply for large-scale use in academic research, pharmaceutical industry, and clinical application. For our studies on natural compound-treated hAESCs, we received the cells from 'The Tsukuba Human Tissue Biobank Center (THB)' established at the University of Tsukuba Hospital in 2013 (Takeuchi et al., 2016). The hAESCs were isolated from the mothers' donated placenta who underwent cesarean section. Biobanking of perinatal stem cells began over three decades ago with the establishment of umbilical cord blood biobank. However, as the field of perinatal cells and regenerative medicine is progressing rapidly, biobanking of other types of perinatal stem cells, including hAESCs, will be an integral part of successful cell-based therapy.

Recent advances in genome-wide expression profiling, single-cell multi-omics analysis followed by machine learning-based analyses permit systematic approaches to the biological discovery of regulatory mechanisms and biochemical pathways (Chavan et al., 2006; Kumar et al., 2012). They have indeed provided certain unique opportunities for widening the application of hAESC research platform.

In the future, integrating natural compounds to hAESCs to establish an optimal culture condition, to achieve appropriate preconditioning for enhancing the therapeutic potential would be new opportunities for further investigation.

DATA AVAILABILITY STATEMENT

Publicly available datasets were analyzed in this study. This data can be found here: Microarray data are deposited in the Gene Expression Omnibus (GEO) under accession numbers GSE148776 (CY3G), GSE188411 (EEASQ), GSE148777 (Isorhamnetin), GSE133277 (Rosmarinic acid), GSE153617 (TCQA), and GSE137061 (Verbenalin).

AUTHOR CONTRIBUTIONS

FF: conceptualization, data curation, formal analysis, visualization, writing—original draft; HI: conceptualization, funding acquisition, project administration, supervision and writing—review and editing. Both authors made substantial contributions to this article and approved the final article.

FUNDING

This research was supported by Japan Science and Technology Agency (JST)-Science and Technology Research Partnership for Sustainable Development (SATREPS, Grant No. JPMJSA1506).

ACKNOWLEDGMENTS

We thankfully acknowledge Professor Nobuhiro Ohkohchi, Professor Yun-Wen Zheng, Dr. Kazunori Sasaki and Dr. Kinji Furuya for their active contribution to this project.

SUPPLEMENTARY MATERIAL

The Supplementary Material for this article can be found online at: https://www.frontiersin.org/articles/10.3389/fcell.2022.865810/full#supplementary-material

REFERENCES

Akle, C. A., Welsh, K. I., Adinolfi, M., Leibowitz, S., and McColl, I. (1981). Immunogenicity of Human Amniotic Epithelial Cells after Transplantation into Volunteers. *The Lancet* 318 (8254), 1003–1005. doi:10.1016/s0140-6736(81)91212-5

Antoniadou, E., and David, A. L. (2016). Placental Stem Cells. *Best Pract. Res. Clin. Obstet. Gynaecol.* 31, 13–29. doi:10.1016/j.bpobgyn.2015.08.014

Aonuma, K., Ferdousi, F., Xu, D., Tominaga, K., and Isoda, H. (2020). Effects of Isorhamnetin in Human Amniotic Epithelial Stem Cells *In Vitro* and its Cardioprotective Effects *In Vivo*. *Front Cell Dev Biol* 8, 578197. doi:10.3389/fcell.2020.578197

Bai, X., Liu, J., Yuan, W., Liu, Y., Li, W., Cao, S., et al. (2020). Therapeutic Effect of Human Amniotic Epithelial Cells in Rat Models of Intrauterine Adhesions. *Cell Transpl.* 29, 963689720908495. doi:10.1177/0963689720908495

Bejaoui, M., Ferdousi, F., Zheng, Y.-W., Oda, T., and Isoda, H. (2021). Regulating Cell Fate of Human Amnion Epithelial Cells Using Natural Compounds: an Example of Enhanced Neural and Pigment Differentiation by 3,4,5-Tri-O-Caffeoylquinic Acid. *Cell Commun Signal* 19 (1), 26. doi:10.1186/s12964-020-00697-5

Bejaoui, M., Villareal, M. O., and Isoda, H. (2020). 3,4,5-Tri-O-Caffeoylquinic Acid Promoted Hair Pigmentation through β-Catenin and its Target Genes. *Front. Cell Dev. Biol.* 8, 175. doi:10.3389/fcell.2020.00175

Bejaoui, M., Villareal, M. O., and Isoda, H. (2019). β-catenin-mediated Hair Growth Induction Effect of 3,4,5-Tri-O-Caffeoylquinic Acid. *Aging* 11 (12), 4216–4237. doi:10.18632/aging.102048

Bryzek, A., Czekaj, P., Plewka, D., Komarska, H., Tomsia, M., Lesiak, M., et al. (2013). Expression and Co-expression of Surface Markers of Pluripotency on Human Amniotic Cells Cultured in Different Growth media. *Ginekol Pol.* 84 (12), 1012–1024. doi:10.17772/gp/1673

Cai, Z., Pan, L., and Shu, J. (2005). Specific Proteins of Neural Stem Cell Expressed by Human Amnion Cells. *Chin. J. Rehabil. Theor. Pract.* 11 (12), 965–967.

Cargnoni, A., Farigu, S., Cotti Piccinelli, E., Bonassi Signoroni, P., Romele, P., Vanosi, G., et al. (2018). Effect of Human Amniotic Epithelial Cells on Pro-fibrogenic Resident Hepatic Cells in a Rat Model of Liver Fibrosis. *J. Cell Mol Med* 22 (2), 1202–1213. doi:10.1111/jcmm.13396

Centurione, L., Passaretta, F., Centurione, M. A., De Munari, S., Vertua, E., Silini, A., et al. (2018). Mapping of the Human Placenta. *Cell Transpl.* 27 (1), 12–22. doi:10.1177/0963689717725078

Chavan, P., Joshi, K., and Patwardhan, B. (2006). DNA Microarrays in Herbal Drug Research. *Evidence-Based Complement. Altern. Med.* 3 (4), 447–457. doi:10.1093/ecam/nel075

De Coppi, P., and Atala, A. (2019). "Stem Cells from the Amnion," in *Principles of Regenerative Medicine* (Cambridge, Massachusetts: Academic Press, Elsevier), 133–148. doi:10.1016/b978-0-12-809880-6.00009-6

Di Germanio, C., Bernier, M., de Cabo, R., and Barboni, B. (2016). Amniotic Epithelial Cells: A New Tool to Combat Aging and Age-Related Diseases? *Front. Cell Dev. Biol.* 4, 135. doi:10.3389/fcell.2016.00135

Ebert, A. D., and Svendsen, C. N. (2010). Human Stem Cells and Drug Screening: Opportunities and Challenges. *Nat. Rev. Drug Discov.* 9 (5), 367–372. doi:10.1038/nrd3000

Engle, S. J., and Puppala, D. (2013). Integrating Human Pluripotent Stem Cells into Drug Development. *Cell stem cell* 12 (6), 669–677. doi:10.1016/j.stem.2013.05.011

Fang, C.-H., Jin, J., Joe, J.-H., Song, Y.-S., So, B.-I., Lim, S. M., et al. (2012). *In Vivo* differentiation of Human Amniotic Epithelial Cells into Cardiomyocyte-like Cells and Cell Transplantation Effect on Myocardial Infarction in Rats: Comparison with Cord Blood and Adipose Tissue-Derived Mesenchymal Stem Cells. *Cell Transpl.* 21 (8), 1687–1696. doi:10.3727/096368912x653039

Ferdousi, F., Furuya, K., Sasaki, K., Zheng, Y.-W., Oda, T., and Isoda, H. (2021). DNA Microarray-Based Global Gene Expression Profiling in Human Amniotic Epithelial Cells Predicts the Potential of Microalgae-Derived Squalene for the Nervous System and Metabolic Health. *Biomedicines* 10 (1), 48. doi:10.3390/biomedicines10010048

Ferdousi, F., Kondo, S., Sasaki, K., Uchida, Y., Ohkohchi, N., Zheng, Y.-W., et al. (2020). Microarray Analysis of Verbenalin-Treated Human Amniotic Epithelial Cells Reveals Therapeutic Potential for Alzheimer's Disease. *Aging* 12 (6), 5516–5538. doi:10.18632/aging.102985

Ferdousi, F., Sasaki, K., Uchida, Y., Ohkohchi, N., Zheng, Y.-W., and Isoda, H. (2019). Exploring the Potential Role of Rosmarinic Acid in Neuronal Differentiation of Human Amnion Epithelial Cells by Microarray Gene Expression Profiling. *Front. Neurosci.* 13, 779. doi:10.3389/fnins.2019.00779

Furuya, K., Zheng, Y.-W., Sako, D., Iwasaki, K., Zheng, D.-X., Ge, J.-Y., et al. (2019). Enhanced Hepatic Differentiation in the Subpopulation of Human Amniotic Stem Cells under 3D Multicellular Microenvironment. *Wjsc* 11 (9), 705–721. doi:10.4252/wjsc.v11.i9.705

Gaggi, G., Di Credico, A., Izzicupo, P., Antonucci, I., Crescioli, C., Di Giacomo, V., et al. (2020). Epigenetic Features of Human Perinatal Stem Cells Redefine Their Stemness Potential. *Cells* 9 (5), 1304. doi:10.3390/cells9051304

Ganbold, M., Owada, Y., Ozawa, Y., Shimamoto, Y., Ferdousi, F., Tominaga, K., et al. (2019). Isorhamnetin Alleviates Steatosis and Fibrosis in Mice with Nonalcoholic Steatohepatitis. *Sci. Rep.* 9 (1), 16210–16211. doi:10.1038/s41598-019-52736-y

Gao, S., Ding, J., Xiao, H.-J., Li, Z.-Q., Chen, Y., Zhou, X.-S., et al. (2014). Anti-inflammatory and Anti-apoptotic Effect of Combined Treatment with Methylprednisolone and Amniotic Membrane Mesenchymal Stem Cells after Spinal Cord Injury in Rats. *Neurochem. Res.* 39 (8), 1544–1552. doi:10.1007/s11064-014-1344-9

Ghamari, S.-H., Abbasi-Kangevari, M., Tayebi, T., Bahrami, S., and Niknejad, H. (2020). The Bottlenecks in Translating Placenta-Derived Amniotic Epithelial and Mesenchymal Stromal Cells into the Clinic: Current Discrepancies in Marker Reports. *Front. Bioeng. Biotechnol.* 8, 180. doi:10.3389/fbioe.2020.00180

Gottipamula, S., and Sridhar, K. N. (2018). Large-scale Isolation, Expansion and Characterization of Human Amniotic Epithelial Cells. *Ijsc* 11 (1), 87–95. doi:10.15283/ijsc18001

Gramignoli, R., Srinivasan, R. C., Kannisto, K., and Strom, S. C. (2016). Isolation of Human Amnion Epithelial Cells According to Current Good Manufacturing Procedures. *Curr. Protoc. Stem Cell Biol* 37 (1), 1E–13E. doi:10.1310.1002/cpsc.2

Grskovic, M., Javaherian, A., Strulovici, B., and Daley, G. Q. (2011). Induced Pluripotent Stem Cells - Opportunities for Disease Modelling and Drug Discovery. *Nat. Rev. Drug Discov.* 10 (12), 915–929. doi:10.1038/nrd3577

Hu, J., Cai, Z., and Zhou, Z. (2009). Progress in Studies on the Characteristics of Human Amnion Mesenchymal Cells. *Prog. Nat. Sci.* 19 (9), 1047–1052. doi:10.1016/j.pnsc.2008.12.005

Ilancheran, S., Michalska, A., Peh, G., Wallace, E. M., Pera, M., and Manuelpillai, U. (2007). Stem Cells Derived from Human Fetal Membranes Display Multilineage Differentiation Potential. *Biol. Reprod.* 77 (3), 577–588. doi:10.1095/biolreprod.106.055244

Ishii, T., Ohsugi, K., Nakamura, S., Sato, K., Hashimoto, M., Mikoshiba, K., et al. (1999). Gene Expression of Oligodendrocyte Markers in Human Amniotic Epithelial Cells Using Neural Cell-type-specific Expression System. *Neurosci. Lett.* 268 (3), 131–134. doi:10.1016/s0304-3940(99)00297-9

Ito, N., Yabe, T., Gamo, Y., Nagai, T., Oikawa, T., Yamada, H., et al. (2008). Rosmarinic Acid from Perillae Herba Produces an Antidepressant-like Effect in Mice through Cell Proliferation in the hippocampus. *Biol. Pharm. Bull.* 31 (7), 1376–1380. doi:10.1248/bpb.31.1376

Kamiya, K., Wang, M., Uchida, S., Amano, S., Oshika, T., Sakuragawa, N., et al. (2005). Topical Application of Culture Supernatant from Human Amniotic Epithelial Cells Suppresses Inflammatory Reactions in Cornea. *Exp. Eye Res.* 80 (5), 671–679. doi:10.1016/j.exer.2004.11.018

Kim, K., Suh, Y.-H., and Chang, K.-A. (2020). Therapeutic Effects of Human Amniotic Epithelial Stem Cells in a Transgenic Mouse Model of Alzheimer's Disease. *Ijms* 21 (7), 2658. doi:10.3390/ijms21072658

Kolanko, E., Kopaczka, K., Koryciak-Komarska, H., Czech, E., Szmytkowska, P., Gramignoli, R., et al. (2019). Increased Immunomodulatory Capacity of Human Amniotic Cells after Activation by Pro-inflammatory Chemokines. *Eur. J. Pharmacol.* 859, 172545. doi:10.1016/j.ejphar.2019.172545

Kondo, S., El Omri, A., Han, J., and Isoda, H. (2015). Antidepressant-like Effects of Rosmarinic Acid through Mitogen-Activated Protein Kinase Phosphatase-1 and Brain-Derived Neurotrophic Factor Modulation. *J. Funct. Foods* 14, 758–766. doi:10.1016/j.jff.2015.03.001

Kornicka, K., Kocherova, I., and Marycz, K. (2017). The Effects of Chosen Plant Extracts and Compounds on Mesenchymal Stem Cells-A Bridge between Molecular Nutrition and Regenerative Medicine- Concise Review. *Phytother. Res.* 31 (7), 947–958. doi:10.1002/ptr.5812

Kumar, A., Asthana, M., Sharma, S., Roy, P., Amdekar, S., Singh, V., et al. (2012). Importance of Using DNA Microarray in Studying Medicinal Plant.

Laustriat, D., Gide, J., and Peschanski, M. (2010). Human Pluripotent Stem Cells in Drug Discovery and Predictive Toxicology. *Biochem. Soc. Trans.* 38 (4), 1051–1057.

Lee, M.-K., Yang, H.-K., Ha, N.-R., Sung, S.-H., and Kim, Y.-C. (2008). Isorhamnetin from Oenanthe Javanica Attenuates Fibrosis in Rat Hepatic Stellate Cells via Inhibition of ERK Signaling Pathway. *Nat. Product. Sci.* 14 (2), 81–85.

Li, H., Chu, Y., Zhang, Z., Zhang, G., Jiang, L., Wu, H., et al. (2012). Construction of Bilayered Tissue-Engineered Skin with Human Amniotic Mesenchymal Cells and Human Amniotic Epithelial Cells. *Artif. organs* 36 (10), 911–919. doi:10.1111/j.1525-1594.2012.01461.x

Li, H., Niederkorn, J. Y., Neelam, S., Mayhew, E., Word, R. A., McCulley, J. P., et al. (2005). Immunosuppressive Factors Secreted by Human Amniotic Epithelial Cells. *Invest. Ophthalmol. Vis. Sci.* 46 (3), 900–907. doi:10.1167/iovs.04-0495

Liu, N., Feng, J., Lu, X., Yao, Z., Liu, Q., Lv, Y., et al. (2019). Isorhamnetin Inhibits Liver Fibrosis by Reducing Autophagy and Inhibiting Extracellular Matrix Formation *via* the TGF-β1/Smad3 and TGF-B1/p38 MAPK Pathways. *Mediators Inflamm.* 2019. doi:10.1155/2019/6175091

Liu, Y. H., Vaghjiani, V., Tee, J. Y., To, K., Cui, P., Oh, D. Y., et al. (2012). Amniotic Epithelial Cells from the Human Placenta Potently Suppress a Mouse Model of Multiple Sclerosis. *PloS one* 7 (4), e35758. doi:10.1371/journal.pone.0035758

Maeda, A. (2020). Recruitment of Mesenchymal Stem Cells to Damaged Sites by Plant-Derived Components. *Front. Cell Dev. Biol.* 8, 437. doi:10.3389/fcell.2020.00437

Makhathini, K. B., Mabandla, M. V., and Daniels, W. M. U. (2018). Rosmarinic Acid Reverses the Deleterious Effects of Repetitive Stress and Tat Protein. *Behav. Brain Res.* 353, 203–209. doi:10.1016/j.bbr.2018.07.010

Manuelpillai, U., Lourensz, D., Vaghjiani, V., Tchongue, J., Lacey, D., Tee, J.-Y., et al. (2012). Human Amniotic Epithelial Cell Transplantation Induces Markers of Alternative Macrophage Activation and Reduces Established Hepatic Fibrosis. *PloS one* 7 (6), e38631. doi:10.1371/journal.pone.0038631

Marion, N. W., and Mao, J. J. (2006). Mesenchymal Stem Cells and Tissue Engineering. *Methods Enzymol.* 420, 339–361. doi:10.1016/s0076-6879(06)20016-8

Marongiu, F., Gramignoli, R., Dorko, K., Miki, T., Ranade, A. R., Paola Serra, M., et al. (2011). Hepatic Differentiation of Amniotic Epithelial Cells. *Hepatology* 53 (5), 1719–1729. doi:10.1002/hep.24255

Matsukawa, T., Inaguma, T., Han, J., Villareal, M. O., and Isoda, H. (2015). Cyanidin-3-glucoside Derived from Black Soybeans Ameliorate Type 2 Diabetes through the Induction of Differentiation of Preadipocytes into Smaller and Insulin-Sensitive Adipocytes. *J. Nutr. Biochem.* 26 (8), 860–867. doi:10.1016/j.jnutbio.2015.03.006

Maymó, J. L., Riedel, R., Pérez-Pérez, A., Magatti, M., Maskin, B., Dueñas, J. L., et al. (2018). Proliferation and Survival of Human Amniotic Epithelial Cells during Their Hepatic Differentiation. *PloS one* 13 (1), e0191489.

McDonald, C., Siatskas, C., and C.A. Bernard, C. (2011). The Emergence of Amnion Epithelial Stem Cells for the Treatment of Multiple Sclerosis. *Inflamm. Regen.* 31 (3), 256–271. doi:10.2492/inflammregen.31.256

McNeish, J. (2004). Embryonic Stem Cells in Drug Discovery. *Nat. Rev. Drug Discov.* 3 (1), 70–80. doi:10.1038/nrd1281

Miki, T., Marongiu, F., Dorko, K., Ellis, E. C., and Strom, S. C. (2010). Isolation of Amniotic Epithelial Stem Cells. *Curr. Protoc. Stem Cell Biol.* 12, 1E.3.1–1E.3.10. doi:10.1002/9780470151808.sc01e03s12

Miki, T. (2016). A Rational Strategy for the Use of Amniotic Epithelial Stem Cell Therapy for Liver Diseases. *Stem Cell translational Med.* 5 (4), 405–409. doi:10.5966/sctm.2015-0304

Miki, T. (2011). Amnion-derived Stem Cells: in Quest of Clinical Applications. *Stem Cell Res Ther* 2 (3), 25. doi:10.1186/scrt66

Miki, T., Lehmann, T., Cai, H., Stolz, D. B., and Strom, S. C. (2005). Stem Cell Characteristics of Amniotic Epithelial Cells. *Stem cells* 23 (10), 1549–1559. doi:10.1634/stemcells.2004-0357

Miki, T., Mitamura, K., Ross, M. A., Stolz, D. B., and Strom, S. C. (2007). Identification of Stem Cell Marker-Positive Cells by Immunofluorescence in Term Human Amnion. *J. Reprod. Immunol.* 75 (2), 91–96. doi:10.1016/j.jri.2007.03.017

Miki, T., and Strom, S. C. (2006). Amnion-derived Pluripotent/multipotent Stem Cells. *Stem Cell Rev* 2 (2), 133–141. doi:10.1007/s12015-006-0020-0

Murphy, S., Rosli, S., Acharya, R., Mathias, L., Lim, R., Wallace, E., et al. (2010). Amnion Epithelial Cell Isolation and Characterization for Clinical Use. *Curr. Protoc. Stem Cell Biol* 13, 1E.6.1–1E.6.25. doi:10.1002/9780470151808.sc01e06s13

Niknejad, H., Peirovi, H., Peirovi, H., Ahmadiani, A., Ghanavi, J., and Jorjani, M. (2010). Differentiation Factors that Influence Neuronal Markers Expression *In Vitro* from Human Amniotic Epithelial Cells. *eCM* 19, 22–29. doi:10.22203/ecm.v019a03

Okawa, H., Okuda, O., Arai, H., Sakuragawa, N., and Sato, K. (2001). Amniotic Epithelial Cells Transform into Neuron-like Cells in the Ischemic Brain. *Neuroreport* 12 (18), 4003–4007. doi:10.1097/00001756-200112210-00030

Olivas-Aguirre, F., Rodrigo-García, J., Martínez-Ruiz, N., Cárdenas-Robles, A., Mendoza-Díaz, S., Álvarez-Parrilla, E., et al. (2016). Cyanidin-3-O-glucoside: Physical-Chemistry, Foodomics and Health Effects. *Molecules* 21 (9), 1264. doi:10.3390/molecules21091264

Pan, L., Shu, J., and Cai, Z. (2006). The Morphologic Study of the Characteristics of Neurobiology of the Amniotic Membrane. *Chin. J. Rehabil. Med.* 21 (1), 46–49.

Parmar, D. N., Alizadeh, H., Awwad, S. T., Li, H., Neelam, S., Bowman, R. W., et al. (2006). Ocular Surface Restoration Using Non-surgical Transplantation of Tissue-Cultured Human Amniotic Epithelial Cells. *Am. J. Ophthalmol.* 141 (2), 299–307. doi:10.1016/j.ajo.2005.09.008

Raghavan, R. N., Somanathan, N., and Sastry, T. P. (2013). Evaluation of Phytochemical-Incorporated Porous Polymeric Sponges for Bone Tissue Engineering: a Novel Perspective. *Proc. Inst. Mech. Eng. H* 227 (8), 859–865. doi:10.1177/0954411913489804

Rubin, L. L., and Haston, K. M. (2011). Stem Cell Biology and Drug Discovery. *BMC Biol.* 9 (1), 42–11. doi:10.1186/1741-7007-9-42

Sakuragawa, N., Thangavel, R., Mizuguchi, M., Hirasawa, M., and Kamo, I. (1996). Expression of Markers for Both Neuronal and Glial Cells in Human Amniotic Epithelial Cells. *Neurosci. Lett.* 209 (1), 9–12. doi:10.1016/0304-3940(96)12599-4

Sanluis-Verdes, A., Sanluis-Verdes, N., Manso-Revilla, M. J., Castro-Castro, A. M., Pombo-Otero, J., Fraga-Mariño, M., et al. (2017). Tissue Engineering for Neurodegenerative Diseases Using Human Amniotic Membrane and Umbilical Cord. *Cell Tissue Bank* 18 (1), 1–15. doi:10.1007/s10561-016-9595-0

Sasaki, K., Davies, J., Doldán, N. G., Arao, S., Ferdousi, F., Szele, F. G., et al. (2019a). 3,4,5-Tricaffeoylquinic Acid Induces Adult Neurogenesis and Improves Deficit of Learning and Memory in Aging Model Senescence-Accelerated Prone 8 Mice. *Aging* 11 (2), 401–422. doi:10.18632/aging.101748

Sasaki, K., El Omri, A., Kondo, S., Han, J., and Isoda, H. (2013). Rosmarinus Officinalis Polyphenols Produce Anti-depressant like Effect through Monoaminergic and Cholinergic Functions Modulation. *Behav. Brain Res.* 238, 86–94. doi:10.1016/j.bbr.2012.10.010

Sasaki, K., Geribaldi-Doldan, N., Wu, Q., Davies, J., Szele, F. G., and Isoda, H. (2020). The Microalgae Aurantiochytrium Sp. Increases Neurogenesis and Improves Spatial Learning and Memory in Senescence-Accelerated Prone 8 Mice. *Front. Cell Developmental Biol.* 8, 1877.

Sasaki, K., Othman, M. B., Ferdousi, F., Yoshida, M., Watanabe, M., Tominaga, K., et al. (2019b). Modulation of the Neurotransmitter Systems through the Anti-inflammatory and Antidepressant-like Effects of Squalene from Aurantiochytrium Sp. *Plos one* 14 (6), e0218923. doi:10.1371/journal.pone.0218923

Saud, B., Malla, R., and Shrestha, K. (2019). A Review on the Effect of Plant Extract on Mesenchymal Stem Cell Proliferation and Differentiation. *Stem Cell Int.* 2019. doi:10.1155/2019/7513404

Saulite, L., Jekabsons, K., Klavins, M., Muceniece, R., and Riekstina, U. (2019). Effects of Malvidin, Cyanidin and Delphinidin on Human Adipose Mesenchymal Stem Cell Differentiation into Adipocytes, Chondrocytes and Osteocytes. *Phytomedicine* 53, 86–95. doi:10.1016/j.phymed.2018.09.029

Serra, M., Marongiu, M., Contini, A., Miki, T., Cadoni, E., Laconi, E., et al. (2018). Evidence of Amniotic Epithelial Cell Differentiation toward Hepatic Sinusoidal Endothelial Cells. *Cell Transpl.* 27 (1), 23–30. doi:10.1177/0963689717727541

Szukiewicz, D., Pyzlak, M., Stangret, A., Rongies, W., and Maslinska, D. (2010). Decrease in Expression of Histamine H2 Receptors by Human Amniotic Epithelial Cells during Differentiation into Pancreatic Beta-like Cells. *Inflamm. Res.* 59 (2), S205–S207. doi:10.1007/s00011-009-0131-6

Takahashi, S., Ferdousi, F., Zheng, Y.-W., Oda, T., and Isoda, H. (2021). Human Amniotic Epithelial Cells as a Tool to Investigate the Effects of Cyanidin 3-O-Glucoside on Cell Differentiation. *Ijms* 22 (7), 3768. doi:10.3390/ijms22073768

Takeda, H., Tsuji, M., Miyamoto, J., and Matsumiya, T. (2002). Rosmarinic Acid and Caffeic Acid Reduce the Defensive Freezing Behavior of Mice Exposed to Conditioned Fear Stress. *Psychopharmacology* 164 (2), 233–235. doi:10.1007/s00213-002-1253-5

Takeuchi, T., Noguchi, M., Kawakami, Y., and Ohkohchi, N. (2016). Use of Human Biospecimen Resources for Drug Discovery —Approach of Tsukuba Human Tissue Biobank Center—. *Regul. Sci. Med. Prod.* 6 (1), 57–63. doi:10.14982/rsmp.6.57

Tan, J. L., Chan, S. T., Wallace, E. M., and Lim, R. (2014). Human Amnion Epithelial Cells Mediate Lung Repair by Directly Modulating Macrophage Recruitment and Polarization. *Cell Transpl.* 23 (3), 319–328. doi:10.3727/096368912x661409

Tan, J. L., Tan, Y. Z., Muljadi, R., Chan, S. T., Lau, S. N., Mockler, J. C., et al. (2017). Amnion Epithelial Cells Promote Lung Repair *via* Lipoxin A4. *Stem Cell translational Med.* 6 (4), 1085–1095. doi:10.5966/sctm.2016-0077

Toda, A., Okabe, M., Yoshida, T., and Nikaido, T. (2007). The Potential of Amniotic Membrane/amnion-Derived Cells for Regeneration of Various Tissues. *J. Pharmacol. Sci.* 105 (3), 215–228. doi:10.1254/jphs.cr0070034

Uchida, Y., Ferdousi, F., Zheng, Y.-W., Oda, T., and Isoda, H. (2020). Global Gene Expression Profiling Reveals Isorhamnetin Induces Hepatic-Lineage Specific Differentiation in Human Amniotic Epithelial Cells. *Front. Cell Dev. Biol.* 8 (1260). doi:10.3389/fcell.2020.578036

Udalamaththa, V. L., Jayasinghe, C. D., and Udagama, P. V. (2016). Potential Role of Herbal Remedies in Stem Cell Therapy: Proliferation and Differentiation of Human Mesenchymal Stromal Cells. *Stem Cell Res Ther* 7 (1), 110. doi:10.1186/s13287-016-0366-4

Vidya Udagama, P., and Udalamaththa, V. (2018). "Application of Herbal Medicine as Proliferation and Differentiation Effectors of Human Stem Cells," in *Herbal Medicine. IntechOpen* (London: IntechOpen Limited). doi:10.5772/intechopen.72711

Xu, Z., Liu, C., Wang, R., Gao, X., Hao, C., and Liu, C. (2021). A Combination of Lycopene and Human Amniotic Epithelial Cells Can Ameliorate Cognitive Deficits and Suppress Neuroinflammatory Signaling by Choroid Plexus in Alzheimer's Disease Rat. *J. Nutr. Biochem.* 88, 108558. doi:10.1016/j.jnutbio.2020.108558

Xue, S., Chen, C., Dong, W., Hui, G., Liu, T., and Guo, L. (2012). Therapeutic Effects of Human Amniotic Epithelial Cell Transplantation on Double-Transgenic Mice Co-expressing APPswe and PS1ΔE9-Deleted Genes. *Sci. China Life Sci.* 55 (2), 132–140. doi:10.1007/s11427-012-4283-1

Yang, P.-j., Yuan, W.-x., Liu, J., Li, J.-y., Tan, B., Qiu, C., et al. (2018). Biological Characterization of Human Amniotic Epithelial Cells in a Serum-free System and Their Safety Evaluation. *Acta Pharmacol. Sin* 39 (8), 1305–1316. doi:10.1038/aps.2018.22

Yang, X., Song, L., Wu, N., Liu, Z., Xue, S., and Hui, G. (2010). An Experimental Study on Intracerebroventricular Transplantation of Human Amniotic Epithelial Cells in a Rat Model of Parkinson's Disease. *Neurol. Res.* 32 (10), 1054–1059. doi:10.1179/016164110x12681290831207

Zhao, B., Li, X., Shi, X., Shi, X., Zhang, W., Wu, G., et al. (2018). Exosomal microRNAs Derived from Human Amniotic Epithelial Cells Accelerate Wound Healing by Promoting the Proliferation and Migration of Fibroblasts. *Stem Cell Int.* 2018. doi:10.1155/2018/5420463

Zheng, Y., Zheng, S., Fan, X., Li, L., Xiao, Y., Luo, P., et al. (2018). Amniotic Epithelial Cells Accelerate Diabetic Wound Healing by Modulating Inflammation and Promoting Neovascularization. *Stem Cell Int* 2018, 1082076. doi:10.1155/2018/1082076

Zhou, K., Koike, C., Yoshida, T., Okabe, M., Fathy, M., Kyo, S., et al. (2013). Establishment and Characterization of Immortalized Human Amniotic Epithelial Cells. *Cell reprogramming* 15 (1), 55–67. doi:10.1089/cell.2012.0021

Conflict of Interest: The authors declare that the research was conducted in the absence of any commercial or financial relationships that could be construed as a potential conflict of interest.

Publisher's Note: All claims expressed in this article are solely those of the authors and do not necessarily represent those of their affiliated organizations, or those of the publisher, the editors and the reviewers. Any product that may be evaluated in this article, or claim that may be made by its manufacturer, is not guaranteed or endorsed by the publisher.

frontiers | Frontiers in Cell and Developmental Biology

MINI REVIEW
published: 11 May 2022
doi: 10.3389/fcell.2022.891569

The Field of Cell Competition Comes of Age: Semantics and Technological Synergy

Kieran Maheden, Vivian Weixuan Zhang and Nika Shakiba *

School of Biomedical Engineering, University of British Columbia, Vancouver, BC, Canada

Stem cells experience many selective pressures which shape their cellular populations, potentially pushing them to skew towards dominance of a few break-through clones. An evolutionarily conserved answer to curb these aberrant selective pressures is cell competition, the elimination of a subset of cells by their neighbours in a seemingly homogenous population. Cell competition in mammalian systems is a relatively recent discovery that has now been observed across many tissue systems, such as embryonic, haematopoietic, intestinal, and epithelial compartments. With this rapidly growing field, there is a need to revisit and standardize the terminology used, much of which has been co-opted from evolutionary biology. Further, the implications of cell competition across biological scales in organisms have been difficult to capture. In this review, we make three key points. One, we propose new nomenclature to standardize concepts across dispersed studies of different types of competition, each of which currently use the same terminology to describe different phenomena. Second, we highlight the challenges in capturing information flow across biological scales. Third, we challenge the field to incorporate next generation technologies into the cell competition toolkit to bridge these gaps. As the field of cell competition matures, synergy between cutting edge tools will help elucidate the molecular events which shape cellular growth and death dynamics, allowing a deeper examination of this evolutionarily conserved mechanism at the core of multicellularity.

Keywords: synthetic biology, cell competition, development, stem cells, molecular recording

OPEN ACCESS

Edited by:
Valerie Kouskoff,
The University of Manchester,
United Kingdom

Reviewed by:
Maximiliano Portal,
The University of Manchester,
United Kingdom
Ezio Laconi,
University of Cagliari, Italy

***Correspondence:**
Nika Shakiba
nika.shakiba@ubc.ca

Specialty section:
This article was submitted to Stem Cell Research, a section of the journal Frontiers in Cell and Developmental Biology

Received: *07 March 2022*
Accepted: *20 April 2022*
Published: *11 May 2022*

Citation:
Maheden K, Zhang VW and Shakiba N (2022) The Field of Cell Competition Comes of Age: Semantics and Technological Synergy. Front. Cell Dev. Biol. 10:891569. doi: 10.3389/fcell.2022.891569

CLONALITY AND COMPETITION

The life of a stem cell is that of growth or death, persistence or differentiation. Across generations and within our tissues, these cells find themselves racing towards their limits—space, molecular signals, and the abundance of their progeny relative to peers. These selective pressures inherently define cellular populations, shaping them over the organism's lifetime depending on the demands of the environment. Heterogeneity is lost over time in several stem cell populations, as a few cells give rise to offspring that outlast and overtake neighbouring clones. Intestinal stem cells, caught in a perpetual rush to out-divide each other, come to grow in abundance and their progeny dominate an environment either by chance or by mutations that provide an edge over their neighbours (Lopez-Garcia et al., 2010; Snippert et al., 2010; Baker et al., 2014; Snippert et al., 2014). As a result, intestinal tissue and the constituent crypts eventually become more homogenous as individual clones out-persist the multicellular population. Interestingly, the reverse phenomenon is seen in epithelial tissues, where clonal diversity increases as cells acquire mutations, giving rise to a birth of

clones with divergent family trees (Alcolea et al., 2014; Colom et al., 2021). This ultimately culminates with a single clone "breaking through", gaining mutations that allow it to overtake its environment. One key difference between these two patterns of cellular competition is the nature of the tissue it occurs within—where one clone may come to outcompete its neighbours in an epithelial layer, spatially separated crypts isolate clones, limiting their spread. While perhaps seeming straightforward, the dynamics of clonal competition and neoplastic growth are increasingly complex, and have been recently well reviewed elsewhere (Marongiu et al., 2021).

Competition between cellular neighbours has been reported in several stem cell populations. Haematopoietic stem cell populations tend towards clonality in an age-dependent manner (Genovese et al., 2014; Jaiswal and Ebert, 2019; Silver et al., 2021). Similarly, a small set of embryonic stem cells establish clonal contributions to reproductive tissue (Kanatsu-Shinohara et al., 2006; Kanatsu-Shinohara et al., 2016; Nguyen and Laird, 2021; Yang et al., 2021) and exhibit skewed contributions to germ layer specification during embryonic development (Park et al., 2021). Despite the clear importance of clonal dynamics in many of our tissues, we lack an understanding of the implications of these differences and how they arise. Often, these changes in clonality are associated with oncogenesis or tissue function detereriation (Suda et al., 2018; Yokoyama et al., 2019), but the impact of tissue-specific clonality or *aclonality* at the organism level remains relatively unexplored. This dynamic, where stochasticity or chance mutations heavily skew a valuable stem cell population, creates a pressure for "cheater" clones to emerge and overtake a bodily niche—often at the expense of organism survival.

One evolutionarily conserved answer to control this selective pressure is a set of cellular interactions dubbed cell competition (CC). CC has traditionally been defined as the elimination of a subset of cells by their neighbours within a seemingly homogenous cell population. This dynamic has been proposed as a conserved quality control mechanism, functioning to select against deleterious mutations (Sancho et al., 2013; Ji et al., 2021). To date, CC has been demonstrated in embryonic (Clavería et al., 2013; Sancho et al., 2013; Ellis et al., 2019), intestinal (Snippert et al., 2014; Suijkerbuijk et al., 2016; Ellis et al., 2019; Flanagan et al., 2021; Scheuer et al., 2021), haematopoietic (Bondar and Medzhitov, 2010), gonadal (Jin et al., 2008; Rhiner et al., 2009; Nguyen and Laird, 2021), and epithelial tissues (Snippert et al., 2014; Suijkerbuijk et al., 2016; Kon et al., 2017; Ellis et al., 2019; Flanagan et al., 2021; Scheuer et al., 2021) scattered throughout several model species. The "why" of cell competition is mostly unknown, however insights from embryonic competition suggest cell function is a determinant of competitive ability (Clavería et al., 2013; Hashimoto and Sasaki, 2019). Indeed, literature on competition has outlined its role in monitoring for epithelial cell polarity (Brumby and Richardson, 2003; Igaki et al., 2009), embryonic tissue size and morphology (Orietti et al., 2021), and in maintaining an organism's lifespan (Merino et al., 2015).

To date, the field of CC has mostly been concerned with the novelty of "loser" cell removal by neighbouring "winners." However, how these dynamics impact the residing tissue and its function, or the implications for the host organism are broadly unknown. The field, as it progresses, is then faced with a challenge: designing experiments and formulating hypotheses that encompass the full complexity of multicellular systems at the cellular, tissue, and organism scale. Ultimately, in capturing and understanding the information flow between these scales, we can learn the processes by which these levels shape each other. This is key to connecting the evolutionary basis and molecular mechanisms that orchestrate the competition that shapes multicellular populations (Maheden et al., 2021).

CLARIFYING COMPETITION

As the field of cell competition has grown quickly, so too has the number of terms used to describe these cellular interactions. With reports of CC becoming commonplace across tissues and organisms, it is timely to revisit and standardize vocabulary across the field. Since the earliest examples of CC were reported, the field has borrowed terminology from evolutionary biology, which has an established and rich history of capturing inter-species competition. However, the broad use of the same terms in evolutionary and developmental biology may be a source of confusion for those new to the field.

The use of the term "fitness" is a clear example of this. In the context of CC, "fitness" is widely used to describe the inherent qualities of winner cells that confer their ability to eliminate losers (Clavería et al., 2013; Sancho et al., 2013; Bowling et al., 2019; Madan et al., 2019; Lima et al., 2021). However, the ability to eliminate losers is often defined by the cell's "fitness"; an argument that begins where it ends. Indeed, there is no agreed-upon definition for "fitness", even in the ecological realm (Peacock, 2011); so too, there is a discrepancy in how different experts may interpret the mechanistic underpinnings of cellular "fitness". An example of this disconnect is seen in the comparison between "fitness" in *Drosophila* epithelial cells as compared to the mammalian haematopoietic system. Cell competition studies using the haematopoietic system describe "fitter" cells as those that exhibit a growth advantage, often conferred by genetic mutations that allow these clones to overtake the niche (Watson et al., 2020). In contrast, cell competition studies involving *Drosophila* describe "fitter" cells as those that are able to eliminate neighbouring cells that are less fit by inducing their apoptosis (Casas-Tinto et al., 2010; De La Cova et al., 2014; Nagata and Igaki, 2018). This demonstrates the disconnect in the use of the term "fitness" across different subfields of competition: the same term is used to describe different phenomena in a context-dependent manner. Indeed, the historical use of the term "fitness" makes it particularly challenging to adapt for the CC field and may warrant careful use as a result.

More specific and nuanced terminology may help the budding CC field avoid inadvertently grouping together distinct biological phenomena and allow for the growing library of CC mechanisms to be catalogued. At the moment, "fitness" is used as a non-specific umbrella term to describe different facets of a cell's ability to dominate in a given niche. As the field matures, and a more

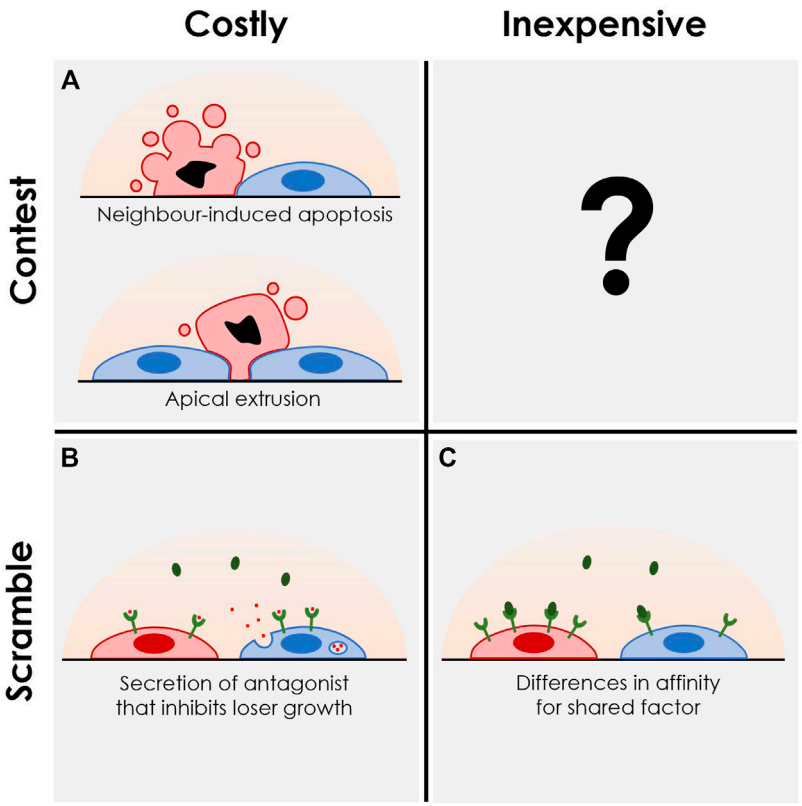

FIGURE 1 | Systematic characterization of the various modes of cell competition. We propose contextualizing competitive interactions *via* two axes: *Costly* versus *inexpensive*; *scramble* versus *contest*. "Costly competition" includes behaviours or molecular interactions that do not yield immediate benefit for the cell or population outside of the elimination of loser cells from that population. "Inexpensive competition" involves less risk as these behaviours or interactions would be expected to always benefit the cell, regardless of environment. "Scramble" involves a rush to accumulate a limited number of resources, whereas "contests" involve direct interactions, comparisons, or sensing between competing cell populations. **(A)** Examples of "costly contests" include direct apoptotic induction of loser cells by winners as seen in mouse embryonic stem cell models (Díaz-Díaz et al., 2017; Bowling et al., 2018b; Lima et al., 2021), or *via* extrusion of losers from the underlying substrate by neighbours as seen in tissue culture models (Hogan et al., 2009; Kajita et al., 2010). **(B)** "Costly scrambles" have been seen in intestinal stem cell models, where *apc*-mutant cells with constitutive WNT signaling secrete a WNT antagonist, NOTUM, crippling WNT signaling in their wildtype neighbours and limiting their ability to persist in the stem cell state (Flanagan et al., 2021; Scheuer et al., 2021). **(C)** "Inexpensive scramble" encompasses a wide range of mechanisms which ultimately result in differences in abundances between two populations by affecting the independent growth or survival of the competitors. This can be driven by different cell cycle rates, death rates, or different required thresholds and affinities for environmental factors, all ultimately resulting in inequality of effective growth rates independent of intercellular interactions. A straightforward example can be seen again within the intestinal stem cell niche, where faster-dividing mutant intestinal stem cells overtake their wildtype neighbours over time (Snippert et al., 2014), or with hematopoietic stem cells having different abilities to persist long term based on growth factor receptor expression (Cosgun et al., 2014; Shin et al., 2014). To date, no clear examples of "inexpensive contest" have been observed.

nuanced understanding of the various mechanistic drivers of this phenotype develops, the catch-all term "fitness" can be replaced by more specific terminology.

Similarly, "competition" is used to describe distinct phenomena across fields. We propose to redefine "competition" along two dimensions, each serving to capture distinct biological mechanisms that lead to cellular elimination in multicellular settings: *costly* versus *inexpensive* competition, and cellular *contest* versus *scramble* (**Figure 1**) (Hibbing et al., 2010). *Costly* competition invovles situations in which a cell or population of cells expend energy to eliminate other competitors, while experiencing no immediate benefit in terms of proliferation or abundance. On the other hand, *inexpensive* competition describes situations where competition is driven by processes that directly increase the abundance of the cells or populations involved. This is seen in situations where one cell population has a cell-autonomous propensity to outgrow or outpersist other populations in a given niche—a property that remains unchanged in the presence of a competitor cell population. *Scramble* refers to competition that affects an extracellular intermediate that drives a change to the cellular microenvironment. By contrast, *contest* refers to a direct action between cells, without involvement of an intermediate resource, such as when cells induce apoptosis in or extrude their neighbours (Sun et al., 2014; Bowling et al., 2018a).

Published reports of CC in various organisms and tissue types can be categorized along these two axes, which together define four quadrants (**Figure 1**). As an example of a *costly contest*, loser mouse embryonic stem cells undergo apoptosis when mixed with neighbouring winner cells (**Figure 1A**) (Díaz-Díaz et al., 2017).

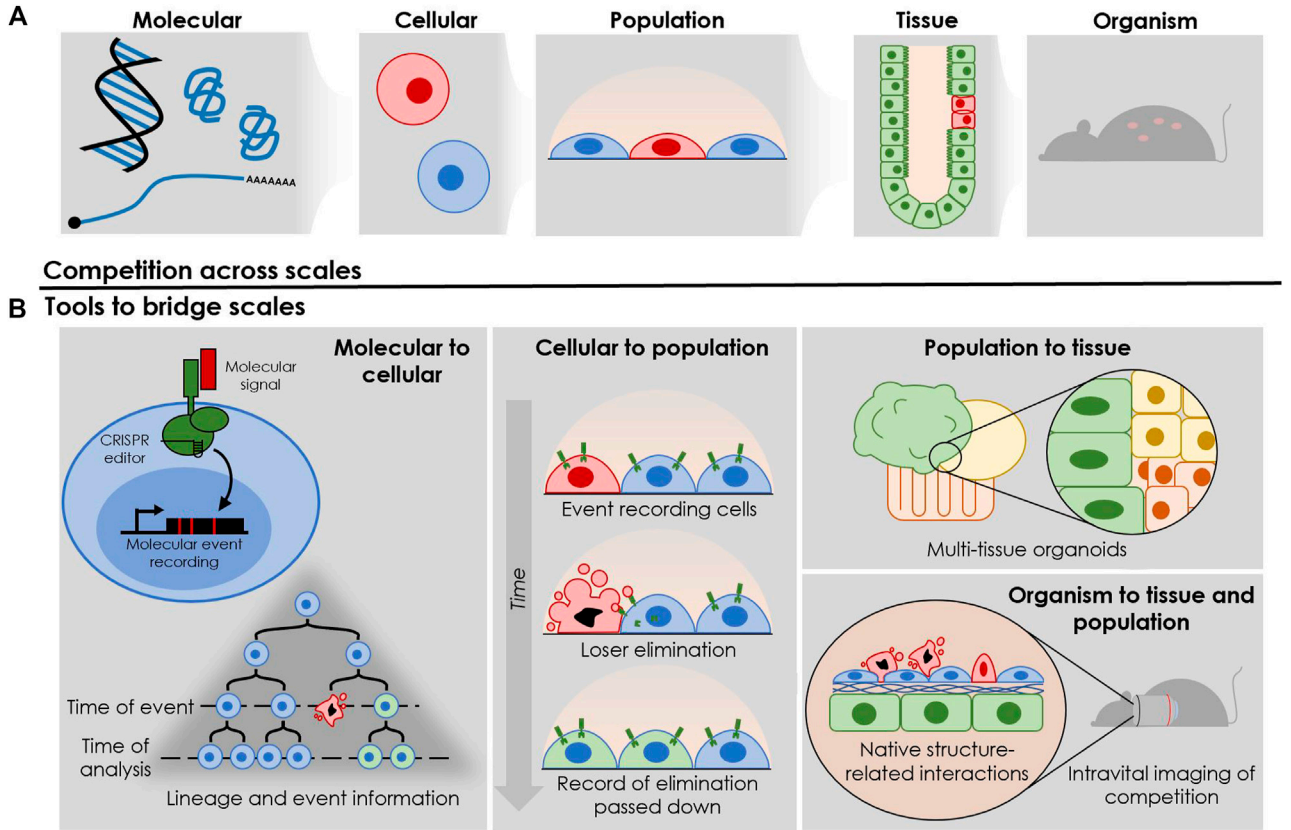

FIGURE 2 | Utilizing recent technological advancements to gain insights into various layers of complexity during cell competition. **(A)** The different biological levels influencing and influenced by competitive interactions between cells. **(B)** Following the biological levels shown in **Figure 2A**, recent technologies provide unprecedented access to information flow across scales. Molecular level: event recording allows for the tracking of molecular events with single-cell resolution—in this case, the elimination of a loser cell from a mosaic tissue. Cellular level: the surrounding cells can record this elimination, allowing researchers to observe this molecular event in the cellular history through end-point single-cell analysis. Cell population level: complex, multi-organoid systems allow for interplay between tissue types, and for emergent behaviours between cells that typically interact *in vivo* but are traditionally isolated in simple 2-dimentional cultures *in vitro*. Tissue and organism level: intravital imaging enables the investigation of interactions in their *in vivo* context, allowing access to competitive interactions in complex tissue architecture and cellular milieu.

From the standpoint of these winners, elimination of loser clones requires energy and time and does not yield immediate benefit (i.e., an increase in winner cell numbers) if the loser were not present. An example of a *costly scramble* is shown by Flanagan et al. in which secretion of NOTUM by *apc*-mutant winner cells suppresses wildtype losers' ability to persist in the niche by targeting their WNT signaling (**Figure 1B**) (Flanagan et al., 2021). In such a situation, NOTUM production and secretion presents as the cost of eliminating wildtype neighbours, with the ultimate benefit of increased availability of the stem cell niche for these *apc* mutants due to their lack of dependence on WNT signaling. Other examples may involve cells competing by racing for access to a limited nutrient or physical space within a niche. On the other hand, *inexpensive scramble* has been seen in hematopoietic stem cell competition, where clones of stem cells with specific receptor expression levels or mutations predispose them to surviving in that stem cell state over the long term (**Figure 1C**) (Cosgun et al., 2014; Shin et al., 2014; Bowman et al., 2018; Jaiswal and Ebert, 2019). While an example of an *inexpensive contest* has not been reported to our knowledge, a possible example could involve a contact-mediated elimination of loser cells based on differential expression of surface proteins involved in cell adhesion. In this way, the removal of loser cells from an adherent substrate or cellular niche would be driven by a passive differential adhesion mechanism rather than an active process of extrusion by winners. Ultimately, we hope that this standardization of the vocabulary used by researchers will aid in the discovery and communication of nuanced insights in this burgeoning field.

CELL COMPETITION ACROSS SCALES

Cell competition is a phenomenon that bridges across scales, where molecular changes at the single cell level drive phenotypic changes within multicellular tissues (**Figure 2A**). These underlying dynamics ultimately shape the highest biological scale—that of organism viability, which is the level at which evolutionary selection pressures are dealt. Current assays used to investigate CC typically do not span multiple biological scales: molecular, single cell, cell population, tissue, and organism. This leaves a mechanistic disconnect in our understanding of how

changes involving CC at one biological level drive outcomes at another. Here, we will review how current assays characterize CC at various scales, outlining gaps in our collective understanding of the biology while highlighting opportunities to push the boundaries of the field through cutting-edge advances in genetic and cellular technologies.

At the molecular level, studies have explored the impact of genetic perturbations on the ability of winner cells to contribute to cellular populations, both *in vitro* and *in vivo*. Claveria et al. and Sancho et al. both show that early embryonic cells measure Myc content relative to their neighbours, and cells with lower Myc levels are eliminated by neighbours with higher Myc (Clavería et al., 2013; Sancho et al., 2013). While these studies reveal the impact of key genetic perturbations in driving the ability of individual cells to overtake populations, they do not capture their impact on higher-level tissue function or structure, and organism outcomes. Of note is that changes to gene expression shown to drive CC need not involve genetic engineering or mutations to the DNA itself. Cells may receive signals from their microenvironment, including cell-cell interactions, that converge on the cellular processor and drive CC behavour by affecting gene expression (Maheden et al., 2021; Shakiba et al., 2021). Similarly, epigenetic changes can also drive CC-relevant gene expression changes. Exciting open questions remain to be answered, including exploring the contributions of inputs to the cellular processor on CC outcomes.

Others have investigated competition at the tissue level. Bondar and Medzhitov demonstrated cell competition in haematopoietic stem and progenitor cells using an *in vivo* bone marrow repopulation assay (Bondar and Medzhitov, 2010). Here, the connection is made between molecular perturbations and population level outcomes, as increased relative p53 expression was shown to confer loser status by marking cells for senescence and extrusion from the niche (Bondar and Medzhitov, 2010). Follow-up studies on the long-term health and blood compartment function of the recipient mice may provide more insight into how winner-loser status at the tissue level shapes survival and viability at the organism level. Indeed, these findings would help to bridge our understanding of the evolutionary role of CC.

Our understanding of the role of CC at the organismal level is relatively underdeveloped. The clearest example comes from work in *Drosophila*, studying the gene *azot*, a gene required for loser cell elimination (Merino et al., 2015). This work outlined several roles for *azot*, showing it is critical for survival post-UV irradiation and maintanence of a normal lifespan through elimination of loser clones arising during both. The connection between competition and lifespan or survivial post-insult has not been made in mammalian systems, and the percise implications of carrying tissues rife with uneliminated losers is an open question.

The phenomenon of CC has captured the attention of scientists with core expertise that span different model systems, technical skills, and cell types. With the exciting interdisciplinary nature of the field comes the challenge of interpreting results that span different biological scales and systems. Mixing assays, involving *in vitro* co-culturing of winner and loser cells on a 2-dimensional surface, have traditionally dominated the field. These assays connect molecular-level genetic perturbations to cell-level events such as apoptosis, killng, and proliferation. Tissue-level studies connect genetic perturbations to the succesful function of the organ, and so on with organismal studies. The disconnect lies in the fact that cell mixing assays provide little insight into the impact of genetic perturbations on any level above that of the cellular. On the other hand, organism-level assays often do not preserve information about underlying genetic perturbations and how they affect cellular and tissue function.

While an understanding of how genetic perturbations drive CC outcomes at the cellular level is powerful for some contexts, such as engineering cells that survive and thrive in cell manufacturing bioprocesses, expanding the scope of our studies to incorporate how these perturbations shape the emergent structure and function of tissues may open the door to the robust derivation of lab-grown tissues for regenerative medicine. Undoubtedly, these insights would also be powerful for our fundamental biological understanding of tissue development and homeostasis as well, with implications for treating disease. Increased cross-disciplinary collaboration would benefit the field by connecting scientists investigating CC from different angles and encouraging broader perspectives.

In mammalian systems, much has recently been learned from pushing beyond *in vitro* mixing studies. During development, it was shown that the same mosaic *epidermis* consisting of a pair of genotypes would show differing mechanisms of elimination, depending on the timing and maturity of the tissue (Ellis et al., 2019). The same work showed that when competition and elimination of one of the genotypes was blocked, tight-junction organization and barrier function was compromised. A recent example leveraging intravital imaging further outlined the critical role of tissue architecture in defining competitive interactions. In skin epithelium, consisting of mosaic hair follicle stem cells (wildtype or with hyperactive WNT/β-catenin signaling), it was shown that mutant cells form growths and protrusions that are encapsulated and stifled by surrounding wildtype cells. This dynamic eventually resulted in a return to homeostatic tissue organization and elimination of mutant cells, a phenomenon only observable when studying the original cellular architecture.

EXPANDING THE COMPETITION ASSAY TOOLKIT

As the field of CC progresses and the complexity of our questions increase, there are opportunities to engage cutting-edge techniques from the fields of systems and synthetic biology (**Figure 2B**). Looking to previous work, mathematical modeling has played a critical role in understanding the evolutionary pressures that drive clonal competition in cancer (Gatenby and Vincent, 2003; Vermeulen et al., 2013). Indeed, computational approaches using live-cell imaging data have been successful at disentangling cellular factors involved in 2-dimensional mechanical competition (Gradeci et al., 2019). Additionally, modeling of intestinal stem cell clonality over

time initially predicted that the progressive clonal takeover of intestinal crypts fit well with a stochastic model, indicating that neutral drift was the driver of clonality in non-oncogenic situations (Snippert et al., 2010).

Another powerful tool in understanding competition and clonal dynamics is that of lineage tracing (Wagner and Klein, 2020). Somatic mutations have been used to map clonal contributions in the early embryo, creating a family tree of cells within our earliest stages of development (Park et al., 2021). The combination of mathematical modeling and a static, lentiviral barcode has also provided insight into clonal dynamics over the process of reprogramming, revealing competitive interactions (Shakiba et al., 2019). Additionally, as assays grow in complexity and adopt additional layers, cell types, and tissue architectures, single cell sequencing and lineage tracing will further enable us to understand the interplay between clonality and tissue identity, revealing hidden layers of homogeneity or heterogeneity that would otherwise be missed (Mckenna et al., 2016; He et al., 2021). One recent example looking at the haematopoietic compartment performed single cell RNA-seq with a modified pipeline, capturing both mtRNA and mRNA at single cell resolution from human samples (Miller et al., 2022). Using mtRNA to identify mutations, the authors were able to map the haematopoietic stem cell lineage. Using accompanying transcriptomic data, they correlated divergent differentiation trajectories with specific haematopoietic clones, connecting tissue-level function with clonal contributions to that function.

Finally, when looking to how the field of CC might aim to understand the flow of information from the cellular, to the tissue, and finally to the organism scale, key advances in molecular event recording technologies, which leverage the DNA as a data storage device, may bridge the gap. Early event recording technologies demonstrated the possibility for both recording and recovering cellular events in the history of individual cells from a single molecular input (Perli et al., 2016), with later works demonstrating recording systems that require two distinct signals to activate (Tang and Liu, 2018). As our knowledge of the molecular events and markers of competition grow, building synthetic genetic systems to record their presence and encode that information for recovery with single-cell resolution allows us to correlate molecular and cellular events with tissue-level outcomes through time (Sheth and Wang, 2018; Ishiguro et al., 2019). Critically, this removes the need to take snapshots of molecular events, instead allowing us to look back through the life-history of our model, identifying potentially complex events that have taken place days or weeks past.

To go beyond simple *in vitro* mixing assays, designing culture conditions that mimic the *in vivo* reality of multicellular systems would help bridge the gap. Advances in organoid tissue models have allowed for accurate representations of *in vivo* architecture while also incorporating cross-talk between multiple tissue types, striking a balance between biological reality and feasibility (Wimmer et al., 2019; Koike et al., 2021). With multi-organoid systems engineered from the ground up, we gain the ability to probe and control interactions between tissue types, capturing complexity that would otherwise be missed.

Synergy between the above tools provides a strategy to approach capturing information at the molecular, cellular, tissue, and organismal level. When conceptualizing an idealized competition experiment, the combination of competitive event recording and clonal lineage tracing in a full animal model would allow researchers to discover where these cellular battlefields lie, and which clones have shaped and overtaken their environment *via* these interactions. Coupling this molecular information with tissue function and organismal readouts would allow direct connection between molecular interactions and outcomes of the animal. Additionally, it would become possible to work backwards, performing insults or creating conditions that have been shown to affect organismal or tissue health and characterizing clonal or competitive interactions at the molecular level.

Ultimately, the field of cell competition is poised to mature from a novelty of mixing cells to a holistic process at the core of multicellularity, one that is a driving force in tissue homeostasis and function. Facilitating this transition are numerous advancements in adjacent fields, giving researchers the capability to ask deeper questions on the nature and evolutionary basis of the intriguing cellular behaviour that is CC.

AUTHOR CONTRIBUTIONS

KM, VZ, and NS all contributed to ideation, writing, and figure generation for this article.

FUNDING

The authors were supported by a Natural Sciences and Engineering Research Council of Canada (NSERC) Discovery Grant. The authors were also supported by an Allen Distinguished Investigator Award, a Paul G. Allen Frontiers Group advised grant of the Paul G. Allen Family Foundation. NS is a recipient of a Michael Smith Health Research BC Scholar Award. KM was supported by a NSERC CGS-M award.

ACKNOWLEDGMENTS

The authors would like to acknowledge the many contributions to the field that were not cited in this work due to space limitations, as well as the funding agencies that provided this opportunity.

REFERENCES

Alcolea, M. P., Greulich, P., Wabik, A., Frede, J., Simons, B. D., and Jones, P. H. (2014). Differentiation Imbalance in Single Oesophageal Progenitor Cells Causes Clonal Immortalization and Field Change. *Nat. Cell Biol.* 16, 612–619. doi:10.1038/ncb2963

Baker, A.-M., Cereser, B., Melton, S., Fletcher, A. G., Rodriguez-Justo, M., Tadrous, P. J., et al. (2014). Quantification of Crypt and Stem Cell Evolution in the Normal and Neoplastic Human Colon. *Cell Rep.* 8, 940–947. doi:10.1016/j.celrep.2014.07.019

Bondar, T., and Medzhitov, R. (2010). p53-Mediated Hematopoietic Stem and Progenitor Cell Competition. *Cell Stem Cell* 6, 309–322. doi:10.1016/j.stem.2010.03.002

Bowling, S., Di Gregorio, A., Sancho, M., Pozzi, S., Aarts, M., Signore, M., et al. (2018a). P53 and mTOR Signalling Determine Fitness Selection through Cell Competition during Early Mouse Embryonic Development. *Nat. Commun.* 9, 1763. doi:10.1038/s41467-018-04167-y

Bowling, S., Di Gregorio, A., Sancho, M., Pozzi, S., Aarts, M., Signore, M., et al. (2018b). P53 and mTOR Signalling Determine Fitness Selection through Cell Competition during Early Mouse Embryonic Development. *Nat. Commun.* 9, 1763. doi:10.1038/s41467-018-04167-y

Bowling, S., Lawlor, K., and Rodríguez, T. A. (2019). Cell Competition: the Winners and Losers of Fitness Selection. *Development* 146, dev167486. doi:10.1242/dev.167486

Bowman, R. L., Busque, L., and Levine, R. L. (2018). Clonal Hematopoiesis and Evolution to Hematopoietic Malignancies. *Cell Stem Cell* 22, 157–170. doi:10.1016/j.stem.2018.01.011

Brumby, A. M., and Richardson, H. E. (2003). Scribble Mutants Cooperate with Oncogenic Ras or Notch to Cause Neoplastic Overgrowth in Drosophila. *EMBO J.* 22, 5769–5779. doi:10.1093/emboj/cdg548

Casas-Tinto, S., López-Gay, J. M., Soldini, D., Martín, F. A., Lombardía, L., and Moreno, E. (2010). Flower Forms an Extracellular Code that Reveals the Fitness of a Cell to its Neighbors in Drosophila. *Dev. Cel.* 18, 985–998. doi:10.1016/j.devcel.2010.05.010

Clavería, C., Giovinazzo, G., Sierra, R., and Torres, M. (2013). Myc-Driven Endogenous Cell Competition in the Early Mammalian Embryo. *Nature* 500, 39–44. doi:10.1038/nature12389

Colom, B., Herms, A., Hall, M. W. J., Dentro, S. C., King, C., Sood, R. K., et al. (2021). Mutant Clones in Normal Epithelium Outcompete and Eliminate Emerging Tumours. *Nature* 598, 510–514. doi:10.1038/s41586-021-03965-7

Cosgun, K. N., Rahmig, S., Mende, N., Reinke, S., Hauber, I., Schäfer, C., et al. (2014). Kit Regulates HSC Engraftment across the Human-Mouse Species Barrier. *Cell Stem Cell* 15, 227–238. doi:10.1016/j.stem.2014.06.001

De La Cova, C., Senoo-Matsuda, N., Ziosi, M., Wu, D. C., Bellosta, P., Quinzii, C. M., et al. (2014). Supercompetitor Status of drosophila Myc Cells Requires P53 as a Fitness Sensor to Reprogram Metabolism and Promote Viability. *Cell Metab.* 19, 470–483. doi:10.1016/j.cmet.2014.01.012

Díaz-Díaz, C., Fernandez de Manuel, L., Jimenez-Carretero, D., Montoya, M. C., Clavería, C., and Torres, M. (2017). Pluripotency Surveillance by Myc-Driven Competitive Elimination of Differentiating Cells. *Dev. Cel.* 42, 585–599. doi:10.1016/j.devcel.2017.08.011

Ellis, S. J., Gomez, N. C., Levorse, J., Mertz, A. F., Ge, Y., and Fuchs, E. (2019). Distinct Modes of Cell Competition Shape Mammalian Tissue Morphogenesis. *Nature* 569, 497–502. doi:10.1038/s41586-019-1199-y

Flanagan, D. J., Pentinmikko, N., Luopajärvi, K., Willis, N. J., Gilroy, K., Raven, A. P., et al. (2021). NOTUM from Apc-Mutant Cells Biases Clonal Competition to Initiate Cancer. *Nature* 594, 430–435. doi:10.1038/s41586-021-03525-z

Gatenby, R. A., and Vincent, T. L. (2003). An Evolutionary Model of Carcinogenesis. *Cancer Res.* 63, 6212–6220.

Genovese, G., Kähler, A. K., Handsaker, R. E., Lindberg, J., Rose, S. A., Bakhoum, S. F., et al. (2014). Clonal Hematopoiesis and Blood-Cancer Risk Inferred from Blood DNA Sequence. *N. Engl. J. Med.* 371, 2477–2487. doi:10.1056/nejmoa1409405

Gradeci, D., Bove, A., Vallardi, G., Lowe, A. R., Banerjee, S., and Charras, G. (2019). Cell-Scale Biophysical Determinants of Cell Competition in Epithelia. *Elife*. doi:10.1101/729731

Hashimoto, M., and Sasaki, H. (2019). Epiblast Formation by TEAD-YAP-Dependent Expression of Pluripotency Factors and Competitive Elimination of Unspecified Cells. *Dev. Cel.* 50, 139–154.e5. doi:10.1016/j.devcel.2019.05.024

He, Z., Maynard, A., Jain, A., Gerber, T., Petri, R., and Chuan Lin, H. (2021). Lineage Recording in Human Cerebral Organoids. *Nat. Methods* 19, 90–99. doi:10.1038/s41592-021-01344-8

Hibbing, M. E., Fuqua, C., Parsek, M. R., and Peterson, S. B. (2010). Bacterial Competition: Surviving and Thriving in the Microbial Jungle. *Nat. Rev. Microbiol.* 8, 15–25. doi:10.1038/nrmicro2259

Hogan, C., Dupré-Crochet, S., Norman, M., Kajita, M., Zimmermann, C., Pelling, A. E., et al. (2009). Characterization of the Interface between Normal and Transformed Epithelial Cells. *Nat. Cell Biol.* 11, 460–467. doi:10.1038/ncb1853

Igaki, T., Pastor-Pareja, J. C., Aonuma, H., Miura, M., and Xu, T. (2009). Intrinsic Tumor Suppression and Epithelial Maintenance by Endocytic Activation of Eiger/TNF Signaling in Drosophila. *Dev. Cel.* 16, 458–465. doi:10.1016/j.devcel.2009.01.002

Ishiguro, S., Mori, H., and Yachie, N. (2019). DNA Event Recorders Send Past Information of Cells to the Time of Observation. *Curr. Opin. Chem. Biol.* 52, 54–62. doi:10.1016/j.cbpa.2019.05.009

Jaiswal, S., and Ebert, B. L. (2019). Clonal Hematopoiesis in Human Aging and Disease. *Science* 366, eaan4673. doi:10.1126/science.aan4673

Ji, Z., Chuen, J., Kiparaki, M., and Baker, N. (2021). Cell Competition Removes Segmental Aneuploid Cells from drosophila Imaginal Disc-Derived Tissues Based on Ribosomal Protein Gene Dose. *Elife* 10, e61172. doi:10.7554/elife.61172

Jin, Z., Kirilly, D., Weng, C., Kawase, E., Song, X., Smith, S., et al. (2008). Differentiation-Defective Stem Cells Outcompete Normal Stem Cells for Niche Occupancy in the Drosophila Ovary. *Cell Stem Cell* 2, 39–49. doi:10.1016/j.stem.2007.10.021

Kajita, M., Hogan, C., Harris, A. R., Dupre-Crochet, S., Itasaki, N., Kawakami, K., et al. (2010). Interaction with Surrounding Normal Epithelial Cells Influences Signalling Pathways and Behaviour of Src-Transformed Cells. *J. Cell Sci.* 123, 171–180. doi:10.1242/jcs.057976

Kanatsu-Shinohara, M., Inoue, K., Miki, H., Ogonuki, N., Takehashi, M., Morimoto, T., et al. (2006). Clonal Origin of Germ Cell Colonies after Spermatogonial Transplantation in Mice1. *Biol. Reprod.* 75, 68–74. doi:10.1095/biolreprod.106.051193

Kanatsu-Shinohara, M., Naoki, H., and Shinohara, T. (2016). Nonrandom Germline Transmission of Mouse Spermatogonial Stem Cells. *Dev. Cel.* 38, 248–261. doi:10.1016/j.devcel.2016.07.011

Koike, H., Iwasawa, K., Ouchi, R., Maezawa, M., Kimura, M., Kodaka, A., et al. (2021). Engineering Human Hepato-Biliary-Pancreatic Organoids from Pluripotent Stem Cells. *Nat. Protoc.* 16, 919–936. doi:10.1038/s41596-020-00441-w

Kon, S., Ishibashi, K., Katoh, H., Kitamoto, S., Shirai, T., Tanaka, S., et al. (2017). Cell Competition with Normal Epithelial Cells Promotes Apical Extrusion of Transformed Cells through Metabolic Changes. *Nat. Cell Biol.* 19, 530–541. doi:10.1038/ncb3509

Lima, A., Lubatti, G., Burgstaller, J., Hu, D., Green, A. P., and Di Gregorio, A. (2021). Cell Competition Acts as a Purifying Selection to Eliminate Cells with Mitochondrial Defects during Early Mouse Development. *Nat. Metab.* 3, 1091–1108. doi:10.1038/s42255-021-00422-7

Lopez-Garcia, C., Klein, A. M., Simons, B. D., and Winton, D. J. (2010). Intestinal Stem Cell Replacement Follows a Pattern of Neutral Drift. *Science* 330, 822–825. doi:10.1126/science.1196236

Madan, E., Pelham, C. J., Nagane, M., Parker, T. M., Canas-Marques, R., Fazio, K., et al. (2019). Flower Isoforms Promote Competitive Growth in Cancer. *Nature* 572, 260–264. doi:10.1038/s41586-019-1429-3

Maheden, K., Bashth, O. S., and Shakiba, N. (2021). Evening the Playing Field: Microenvironmental Control over Stem Cell Competition during Fate Programming. *Curr. Opin. Genet. Dev.* 70, 66–75. doi:10.1016/j.gde.2021.05.008

Marongiu, F., Cheri, S., and Laconi, E. (2021). Cell Competition, Cooperation, and Cancer. *Neoplasia* 23, 1029–1036. doi:10.1016/j.neo.2021.08.001

Mckenna, A., Findlay, G. M., Gagnon, J. A., Horwitz, M. S., Schier, A. F., and Shendure, J. (2016). Whole-organism Lineage Tracing by Combinatorial and Cumulative Genome Editing. *Science* 353, aaf7907. doi:10.1126/science.aaf7907

Merino, M. M., Rhiner, C., Lopez-Gay, J. M., Buechel, D., Hauert, B., and Moreno, E. (2015). Elimination of Unfit Cells Maintains Tissue Health and Prolongs Lifespan. *Cell* 160, 461–476. doi:10.1016/j.cell.2014.12.017

Miller, T. E., Lareau, C. A., Verga, J. A., DePasquale, E. A. K., Liu, V., Ssozi, D., et al. (2022). Mitochondrial Variant Enrichment from High-Throughput Single-Cell RNA Sequencing Resolves Clonal Populations. *Nat. Biotechnol.* doi:10.1038/s41587-022-01210-8

Nagata, R., and Igaki, T. (2018). Cell Competition: Emerging Mechanisms to Eliminate Neighbors. *Dev. Growth Differ.* 60, 522–530. doi:10.1111/dgd.12575

Nguyen, D. H., and Laird, D. J. (2021). Natural Selection at the Cellular Level: Insights from Male Germ Cell Differentiation. *Cell Death Differ.* 28, 2296–2299. doi:10.1038/s41418-021-00812-0

Orietti, L. C., Rosa, V. S., Antonica, F., Kyprianou, C., Mansfield, W., and Marques-Souza, H. (2021). Embryo Size Regulates the Timing and Mechanism of Pluripotent Tissue Morphogenesis. *Stem Cell Rep.* 16, 1182–1196. doi:10.1016/j.stemcr.2020.09.004

Park, S., Mali, N. M., Kim, R., Choi, J.-W., Lee, J., Lim, J., et al. (2021). Clonal Dynamics in Early Human Embryogenesis Inferred from Somatic Mutation. *Nature* 597, 393–397. doi:10.1038/s41586-021-03786-8

Peacock, K. A. (2011). The Three Faces of Ecological Fitness. *Stud. Hist. Philos. Biol. Biomed. Sci.* 42, 99–105. doi:10.1016/j.shpsc.2010.11.011

Perli, S. D., Cui, C. H., and Lu, T. K. (2016). Continuous Genetic Recording with Self-Targeting CRISPR-Cas in Human Cells. *Science* 353, aag0511. doi:10.1126/science.aag0511

Rhiner, C., Dìaz, B., Portela, M., Poyatos, J. F., Fernàndez-Ruiz, I., and Lòpez-Gay, J. M. (2009). Persistent Competition Among Stem Cells and Their Daughters in theDrosophilaovary Germline Niche. *Development* 136, 995–1006. doi:10.1242/dev.033340

Sancho, M., Di-Gregorio, A., George, N., Pozzi, S., Sánchez, J. M., and Pernaute, B. (2013). Competitive Interactions Eliminate Unfit Embryonic Stem Cells at the Onset of Differentiation. *Dev. Cel.* 26, 19–30. doi:10.1016/j.devcel.2013.06.012

Scheuer, C., Pekka, K., and Sansom, O. J. (2021). Apc-Mutant Cells Deploy Notum to Bias Clonal Competition and Drive Tumorigenesis. *Nature* 594, 343–354. doi:10.2/JQUERY.MIN.JS

Shakiba, N., Fahmy, A., Jayakumaran, G., McGibbon, S., David, L., and Trcka, D. (2019). Cell Competition during Reprogramming Gives Rise to Dominant Clones. *Science* 364, eaan0925. doi:10.1126/science.aan0925

Shakiba, N., Jones, R. D., Weiss, R., and Del Vecchio, D. (2021). Context-Aware Synthetic Biology by Controller Design: Engineering the Mammalian Cell. *Cell Syst.* 12, 561–592. doi:10.1016/j.cels.2021.05.011

Sheth, R. U., and Wang, H. H. (2018). DNA-Based Memory Devices for Recording Cellular Events. *Nat. Rev. Genet.* 19, 718–732. doi:10.1038/s41576-018-0052-8

Shin, J. Y., Hu, W., Naramura, M., and Park, C. Y. (2014). High C-Kit Expression Identifies Hematopoietic Stem Cells with Impaired Self-Renewal and Megakaryocytic Bias. *J. Exp. Med.* 211, 217–231. doi:10.1084/jem.20131128

Silver, A. J., Bick, A. G., and Savona, M. R. (2021). Germline Risk of Clonal Haematopoiesis. *Nat. Rev. Genet.* 22, 603–617. doi:10.1038/s41576-021-00356-6

Snippert, H. J., van der Flier, L. G., Sato, T., van Es, J. H., van den Born, M., and Kroon-Veenboer, C. (2010). Intestinal Crypt Homeostasis Results from Neutral Competition between Symmetrically Dividing Lgr5 Stem Cells. *Cell* 143, 134–144. doi:10.1016/j.cell.2010.09.016

Snippert, H. J., Schepers, A. G., Es, J. H., Simons, B. D., and Clevers, H. (2014). Biased Competition between Lgr5 Intestinal Stem Cells Driven by Oncogenic Mutation Induces Clonal Expansion. *EMBO Rep.* 15, 62–69. doi:10.1002/embr.201337799

Suda, K., Nakaoka, H., Yoshihara, K., Ishiguro, T., Tamura, R., and Mori, Y. (2018). Clonal Expansion and Diversification of Cancer-Associated Mutations in Endometriosis and Normal Endometrium. *Cell Rep.* 24, 1777–1789. doi:10.1016/j.celrep.2018.07.037

Suijkerbuijk, S. J. E., Kolahgar, G., Kucinski, I., and Piddini, E. (2016). Cell Competition Drives the Growth of Intestinal Adenomas in Drosophila. *Curr. Biol.* 26, 428–438. doi:10.1016/j.cub.2015.12.043

Sun, Q., Luo, T., Ren, Y., Florey, O., Shirasawa, S., and Sasazuki, T., (2014). Competition between Human Cells by Entosis. *Cell Res.* 24, 1299–1310. doi:10.1038/cr.2014.138

Tang, W., and Liu, D. R. (2018). Rewritable Multi-Event Analog Recording in Bacterial and Mammalian Cells. *Science* 360, 360. doi:10.1126/science.aap8992

Vermeulen, L., Morrissey, E., van der Heijden, M., Nicholson, A. M., Sottoriva, A., and Buczacki, S., (2013). Defining Stem Cell Dynamics in Models of Intestinal Tumor Initiation. *Science* 342, 995–998. doi:10.1126/science.1243148

Wagner, D. E., and Klein, A. M. (2020). Lineage Tracing Meets Single-Cell Omics: Opportunities and Challenges. *Nat. Rev. Genet.* 21, 410–427. doi:10.1038/s41576-020-0223-2

Watson, C. J., Papula, A. L., Poon, G. Y. P., Wong, W. H., Young, A. L., and Druley, T. E. (2020). The Evolutionary Dynamics and Fitness Landscape of Clonal Hematopoiesis. *Science* 367, 1449–1454. doi:10.1126/science.aay9333

Wimmer, R. A., Leopoldi, A., Aichinger, M., Wick, N., Hantusch, B., and Novatchkova, M. (2019). Human Blood Vessel Organoids as a Model of Diabetic Vasculopathy. *Nature* 565, 505–510. doi:10.1038/s41586-018-0858-8

Yang, X., Breuss, M. W., Xu, X., Antaki, D., James, K. N., and Stanley, V. (2021). Developmental and Temporal Characteristics of Clonal Sperm Mosaicism. *Cell* 184, 4772e15–4783. doi:10.1016/j.cell.2021.07.024

Yokoyama, A., Kakiuchi, N., Yoshizato, T., Nannya, Y., Suzuki, H., and Takeuchi, Y. (2019). Age-related Remodelling of Oesophageal Epithelia by Mutated Cancer Drivers. *Nature* 565, 312–317. doi:10.1038/s41586-018-0811-x

Conflict of Interest: The authors declare that the research was conducted in the absence of any commercial or financial relationships that could be construed as a potential conflict of interest.

Publisher's Note: All claims expressed in this article are solely those of the authors and do not necessarily represent those of their affiliated organizations, or those of the publisher, the editors and the reviewers. Any product that may be evaluated in this article, or claim that may be made by its manufacturer, is not guaranteed or endorsed by the publisher.

frontiers | Frontiers in Cell and Developmental Biology

ORIGINAL RESEARCH
published: 16 May 2022
doi: 10.3389/fcell.2022.820255

Esrrb Regulates Specific Feed-Forward Loops to Transit From Pluripotency Into Early Stages of Differentiation

*Amin R. Mazloom[1], Huilei Xu[1], Jaume Reig-Palou[2], Ana Vasileva[3], Angel-Carlos Román[4], Sonia Mulero-Navarro[4], Ihor R. Lemischka[5,6] and Ana Sevilla[2,5,6,7]**

[1]Department of Pharmacology and Systems Therapeutics, Icahn School of Medicine at Mount Sinai, New York, NY, United States, [2]Department of Cell Biology, Physiology and Immunology, Faculty of Biology, University of Barcelona, Barcelona, Spain, [3]Center for Radiological Research, Columbia University, New York, NY, United States, [4]Department of Biochemistry, Molecular Biology and Genetics, University of Extremadura, Badajoz, Spain, [5]Department of Developmental and Regenerative Biology, Icahn School of Medicine at Mount Sinai, New York, NY, United States, [6]Black Family Stem Cell Institute, Icahn School of Medicine at Mount Sinai, New York, NY, United States, [7]Institute of Biomedicine of the University of Barcelona (IBUB), Barcelona, Spain

OPEN ACCESS

Edited by:
Atsushi Asakura, University of Minnesota Twin Cities, United States

Reviewed by:
Cristina Pina, Brunel University London, United Kingdom
Constance Ciaudo, ETH Zürich, Switzerland
Nicola Festuccia, Institute Pasteur, France

***Correspondence:**
Ana Sevilla
anasevilla@ub.edu

Specialty section:
This article was submitted to Stem Cell Research, a section of the journal Frontiers in Cell and Developmental Biology

Received: *22 November 2021*
Accepted: *24 March 2022*
Published: *16 May 2022*

Citation:
Mazloom AR, Xu H, Reig-Palou J, Vasileva A, Román A-C, Mulero-Navarro S, Lemischka IR and Sevilla A (2022) Esrrb Regulates Specific Feed-Forward Loops to Transit From Pluripotency Into Early Stages of Differentiation. Front. Cell Dev. Biol. 10:820255. doi: 10.3389/fcell.2022.820255

Characterization of pluripotent states, in which cells can both self-renew or differentiate, with the irreversible loss of pluripotency, are important research areas in developmental biology. Although microRNAs (miRNAs) have been shown to play a relevant role in cellular differentiation, the role of miRNAs integrated into gene regulatory networks and its dynamic changes during these early stages of embryonic stem cell (ESC) differentiation remain elusive. Here we describe the dynamic transcriptional regulatory circuitry of stem cells that incorporate protein-coding and miRNA genes based on miRNA array expression and quantitative sequencing of short transcripts upon the downregulation of the Estrogen Related Receptor Beta (Esrrb). The data reveals how Esrrb, a key stem cell transcription factor, regulates a specific stem cell miRNA expression program and integrates dynamic changes of feed-forward loops contributing to the early stages of cell differentiation upon its downregulation. Together these findings provide new insights on the architecture of the combined transcriptional post-transcriptional regulatory network in embryonic stem cells.

Keywords: estrogen related receptor beta, feed-forward loops, MicroRNAs, mouse embryonic stem cells, network dynamic analysis

INTRODUCTION

Naïve pluripotent embryonic stem cells (ESCs) and epiblast stem cells (EpiSCs) constitute different developmental stages, mimicking the pre- and the post-implantation events during the embryo development respectively (Semi and Takashima, 2021). The complex molecular mechanisms governing this cellular stage transition are orchestrated by fluctuating levels of pluripotency transcription factors and wide-range modelling of the epigenetic landscape (Sevilla et al., 2021). Recently, microRNAs (miRNAs) have also emerged as important post-transcriptional regulators of cell fate (Leung et al., 2011; Li et al., 2021). In particular, miRNAs have been shown to play a key role in mammalian cell differentiation for proper embryonic development into the three germ layers (Cirera-Salinas et al., 2017; Cui et al., 2021). Additionally, recent studies focused on deconstructing

the transcriptional heterogeneity of ESCs, have identified certain differentially expressed miRNAs as key mediators of this transcriptional heterogeneity that facilitate the transitions into different cellular states (Kumar et al., 2014; Chakraborty et al., 2020).

Among the mechanisms to control the ESC miRNA expression program, we find the direct binding of certain transcription factors like Oct4, Sox2, Nanog and Tcf3 to their specific miRNA promoter regions (Marson et al., 2008). These miRNAs or small non-coding RNA molecules with approximately 23 nucleotides (nt) in length, regulate in turn the expression of a large set of genes as well as the pluripotency transcription factors themselves. Their way to modulate the expression of large groups of target genes is by base pairing with complementary sequences in mRNAs to induce mRNA decay and translational repression (Bartel, 2009). From this point of view, the deep understanding of network regulatory functions involves the coordination of several molecular regulatory mechanisms over time.

As key regulators of gene expression, transcription factors (TFs) and miRNAs are able to co-regulate the expression of targets in form of feed-forward loops (FFLs) and feedback loops (FBLs) (Eduati et al., 2012; Macarthur et al., 2012; Bo et al., 2021; Sevilla et al., 2021). These two kind of loops are important motifs in gene regulatory networks, which were initially proposed to describe co-regulation between different TFs on the same target (Kalir et al., 2005; Hirashima et al., 2008). In this regard, we already have been able to identify certain FFLs between Esrrb and Nanog regulating the expression of common target genes (Sevilla et al., 2021). Here, we hypothesize that TFs and miRNAs can co-regulate gene expression in a similar manner when cells transit into early differentiation stages.

In particular, it is well known that an intricate network of miRNAs participates in the regulation of the ESC cell cycle, ESC self-renewal and reprograming and ESC differentiation (Li et al., 2017). In the pluripotency state, the miRNA 290–295 cluster accounts for more than 60% of the miRNA population (Yuan et al., 2017). Indeed, components of this cluster, such as the mmu-mir-294 promote pluripotency by regulating a subset of c-Myc target genes through feed-forward loops and directly upregulating pluripotency-associated genes such as Lin 28 (Hanina et al., 2010). In this regard, work pioneered by Marson and others also proposed the presence of incoherent feed-forward loops among Oct4, Sox2, Nanog and Tcf3 and the miR 290–295 cluster (Marson et al., 2008).

To extend these studies, we have centred this study in mapping the direct miRNA targets of the Estrogen related receptor beta, (Esrrb), and observed their miRNA dynamic changes once integrated into gene regulatory networks with their gene target transcripts. Studying the dynamic changes of these feedforward motifs participating miRNAs will give us a better understanding on this stem cell transition upon Esrrb downregulation.

Esrrb was discovered as a key pluripotency transcription factor (TF) with Pou5f1, Nanog and Sox2 from loss of function studies (Ivanova et al., 2006). Results from its depletion evidenced loss of pluripotency and certain cellular commitment towards epiblast-derived lineages, such as mesoderm and neuroectoderm (Ivanova et al., 2006; Festuccia et al., 2018). It has been shown that Esrrb is among the key TFs present in ESC while absent in more mature epiblast-derived stem cells (EpiSC) (Hutchins et al., 2013). In ESCs, Esrrb and Sox2 positively co-regulate at the transcriptional level, certain pluripotent genes and co-binding with Oct4 is capable to activate Nanog promoter (van den Berg et al., 2008).

Interestingly, further observations of our previous studies in protein/mRNA content (Lu et al., 2009), highlighted the important and largely underappreciated role(s) of translational and post-translational regulation in ESC biology. To address this issue in more detail, we have integrated miRNA expression analyses into our regulatory networks providing a more comprehensive view of the stem cell transition towards a differentiation state. We identify a set of feed-forward loops (FFL) where Esrrb (and likely other transcription factors) simultaneously regulate the expression of mRNA coding genes and miRNA genes whose products have been experimentally proved to target these mRNAs. Thus, Esrrb simultaneously regulates protein-coding genes as well as the post-transcriptional machinery for fine-tuning the transition from pluripotency into an early differentiation state. Overall, our results reveal the amazing degree of biological complexity that can be "encoded" even with apparently "simple" regulatory network sub-circuits.

MATERIALS AND METHODS

ES Cell Culture

The murine ESC line with controllable Esrrb expression (Esrrb_R) was constructed and characterized previously (Ivanova et al., 2006), and was maintained as described on irradiated primary mouse embryonic fibroblasts (MEFs). For all experiments, ESCs were cultured on 0.1% gelatin-coated tissue culture plates without feeder cells. To induce differentiation, we plated the cells at a density of 3×10^5 cells per 10 cm dish and we withdrew Doxycycline (Dox) (1 μg/ml, Sigma) from the media while maintaining all other routine ESC nutrients: D-MEM–High Glucose (Dulbecco's modified Eagle's medium-1X-High Glucose) (Gibco®, Invitrogen), 15% FBS (Fetal bovine serum) (Hyclone, Thermo Scientific), 100 mM MEM non-essential amino acids, 0.1 mM 2-mercaptoethanol, 1 mM L-glutamine, Penicillin/Streptomycin (Gibco, Invitrogen) and 10^3 U/ml LIF (Chemicon, Millipore). All cell cultures were maintained at 37°C with 5% CO_2.

Alkaline Phosphatase

Alkaline phosphatase activity was examined using Alkaline Phosphatase Staining Kit (Red) from abcam (ab242286) following manufacturer´s instructions.

Real Time Quantitative PCR (RT-qPCR)

Cells were trypsinized and collected at specific time points. Total RNA was extracted using Trizol Reagent (Invitrogen), column-purified with RNeasy kit (Qiagen) and treated with RNase-free DNase (Qiagen). Total RNA (1 μg) was reverse transcribed using a high-capacity reverse transcription kit (Applied Biosystems).

All quantitative PCR analyses were performed using the Fast SYBR Green Master Mix (Applied Biosystems) following the manufacturer's protocols on the StepOne Plus Real-Time PCR System (Applied Biosystems). Gene-specific primers used for this study are listed in **Supplementary Table S1**.

MiRNA qRT-PCR

MiRNA expression levels were quantified in total RNA from cell extracts at days 0, 1, 3 and 5 using Trizol and MiRNase kit (QIAGEN). TaqMan mouse MicroRNA assays (Applied Biosystems) were used to quantify mature miRNA expression levels as previously described (Chen et al., 2005) (**Supplementary Table S1**). Reverse-transcriptase reactions were performed using the TaqMan MicroRNA Reverse Transcription kit (Applied Biosystems) according to manufacturer´s recommendations. Basically, the reaction contained 10 ng of total RNA, 50 nM reverse transcription (RT) primer, 1x RT buffer, 0.25 mM each of dNTPs, 3.33 U/ml MultiScribe reverse transcriptase and 0.25 U/ml RNase inhibitor. The 7.5 µl reactions were incubated in an Applied Biosystems 9,700 Thermocycler in a 96-well plate for 30 min at 16°C, 30 min at 42°C, and 5 min at 85°C and then held at 4°C. Quantitative real-time PCR was performed using TaqMan universal PCR Master Mix, No AmpErases UNG (Applied Biosystems) on the StepOnePlus Real-Time PCR Systems (Applied Biosystems). The 10 µl PCR mix included 0.67 µl RT product, 1x TaqMan universal PCR Master Mix, and 0.2 mM TaqMan probe. The reactions were incubated in a 96-well plate at 95°C for 10 min, followed by 40 cycles of 95°C for 15 s and 60°C for 1 min. All reactions were run in triplicate. All TaqMan miRNA assays are available through Applied Biosystems. MiRNA expressions were normalized to the expression of U6 probe (Applied Biosystems) as endogenous control.

Chromatin Immunoprecipitation

Data from the Esrrb ChIP using the PP-H6707-00 antibody, clone H6707 (R&D Systems) was obtained from the GEO database under the accession numbers GSM785839 and GSM785840. See Supplementary Material and our previous work for experimental details (Sevilla et al., 2021).

Analysis of Mature miRNA Frequencies by Solexa Sequencing

The method for cloning cDNAs from 18–30 nt transcripts was slightly modified from the previously described to allow its use in the Solexa sequencing platform (Illumina) (Lau et al., 2001). Short transcript libraries were generated using size selected RNA. Total RNA at different time points after Esrrb downregulation, was extracted with Qiazol® (Qiagen) with subsequent enrichment for small RNAs (<200 bp) using the miRNeasy® Mini purification kit according to the manufacturers' instructions for total RNA isolation that includes the small fraction. Extracted RNA (40 µg) was combined with trace amounts of 5′-^{32}P-labeled RNA standards (See, **Supplementary Table S1**). RNA was then fractionated on a 15% polyacrylamide, 8 M urea gel (Bio-Rad). A gel fragment spanning both the 18 nt and 24–26 nt internal standards was excised, and RNA was eluted and ethanol-precipitated in siliconized tubes, with 20 µg of glycogen as carrier. Gel-purified 18–26 nt RNA was incubated with 50 µM pre-adenylylated 3′-adaptor oligonucleotide (Modban), 10X ATP-free ligase Buffer (500 mM Tri-HCl (pH = 7.5–7.6), 100 mM $MgCl_2$, 100 mM DTT, 600 µg/ml BSA), and T4 RNA Ligase 2, truncated (New England BioLabs) in a 20 µl reaction at 37°C for 1 h. The T4 RNA ligase reaction was purified on a 15% polyacrylamide, 8 M urea gel (Bio-Rad) by using the ligated forms of the standards as a guide for band excision. RNAs ligated with 3′-adaptor oligonucleotide were eluted and ethanol-precipitated in siliconized tubes, with 20 µg of glycogen. Ligated RNA product was used in a second T4 RNA ligase reaction for the 5′-adaptor oligonucleotide (Solexa Linker). Ligated products were gel-purified, excising the gel fragment spanning the doubly ligated standards. Gel-purified doubly ligated RNA was used in a standard 20 µl RT reaction (SuperScript III, Invitrogen) with the RT BanOne primer. The cDNA was PCR amplified with the 5′and 3′primers, generating products with an extended 3′ adaptor sequence. PCR products were digested with Pme I (NEB) at 37°C for 3 h. DNA fragments ranging from 108–113 bp were isolated from a low-melting point agarose gel. After further phenol extraction and ethanol precipitation, DNA samples were resuspended in Elution buffer (10 mM Tris/0.1% Tween) and then used according to the standard Solexa sequencing protocol (Illumina). Each library was run on one lane of the Solexa sequencer at the Genomic Sequencing Core at Icahn School of Medicine at Mount Sinai. MiRNA-Seq data analysis is described in the **Supplementary Material** and primer sequences for this analysis can be obtained from (**Supplementary Table S1**).

Gene Ontology

Gene ontology analysis was performed using David bioinformatic resources https://david.ncifcrf.gov/tools.jsp (Huang et al., 2008).

qRT-PCR of Primary miRNAs

qPCR primers were designed using the standard specifications of Primer 3 for real time primer design (Rozen and Skaletsky, 2000). Pri-miR 290–295 expression levels were analysed by SybrGreen quantitative PCR on the StepOnePlus Real-Time PCR system (Applied Biosystems) using specific primers (**Supplementary Table S1**). Expression levels were calculated relative to actin mRNA levels.

miRNA Microarray Expression Analysis

RNA from the Esrrb_R rescue clone was extracted with the miRNeasy mini kit (Qiagen) at the different time points. Total RNA (5 µg) from days 1, 3 and 5 after Esrrb downregulation and day 0 as a reference sample were labelled with Hy3™ and Hy5™ fluorescent labels, using the miRCURY™ LNA Array labelling kit (Exiqon, Denmark) according to the manufacturer's protocol. The labelled samples were mixed pairwise and hybridized to the miRNA arrays printed using miRCURY™ LNA oligo set, fifth generation (Exiqon, Denmark). Analyses were performed in triplicate for a total of 12 microarrays. Each miRNA was printed in duplicate, on code link slides (GE), using Gene

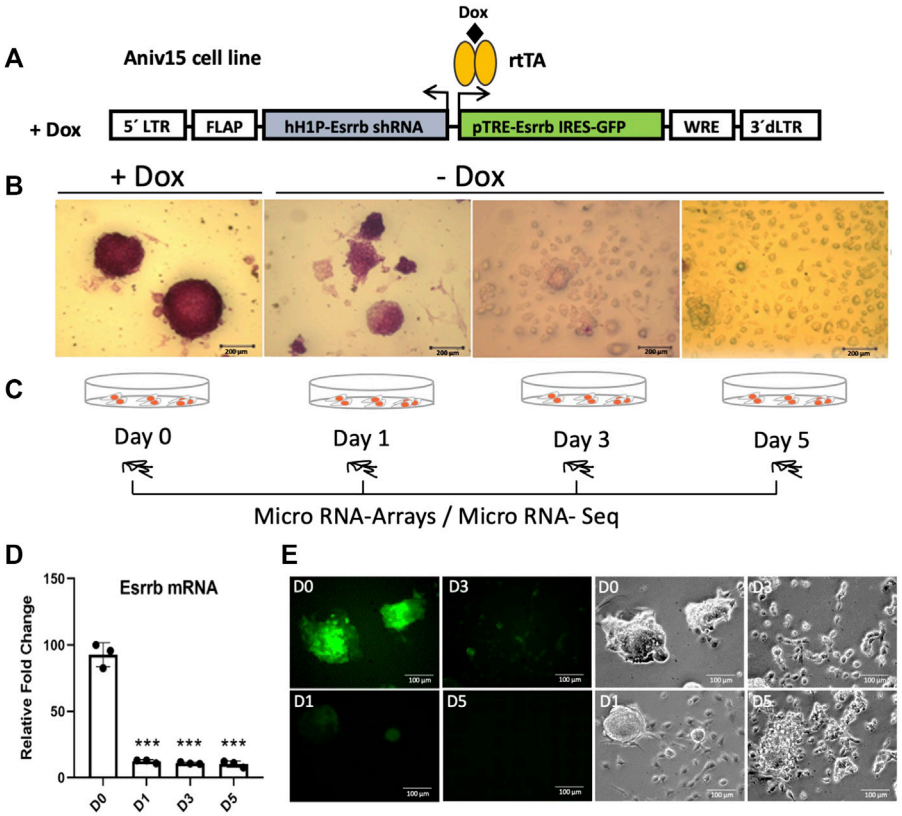

FIGURE 1 | Downregulation of Esrrb induces cell differentiation **(A)** Structure of the lentiviral vector for conditional expression of Esrrb (Ivanova et al., 2006). Endogenous Esrrb is depleted with short hairpin (sh) RNA and complemented by shRNA¨immune¨version of Esrrb expressed in a doxycycline (Dox)-dependent manner. Dox withdrawal results in downregulation of the exogenous Esrrb leading to stem cell differentiation. hH1P-Esrrb is the endogenous Esrrb specific shRNA cassette (in light grey); pTRE-Esrrb is GFP-tagged exogenous Esrrb cassette (in green) **(B)** Experimental time series inducing differentiation from day 1 to day 5 by Dox removal and measurement of the alkaline phosphatase activity to confirm stem cell differentiation. Scale bar 200 μm. **(C)** Experimental time course for miRNA gene expression analysis. At day 0, Esrrb is expressed in the presence of Dox; at day 1, 3 and 5 time points, Esrrb is downregulated following Dox withdrawal. **(D)** Gene expression analysis of Esrrb after Dox withdrawal. Endogenous levels of Esrrb mRNA are undetectable due to the constitutive shRNA. Quantitative PCR data confirm the expression of the exogenous form of Esrrb in the presence of Dox (mean ±3 replicates (n = 3)). Significance was tested comparing each day to day 0 using a two-tailed Student´s *t*-test with ***$p < 0.001$) **(E)** GFP expression at day 0 in the presence of Doxycycline. Removal of Doxycycline results in the downregulation of the exogenous Esrrb-GFP leading to stem cell differentiation. Scale bars 100 μm.

Machines Omnigrid 100. Hybridizations were performed overnight at 60°C using the Agilent Hybridization system (SurHyb), after which the slides were washed using the miRCURY™ LNA washing buffer kit (Exiqon, Denmark) following the manufacturer's protocol. The slides were scanned using an Axon 4000B scanner and image analyses were performed using the Genepix Pro 6.0 software package. MiRNA microarray expression data analysis is depicted in the **Supplementary Material**.

RESULTS

Esrrb Downregulation Changes the miR Transcriptome Landscape

To explore the Esrrb miRNA specific program, we started analysing miRNA dynamic changes upon its downregulation. For that, we took advantage of the lentiviral/shRNA-based genetic complementation system to deplete Esrrb under serum/Lif conditions (Ivanova et al., 2006; Lee et al., 2012; Sevilla et al., 2021) (**Figure 1A**). This lentiviral system carries a constitutively expressed shRNA for Esrrb and a TRE-controlled immune-deficient version of Esrrb linked to GFP expression, into transactivator (rtTA)-expressing mouse Ainv15 ESCs. Therefore, in the presence of doxycycline (day 0), Esrrb is expressed but upon doxycycline removal, Esrrb expression downregulates and cells differentiate. Stem cell differentiation at days 1, 3 and 5, was confirmed by the loss of alkaline phosphatase activity in comparison to day 0 (**Figure 1B**). Using this system, we profiled miRNA expression at day 0, when Esrrb was expressed and at days 1, 3 and 5, where Esrrb downregulation was induced (**Figures 1C–E**), by exiqon microarrays and miRNA-Seq.

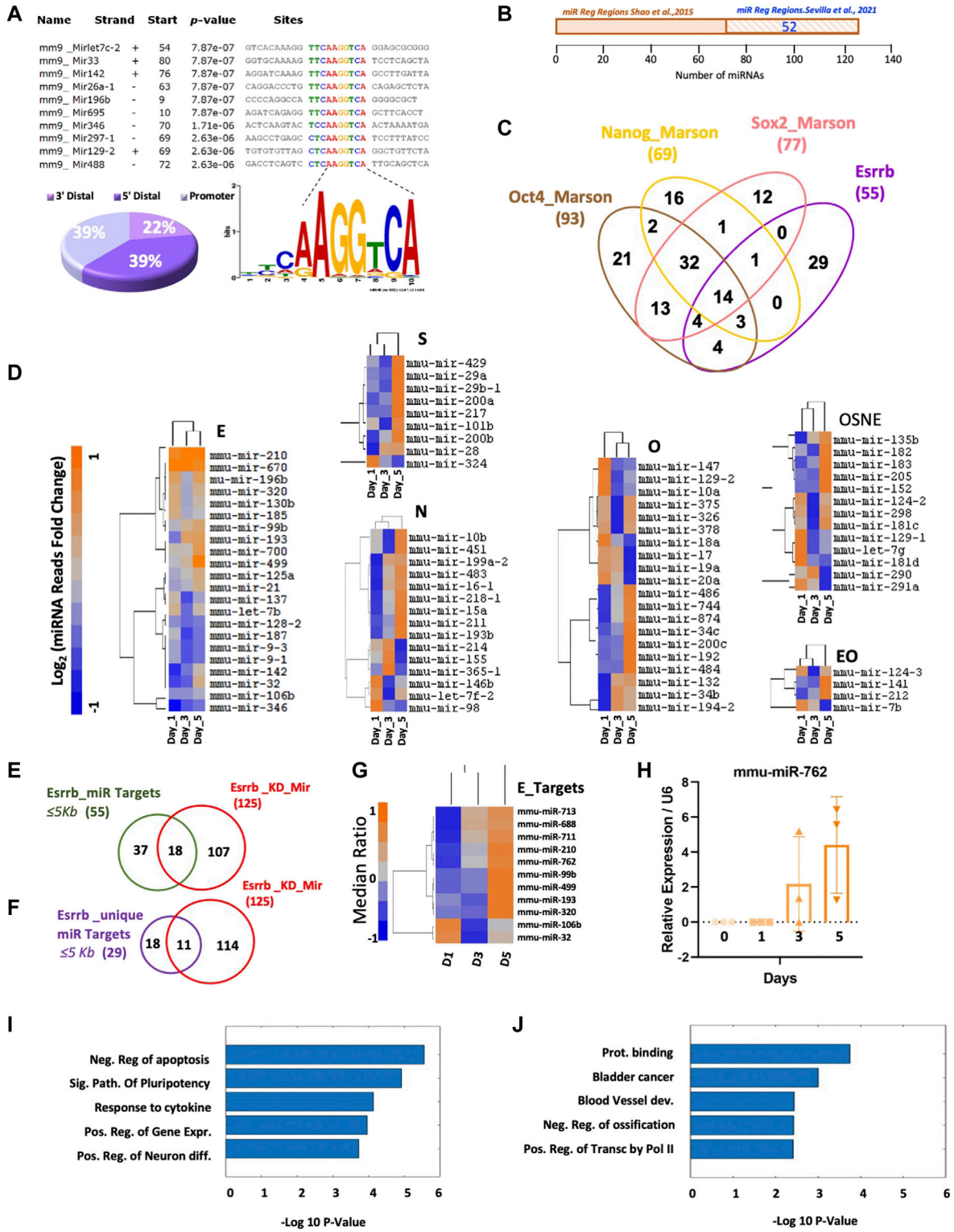

FIGURE 2 | Direct regulation of miRNA expression by Esrrb. **(A)** Motif Esrrb peak distribution at miRNA promoters, (22%) 3′Distal (39%) 5′Distal and (39%) Promoter. **(B)** Venn diagram generated by the Venny 2.1.0 tool https://bioinfogp.cnb.csic.es/tools/venny/(Oliveros, 2007) showing the overlap between the Esrrb miRNA target genes identified by Shao et al. (2015) and the Esrrb miRNA target genes identified in our Esrrb ChIP-Seq data (Sevilla et al., 2021) **(C)** Venn diagram generated by the Venny 2.1.0 tool https://bioinfogp.cnb.csic.es/tools/venny/(Oliveros, 2007) showing the overlaps among miRNAs bound by Esrrb, and those bound by Oct4, Sox2 and Nanog (Marson et al., 2008). Binding sites were identified at ≤5 Kb distance from the transcription start site (TSS) for all four-transcription

(*Continued*)

FIGURE 2 | factors. Numbers in parentheses represent the total number of miR genes bound by each respective TF. **(D)** Dynamic miRNA expression level changes of miRNA genes that are targets of Esrrb (letter E) Oct4 (letter O), Nanog (letter N), Sox2 (letter S), the combination of all four transcription factors (letters OSNE) and the combination of only Oct4 and Esrrb (letters EO) following Esrrb depletion. Analysis and normalization details are described in Material and Methods, Supplementary Material and **Supplementary Figure S1**. A full list of the miRNA reads differentially expressed can be found in (**Supplementary Table S5**) **(E)** Venn diagram showing the overlap between the 55 Esrrb miRNA targets and the 125 differentially expressed miRNAs analyzed by microarrays. Anova p-Value ≤ 0.05 after Bonferroni correction (**Supplementary Table S6**) **(F)** Venn diagram showing the overlap between the 29 unique Esrrb miRNA targets and the 125 differentially expressed miRNAs analyzed by microarrays (**Supplementary Table S6**). Anova p-Value ≤ 0.05 after Bonferroni correction. **(G)** Hierarchical clustering of the miRNAs that are specifically regulated by Esrrb, but not by Oct4, Sox2 or Nanog that significantly change in expression after Esrrb knockdown. Expression levels are represented as ratios of the median. **(H)** Relative expression of the mature mmu-mir-762 over the time series. Error bars indicate standard deviation derived from three independent time series experiments (n = 3). **(I)** Bars representing the five top Gene ontology (GO) terms obtained, using David bioinformatics resources https://david.ncifcrf.gov/tools.jsp (Huang et al., 2008), in the set of genes that are directly bound by Esrrb as transcription factor and also modulated by Esrrb-regulated miRNAs. **(J)** GO results from the set of genes that are only modulated by Esrrb-regulated miRNAs.

Surprisingly, in genomic localization analyses, when we incorporate our published Esrrb ChiP-Seq data GSM785839 (Sevilla et al., 2021) to our miRNA analysis, we observed that 39% of Esrrb binding sites are located near miR gene promoter regions and these binding sites contain the previously reported Esrrb binding motif TCAAGGTCA (Chen et al., 2008) (**Figure 2A** and **Supplementary Table S2**). Comparison of our Esrrb miRNA targets with the ones previously published showed an overlap of 52 miRNAs (57%) (Shao et al., 2015) (**Figure 2B** and **Supplementary Table S3**). Integration of Esrrb miRNAs binding sites with the other core transcription factors, all within ≤5 Kb from the transcription start site (TSS), showed a total of 14 Esrrb miRNA targets that are co-occupied by Esrrb, Oct4, Sox2 and Nanog and 29 that are uniquely bound by Esrrb (**Figure 2C** and **Supplementary Table S4**). MiRNA-Seq analysis of the dynamic changes of the miRNAs regulated by each transcription factor independently showed specific miRNAs like mmu-mir-210, mmu-mir-99b, mmu-mir-499, mmu-mir-196b, mmu-mir-320, mmu-mir-106b and mmu-mir-32 among others to be regulated by Esrrb whereas, other miRNAs like mmu-mir-182, mmu-mir-183, mmu-mir -290 and mmu-mir-291a appeared to be regulated by the whole core of transcription factors Oct4, Sox2, Nanog, and Esrrb (OSNE) (**Figure 2D**, **Supplementary Table S5**).

Further comparison of the fifty-five Esrrb miRNA targets with the miRNA transcriptome microarray data performed in the Esrrb knockdown time series, revealed significant changes of expression in eighteen out of the fifty-five (**Figure 2E**, **Supplementary Table S6**). Notably, eleven out of the eighteen miRNAs identified were uniquely regulated by Esrrb (**Figure 2F**, **Supplementary Table S6**). Heatmap showing the miRNA expression values, from our microarray data along the time series, showed that most of them are upregulated (**Figure 2G**, **Supplementary Table S6**). Additional experimental confirmation for mmu-mir-762, from three independent experimental time series, confirmed this upregulation as well (**Figure 2H**).

Next, we explored if the main transcriptional changes upon Esrrb downregulation of these eleven miRNAs were attributed to regulation through the modulation of miRNAs or to a direct control as a transcription factor. For that, we identified the miRNA target genes of these eleven Esrrb regulated miRNAs using the miRNet 2.0 network-based visual analytics for miRNA functional analysis www.mirnet.ca (Chang et al., 2020) and we classified those genes as being regulated by Esrrb as a transcription factor or not based on the presence or absence of peaks at (≤5 Kb from TSS) using the data from our previous publication (Sevilla et al., 2021). Interestingly, gene ontology analysis using David bioinformatic resources https://david.ncifcrf.gov/tools.jsp (Huang et al., 2008) of these eleven Esrrb miRNA target genes showed a significant enrichment in the categories of negative regulation of apoptosis, signaling pathways of pluripotency and positive regulation of gene expression for those genes that are both regulated directly by Esrrb as a transcription factor (≤5 Kb from TSS), and also modulated by Esrrb through the regulation of miRNAs, (**Figure 2I** and **Supplementary Table S7**). However, in the set of genes that are only regulated by Esrrb through the modulation of miRNAs, we observed an enrichment in more diverse categories such as protein binding, bladder cancer and blood vessel development (**Figure 2J** and **Supplementary Table S7**). These results reinforce the role of Esrrb as a transcription factor not only interacting directly at the promoter region of the genes but also binding at the promoter regions of certain miRNAs whose target genes are also involved in regulating gene expression.

Further analysis of the targets of each miRNA showed that not all the miRNAs regulate the same number of genes. For instance, mmu-mir-688, mmu-mir-711, mmu-mir-99b and mmu-mir-193 have less weight in the Esrrb miRNA regulation as each of them regulate less than 10 target genes. In contrast, mmu-mir-713, mmu-mir-210, mmu-mir-762, mmu-mir-499, mmu-mir-320, mmu-mir-106b, and mmu-mir-320 each of them regulate, up or down, more than 10 target genes. As we can observe, the response is quite specific for each miRNA and each target (**Supplementary Figure S2** and **Supplementary Table S8**).

Esrrb Contributes With the Core Transcription Factors Oct4, Sox2 and Nanog in the miR 290–295 Cluster Regulation

In mESC, the miR 290–295 cluster inhibits differentiation among other functions (Yuan et al., 2017). Analysis from our high-resolution Esrrb location analysis confirmed a clear peak within ≤5 Kb of the TSS on the miR 290–295 promoter (**Figure 3A**, **Supplementary Table S2**). Analysis of the primary miR-290–295

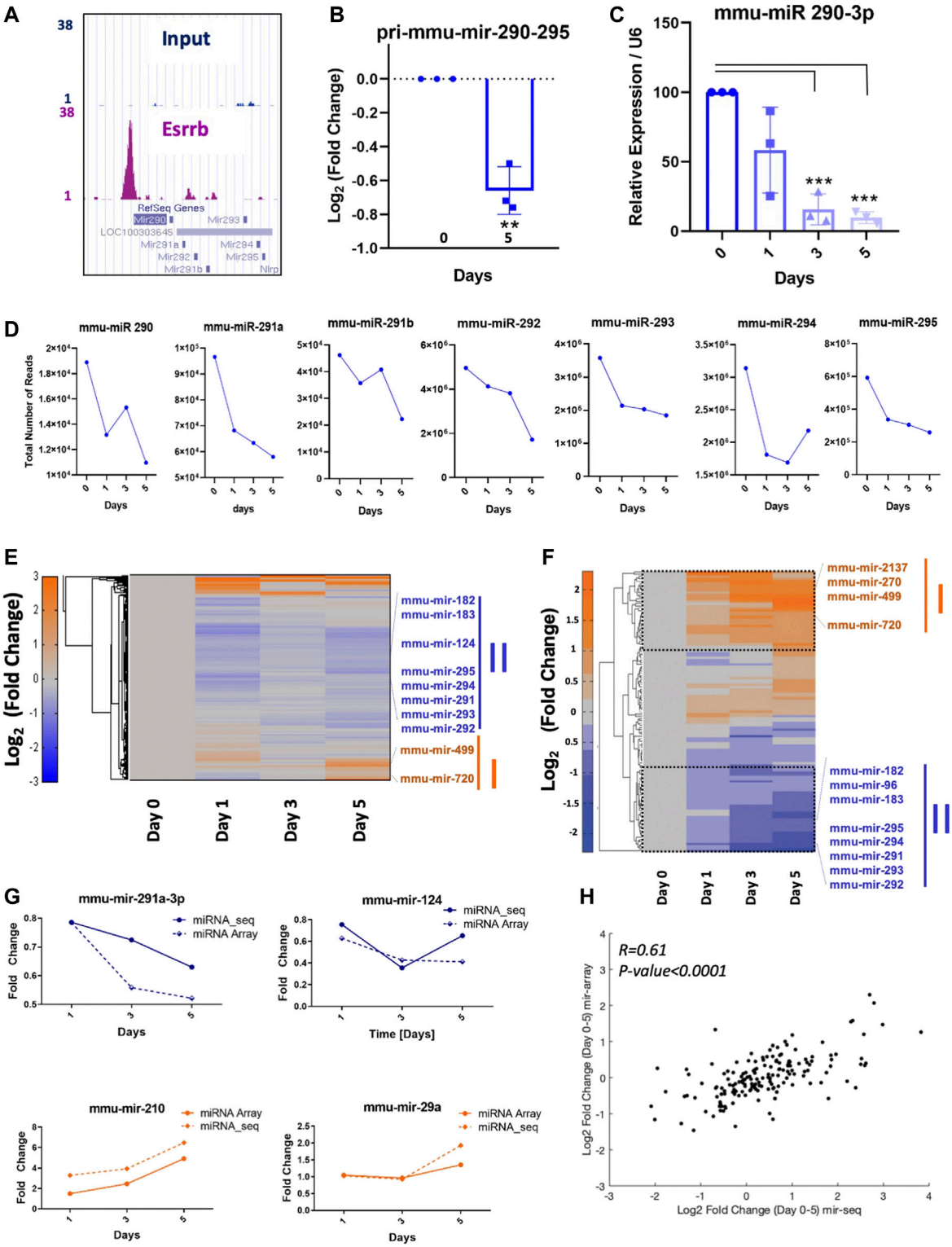

FIGURE 3 | Direct regulation of miRNA expression by Esrrb **(A)** Genome Browser screenshot of the Esrrb binding site in the promoter region of the miR-290–295 cluster (http://genome.ucsc.edu) (Kent et al., 2002). **(B)** Quantitative PCR measurements of changes in pri-mmu-mir-290–295 expression levels. Error bars indicate standard deviation derived from three independent time series. Significance was tested with a two-tailed Student´s *t*-test, with $^{**}p < 0.001$ **(C)** Relative expression of mature mmu-mir-290-3p over the time series. Error bars indicate standard deviation derived from three independent experiments (n = 3). Significance was tested comparing each day to day 0 using a two-tailed Student´s *t*-test with $^{***}p < 0.0001$) (D) Total number of reads for mmu-mir-290, mmu-mir-291a, mmu-mir-291b, mmu-

(*Continued*)

FIGURE 3 | mir-292, mmu-mir-293, mmu-mir-294, mmu-mir-295 at days d0, d1, d3 and d5. **(E)** Hierarchical clustering of the $\log_2$ (fold change) miRNA-Seq read counts after Esrrb knockdown. **(F)** Hierarchical clustering of the most significant miRNA level changes analysed by microarrays (Exiqon). **(G)** Similar expression profiles of miRNAs from the miRNA-Seq and the microarray data. **(H)** Correlation plot between microRNAs obtained in microarrays and miRNA-Seq using the log2 of the fold change between day 0 and day 5. Correlation coefficient R = 0.61 with a *p*-Value $p < 0.0001$.

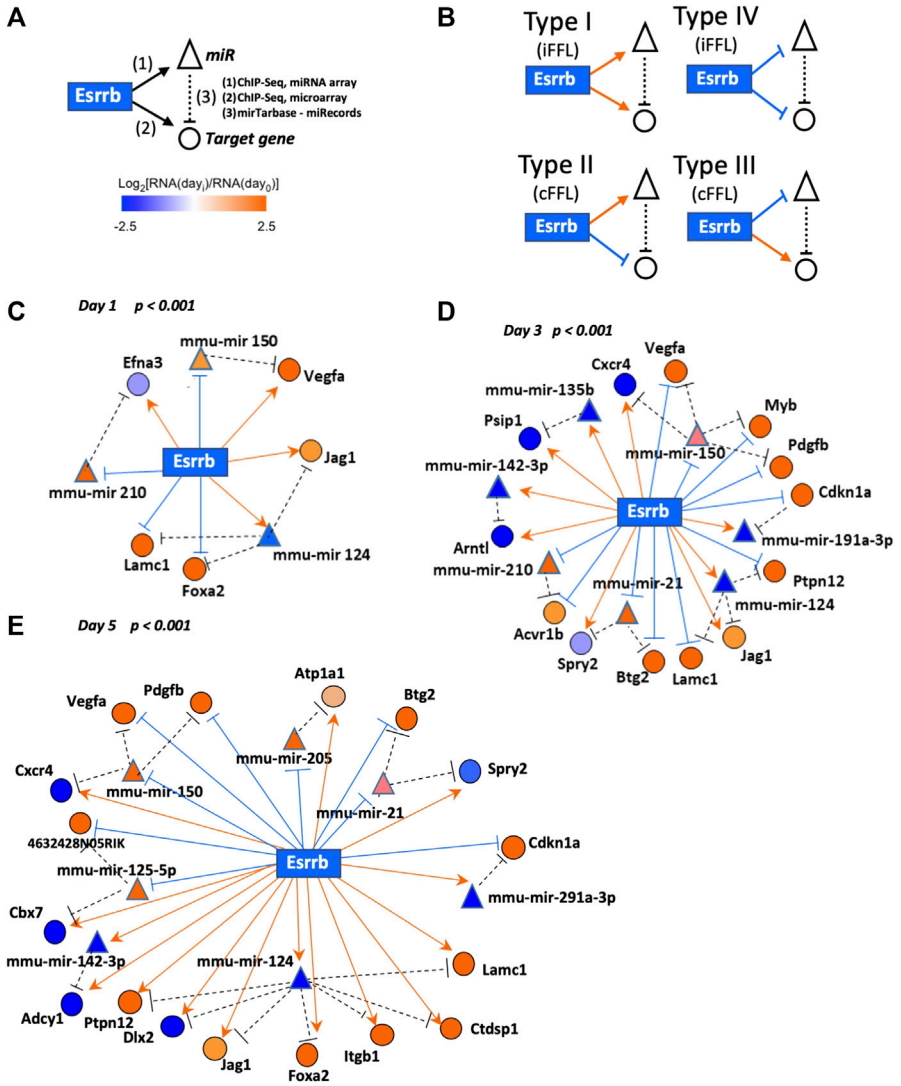

FIGURE 4 | Esrrb regulated mRNA/miRNA feed-forward network motif. **(A)** Schematic view of the Esrrb regulated feed-forward network motif. Esrrb directly regulates expression of many target genes (1) as well as miRNAs (2), which in turn regulate expression levels of Esrrb protein-coding target genes (3). Interactions have been mapped according to experimentally validated post-translational regulations reported by either miRTarBase (last update January 2022) https://mirtarbase.cuhk.edu.cn/~miRTarBase/miRTarBase_2022/php/index.php (Hsu et al., 2014) or miRecords (last update 03–09-2021) http://c1.accurascience.com/miRecords/(Xiao et al., 2009) databases. **(B)** Detected network motif types connecting Esrrb, miRNAs and their mRNA target genes. **(C–E)** Representation of the day 1, day 3 and day 5 networks linking together Esrrb, miRNA target genes and their experimentally validated mRNA targets. Esrrb is the central rectangle; circles and triangles designate protein-coding and miRNA-coding target genes, respectively. Edges are formatted either in bright orange arrows (activation) or blue hammerheads (repression). Nodes are coloured in orange or blue for both target genes and miRNAs, depending on their expression levels increase or decrease respectively, relative to day 0 levels. Only motifs that passed the Bonferroni corrected *p*-value ($p < 0.001$) during the Esrrb downregulation time course are depicted.

expression levels assessed by quantitative qPCR showed a significant downregulation of the primary transcript at day 5 (**Figure 3B**). In the same line, relative expression values of the mature mmu-miR-290-3p were significantly downregulated at day 3 and day 5 with respect to day 0 (**Figure 3C**). Effects on mature miR regulation were measured globally at day 0 in the

presence of doxycycline and on days 1, 3 and 5 upon doxycycline removal using quantitative sequencing of short RNAs (18–30 nucleotides). Although, mature miRNAs might have long half-lives, a reduction in the mmu-mir-290, mmu-mir-291a, mmu-mir-291b, mmu-mir-292, mmu-mir-293, mmu-mir-294 and mmu-mir-295 was observed (**Figure 3D** and **Supplementary Table S5**). Clustering analysis of the miRNA-Seq data (**Figure 3E**) and the miRNA expression data analysed by the miRCURY LNA array platform (**Figure 3F**), showed comparable results for several miRNAs showing concordance in the downregulation or upregulation of many miRNAs (**Figure 3G**). This result was also confirmed by analyzing the correlation between the miRNAs obtained in the microarrays and the ones obtained in the miRNA-Seq analysis. Strong similarities were observed when the $\log_2$ fold change between day 0 and day 5 was compared (**Figure 3H**).

Esrrb is part a of mixed-type mRNA/microRNA feed-forward loop motif network that controls stem cell transition from pluripotency into early differentiation states.

As many gene-products are regulated by miRNAs, the functions of potential regulatory network motifs containing both miRNAs and protein coding genes/gene products are gaining special interest (Zhang et al., 2015). For this reason, we focused our analysis on elucidating the presence of possible recurring Esrrb-controlled feed-forward loop network motifs (FFLs). These (FFL) motifs present three nodes: an upstream regulator X (Esrrb) that regulates both a downstream regulator Y (miR), and a downstream target Z (target-gene). An additional edge is directed from Y (miRNA) to Z (target-gene), thus closing the unidirectional "loop" (**Figure 4A**). FFLs can be divided into three types according to the master regulator: TF-FFL, miRNA-FFL and composite FFL in which TF and miRNA regulate each other (Shen-Orr et al., 2002; Zhang et al., 2013). Here we have considered the TF-FFLs where the TF (Esrrb) is the master regulator, which regulates its partner miRNA and their mutual target gene.

In our analysis, we found four types of feed-forward loop (FFL) motifs where Esrrb is the source transcriptional regulatory node by integrating, our previously published data of Esrrb genomic localization by Chip-Seq and, gene expression changes experimentally determined by the Affymetrix Gene 1.0 ST Array (Sevilla et al., 2021) with our miRNA expression changes experimentally analyzed in this study by miRCURY LNA™ miRNA Array followed by Esrrb downregulation (**Supplementary Table S6**). MiRNA/mRNA interacting pairs have been taken from the miRNA-target interactions experimentally validated databases miRTarBase https://mirtarbase.cuhk.edu.cn/~miRTarBase/miRTarBase_2022/php/index.php (last update January 2022) (Hsu et al., 2014) or miRecords (last update 03–09-2021) http://c1.accurascience.com/miRecords/(Xiao et al., 2009) (**Supplementary Table S9**).

Based on the effects of TFs and miRNAs on their mutual target, FFLs can be classified in coherent and incoherent FFLs (**Figure 4B**). In incoherent FFLs, the expression of the target is controlled by two reverse paths, both miRNA and target gene interactions increase or decrease in expression together (Types I and IV), whereas in coherent FFLs, the regulatory paths have the same effects on the target (either activation or repression) and therefore, one interaction increase meanwhile the other decrease (Types II and III). In the case of coherent FFLs, the miRNA can help the transcriptional activation or repression of a target protein in the cell at a particular time acting as a post-transcriptional failsafe control whereas in the case of incoherent FFLs, the miRNA contributes more in fine-tuning the protein expression levels at the correct functional range (Osella et al., 2011; Zhang et al., 2013). Integration of the identified individual motifs revealed three networks corresponding to each day of the differentiation process with significant presence of specific Esrrb-regulated miRs (**Figures 4C–E**, **Supplementary Table S9**). As cells differentiate over time, more genes became differentially expressed and as a result, the subnetwork of FFL motifs grows. Although some of the miRNAs such as mmu-mir-150 and mmu-mir-124, are present in all the networks, the response is very dynamic as more targets are being affected by these miRNAs over time and because not all the targets are conserved over time. This effect is more evident between day 3 and day 5 were the number of targets increase and diversify. Only two miRNAs, mmu-miR-21 and mmu-miR-291-3p maintained the same targets from day 3 to day 5, whereas mmu-miR-135b appears only at day3.

Collectively, our data show that Esrrb controls FFLs involving both the protein coding target genes and miRNAs to guarantee the smooth transit from the pluripotency state into the early differentiation state in a precise controlled manner.

DISCUSSION

Gene expression regulation during the transition from pluripotency into the early stages of stem cell differentiation, is a complex process involving various regulatory biomolecules across different levels (MacNeil and Walhout, 2011). Transcription factors and miRNAs are the most common regulatory biomolecules that fine-tune gene expression by regulating at transcriptional and post-transcriptional level respectively (Martinez and Walhout, 2009). Although initially they were known to regulate gene expression independently, now increasing evidence shows that miRNAs and TFs also work synergistically in the form of complex networks to regulate the gene expression, which further modulates cellular and molecular processes (Qin et al., 2020; You et al., 2020; Bo et al., 2021). These complex regulatory interactions can be best viewed using TF-miRNA-Target Gene co-regulatory networks. These co-regulatory networks are responsible for the impressive degree of complexity in gene-regulation in higher eucaryotes (Cora et al., 2017).

Here we provide dynamic time series of miRNA significant changes after Esrrb downregulation in mouse ESCs (**Figures 1D,E**) and we connect this data with previously published high-resolution, genome-wide maps of Esrrb binding sites at promoter regions for most miRNA genes (Sevilla et al., 2021). From binding motif identification (**Figure 2A**), and changes in

miRNA transcription, from the time series data generated in the present study (**Figure 2D**, **Supplementary Tables S5, S6**), we have identified the most significant Esrrb miRNAs target genes having a 57% of overlap with the previously identified Esrrb miRNA targets (Shao et al., 2015). Cross comparison of Esrrb miRNA targets with the other core transcription factors (Oct4, Sox2 and Nanog) miRNA targets, revealed twenty-nine miRNAs regulated uniquely by Esrrb. From them, 11 showed significant changes in their miRNA expression profiles upon Esrrb downregulation (**Supplementary Table S6**). Notably, those miRNA target genes that were also regulated by Esrrb as a transcription factor were target genes involved in signalling pathways related with pluripotency and negative regulation of apoptosis showing the complex regulatory mechanisms to maintain pluripotency (**Figure 2I**).

Among its direct targets, Esrrb regulates the miR 290–295 cluster (**Figures 3A–D**) as previously has been also proven to be regulated by other core transcription factors such as Oct4, Sox2, Nanog and Tcl3 (Marson et al., 2008). This cluster controls a wide variety of functions such as the regulation of expression of the core transcription factors, stem cell metabolism, cell proliferation and the cell cycle of ESCs whose phase distribution changes are critical for adequate stem cell differentiation (Yuan et al., 2017).

Additionally, special attention should be given to those miRNAs regulated by the core of transcription factors (OSNE) (**Figure 2D**). Among them we have the mmu-mir-182, which shows a clear upregulation by day 5 upon Esrrb downregulation in the absence of external signals. This upregulation is in line with recent studies where they show that the mmu-miR-182 and other differentially expressed miRNAs, act on neighborhoods of pluripotency genes to increase variation of target genes. Thus, through this mechanism, pluripotent stem cells could be driving cell diversification into new states without the need of external signals (Chakraborty et al., 2020).

Additionally, considering that Esrrb has a bimodal expression and that some of the differentially expressed miRNAs are regulated by Esrrb, the possibilities of cell diversification multiply exponentially since both mechanisms increase transcriptional variation (Kumar et al., 2014).

Our analyses of Esrrb-mediated miRNA gene regulation add a new element to the view of cell fate regulatory networks, a feed-forward control loop (FFL), consisted by Esrrb, direct miRNA targets and a protein coding gene transcriptionally regulated by Esrrb with further mRNA regulation by the miRNAs (**Figures 4A,B**). Our network studies show a novel approach to analyse miRNA expression dynamics during ESC differentiation, particularly at early stages when the cells transit from the pluripotency state into the differentiation fates.

Thoroughly observation of the connections between mRNA and miRNA-encoding genes, allowed the identification of frequently occurring feed-forward motifs composed of Esrrb as the central transcriptional regulatory node controlling the expression of mRNAs of certain genes as well as miRNAs that target these mRNAs (**Figures 4C–E**). Thus, from this data it appears that Esrrb and likely, other transcriptional regulators simultaneously control the expression of protein-coding genes as well as the miRNA-based machinery for post-transcriptional failsafe control or for fine-tuning protein levels. Through this mechanism cells presumably smoothly transit into early differentiation cell commitment.

ESCs exhibit a very unusual cell cycle structure, consisting mainly of an S phase and a short G1 phase, but lack of a G1/S checkpoint. In this study, downregulation of Esrrb elucidates a recurrent coherent motif type II (cFFL-type II) found at day 3 and day 5, formed by the mmu-mir-291a-3p and the target gene *Cdkn1a*. Previous studies lead by Blelloch and others have extensively characterize by luciferase reporter assays and qPCR the post-transcriptionally regulation of *Cdkn1a* by several members of the miR-290–295 cluster, in particular the mmu-mir-291a-3p, mmu-mir-291b-3p, mmu-mir-294 and mmu-mir-295 (Wang et al., 2008). Downregulation of mmu-mir-291a-3p abrogates the suppressing effect on *Cdkn1a,* an inhibitor of the cyclinE-Cdk2 complex. This mechanism slows down the cellular cell cycle for proper stem cell differentiation. Our data shows that, in this cell fate transition towards differentiation, the expression levels of this cell cycle inhibitor p21 (Cdkn1a) are post-transcriptionally regulated through an Esrrb-mmu-mir-291-3p-Cdkn1a coherent FFL type II motif acting as a failsafe control. Down-regulation of Esrrb reduces the expression of the mmu-mir-291a-3p which allows the expression of p21(Cdkn1a) (**Supplementary Figure S3**) (Wang et al., 2008).

In parallel, we have also observed several FFLs that could be involved in early stages of stem cell differentiation. One example is the FFL among Esrrb-mmu-mir-21 and Sprouty (Spry2), whose post-transcriptional regulation has been previously validated experimentally by luciferase reporter assays and western blot (Sayed et al., 2008; Mei et al., 2013). This Esrrb-mmu-mir-21-Spry2 FFL is present in our network as a coherent FFL type III (**Figure 4** and **Supplementary Figure S3**). Previous studies have reported about this post transcriptional regulation of Spry2 by the mmu-mir-21 in cardiac and mesenchymal stem cell differentiation (Sayed et al., 2008; Mei et al., 2013).

Similarly, we have observed two other FFLs under the mmu-mir-124 regulating the expression of Lacm1 and the Notch ligand Jag1. A significant decrease in the luciferase activity for Jag1 has been observed in the presence of the mmu-mir-124 (Cheng et al., 2009) as well as a reduction of Lacm1 expression levels in the presence of mmu-mir-124 (Conaco et al., 2006). Both genes are known to regulate proliferation and self-renewal of neuronal stem cells (NSCs) (Stump et al., 2002; Cao et al., 2007). This finding supports previous reports where Esrrb depletion evidenced loss of pluripotency and certain cellular commitment towards neuroectoderm (Ivanova et al., 2006; Festuccia et al., 2018).

Finally, given that FFLs are generally not topologically isolated within the transcriptional regulatory network, they may be susceptible to; cross-talks among them, the transient dynamics of other regulatory modules, network motifs, or expressed proteins (Rowland et al., 2017). In this regard, our analysis considers the FFL networks at different days, as crucial events that control cell fate decisions, are likely to occur as regulatory networks process biological information in real time. Indeed, specific decisions may, in fact, be "emergent"

properties of collective network dynamics. We hope that our novel systems biology approach and results will deeply influence future views and analyses of cell fate determination and more generally, the functions of biological regulatory networks.

CONCLUSION

In summary, we have confirmed that TFs and miRNAs can jointly regulate target gene expression in the form of FFLs to transit from the pluripotency state into the early differentiation stages and that these TF-miRNA-Target Gene motifs are important genetic overrepresented motif patterns that occur more often than by chance in biological networks. Hence, FFLs in coregulatory networks are crucial in providing new insights into the logic and evolution of a new regulatory layer of the complex eukaryotic genome.

DATA AVAILABILITY STATEMENT

The data presented in this study can be found in the online repository Gene Expression Omnibus (GEO) (Edgar et al., 2002; Barrett et al., 2011) under the accession numbers GSE57371, GSE189678 and the Esrrb ChiP-Seq data is under the accession numbers GSM785839 and GSM785840.

AUTHOR CONTRIBUTIONS

AM, HX, JR, and A-CR performed bioinformatic analyses. AV and SM-N performed experiments. IL prepared the manuscript. AS designed the project, performed experiments, and prepared the manuscript. All authors reviewed and approved the manuscript.

FUNDING

This research was funded by grants from the National Institutes of Health (NIH) to IL (5R01GM078465), the Empire State Stem Cell Fund through New York State Department of Health (NYSTEM) C024410 and C024176 (HESC-SRF) to IL. A-CR and SM-N recognize funding by the spanish ministry of sciences (PID 2020-117467RB-I0) and the regional government of Extremadura (IB20174). AS was funded through the project PGC2018-098626-B100) funded by the MCIN/AEI/10.13039/501100011033/ERDF "A way of making Europe" and the Merck Salud Foundation. AS is a recipient of a Ramón y Cajal contract (RYC-2016-19962) funded by the MCIN/AEI/10.13039/501100011033 and "ESF Investing in your Future".

ACKNOWLEDGMENTS

We thank A. Gordon from G. Hannon's laboratory for the pipeline analyses suggestions.

SUPPLEMENTARY MATERIAL

The Supplementary Material for this article can be found online at: https://www.frontiersin.org/articles/10.3389/fcell.2022.820255/full#supplementary-material

REFERENCES

Barrett, T., Troup, D. B., Wilhite, S. E., Ledoux, P., Evangelista, C., Kim, I. F., et al. (2011). NCBI GEO: Archive for Functional Genomics Data Sets--10 Years on. *Nucleic Acids Res.* 39, D1005–D1010. doi:10.1093/nar/gkq1184

Bartel, D. P. (2009). MicroRNAs: Target Recognition and Regulatory Functions. *Cell* 136, 215–233. doi:10.1016/j.cell.2009.01.002

Bo, C., Zhang, H., Cao, Y., Lu, X., Zhang, C., Li, S., et al. (2021). Construction of a TF-miRNA-Gene Feed-Forward Loop Network Predicts Biomarkers and Potential Drugs for Myasthenia Gravis. *Sci. Rep.* 11, 1–15. doi:10.1038/s41598-021-81962-6

Cao, X., Pfaff, S. L., and Gage, F. H. (2007). A Functional Study of miR-124 in the Developing Neural Tube. *Genes Dev.* 21, 531–536. doi:10.1101/GAD.1519207

Chakraborty, M., Hu, S., Visness, E., Del Giudice, M., De Martino, C., Sharp, P. A., et al. (2020). MicroRNAs Organize Intrinsic Variation into Stem Cell States. *Proc. Natl. Acad. Sci. U.S.A.* 117, 6942–6950. doi:10.1073/PNAS.1920695117/-/DCSUPPLEMENTAL

Chang, L., Zhou, G., Soufan, O., and Xia, J. (2020). miRNet 2.0: Network-Based Visual Analytics for miRNA Functional Analysis and Systems Biology. *Nucleic Acids Res.* 48, W244–W251. doi:10.1093/NAR/GKAA467

Chen, C., Ridzon, D. A., Broomer, A. J., Zhou, Z., Lee, D. H., Nguyen, J. T., et al. (2005). Real-time Quantification of microRNAs by Stem-Loop RT-PCR. *Nucleic Acids Res.* 33, e179. doi:10.1093/NAR/GNI178

Chen, X., Xu, H., Yuan, P., Fang, F., Huss, M., Vega, V. B., et al. (2008). Integration of External Signaling Pathways with the Core Transcriptional Network in Embryonic Stem Cells. *Cell* 133, 1106–1117. doi:10.1016/j.cell.2008.04.043

Cheng, L.-C., Pastrana, E., Tavazoie, M., and Doetsch, F. (2009). miR-124 Regulates Adult Neurogenesis in the Subventricular Zone Stem Cell Niche. *Nat. Neurosci.* 12, 399–408. doi:10.1038/NN.2294

Cirera-Salinas, D., Yu, J., Bodak, M., Ngondo, R. P., Herbert, K. M., and Ciaudo, C. (2017). Noncanonical Function of DGCR8 Controls mESC Exit from Pluripotency. *J. Cel Biol.* 216, 355–366. doi:10.1083/JCB.201606073

Conaco, C., Otto, S., Han, J.-J., and Mandel, G. (2006). Reciprocal Actions of REST and a microRNA Promote Neuronal Identity. *Proc. Natl. Acad. Sci. U.S.A.* 103, 2422–2427. doi:10.1073/PNAS.0511041103

Cora', D., Re, A., Caselle, M., and Bussolino, F. (2017). MicroRNA-mediated Regulatory Circuits: Outlook and Perspectives. *Phys. Biol.* 14, 045001. doi:10.1088/1478-3975/AA6F21

Cui, Y., Lyu, X., Ding, L., Ke, L., Yang, D., Pirouz, M., et al. (2021). Global miRNA Dosage Control of Embryonic Germ Layer Specification. *Nature* 593, 602–606. doi:10.1038/s41586-021-03524-0

Edgar, R., Domrachev, M., and Lash, A. E. (2002). Gene Expression Omnibus: NCBI Gene Expression and Hybridization Array Data Repository. *Nucleic Acids Res.* 30, 207–210. doi:10.1093/nar/30.1.207

Eduati, F., Di Camillo, B., Karbiener, M., Scheideler, M., Corà, D., Caselle, M., et al. (2012). Dynamic Modeling of miRNA-Mediated Feed-Forward Loops. *J. Comput. Biol.* 19, 188–199. doi:10.1089/CMB.2011.0274

Festuccia, N., Owens, N., and Navarro, P. (2018). Esrrb, an Estrogen-Related Receptor Involved in Early Development, Pluripotency, and Reprogramming. *FEBS Lett.* 592, 852–877. doi:10.1002/1873-3468.12826

Hanina, S. A., Mifsud, W., Down, T. A., Hayashi, K., O'Carroll, D., Lao, K., et al. (2010). Genome-Wide Identification of Targets and Function of Individual MicroRNAs in Mouse Embryonic Stem Cells. *PLOS Genet.* 6, e1001163. doi:10.1371/JOURNAL.PGEN.1001163

Hirashima, T., Iwasa, Y., and Morishita, Y. (2008). Distance between AER and ZPA Is Defined by Feed-Forward Loop and Is Stabilized by Their Feedback Loop in Vertebrate Limb Bud. *Bull. Math. Biol.* 70, 438–459. doi:10.1007/s11538-007-9263-4

Hsu, S.-D., Tseng, Y.-T., Shrestha, S., Lin, Y.-L., Khaleel, A., Chou, C.-H., et al. (2014). MiRTarBase Update 2014: An Information Resource for Experimentally Validated miRNA-Target Interactions. *Nucl. Acids Res.* 42, D78–D85. doi:10.1093/nar/gkt1266

Huang, D. W., Sherman, B. T., and Lempicki, R. A. (2008). Systematic and Integrative Analysis of Large Gene Lists Using DAVID Bioinformatics Resources. *Nat. Protoc.* 4, 44–57. doi:10.1038/NPROT.2008.211

Hutchins, A. P., Choo, S. H., Mistri, T. K., Rahmani, M., Woon, C. T., Keow Leng Ng, C., et al. (2013). Co-motif Discovery Identifies an Esrrb-Sox2-DNA Ternary Complex as a Mediator of Transcriptional Differences between Mouse Embryonic and Epiblast Stem Cells. *Stem Cells* 31, 269–281. doi:10.1002/stem.1279

Ivanova, N., Dobrin, R., Lu, R., Kotenko, I., Levorse, J., DeCoste, C., et al. (2006). Dissecting Self-Renewal in Stem Cells with RNA Interference. *Nature* 442, 533–538. doi:10.1038/nature04915

Kalir, S., Mangan, S., and Alon, U. (2005). A Coherent Feed-forward Loop with a SUM Input Function Prolongs Flagella Expression in *Escherichia coli*. *Mol. Syst. Biol.* 1. doi:10.1038/msb4100010

Kent, W. J., Sugnet, C. W., Furey, T. S., Roskin, K. M., Pringle, T. H., Zahler, A. M., et al. (2002). The Human Genome Browser at UCSC. *Genome Res.* 12, 996–1006. doi:10.1101/GR.229102

Kumar, R. M., Cahan, P., Shalek, A. K., Satija, R., Jay DaleyKeyser, A., Li, H., et al. (2014). Deconstructing Transcriptional Heterogeneity in Pluripotent Stem Cells. *Nature* 516, 56–61. doi:10.1038/nature13920

Lau, N. C., Lim, L. P., Weinstein, E. G., and Bartel, D. P. (2001). An Abundant Class of Tiny RNAs with Probable Regulatory Roles in *Caenorhabditis elegans*. *Science* 294, 858–862. doi:10.1126/science.1065062

Lee, D.-F., Su, J., Sevilla, A., Gingold, J., Schaniel, C., and Lemischka, I. R. (2012). Combining Competition Assays with Genetic Complementation Strategies to Dissect Mouse Embryonic Stem Cell Self-Renewal and Pluripotency. *Nat. Protoc.* 7, 729–748. doi:10.1038/nprot.2012.018

Leung, A. K. L., Young, A. G., Bhutkar, A., Zheng, G. X., Bosson, A. D., Nielsen, C. B., et al. (2011). Genome-wide Identification of Ago2 Binding Sites from Mouse Embryonic Stem Cells with and without Mature microRNAs. *Nat. Struct. Mol. Biol.* 18, 237–244. doi:10.1038/nsmb.1991

Li, C. J., Liau, E. S., Lee, Y. H., Huang, Y. Z., Liu, Z., Willems, A., et al. (2021). MicroRNA Governs Bistable Cell Differentiation and Lineage Segregation via a Noncanonical Feedback. *Mol. Syst. Biol.* 17, e9945. doi:10.15252/MSB.20209945

Li, N., Long, B., Han, W., Yuan, S., and Wang, K. (2017). MicroRNAs: Important Regulators of Stem Cells. *Stem Cel Res. Ther.* 8, 110–117. doi:10.1186/S13287-017-0551-0/TABLES/1

Lu, R., Markowetz, F., Unwin, R. D., Leek, J. T., Airoldi, E. M., MacArthur, B. D., et al. (2009). Systems-level Dynamic Analyses of Fate Change in Murine Embryonic Stem Cells. *Nature* 462, 358–362. doi:10.1038/NATURE08575

Macarthur, B. D., Sevilla, A., Lenz, M., Müller, F.-J., Schuldt, B. M., Schuppert, A. A., et al. (2012). Nanog-dependent Feedback Loops Regulate Murine Embryonic Stem Cell Heterogeneity. *Nat. Cel Biol.* 14, 1139–1147. doi:10.1038/ncb2603

MacNeil, L. T., and Walhout, A. J. M. (2011). Gene Regulatory Networks and the Role of Robustness and Stochasticity in the Control of Gene Expression. *Genome Res.* 21, 645–657. doi:10.1101/GR.097378.109

Marson, A., Levine, S. S., Cole, M. F., Frampton, G. M., Brambrink, T., Johnstone, S., et al. (2008). Connecting microRNA Genes to the Core Transcriptional Regulatory Circuitry of Embryonic Stem Cells. *Cell* 134, 521–533. doi:10.1016/J.CELL.2008.07.020

Martinez, N. J., and Walhout, A. J. M. (2009). The Interplay between Transcription Factors and microRNAs in Genome-Scale Regulatory Networks. *Bioessays* 31, 435–445. doi:10.1002/BIES.200800212

Mei, Y., Bian, C., Li, J., Du, Z., Zhou, H., Yang, Z., et al. (2013). miR-21 Modulates the ERK-MAPK Signaling Pathway by Regulating SPRY2 Expression during Human Mesenchymal Stem Cell Differentiation. *J. Cel. Biochem.* 114, 1374–1384. doi:10.1002/JCB.24479

Oliveros, J. C. (2007). Venny. An Interactive Tool for Comparing Lists with Venn's Diagrams. Available at: https://bioinfogp.cnb.csic.es/tools/venny/index.html.

Osella, M., Bosia, C., Corá, D., and Caselle, M. (2011). The Role of Incoherent microRNA-Mediated Feedforward Loops in Noise Buffering. *Plos Comput. Biol.* 7, e1001101. doi:10.1371/journal.pcbi.1001101

Qin, G., Mallik, S., Mitra, R., Li, A., Jia, P., Eischen, C. M., et al. (2020). MicroRNA and Transcription Factor Co-regulatory Networks and Subtype Classification of Seminoma and Non-seminoma in Testicular Germ Cell Tumors. *Sci. Rep.* 10, 1–14. doi:10.1038/s41598-020-57834-w

Rowland, M. A., Abdelzaher, A., Ghosh, P., and Mayo, M. L. (2017). Crosstalk and the Dynamical Modularity of Feed-Forward Loops in Transcriptional Regulatory Networks. *Biophysical J.* 112, 1539–1550. doi:10.1016/J.BPJ.2017.02.044

Rozen, S., and Skaletsky, H. (2000). Primer3 on the WWW for General Users and for Biologist Programmers. *Methods Mol. Biol.* 132, 365–386. doi:10.1385/1-59259-192-2:365

Sayed, D., Rane, S., Lypowy, J., He, M., Chen, I.-Y., Vashistha, H., et al. (2008). MicroRNA-21 Targets Sprouty2 and Promotes Cellular Outgrowths. *MBoC* 19, 3272–3282. doi:10.1091/MBC.E08-02-0159

Semi, K., and Takashima, Y. (2021). Pluripotent Stem Cells for the Study of Early Human Embryology. *Develop. Growth Differ.* 63, 104–115. doi:10.1111/DGD.12715

Sevilla, A., Papatsenko, D., Mazloom, A. R., Xu, H., Vasileva, A., Unwin, R. D., et al. (2021). An Esrrb and Nanog Cell Fate Regulatory Module Controlled by Feed Forward Loop Interactions. *Front. Cel Dev. Biol.* 9, 630067. doi:10.3389/fcell.2021.630067

Shao, M., Sun, Y., and Zhou, S. (2015). Identifying TF-MiRNA Regulatory Relationships Using Multiple Features. *PLoS One* 10, e0125156. doi:10.1371/JOURNAL.PONE.0125156

Shen-Orr, S. S., Milo, R., Mangan, S., and Alon, U. (2002). Network Motifs in the Transcriptional Regulation Network of *Escherichia coli*. *Nat. Genet.* 31, 64–68. doi:10.1038/ng881

Stump, G., Durrer, A., Klein, A.-L., Lütolf, S., Suter, U., and Taylor, V. (2002). Notch1 and its Ligands Delta-like and Jagged Are Expressed and Active in Distinct Cell Populations in the Postnatal Mouse Brain. *Mech. Develop.* 114, 153–159. doi:10.1016/S0925-4773(02)00043-6

van den Berg, D. L. C., Zhang, W., Yates, A., Engelen, E., Takacs, K., Bezstarosti, K., et al. (2008). Estrogen-Related Receptor Beta Interacts with Oct4 to Positively Regulate Nanog Gene Expression. *Mol. Cel. Biol.* 28, 5986–5995. doi:10.1128/mcb.00301-08

Wang, Y., Baskerville, S., Shenoy, A., Babiarz, J. E., Baehner, L., and Blelloch, R. (2008). Embryonic Stem Cell-specific microRNAs Regulate the G1-S Transition and Promote Rapid Proliferation. *Nat. Genet.* 40, 1478–1483. doi:10.1038/NG.250

Xiao, F., Zuo, Z., Cai, G., Kang, S., Gao, X., and Li, T. (2009). miRecords: An Integrated Resource for microRNA-Target Interactions. *Nucleic Acids Res.* 37, D105–D110. doi:10.1093/nar/gkn851

You, G., Zu, B., Wang, B., Fu, Q., and Li, F. (2020). Identification of miRNA-mRNA-TFs Regulatory Network and Crucial Pathways Involved in Tetralogy of Fallot. *Front. Genet.* 11, 552. doi:10.3389/FGENE.2020.00552

Yuan, K., Ai, W.-B., Wan, L.-Y., Tan, X., and Wu, J.-F. (2017). The miR-290-295 Cluster as Multi-Faceted Players in Mouse Embryonic Stem Cells. *Cell Biosci* 7, 38. doi:10.1186/S13578-017-0166-2

Zhang, H.-M., Kuang, S., Xiong, X., Gao, T., Liu, C., and Guo, A.-Y. (2013). Transcription Factor and microRNA Co-regulatory Loops: Important Regulatory Motifs in Biological Processes and Diseases. *Brief. Bioinform.* 16, 45–58. doi:10.1093/bib/bbt085

Zhang, H.-M., Kuang, S., Xiong, X., Gao, T., Liu, C., and Guo, A.-Y. (2015). Transcription Factor and microRNA Co-regulatory Loops: Important

Regulatory Motifs in Biological Processes and Diseases. *Brief. Bioinform.* 16, 45–58. doi:10.1093/BIB/BBT085

Conflict of Interest: The authors declare that the research was conducted in the absence of any commercial or financial relationships that could be construed as a potential conflict of interest.

Publisher's Note: All claims expressed in this article are solely those of the authors and do not necessarily represent those of their affiliated organizations, or those of the publisher, the editors and the reviewers. Any product that may be evaluated in this article, or claim that may be made by its manufacturer, is not guaranteed or endorsed by the publisher.

frontiers | Frontiers in Cell and Developmental Biology

ORIGINAL RESEARCH
published: 23 May 2022
doi: 10.3389/fcell.2022.883314

Xenotransplantation of Human Spermatogonia Into Various Mouse Recipient Models

Dongli Liang[1], Qi Sun[2], Zijue Zhu[3], Chuanyun Wang[2], Shicheng Ye[2], Zheng Li[3] and Yuan Wang[4]**

[1]Laboratory Animal Center, Instrumental Analysis Center, Shanghai Jiao Tong University, Shanghai, China, [2]Shanghai Key Laboratory of Regulatory Biology, Institute of Biomedical Sciences and School of Life Sciences, East China Normal University, Shanghai, China, [3]Department of Andrology, The Center for Men's Health, Urologic Medical Center, Shanghai Key Laboratory of Reproductive Medicine, Shanghai General Hospital, Shanghai Jiao Tong University School of Medicine, Shanghai, China, [4]Department of Animal Sciences, College of Agriculture and Natural Resources, Michigan State University, East Lansing, MI, United States

Spermatogonial stem cells are the foundation of continuous spermatogenesis in adult mammals. Xenograft models have been established to define human SSCs, mostly using infertile and immune-deficient mice as the recipients for human germ cell transplantation. However, it is time-consuming to prepare such recipients using irradiation or chemotherapeutic agents, and this approach may also introduce confounding factors when residual endogenous germ cells recover in transplanted recipients. It remains to be determined whether immune-competent genetically infertile mice can be suitable recipients for xenotransplantation. In this study, we observed similar engraftment efficiencies when using spermatogonia from human biopsied testes across immune-deficient nude mice, immune-competent ICR mice, and genetically infertile *Kit*$^{w/w\text{-}v}$ mice, suggesting minimal immunological rejection from immune-competent mouse recipients upon xenotransplantation of human germ cells. More importantly, we derived EpCAM negative and TNAP positive spermatogonia-like cells (SLCs) from human pluripotent stem cells (PSCs), which highly expressed spermatogonial markers including PLZF, INTERGRINα6, TKTL1, CD90, and DRMT3. We found that upon transplantation, these SLCs proliferated and colonized at the basal membrane of seminiferous tubules in testes of both immune-deficient nude mice and *Kit*$^{w/w\text{-}v}$ mice, though complete spermatogenesis would likely require supporting human signaling factors and microenvironment. Taken together, our study functionally defined the cell identity of PSC-derived SLCs, and supported xenotransplantation using genetically infertile recipients as a convenient model for functionally evaluating spermatogonia derived from different species.

Keywords: spermatogonial stem cells, transplantation, germ cells, immunecompetent mouse, human pluripotent stem cells

OPEN ACCESS

Edited by:
Valerie Kouskoff, The University of Manchester, United Kingdom

Reviewed by:
Morteza Koruji, Iran University of Medical Sciences, Iran
Hinako M. Takase, RIKEN Center for Biosystems Dynamics Research, Japan

****Correspondence:***
Yuan Wang
wangyu81@msu.edu
Zheng Li
lizhengboshi@sjtu.edu.cn

Specialty section:
This article was submitted to Stem Cell Research, a section of the journal Frontiers in Cell and Developmental Biology

Received: *24 February 2022*
Accepted: *20 April 2022*
Published: *23 May 2022*

Citation:
Liang D, Sun Q, Zhu Z, Wang C, Ye S, Li Z and Wang Y (2022) Xenotransplantation of Human Spermatogonia Into Various Mouse Recipient Models. Front. Cell Dev. Biol. 10:883314. doi: 10.3389/fcell.2022.883314

INTRODUCTION

Spermatogonial stem cells (SSCs) provide a pool of undifferentiated spermatogonia to support continual spermatogenesis in adult mammals and are essential for maintaining male fertility (Oatley and Brinster, 2012). Germ cell transplantation was developed in rodents almost 30 years ago and had since become a gold standard to define functional mouse SSCs (Brinster and Avarbock, 1994; Brinster and Zimmermann,

1994). Two types of recipients are widely used for mouse SSC transplantation. One is irradiation- or chemo-treated wildtype male mice, of which, busulfan is the most commonly used chemotherapeutic agent to ablate endogenous germ cells including SSCs from recipients (Russell and Brinster, 1996; Hermann et al., 2007; Morimoto et al., 2021). However, busulfan rarely eradicates all recipient SSCs, and endogenous spermatogenesis may recover over time and thus complicate precise quantitation of unmarked donor SSCs in recipient testes (Morimoto et al., 2021). The other recipient type is $Kit^{w/w\text{-}v}$ genetically infertile mice that contain mutations at the white-spotting (W) genomic locus encoding KIT protein (Nocka et al., 1989; Brinster and Zimmermann, 1994; Ohta et al., 2003). Because the tyrosine kinase receptor KIT plays a critical role in spermatogonial development (Yoshinaga et al., 1991; Rossi et al., 2000), $Kit^{w/w\text{-}v}$ mice with KIT mutations lack endogenous spermatogenesis (Ogawa et al., 2000), which allows accurate quantitation of donor SSCs. Both types of recipients provide a suitable microenvironment for donor mouse SSCs to go through complete spermatogenesis.

Autologous transplantation of human SSCs has been proposed as a strategy to rescue male infertility or restore spermatogenesis in patients after chemotherapy or irradiation treatment in the clinic. In some cases, SSCs collected from fresh testes have to be processed to remove malignant cells, while limited SSCs in cryopreserved testes may need to be expanded before transplantation back to patients (Sadri-Ardekani et al., 2009; Sadri-Ardekani et al., 2011; Koruji et al., 2012; Mirzapour et al., 2012; Jabari et al., 2020). SSC properties and functions could be altered during these procedures, making it necessary to define SSCs *in vivo* before using them for therapeutic applications. Because experimental manipulation involving human subjects is ethically limited, animal xenotransplantation provides a powerful approach to understand the properties of human SSCs. So far, xenotransplantation has been reported using donor germ cells from primates, humans, and many other species (Jiang and Short, 1995; Honaramooz et al., 2002; Nagano et al., 2002; Honaramooz et al., 2003; Hermann et al., 2007; Sadri-Ardekani et al., 2009; Sadri-Ardekani et al., 2011; Kubota and Brinster, 2018; Morimoto et al., 2021). Although human SSCs cannot differentiate and complete spermatogenesis in mouse testes, they do transiently colonize and proliferate at the basement membrane of mouse seminiferous tubules (Nagano et al., 2002; Sadri-Ardekani et al., 2009; Sadri-Ardekani et al., 2011). Notably, published studies mainly used busulfan-treated immunocompromised nude mice as xenotransplantation recipients (Nagano et al., 2002; Sadri-Ardekani et al., 2009; Sadri-Ardekani et al., 2011), though it is unclear whether immunodeficiency may enhance the survival of donor human SSCs in mouse testes. It remains to be determined whether immune-competent or genetically infertile mice (e.g., $Kit^{w/w\text{-}v}$) are suitable recipients for xenotransplantation.

In addition to using SSCs from testes to rescue male infertility, recent technical advances make it possible to derive germ cells from pluripotent stem cells (PSCs) for future therapy of male infertility. PSCs include embryonic stem cells (ESCs) that are derived from embryonic blastocysts (Evans and Kaufman, 1981; Martin, 1981; Thomson et al., 1998), and induced PSCs (iPSCs) from somatic cells (Takahashi and Yamanaka, 2006; Takahashi et al., 2007; Yu et al., 2007; Park et al., 2008). Differentiation protocols have been developed to direct human PSCs into primordial germ cells, spermatogonia-like cells (SLCs) and/or haploid spermatogenic cells (Kee et al., 2009; Easley et al., 2012; Irie et al., 2015; Sasaki et al., 2015; Zhao et al., 2018; Gell et al., 2020). These, coupled with breakthroughs of iPSC research in the last 2 decades, may eventually make it possible to derive autologous germ cells from patient iPSCs for replacement therapy. Yet it is still unknown whether these PSC-derived SLCs behave similarly in testes as *in vivo* developed spermatogonia. Additionally, in treating male infertility using replacement therapy, potential immune responses elicited by PSC-derived spermatogonia need to be considered. Although reports showed minimal immune rejection upon transplantation of syngeneic PSC-derived cells or tissues (Araki et al., 2013; Guha et al., 2013), the immunogenicity of these cells remains to be a highly debatable topic, and may vary by cell types (de Almeida et al., 2013; Liu et al., 2017). Therefore, it is necessary to examine the survival and tolerance of PSC-derived spermatogonia by the host *in vivo*.

In this study, we assessed the engraftment of human spermatogonia derived from different sources in immune-competent and immunocompromised mouse recipients. In addition, by using the xenotransplantation models, we examined the cell identity of EpCAM-/TNAP+ SLCs differentiated from human PSCs. We further demonstrated that xenotransplantation with $Kit^{w/w\text{-}v}$ genetically infertile mice as recipients provided a convenient model to functionally evaluate human spermatogonial property *in vivo*.

MATERIALS AND METHODS

Overall experimental design was shown below. Briefly, we used two types of human spermatogonia for xenotransplantation, one from biopsied human testes, the other from SLCs collected from differentiated PSCs. Three types of recipients were used, including immune-deficient nude mice, immune-competent ICR mice, and genetically infertile $Kit^{w/w\text{-}v}$ mice, as listed on the right of the graph.

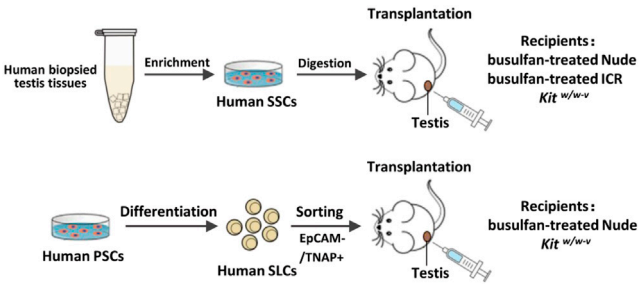

Collection of Male Germ Cells From Human Testicular Tissues

Testicular specimens were biopsied from obstructive azoospermia (OA) patients and immediately placed aseptically into Dulbecco's modified Eagle's medium (DMEM, Gibco) containing 1,000 U/ml penicillin and streptomycin (PS, Gibco) for further processing. The diagnosis of OA patients was

confirmed by pathological examination. This study was approved by the Institutional Ethical Review Committee of Shanghai First People's Hospital (license number 2016KY196), Shanghai Jiao Tong University School of Medicine. All participants had provided written consents. In total, eight testis samples were collected from OA patients from age 25 to 40. Collected testis tissues were cut into small pieces and placed in the cryopreservation medium consisting of DMEM, 20% fetal bovine serum (FBS, Hyclone), 10% dimethyl sulfoxide (DMSO, Sigma-Aldrich), and stored in liquid nitrogen. For experiments, the testis tissues were rapidly thawed at 37°C and washed in DMEM. Recovered testicular samples were processed with a two-step enzymatic digestion, as described previously (Hermann et al., 2007; Hermann et al., 2009). Briefly, testicular tissues were first digested with collagenase type IV, followed by digestion with 0.25% trypsin, 0.38 g/L of EDTA, and 1.4 mg/ml DNase I for 5 min. The digestion was stopped by adding DMEM with 10% FBS, and dissociated single cells were collected by centrifugation. Cell suspensions were seeded into gelatin-coated culture plates in DMEM/F-12 (Gibco) supplemented with 10% FBS for 24–36 h, according to a procedure previously described (Wu et al., 2009). More than 95% of somatic cells (including Sertoli cells, Leydig cells, and peritubular cells) were attached to culture plates, while non-adherent germ cells were collected by centrifuge. The germ cells were then seeded into laminin-coated culture plates in DMEM/F12 containing 1x PS, 6 mM L-Glutamine (Gibco), 100 μM β-mercaptoethanol (Sigma-Aldrich), 1xB27 (Gibco), 20 ng/ml human GDNF (Sino Biological), and 20 ng/ml human basic fibroblast growth factor (b-FGF, Sino Biological) for 2 days at 34°C in a humidified 5% CO_2 incubator. These freshly isolated laminin-binding cells were enriched with SSCs and spermatogonia. In total, ~5×10^5 human SSCs and spermatogonia were obtained from 8 cryopreserved biopsied samples. After 2-days culture, about 30,000 human germ cells per testis were injected for xenotransplantation.

Animal Experiments and Xenotransplantation

Male nude mice (BALB/c-*nu/nu*) and ICR mice at 6 weeks were injected intraperitoneally with 40 mg/kg busulfan (Sigma-Aldrich) and were subsequently used as recipients 6 weeks later. Male $Kit^{w/w\text{-}v}$ mice at 12-week old were used as recipients. All animals used for this study were housed at an SPF-graded facility with healthy conditions. Germ cells to be transplanted were suspended in ~10 μl PBS with 10% trypan blue (v:v; Invitrogen) and injected into the seminiferous tubules of recipient testes *via* the efferent ducts. The contralateral testis in the same mouse with mock injection with PBS and trypan blue was used as a control. PBS was used to minimize any potential effects of proteins, nutrients, or small molecules in the culture media on germ cell proliferation and development. Six weeks after transplantation, animals were euthanized, and their testes were removed for further analyses. All animal experimental procedures were conducted in accordance with the local Animal Welfare Act and Public Health Service Policy with approval from the Committee of Animal Experimental Ethics at East China Normal University (Ref #:M20170325).

Histology, Immunohistofluorescence and Immunofluorescence Assays

Histology and IHF were performed as previously described (Zhao et al., 2018). Briefly, mouse testis samples were fixed with 4% PFA solution, paraffin-embedded, and sectioned with 4 μm thickness. Following the antigen retrieval by citrate (pH6.0, boiling for 15–20 min and cooling down for 30 min), testis sections were blocked with 1% goat serum (Abcam, ab7481) in PBS at 4°C for 12–16 h, stained with primary antibodies at 4°C for 12–16 h, washed three times (15–30 min each time) with PBS at room temperature, and then stained with goat anti-rabbit IgG AlexaFluor 568 (Invitrogen) and goat anti-mouse IgG AlexaFluor 488 (Invitrogen) at 4°C for 12–16 h, and washed three times (15–30 min each time) in dark with PBS at room temperature. Primary antibodies used in this study: mouse anti-DDX4 (Abcam, ab27591), rabbit anti-DDX4 (Abcam, ab13840), rabbit anti-NuMA (Novus Biologicals, NB100-74636), rabbit anti-GFRα1 (Abcam, ab8026), mouse anti-PCNA (Abcam, ab29), and mouse anti-PLZF (Santa Cruz, sc-28319). The fluorescein-conjugated secondary antibodies were used at 1:300 dilution. Images were obtained with a Leica confocal microscope.

For IF, cells cultured on gelatin-coated coverslips were washed twice with 1× PBS and fixed in 4% PFA for 20 min at room temperature. Alternatively, cells were dissociated by Trypsin (Gibco), placed onto slides by cytospin preparation and fixed in 4% PFA for 20 min at room temperature. IF was performed as previously described (Zhao et al., 2018). Briefly, after treatment with 0.2% Triton-100 for 15 min, fixed cells were stained with primary antibodies at 4°C for 12–16 h, washed three times with PBS (10 min every time), and then stained with goat anti-rabbit IgG AlexaFluor 568 (Invitrogen) at 1:300 dilution at 4°C for 12–16 h, and washed three times (10 min each time) in the dark with PBS at room temperature. Primary antibodies used in this study: DDX4 (Abcam, ab13840), GPR125 (GeneTex, GTX51219), and PLZF (R&D, MAB2944). Images were obtained with a Leica fluorescent microscope.

Human PSC Culture and Differentiation

All PSC culture and differentiation were performed as previously described (Zhao et al., 2018). Briefly, human embryonic stem cell line H1 (WiCell) was maintained in chemically defined Essential 8 medium (Stem Cell Technologies). Cells were passaged every 5–7 days and dissociated by 1 mg/ml Collagenase IV (Millipore). ESCs were induced when reaching 80–90% confluence in differentiation medium [α-MEM (Gibco) containing 2 mM L-glutamine (Gibco), 1× Insulin-Transferrin-Selenium-X (Gibco), 0.2% KnockOut SR XenoFree CTS (Gibco), 1 ng/ml human b-FGF, 20 ng/ml human GDNF (Sino Biological), 0.2% chemically defined lipid concentrate, and 200 μg/ml vitamin C (Sigma)] (Zhao et al., 2018). Medium was changed every day. No

passage of cells was performed during differentiation. By day 12, most cells were PLZF+ SLCs. SLCs were collected for analyses or sorted for transplantation on day 12 of ESC differentiation.

Flow Cytometry Analysis

Mouse peripheral blood samples were obtained *via* tail tip into anticoagulant EDTA-containing tubes. After being treated with red blood cell lysis buffer (Beyotime Biotechnology), blood cells were pelleted at 1,200 rpm for 15 min and re-suspended in DMEM with 10% FBS, followed by incubation with PE-CD3 (Cat. #: 561824), PE-Cy7-CD8 (Cat. #: 561097), FITC-CD4 (Cat. #: 561828) or FITC-CD19 (Cat. #: 561740) antibodies from BD Pharmingen. Subsequently, cells were washed with DMEM and analyzed with a BD Fortessa analyzer (BD Biosciences).

Cells at day 12 of PSC differentiation were prepared for flow cytometry analyses as described previously (Zhao et al., 2018). Briefly, cells were dissociated by TrypLE (Gibco), fixed by 4% PFA for 20 min at room temperature, suspended in FACS buffer (PBS with 5% fetal calf serum, 0.2% Triton-100, and 0.5% Tween 20), and centrifuged at 500×g for 5 min before incubation with antibodies. Antibodies used for examining PSC-derived SLCs: EpCAM (Biolegend, 324203), TNAP (Biolegend, 327305), TRA-1-81 (Santa Cruz, Sc-21706), INTEGRINα6 (Biolegend, 313615) and PLZF (R&D, MAB2944). Subsequently, cells were washed with DMEM and analyzed with a BD Fortessa analyzer (BD Biosciences).

To collect SLCs from *in vitro* differentiated PSCs by flow cytometry, dissociated cells were stained at 4°C for 45–60 min in DMEM containing antibodies and then sorted by a FACS Aria II (BD Biosciences). Antibodies used for SLC sorting: EpCAM (Biolegend, 324203), TNAP (Biolegend, 327305) and CD90 (Abcam, ab133350).

RT-PCR and Quantitative Real-Time PCR

Total RNAs were extracted with Trizol (Thermo Fisher Scientific) and cDNAs were synthesized using a PrimeScript® RT reagent Kit (TaKaRa) following manufacturer's protocols, as previously described (Zhang et al., 2016). *Gapdh* was used as the house-keeping gene to normalize various sorted cell populations. The primer sequences used in this assay are provided in **Supplementary Table S1**.

Statistical Analysis

Data were presented as mean ± standard error (SEM). Unpaired Student's t-test was conducted to examine between-group differences using GraphPad Prism. All experiments were performed independently for more than three times unless otherwise stated. *: $p < 0.05$; **: $p < 0.01$.

RESULTS

Characterize Human Spermatogonia From Obstructive Azoospermia Patients

To obtain *in vivo* developed human spermatogonia, human testicular samples were biopsied from obstructive azoospermia (OA) patients, and the existence of undifferentiated spermatogonia in these samples was confirmed by immunohistofluorescence (IHF) with an antibody against a SSC marker GFRα1 (**Figure 1A**). Biopsied testis tissues were processed with two-step enzymatic digestion as described previously (Hermann et al., 2007; Hermann et al., 2009). Non-adherent germ cells were separated from somatic supporting cells (e.g., Sertoli cells) that were attached on gelatin-coated plates. These germ cells were further seeded onto laminin-coated dishes (**Figure 1B**) and cultured for 2 days to enrich for spermatogonia before immunofluorescence (IF) assay and transplantation. More than 95% (based on 10 fields of view) of the enriched cell population was stained with an antibody against a germ cell-specific protein, DDX4, supporting their germ cell identity (**Figure 1C**). In addition, these cells contain ~80% undifferentiated spermatogonia (based on 10 fields of view), as labeled by the high expression of SSC markers, GPR125 (**Figure 1D**) and PLZF (**Figure 1E**) (Costoya et al., 2004; Seandel et al., 2007; He et al., 2012). In total, human germ cells were collected from eight OA patients.

Characterize Infertile Mouse Models for Xenotransplantation of Human Germ Cells

To explore whether the immune deficiency enhances the engraftment of human spermatogonia, three mouse strains, including nude mice, ICR, and $Kit^{w/w\text{-}v}$ male mice, were used as xenotransplantation recipients. Busulfan-treated nude mice (**Supplementary Figure S1A**) and ICR mice (**Supplementary Figure S1B**) represent immunocompromised and immune-competent recipients, respectively. The ablation effects of endogenous germ cells in these mice by busulfan were confirmed by histology at week 6 post-treatment (**Supplementary Figure S1A, B**). Preparation of infertile mouse recipients using busulfan is time-consuming and may potentially introduce confounding factors when residual endogenous germ cells are left or recovered in recipients. Therefore, $Kit^{w/w\text{-}v}$ genetically infertile mice, which lack endogenous spermatogenesis (Nocka et al., 1990; Reis et al., 2000), were also tested as potential xenotransplantation recipients. Although KIT plays a crucial role in lymphocyte development (Rodewald et al., 1997; Waskow et al., 2002), we observed comparable percentages of $CD3^+$ T cells (**Figure 2A**), $CD8^+$ T cells (**Figure 2B**), and $CD4^+$ T cells (**Figure 2C**), with moderately decreased $CD19^+$ B cells (**Figure 2D**) in $Kit^{w/w\text{-}v}$ mice with those in C57BL/6J wildtype mice (**Supplementary Figure S1C**), suggesting that $Kit^{w/w\text{-}v}$ mice contain intact adaptive immunity.

Human Germ Cells From OA Patients Readily Colonize Both Immune-Competent and Immune-Deficient Infertile Mouse Recipients

About 30,000 human germ cells from OA patients were injected per testis for xenotransplantation. The contralateral testis in the same mouse with mock injection was used as a control. In total, we injected 5 nude mice and 5 ICR mice, both busulfan-treated, as well as 6 $Kit^{w/w\text{-}v}$ mice. Six weeks after transplantation, recipient testes were dissected for histology and IHF. We found germ cells in about 3% seminiferous tubules in ~60% of recipient mice (3 for nude and ICR mice, and 4 for $Kit^{w/w\text{-}v}$ mice) with human spermatogonial injection, and some of them were colonized at the basal membranes (**Supplementary Figure S2**). By contrast,

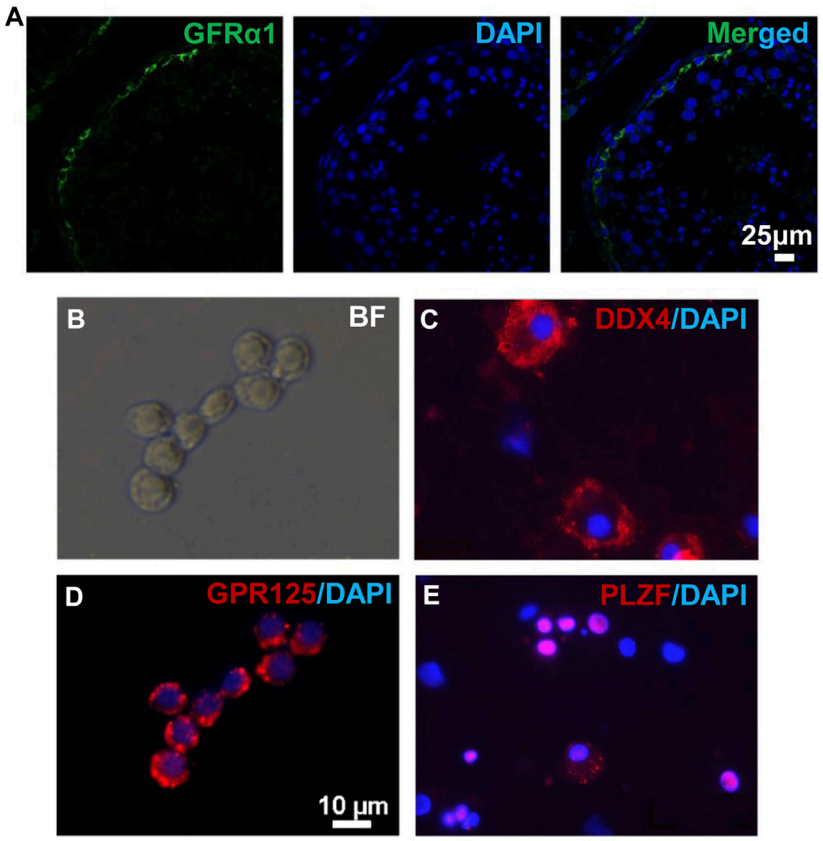

FIGURE 1 | Human germ cells were collected from biopsied testes. **(A)** IHF was performed on biopsied testes from OA patients with a GFRα1 antibody. **(B–E)** Isolated human spermatogonia were observed in bright field **(B)**, and detected by IF with antibodies against DDX4 **(C)**, GPR125 **(D)**, and PLZF **(E)**, counterstained with DAPI. Scale bar: 10 μm **(B,D)** cells were cultured on a cover glass. **(C,E)** cells were spun onto slides by cytospin preparation.

no germ cells were detected in the contralateral testes with mock injection (**Supplementary Figure S2**).

It has reported that endogenous spermatogenesis may recover from busulfan treatment (Morimoto et al., 2021), and occasionally, residue spermatogonia may also exist in *Kit*$^{w/w\text{-}v}$ testes (Kubota et al., 2009). To assess the origin of germ cells in these transplanted mice, NuMA (Merdes and Cleveland, 1998; Taimen et al., 2004), an antibody against human cells, was used. We confirmed that NuMA could specifically detect human but not mouse cells by Western blotting, IHF, and IF (**Supplementary Figure S3**). We performed IHF with this NuMA antibody and an antibody against DDX4, a germ cell-specific protein (Tanaka et al., 2000; Castrillon et al., 2000). No DDX4+/NuMA+ cells were detected in control testes from busulfan-treated nude mice. By contrast, multiple DDX4+/NuMA+ cells were clearly observed at the basal membrane of the contralateral testes from the same mice with transplantation of human germ cells (**Figure 3A**, **Supplementary Figure S4A**). Similar results were observed in both busulfan-treated ICR mice (**Figure 3B**, **Supplementary Figure S4B**) and *Kit*$^{w/w\text{-}v}$ mice (**Figure 3C**, **Supplementary Figure S4C**). Because only undifferentiated spermatogonia would survive long-term in mouse testes, these DDX4+/NuMA+ germ cells were likely human spermatogonia. Indeed, all DDX4+ cells also highly expressed the SSC marker, PLZF (Costoya et al., 2004) (**Figure 3D**). We did not observe significant difference in the number of colonized spermatogonia across these three types of recipients, suggesting that successful engraftments can be achieved with germ cells developed *in vivo* from human testes using both immune-competent and immune-compromised recipients.

Derivation of SLCs From Human PSCs

In a previous study, we robustly derived SLCs from human PSCs (Zhao et al., 2018). These SLCs highly express human spermatogonia-specific genes, including PLZF, CD90, GPR125, DRMT1, and DMRT3 (Zhao et al., 2018). We thus further investigated whether these *in vitro* PSC-derived SLCs behave similarly to *in vivo* developed spermatogonia from human testes. However, upon injection into testes of busulfan-treated nude mice with whole PSC differentiated population, residual undifferentiated PSCs often formed teratoma (data not shown). To exclude contaminating PSCs in transplanted populations, we need to identify appropriate surface antigens to collect SLCs with flow cytometry.

In our SLCs derived from PSCs, PLZF is the most prominently expressed spermatogonial protein (Zhao et al., 2018). Because PLZF is a transcription factor and located in the nucleus, it cannot be used for live-cell sorting. However, we could use PLZF as a marker for spermatogonia to identify surface antigens that are

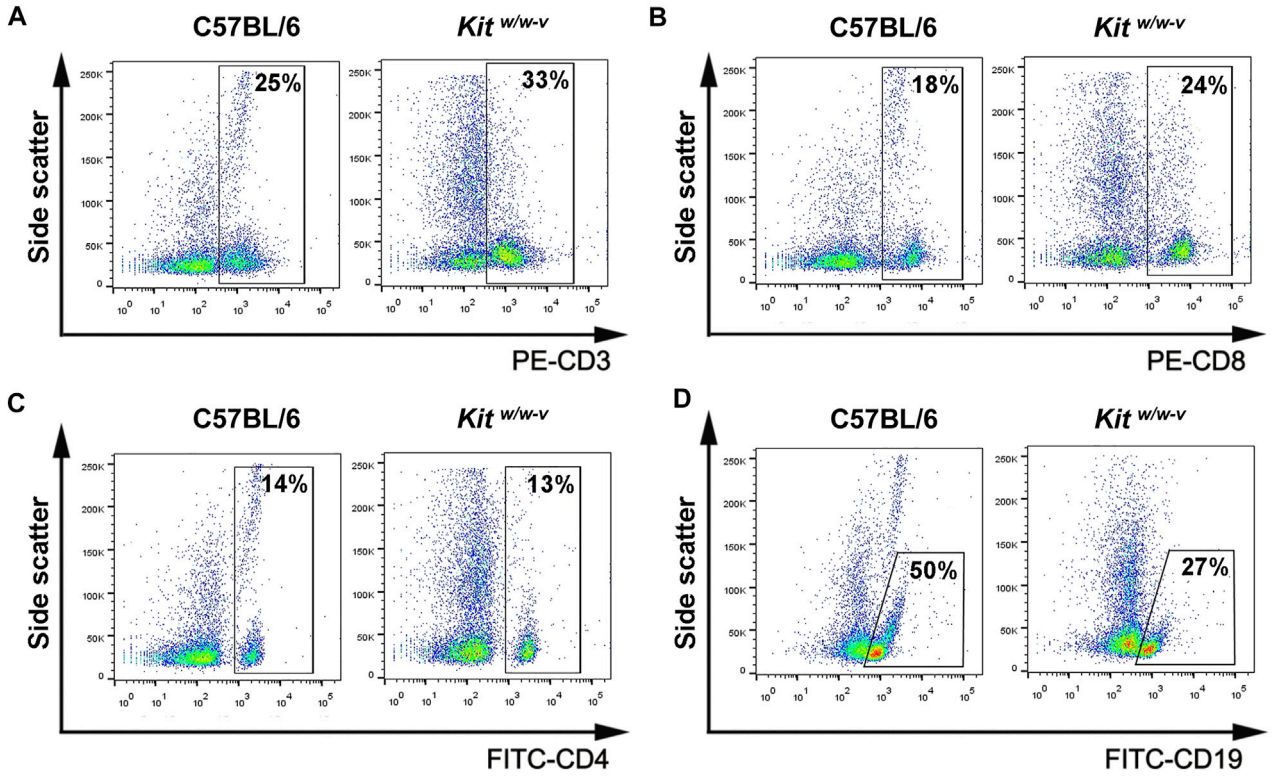

FIGURE 2 | *Kit*$^{w/w-v}$ mice displayed similar peripheral lymphocyte composition, compared to C57BL/6J immune-competent wildtype mice. **(A–D)** The percentages of CD3$^+$, CD8$^+$, and CD4$^+$ T lymphocytes, as well as CD19$^+$ B lymphocytes from peripheral blood from *Kit*$^{w/w-v}$ and C57BL/6 mice were determined with flow cytometry.

enriched in SLCs but not in PSCs with flow cytometry on fixed cells. Because TNAP (tissue non-specific alkaline phosphatase) and EpCAM were reported to be highly expressed in primordial germ cells and pro-spermatogonia (Sasaki et al., 2015), we analyzed their co-existence with PLZF in SLCs differentiated from a human ESC line, H1 (**Supplementary Figure S5**). We found that the majority (92.9%) of PLZF+ SLCs were stained as EpCAM negative (-) and TNAP positive (+) (**Figure 4A**). In addition, 97.4% of EpCAM-/TNAP+ cell population from differentiated PSCs were positive for PLZF (**Figure 4B**) and INTEGRINα6 (**Figure 4C**), a common spermatogonial marker in mouse, monkey and human (Shinohara et al., 1999; Maki et al., 2009; He et al., 2010). Further, TRA-1-81 is a marker for undifferentiated PSCs. We found that 86.2% of TRA-1-81 positive cells were co-stained with EpCAM+/TNAP+ population, while 92.9% of TRA-1-81 negative cells, which lost pluripotency, were EpCAM-/TNAP+ (**Figure 4D**). These data suggest that we may use EpCAM-/TNAP+ to enrich SLCs and to exclude TRA-1-81 + undifferentiated PSCs (**Figure 4E**).

We further evaluated the gene expression of cell populations separated by differential EpCAM and TNAP expressions (**Figure 4F**) with real-time RT-PCR assays. Because CD90 was reported to be spermatogonial marker in mice, primates and humans (Kubota et al., 2003; Maki et al., 2009; He et al., 2010), we also analyzed the cells sorted by EpCAM and CD90 staining (**Figure 4G**). We confirmed that the transcript level of *EpCAM* was dramatically lower while *TNAP* or *CD90* was significantly upregulated in both EpCAM-/TNAP+ and EpCAM-/CD90+ populations, compared to those from the whole differentiated PSC populations (**Figures 4H,I**), supporting reliable sorting results. We also observed that the expression of *TKTL1*, *PLZF*, and *DMRT3*, markers specific for spermatogonia, were significantly elevated in both EpCAM-/TNAP+ and EpCAM-/CD90+ SLCs, with a relatively higher PLZF transcript level in EpCAM-/TNAP+ population (**Figures 4H,I**). These data support the usage of EpCAM-/TNAP+ population to represent PLZF+ SLCs derived from PSCs.

Human PSC-Derived SLCs Colonize Both Immune-Deficient Nude Mice and Genetically Infertile Mouse Recipients

We next injected ~100,000 EpCAM-/TNAP+ SLCs per testis into seminiferous tubules of *Kit*$^{w/w-v}$ mice and busulfan-treated nude mice. The contralateral testis from the same mouse was injected with PBS as a control. No teratoma were found in any of 6 *Kit*$^{w/w-v}$ mice and 4 busulfan-treated nude mice we transplanted, indicating that these SLCs lost pluripotency during PSC differentiation. We found no DDX4+/NuMA+ human germ cells in the control testes of transplanted recipients by IHF. By contrast, in 2 nude mice and all 6 *Kit*$^{w/w-v}$ recipients, DDX4+/NuMA+ germ cells were clearly observed at the basement membrane of the other testis from the same mouse 6 weeks post-injection of EpCAM-/TNAP+ SLCs

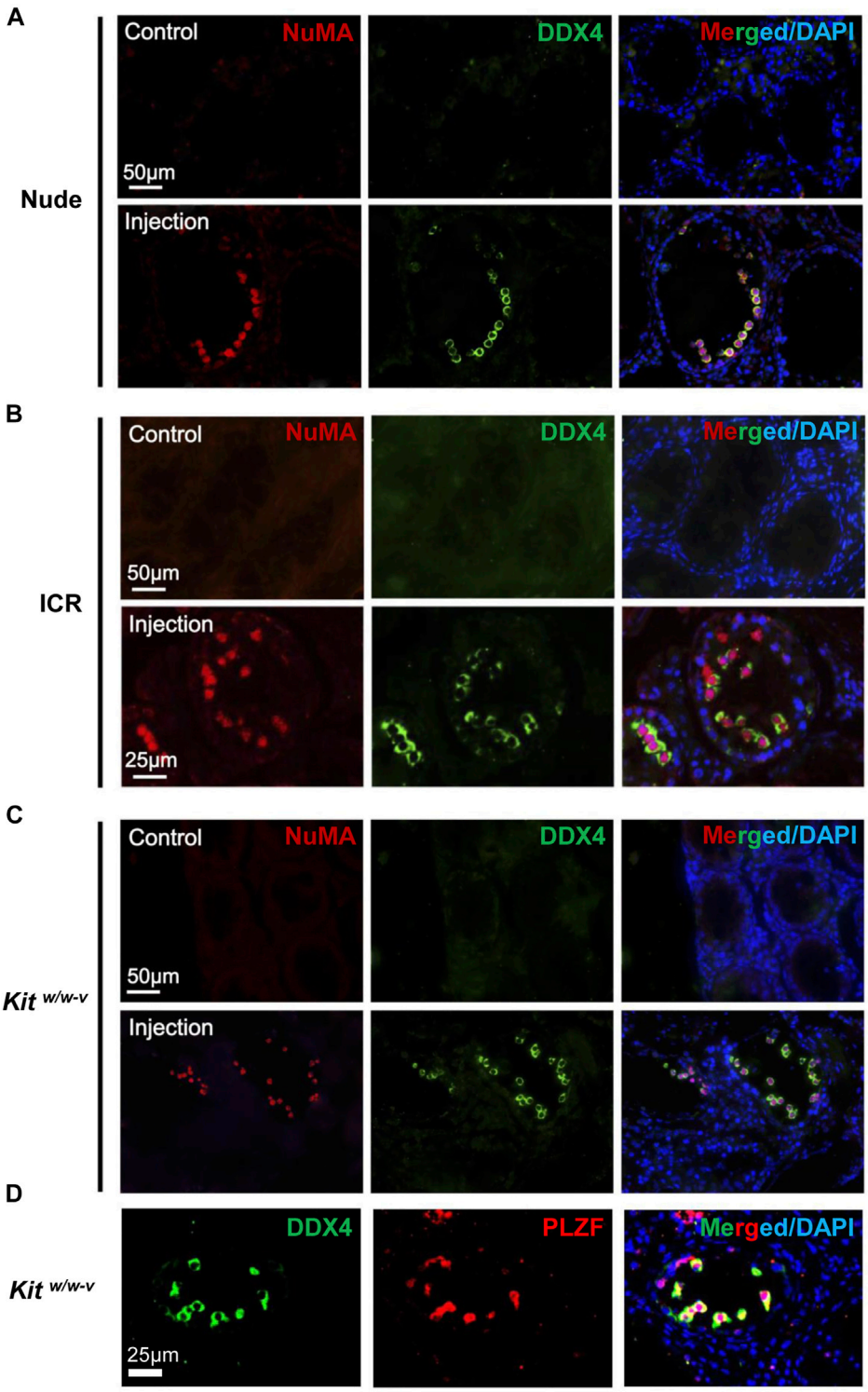

FIGURE 3 | *In vivo* developed human spermatogonia engrafted into testes from both immune-deficient and immune-competent mice. **(A–C)** IHF assays were performed on nude, ICR, and $Kit^{w/w-v}$ testes at 6 weeks post transplantation, with NuMA and DDX4 antibodies, co-stained with DAPI. **(D)** IHF assays were conducted on injected $Kit^{w/w-v}$ testes with antibodies against PLZF and DDX4, counterstained with DAPI. Nude and ICR mice at age 6 weeks were injected intraperitoneally with 40 mg/kg busulfan and were subsequently used as recipients after 6 weeks. $Kit^{w/w-v}$ mice at 12-week old were used as recipients. About 30,000 human germ cells from OA patients were injected per testis for xenotransplantation. The contralateral testis in the same mouse with mock PBS injection was used as a control. In total, 5 nude mice, 5 ICR mice, and 6 $Kit^{w/w-v}$ mice were injected.

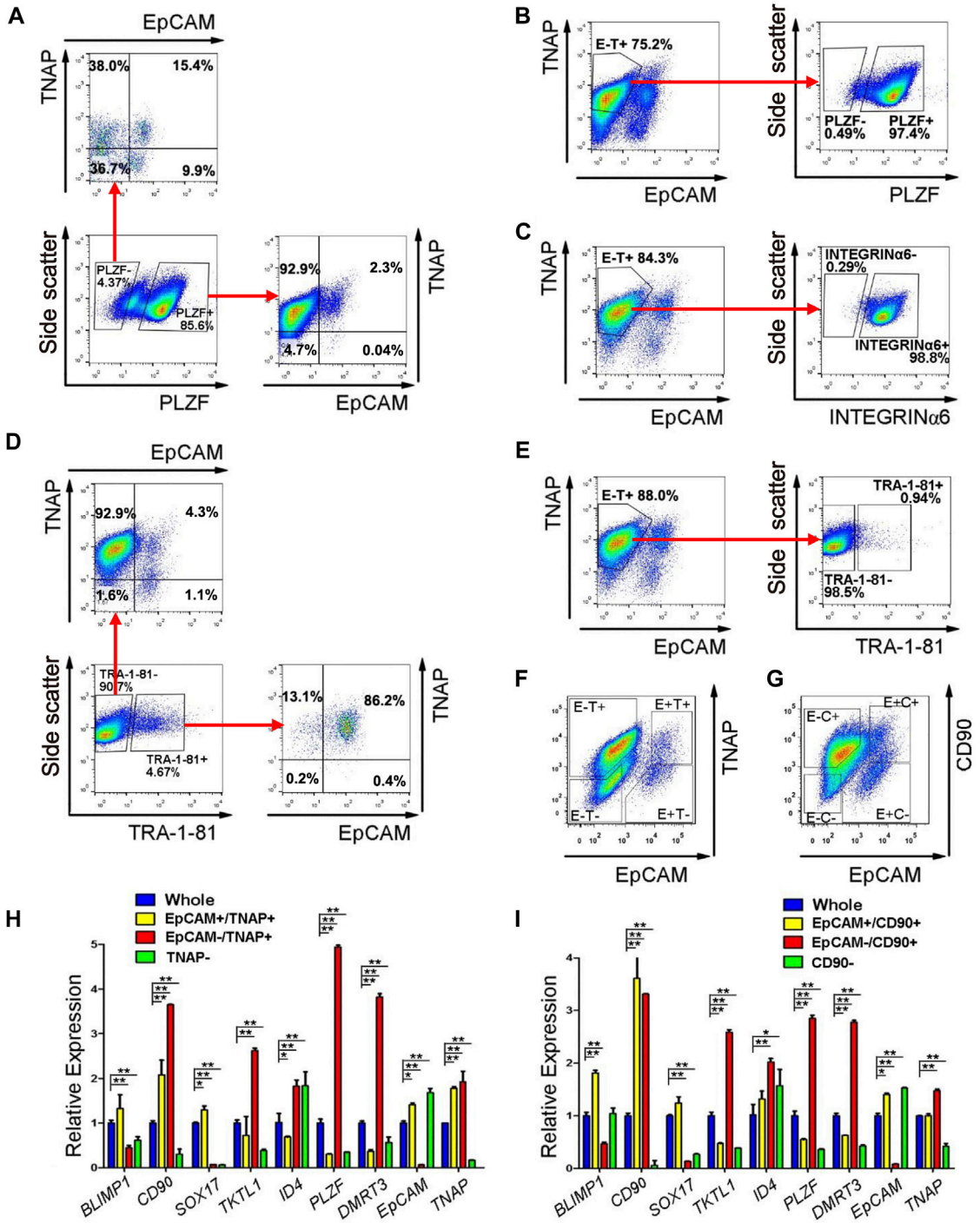

FIGURE 4 | EpCAM-/TNAP+ population is enriched with SLCs differentiated from human PSCs. **(A)** Flow cytometry analyses of EpCAM and TNAP expression in PLZF positive and negative populations from PSCs. **(B,C,E)** Percentage of PLZF **(B)**, INTEGRINα6 **(C)**, and TRA-1-81 **(E)** in EpCAM-/TNAP+ population differentiated from human PSCs, analyzed by flow cytometry. **(D)** Flow cytometry analyses of EpCAM and TNAP expression in TRA-1-81 positive and negative populations from PSCs. **(F–G)** Fluorescence-activated cell sorting was conducted, using EpCAM and TNAP combination **(F)**, or with EpCAM and CD90 antibodies **(G)**. E, EpCAM; T: TNAP; C: CD90 **(H–I)** Real-time RT-PCR analyses of germ cell-specific genes on populations sorted with EpCAM and TNAP **(H)** or with EpCAM and CD90 staining **(I)**. Data represent as the mean ± SEM (n ≥ 3). *: $p < 0.05$; **: $p < 0.01$. Negative gating controls were shown in **Supplementary Figure S5**.

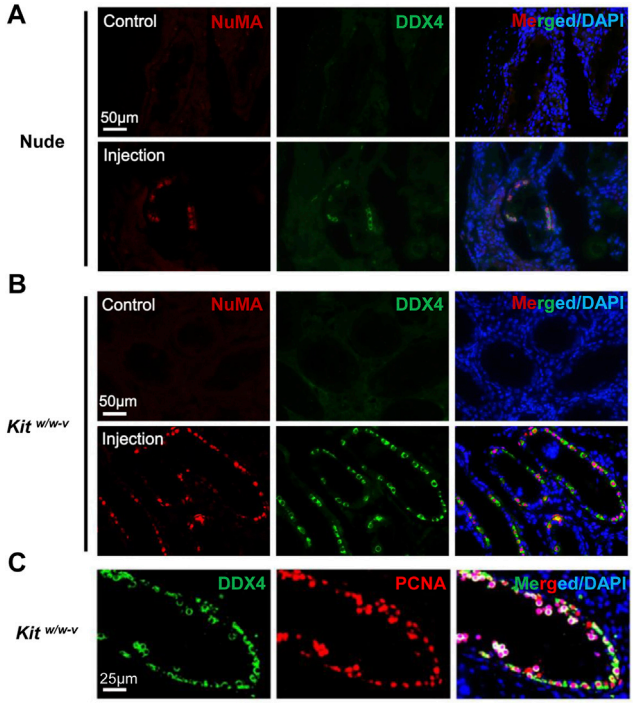

FIGURE 5 | Human SLCs from PSCs readily colonize both nude and *Kit*$^{w/w-v}$ mouse testes. **(A,B)** IHF assays were performed 6 weeks post-transplantation on testes from nude mice and *Kit*$^{w/w-v}$ recipients with antibodies against NuMA and DDX4, counterstained with DAPI. **(C)** IHF assays on testes from *Kit*$^{w/w-v}$ mice with antibodies against PCNA and DDX4, counterstained with DAPI. Nude mice at age 6 weeks were injected intraperitoneally with 40 mg/kg busulfan and were subsequently used as recipients after 6 weeks. Male *Kit*$^{w/w-v}$ mice at 12-week old were used as recipients. About ~100,000 EpCAM-/TNAP+ SLCs were injected per testis for xenotransplantation. The contralateral testis in the same mouse with mock PBS injection was used as a control. In total, 4 nude mice and 6 *Kit*$^{w/w-v}$ mice were injected.

(**Figure 5A**). Interestingly, compared to engrafted nude mice (with ~4% of seminiferous tubules containing human germ cells), much more DDX4+/NuMA+ cells were detected in *Kit*$^{w/w-v}$ testes with ~20% human germ cell-containing seminiferous tubules (**Figure 5B**, **Supplementary Figure S6, 7**), suggesting that *Kit*$^{w/w-v}$ mice provided a suitable microenvironment for the survival of human PSC-derived spermatogonia. In addition, these DDX4+ germ cells in *Kit*$^{w/w-v}$ testes displayed high expression levels of the proliferation marker, proliferating cell nuclear antigen (PCNA) (**Figure 5C**), suggesting that these human SLCs could go through mitotic division in mouse testes. Taken together, our data provide evidence that SLCs derived from human PSCs are indeed undifferentiated spermatogonia, and they maintain their potential to proliferate and repopulate mouse testes upon xenotransplantation.

DISCUSSION

Previous studies mainly used immune-deficient mouse recipients for human spermatogonial xenotransplantation (Nagano et al., 2002; Sadri-Ardekani et al., 2009; Sadri-Ardekani et al., 2011). However, endogenous spermatogenesis that is ablated by irradiation or chemotherapeutic agents may recover over time in these mice, making it difficult in quantifying transplanted germ cells. It remains to be determined whether immune-competent mice or *Kit*$^{w/w-v}$ genetically infertile mice are suitable recipients for xenotransplantation studies. Here, we systematically evaluated engraftments of human spermatogonia in immunocompromised nude mice, immune-competent ICR mice, and *Kit*$^{w/w-v}$ mice. We found that human spermatogonia settled at the basement membrane in seminiferous tubules of all three types of recipients. In addition, the survival and engraftment efficiency of PSC-derived SLCs were much better in *Kit*$^{w/w-v}$ recipients than those in busulfan-treated nude mice. Our data thus support *Kit*$^{w/w-v}$ mice as ideal recipients to assess spermatogonial properties in xenotransplantation.

Notably, nude mice are immunocompromised, lack T cells, and have reduced NK cell activities (Groscurth and Kistler, 1975; Schedi et al., 1975). By contrast, we did not find significant defects in peripheral T and B lymphocyte composition in *Kit*$^{w/w-v}$ mice, compared to wildtype C57B6/J mice, suggesting that adapted immunity in *Kit*$^{w/w-v}$ mice is largely intact. So why PSC-derived SLCs would survive better in *Kit*$^{w/w-v}$ mice? One possibility is that *Kit*$^{w/w-v}$ mice had markedly reduced mast cells (Gregory et al., 2005; Grimbaldeston et al., 2005), while nude mice have normal counts of mast cells (Mayrhofer and Bazin, 1981; Wlodarski et al., 1983). Increased mast cells in nude mice under certain pathological conditions were also reported (Wlodarski et al., 1983). Mast cells are known to participate in both allergic and inflammatory responses to pathogens (Gilfillan and Tkaczyk, 2006; Kolkhir et al., 2021). When abnormally elevated, mast cells may cause tissue fibrosis and sclerosis in the testis, abnormal spermatogenesis, and male infertility (Jezek et al., 1999; Meineke et al., 2000; Fijak and Meinhardt, 2006). It will be interesting to investigate whether low mast cell counts in *Kit*$^{w/w-v}$ protect PSC-derived SLCs from immunological rejection during xenotransplantation.

In a previous study, Reis et al. did not find human germ cells in any recipient (either *Kit*$^{w/w-v}$ mice and SCID mice) post xenotransplantation (Reis et al., 2000). Later, Nagano et al. demonstrated successful colonization of human spermatogonia in busulfan-treated nude mice (Nagano et al., 2002). Although it was unclear why the mouse recipients used in the Reis et al. study failed to support the xenotransplantation of human germ cells, it has been once attributed to potential interspecies non-compatible cell adhesion molecules and/or immunological rejection (Reis et al., 2000). However, these speculations have never been experimentally examined, and it remains elusive whether immune deficiency of recipients improves the survival and engraftment efficiency of transplanted germ cells. Our data demonstrated that human spermatogonia engrafted into both immune-deficient nude mice and immune-competent ICR mice with similar efficiencies. SSCs and spermatogonia reside at the basal compartment of the seminiferous tubules, lying outside of the blood-testis-barrier (BTB). Thus, SSCs and spermatogonia are physically protected from immunological cells/factors only by basement lamina, peritubular myoid cells (PMCs), and endothelial cells of testicular blood vessels (Qu et al., 2020). However, the immune privilege of testis is established not only by BTB, but also by immune-suppressive factors secreted from

testicular supporting cells (e.g., Sertoli cells, Leydig cells, and PMCs) (Kaur et al., 2014; Qu et al., 2020). Tolerance of xenogeneic SSCs and spermatogonia may be induced by local immune-suppressive microenvironment in recipient testis. Consistent with our findings, published reports showed that rat spermatogonia went through complete spermatogenesis in busulfan-treated immune-competent mouse testes (Qu et al., 2012). Although busulfan itself has immune-suppressing effects, the immune system of recipients appeared to recover at the dose to ablate endogenous spermatogenesis (Hirayanagi et al., 2015). Thus, the success of xenotransplantation was not dependent on busulfan-induced immune suppression.

To distinguish transplanted spermatogonia from endogenous spermatogenesis that might recover after busulfan treatment, in this study, we utilized two markers, DDX4 and NuMA, to quantify human spermatogonia in mouse recipients. DDX4 (also called VASA), expressed only in germ cells (Castrillon et al., 2000; Tanaka et al., 2000), was used to detect spermatogonia, while NuMA (Merdes and Cleveland, 1998; Taimen et al., 2004), verified specifically for human cells, efficiently recognized human spermatogonia in mouse testes. The combination of two markers can, to some extent, facilitate the reliable detection of human spermatogonia *in vivo*. We found all DDX4 germ cells were NuMA positive, thus confirming their human origin. These DDX4+ germ cells were also co-stained with a spermatogonial marker, PLZF, suggesting that they are undifferentiated spermatogonia. These findings are consistent with previous studies (Nagano et al., 2002; Sadri-Ardekani et al., 2009; Sadri-Ardekani et al., 2011), indicating that only human spermatogonia survived long-term after xenotransplantation but could not go beyond the spermatogonial stage in mouse testes. Although xenotransplanted cell populations may potentially be contaminated with human testicular somatic cells (e.g., Sertoli cells) during spermatogonial collection from testes or SLC differentiation, very few NuMA positive cells were DDX4 negative. Therefore, we conclude that the human germ cell engraftment was mainly supported by the mouse testis microenvironment rather than by co-transplanted human testicular somatic cells.

The last 2 decades have witnessed remarkable technical advances to reconstitute germ cell development from PSCs *in vitro* (Kee et al., 2009; Hayashi et al., 2011; Easley et al., 2012; Irie et al., 2015; Sasaki et al., 2015; Zhou et al., 2016; Zhao et al., 2018; Gell et al., 2020). These approaches not only offer powerful tools to probe the fundamental regulatory mechanisms of mammalian reproduction, but also open a door for developing replacement therapy of male infertility. Modified from an approach that was originally developed by Easley *et al.* (Easley et al., 2012), we developed a feeder- and xeno-free culture condition that enabled robust derivation of PLZF+ SLCs from human PSCs, including both ESCs we used in this study and patient-derived iPSCs (Zhao et al., 2018). These *in vitro* derived SLCs displayed key features of spermatogonia, with upregulated germline genes and specific epigenetic imprinting patterns (Easley et al., 2012; Zhao et al., 2018). In this study, using a combination of EpCAM and TNAP staining, we further developed a strategy to remove residual ESCs from SLCs. We found that these EpCAM-/TNAP+ cells highly expressed spermatogonial genes, including PLZF, INTERGRINα6, TKTL1, and DMRT3, but were negative for PSC marker TRA-1-81. Upon transplantation, none of these EpCAM-/TNAP+ cells formed teratoma. More importantly, similar to *in vivo* developed human spermatogonia, EpCAM-/TNAP+ SLCs from human ESCs were able to go through the homing process. They were successfully recognized by Sertoli cells in the murine recipients and migrated to the basement membrane of seminiferous tubules of both immunocompromised nude mice and $Kit^{w/w\text{-}v}$ recipients. Our study thus functionally confirmed the cell identity of these EpCAM-/TNAP+ as prospermatogonia or undifferentiated spermatogonia and offered a feasible approach to study germ cell development with a PSC differentiation platform. In addition, the similar SLC derivation procedure can be applied to patient-derived iPSCs to understand the underlying causes and pathological development of male infertility. Although previous reports have shown minimal immune rejection upon transplantation of syngeneic iPSC-derived cells or tissues (Araki et al., 2013; Guha et al., 2013), it remains as a debatable topic whether PSC-derived cells evoke immune responses differently from those developed *in vivo* (de Almeida et al., 2013; Liu et al., 2017). Our study demonstrated negligible immunogenicity of human PSC-derived SLCs in mouse testes, thereby providing strong evidence to support the application of autologous iPSC derivatives for future therapeutic purposes.

DATA AVAILABILITY STATEMENT

The original contributions presented in the study are included in the article/**Supplementary Material**, further inquiries can be directed to the corresponding authors.

ETHICS STATEMENT

The studies involving human participants were reviewed and approved by Institutional Ethical Review Committee of Shanghai First People's Hospital. The patients/participants

provided their written informed consent to participate in this study. The animal study was reviewed and approved by Committee of Animal Experimental Ethics at East China Normal University.

AUTHOR CONTRIBUTIONS

DL, QS, ZZ, CW, and SY performed experiments. ZL diagnosed obstructive azoospermia patients and collected human testes samples. DL and YW designed experiments, analyzed results, and wrote the manuscript.

FUNDING

This work was supported by grants from the Science and Technology Commission of Shanghai Municipality (19JC1412300) and Postdoctoral Science Foundation of China (2018M632064). YW is partially supported by the USDA National Institute of Food and Agriculture Hatch Project (1015058).

SUPPLEMENTARY MATERIAL

The Supplementary Material for this article can be found online at: https://www.frontiersin.org/articles/10.3389/fcell.2022.883314/full#supplementary-material

REFERENCES

Araki, R., Uda, M., Hoki, Y., Sunayama, M., Nakamura, M., Ando, S., Koruji, M., et al. (2013). Negligible Immunogenicity of Terminally Differentiated Cells Derived from Induced Pluripotent or Embryonic Stem Cells. *Nature* 494, 100–104. doi:10.1038/nature11807

Brinster, R. L., and Avarbock, M. R. (1994). Germline Transmission of Donor Haplotype Following Spermatogonial Transplantation. *Proc. Natl. Acad. Sci. U.S.A.* 91, 11303–11307. doi:10.1073/pnas.91.24.11303

Brinster, R. L., and Zimmermann, J. W. (1994). Spermatogenesis Following Male Germ-Cell Transplantation. *Proc. Natl. Acad. Sci. U.S.A.* 91, 11298–11302. doi:10.1073/pnas.91.24.11298

Castrillon, D. H., Quade, B. J., Wang, T. Y., Quigley, C., and Crum, C. P. (2000). The Human VASA Gene Is Specifically Expressed in the Germ Cell Lineage. *Proc. Natl. Acad. Sci. U.S.A.* 97, 9585–9590. doi:10.1073/pnas.160274797

Costoya, J. A., Hobbs, R. M., Barna, M., Cattoretti, G., Manova, K., Sukhwani, M., et al. (2004). Essential Role of Plzf in Maintenance of Spermatogonial Stem Cells. *Nat. Genet.* 36, 653–659. doi:10.1038/ng1367

de Almeida, P. E., Ransohoff, J. D., Nahid, A., and Wu, J. C. (2013). Immunogenicity of Pluripotent Stem Cells and Their Derivatives. *Circ. Res.* 112, 549–561. doi:10.1161/circresaha.111.249243

Easley, C. A., Phillips, B. T., McGuire, M. M., Barringer, J. M., Valli, H., Hermann, B. P., et al. (2012). Direct Differentiation of Human Pluripotent Stem Cells into Haploid Spermatogenic Cells. *Cell. Rep.* 2, 440–446. doi:10.1016/j.celrep.2012.07.015

Evans, M. J., and Kaufman, M. H. (1981). Establishment in Culture of Pluripotential Cells from Mouse Embryos. *Nature* 292, 154–156. doi:10.1038/292154a0

Fijak, M., and Meinhardt, A. (2006). The Testis in Immune Privilege. *Immunol. Rev.* 213, 66–81. doi:10.1111/j.1600-065x.2006.00438.x

Gell, J. J., Liu, W., Sosa, E., Chialastri, A., Hancock, G., Tao, Y., et al. (2020). An Extended Culture System that Supports Human Primordial Germ Cell-like Cell Survival and Initiation of DNA Methylation Erasure. *Stem Cell. Rep.* 14, 433–446. doi:10.1016/j.stemcr.2020.01.009

Gilfillan, A. M., and Tkaczyk, C. (2006). Integrated Signalling Pathways for Mast-Cell Activation. *Nat. Rev. Immunol.* 6, 218–230. doi:10.1038/nri1782

Gregory, G. D., Bickford, A., Robbie-Ryan, M., Tanzola, M., and Brown, M. A. (2005). MASTering the Immune Response: Mast Cells in Autoimmunity. *Novartis Found. Symp.* 271, 215–231. discussion 225-31 (2005).

Grimbaldeston, M. A., Chen, C.-C., Piliponsky, A. M., Tsai, M., Tam, S.-Y., and Galli, S. J. (2005). Mast Cell-Deficient W-Sash C-Kit Mutant KitW-sh/W-Sh Mice as a Model for Investigating Mast Cell Biology *In Vivo*. *Am. J. Pathology* 167, 835–848. doi:10.1016/s0002-9440(10)62055-x

Groscurth, P., and Kistler, G. (1975). Histogenese des Immunsystems der "nude" Maus IV. Ultrastruktur der Thymusanlage 12- und 13tägiger Embryonen. *Beiträge zur Pathol.* 156, 359–375. doi:10.1016/s0005-8165(75)80045-x

Guha, P., Morgan, J. W., Mostoslavsky, G., Rodrigues, N. P., and Boyd, A. S. (2013). Lack of Immune Response to Differentiated Cells Derived from Syngeneic Induced Pluripotent Stem Cells. *Cell. Stem Cell.* 12, 407–412. doi:10.1016/j.stem.2013.01.006

Hayashi, K., Ohta, H., Kurimoto, K., Aramaki, S., and Saitou, M. (2011). Reconstitution of the Mouse Germ Cell Specification Pathway in Culture by Pluripotent Stem Cells. *Cell.* 146, 519–532. doi:10.1016/j.cell.2011.06.052

He, Z., Kokkinaki, M., Jiang, J., Dobrinski, I., and Dym, M. (2010). Isolation, Characterization, and Culture of Human Spermatogonia1. *Biol. Of Reproduction* 82, 363–372. doi:10.1095/biolreprod.109.078550

He, Z., Kokkinaki, M., Jiang, J., Zeng, W., Dobrinski, I., and Dym, M. (2012). "Isolation of Human Male Germ-Line Stem Cells Using Enzymatic Digestion and Magnetic-Activated Cell Sorting,". Editors W. Y. Chan and L. A. Bloomberg, 825, 45–57. doi:10.1007/978-1-61779-436-0_4*Germline Dev. Methods Protoc.*

Hermann, B. P., Sukhwani, M., Lin, C.-C., Sheng, Y., Tomko, J., Rodriguez, M., et al. (2007). Characterization, Cryopreservation, and Ablation of Spermatogonial Stem Cells in Adult Rhesus Macaques. *Stem Cells* 25, 2330–2338. doi:10.1634/stemcells.2007-0143

Hermann, B. P., Sukhwani, M., Simorangkir, D. R., Chu, T., Plant, T. M., and Orwig, K. E. (2009). Molecular Dissection of the Male Germ Cell Lineage Identifies Putative Spermatogonial Stem Cells in Rhesus Macaques. *Hum. Reprod.* 24, 1704–1716. doi:10.1093/humrep/dep073

Hirayanagi, Y., Qu, N., Hirai, S., Naito, M., Terayama, H., Hayashi, S., et al. (2015). Busulfan Pretreatment for Transplantation of Rat Spermatogonia Differentially Affects Immune and Reproductive Systems in Male Recipient Mice. *Anat. Sci. Int.* 90, 264–274. doi:10.1007/s12565-014-0261-y

Honaramooz, A., Behboodi, E., Blash, S., Megee, S. O., and Dobrinski, I. (2003). Germ Cell Transplantation in Goats. *Mol. Reprod. Dev.* 64, 422–428. doi:10.1002/mrd.10205

Honaramooz, A., Megee, S. O., and Dobrinski, I. (2002). Germ Cell Transplantation in Pigs1. *Biol. Reproduction* 66, 21–28. doi:10.1095/biolreprod66.1.21

Irie, N., Weinberger, L., Tang, W. W. C., Kobayashi, T., Viukov, S., Manor, Y. S., et al. (2015). SOX17 Is a Critical Specifier of Human Primordial Germ Cell Fate. *Cell.* 160, 253–268. doi:10.1016/j.cell.2014.12.013

Jabari, A., Sadighi Gilani, M. A., Koruji, M., Gholami, K., Mohsenzadeh, M., rastegar, T., et al. (2020). Three-dimensional Co-culture of Human Spermatogonial Stem Cells with Sertoli Cells in Soft Agar Culture System Supplemented by Growth Factors and Laminin. *Acta Histochem.* 122, 151572. doi:10.1016/j.acthis.2020.151572

Jezek, D., Banek, L., Hittmair, A., Pezerovic-Panijan, R., Goluza, T., and Schulze, W. (1999). Mast Cells in Testicular Biopsies of Infertile Men with 'mixed Atrophy' of Seminiferous Tubules. *Andrologia* 31, 203–210. doi:10.1046/j.1439-0272.1999.00287.x

Jiang, F.-X., and Short, R. V. (1995). Male Germ Cell Transplantation in Rats: Apparent Synchronization of Spermatogenesis between Host and Donor Seminiferous Epithelia. *Int. J. Androl.* 18, 326–330. doi:10.1111/j.1365-2605.1995.tb00570.x

Kaur, G., Thompson, L. A., and Dufour, J. M. (2014). Sertoli Cells - Immunological Sentinels of Spermatogenesis. *Seminars Cell. & Dev. Biol.* 30, 36–44. doi:10.1016/j.semcdb.2014.02.011

Kee, K., Angeles, V. T., Flores, M., Nguyen, H. N., and Reijo Pera, R. A. (2009). Human DAZL, DAZ and BOULE Genes Modulate Primordial Germ-Cell and Haploid Gamete Formation. *Nature* 462, 222–225. doi:10.1038/nature08562

Kolkhir, P., Elieh-Ali-Komi, D., Metz, M., Siebenhaar, F., and Maurer, M. (2021). Understanding Human Mast Cells: Lesson from Therapies for Allergic and Non-allergic Diseases. *Nat. Rev. Immunol.* doi:10.1038/s41577-021-00622-y

Koruji, M., Shahverdi, A., Janan, A., Piryaei, A., Lakpour, M. R., and Gilani Sedighi, M. A. (2012). Proliferation of Small Number of Human Spermatogonial Stem Cells Obtained from Azoospermic Patients. *J. Assist. Reprod. Genet.* 29, 957–967. doi:10.1007/s10815-012-9817-8

Kubota, H., Avarbock, M. R., and Brinster, R. L. (2003). Spermatogonial Stem Cells Share Some, but Not All, Phenotypic and Functional Characteristics with Other Stem Cells. *Proc. Natl. Acad. Sci. U.S.A.* 100, 6487–6492. doi:10.1073/pnas.0631767100

Kubota, H., Avarbock, M. R., Schmidt, J. A., and Brinster, R. L. (2009). Spermatogonial Stem Cells Derived from Infertile Wv/Wv Mice Self-Renew *In Vitro* and Generate Progeny Following Transplantation1. *Biol. Of Reproduction* 81, 293–301. doi:10.1095/biolreprod.109.075960

Kubota, H., and Brinster, R. L. (2018). Spermatogonial Stem Cells†. *Biol. Reproduction* 99, 52–74. doi:10.1093/biolre/ioy077

Liu, X., Li, W., Fu, X., and Xu, Y. (2017). The Immunogenicity and Immune Tolerance of Pluripotent Stem Cell Derivatives. *Front. Immunol.* 8, 645. doi:10.3389/fimmu.2017.00645

Maki, C. B., Pacchiarotti, J., Ramos, T., Pascual, M., Pham, J., Kinjo, J., et al. (2009). Phenotypic and Molecular Characterization of Spermatogonial Stem Cells in Adult Primate Testes. *Hum. Reprod.* 24, 1480–1491. doi:10.1093/humrep/dep033

Martin, G. R. (1981). Isolation of a Pluripotent Cell Line from Early Mouse Embryos Cultured in Medium Conditioned by Teratocarcinoma Stem Cells. *Proc. Natl. Acad. Sci. U.S.A.* 78, 7634–7638. doi:10.1073/pnas.78.12.7634

Mayrhofer, G., and Bazin, H. (1981). Nature of the Thymus Dependency of Mucosal Mast Cells. *Int. Arch. Allergy Immunol.* 64, 320–331. doi:10.1159/000232710

Meineke, V., Frungieri, M. B., Jessberger, B., Vogt, H.-J., and Mayerhofer, A. (2000). Human Testicular Mast Cells Contain Tryptase: Increased Mast Cell Number and Altered Distribution in the Testes of Infertile Men. *Fertil. Steril.* 74, 239–244. doi:10.1016/s0015-0282(00)00626-9

Merdes, A., and Cleveland, D. W. (1998). The Role of NuMA in the Interphase Nucleus. *J. Cell. Sci.* 111, 71–79. doi:10.1242/jcs.111.1.71

Mirzapour, T., Movahedin, M., Tengku Ibrahim, T. A., Koruji, M., Haron, A. W., Nowroozi, M. R., et al. (2012). Effects of Basic Fibroblast Growth Factor and Leukaemia Inhibitory Factor on Proliferation and Short-Term Culture of Human Spermatogonial Stem Cells. *Andrologia* 44 (Suppl. 1), 41–55. doi:10.1111/j.1439-0272.2010.01135.x

Morimoto, H., Ogonuki, N., Kanatsu-Shinohara, M., Matoba, S., Ogura, A., and Shinohara, T. (2021). Spermatogonial Stem Cell Transplantation into Nonablated Mouse Recipient Testes. *Stem Cell. Rep.* 16, 1832–1844. doi:10.1016/j.stemcr.2021.05.013

Nagano, M., Patrizio, P., and Brinster, R. L. (2002). Long-term Survival of Human Spermatogonial Stem Cells in Mouse Testes. *Fertil. Steril.* 78, 1225–1233. doi:10.1016/s0015-0282(02)04345-5

Nocka, K., Majumder, S., Chabot, B., Ray, P., Cervone, M., Bernstein, A., et al. (1989). Expression of C-Kit Gene Products in Known Cellular Targets of W Mutations in Normal and W Mutant Mice-Evidence for an Impaired C-Kit Kinase in Mutant Mice. *Genes Dev.* 3, 816–826. doi:10.1101/gad.3.6.816

Nocka, K., Tan, J. C., Chiu, E., Chu, T. Y., Ray, P., Traktman, P., et al. (1990). Molecular Bases of Dominant Negative and Loss of Function Mutations at the Murine C-Kit/white Spotting Locus: W37, Wv, W41 and W. *EMBO J.* 9, 1805–1813. doi:10.1002/j.1460-2075.1990.tb08305.x

Oatley, J. M., and Brinster, R. L. (2012). The Germline Stem Cell Niche Unit in Mammalian Testes. *Physiol. Rev.* 92, 577–595. doi:10.1152/physrev.00025.2011

Ogawa, T., Dobrinski, I., Avarbock, M. R., and Brinster, R. L. (2000). Transplantation of Male Germ Line Stem Cells Restores Fertility in Infertile Mice. *Nat. Med.* 6, 29–34. doi:10.1038/71496

Ohta, H., Tohda, A., and Nishimune, Y. (2003). Proliferation and Differentiation of Spermatogonial Stem Cells in the W/Wv Mutant Mouse Testis1. *Biol. Reproduction* 69, 1815–1821. doi:10.1095/biolreprod.103.019323

Park, I.-H., Zhao, R., West, J. A., Yabuuchi, A., Huo, H., Ince, T. A., et al. (2008). Reprogramming of Human Somatic Cells to Pluripotency with Defined Factors. *Nature* 451, 141–146. doi:10.1038/nature06534

Qu, N., Naito, M., Li, J., Terayama, H., Hirai, S., and Itoh, M. (2012). Xenogeneic and Endogenous Spermatogenesis Following Transplantation of Rat Germ Cells into Testes of Immunocompetent Mice. *Reprod. Fertil. Dev.* 24, 337–343. doi:10.1071/rd10349

Qu, N., Ogawa, Y., Kuramasu, M., Nagahori, K., Sakabe, K., and Itoh, M. (2020). Immunological Microenvironment in the Testis. *Reprod. Med. Biol.* 19, 24–31. doi:10.1002/rmb2.12293

Reis, M. M., Tsai, M. C., Schlegel, P. N., Feliciano, M., Raffaelli, R., Rosenwaks, Z., et al. (2000). Xenogeneic Transplantation of Human Spermatogonia. *Zygote* 8, 97–105. doi:10.1017/s0967199400000873

Rodewald, H.-R., Ogawa, M., Haller, C., Waskow, C., and DiSanto, J. P. (1997). Pro-Thymocyte Expansion by C-Kit and the Common Cytokine Receptor γ Chain Is Essential for Repertoire Formation. *Immunity* 6, 265–272. doi:10.1016/s1074-7613(00)80329-5

Rossi, P., Sette, C., Dolci, S., and Geremia, R. (2000). Role of C-Kit in Mammalian Spermatogenesis. *J. Endocrinol. Invest.* 23, 609–615. doi:10.1007/bf03343784

Russell, L. D., and Brinster, R. L. (1996). Ultrastructural Observations of Spermatogenesis Following Transplantation of Rat Testis Cells into Mouse Seminiferous Tubules. *J. Androl.* 17, 615–627.

Sadri-Ardekani, H., Akhondi, M. A., van der Veen, F., Repping, S., and van Pelt, A. M. M. (2011). *In Vitro* Propagation of Human Prepubertal Spermatogonial Stem Cells. *Jama* 305, 2416–2418. doi:10.1001/jama.2011.791

Sadri-Ardekani, H., Mizrak, S. C., van Daalen, S. K. M., Korver, C., Roepers-Gajadien, H. L., et al. (2009). Propagation of Human Spermatogonial Stem Cells *In Vitro*. *Jama* 302, 2127–2134. doi:10.1001/jama.2009.1689

Sasaki, K., Yokobayashi, S., Nakamura, T., Okamoto, I., Yabuta, Y., Kurimoto, K., et al. (2015). Robust *In Vitro* Induction of Human Germ Cell Fate from Pluripotent Stem Cells. *Cell. Stem Cell.* 17, 178–194. doi:10.1016/j.stem.2015.06.014

Schedi, M. P., Goldstein, G., and Boyce, E. A. (1975). Differentiation of T Cells in Nude Mice. *Science* 190, 1211–1213. doi:10.1126/science.190.4220.1211

Seandel, M., James, D., Shmelkov, S. V., Falciatori, I., Kim, J., Chavala, S., et al. (2007). Generation of Functional Multipotent Adult Stem Cells from GPR125+ Germline Progenitors. *Nature* 449, 346–350. doi:10.1038/nature06129

Shinohara, T., Avarbock, M. R., and Brinster, R. L. (1999). β 1 - and α 6 -integrin Are Surface Markers on Mouse Spermatogonial Stem Cells. *Proc. Natl. Acad. Sci. U.S.A.* 96, 5504–5509. doi:10.1073/pnas.96.10.5504

Taimen, P., Parvinen, M., Osborn, M., and Kallajoki, M. (2004). NuMA in Rat Testis-Evidence for Roles in Proliferative Activity and Meiotic Cell Division. *Exp. Cell. Res.* 298, 512–520. doi:10.1016/j.yexcr.2004.05.002

Takahashi, K., Tanabe, K., Ohnuki, M., Narita, M., Ichisaka, T., Tomoda, K., et al. (2007). Induction of Pluripotent Stem Cells from Adult Human Fibroblasts by Defined Factors. *Cell.* 131, 861–872. doi:10.1016/j.cell.2007.11.019

Takahashi, K., and Yamanaka, S. (2006). Induction of Pluripotent Stem Cells from Mouse Embryonic and Adult Fibroblast Cultures by Defined Factors. *Cell.* 126, 663–676. doi:10.1016/j.cell.2006.07.024

Tanaka, S. S., Toyooka, Y., Akasu, R., Katoh-Fukui, Y., Nakahara, Y., Suzuki, R., et al. (2000). The Mouse Homolog of Drosophila Vasa Is Required for the Development of Male Germ Cells. *Genes Dev.* 14, 841–853. doi:10.1101/gad.14.7.841

Thomson, J. A., Itskovitz-Eldor, J., Shapiro, S. S., Waknitz, M. A., Swiergiel, J. J., Marshall, V. S., et al. (1998). Embryonic Stem Cell Lines Derived from Human Blastocysts. *Science* 282, 1145–1147. doi:10.1126/science.282.5391.1145

Valli, H., Sukhwani, M., Dovey, S. L., Peters, K. A., Donohue, J., Castro, C. A., et al. (2014). Fluorescence- and Magnetic-Activated Cell Sorting Strategies to Isolate and Enrich Human Spermatogonial Stem Cells. *Fertil. Steril.* 102, 566–580. doi:10.1016/j.fertnstert.2014.04.036

Waskow, C., and Hans-Reimer, R. (2002). "Lymphocyte Development in Neonatal and Adult C-Kit-Deficient (C-Kitw/w) Mice,". Editors S. Gupta, E. Butcher, and W. Paul, 512, 1–10. doi:10.1007/978-1-4615-0757-4_1*Lymphocyte Activation Immune Regul. Ix Homeost. Lymphocyte Traffic*

Wlodarski, K., Rose, N. R., and Morrison, K. (1983). Lymph Node Mast Cells in Athymic "nude" (Nu/Nu) and Thymus Containing (Nu/+ and +/+) Balb/c Mice. *Archivum Immunol. Ther. Exp.* 31, 177–182.

Wu, Z., Falciatori, I., Molyneux, L. A., Richardson, T. E., Chapman, K. M., and Hamra, F. K. (2009). Spermatogonial Culture Medium: An Effective and Efficient Nutrient Mixture for Culturing Rat Spermatogonial Stem Cells1. *Biol. Reprod.* 81, 77–86. doi:10.1095/biolreprod.108.072645

Yoshinaga, K., Nishikawa, S., Ogawa, M., Hayashi, S., Kunisada, T., Fujimoto, T., et al. (1991). Role of C-Kit in Mouse Spermatogenesis: Identification of Spermatogonia as a Specific Site of C-Kit Expression and Function. *Dev. Camb. Engl.* 113, 689–699. doi:10.1242/dev.113.2.689

Yu, J., Vodyanik, M. A., Smuga-Otto, K., Antosiewicz-Bourget, J., Frane, J. L., Tian, S., et al. (2007). Induced Pluripotent Stem Cell Lines Derived from Human Somatic Cells. *Science* 318, 1917–1920. doi:10.1126/science.1151526

Zhang, J., Wang, Q., Wang, M., Jiang, M., Wang, Y., Sun, Y., et al. (2016). GASZ and Mitofusin-mediated Mitochondrial Functions Are Crucial for Spermatogenesis. *EMBO Rep.* 17, 220–234. doi:10.15252/embr.201540846

Zhao, Y., Ye, S., Liang, D., Wang, P., Fu, J., Ma, Q., et al. (2018). *In Vitro* Modeling of Human Germ Cell Development Using Pluripotent Stem Cells. *Stem Cell. Rep.* 10, 509–523. doi:10.1016/j.stemcr.2018.01.001

Zhou, Q., Wang, M., Yuan, Y., Wang, X., Fu, R., Wan, H., et al. (2016). Complete Meiosis from Embryonic Stem Cell-Derived Germ Cells *In Vitro*. *Cell. Stem Cell.* 18, 330–340. doi:10.1016/j.stem.2016.01.017

Conflict of Interest: The authors declare that the research was conducted in the absence of any commercial or financial relationships that could be construed as a potential conflict of interest.

Publisher's Note: All claims expressed in this article are solely those of the authors and do not necessarily represent those of their affiliated organizations, or those of the publisher, the editors and the reviewers. Any product that may be evaluated in this article, or claim that may be made by its manufacturer, is not guaranteed or endorsed by the publisher.

frontiers | Frontiers in Cell and Developmental Biology

MINI REVIEW
published: 27 May 2022
doi: 10.3389/fcell.2022.897831

Air Pollution Exposure Induces Vascular Injury and Hampers Endothelial Repair by Altering Progenitor and Stem Cells Functionality

Alice Costa[1] *and Gianandrea Pasquinelli*[1,2]*

[1]*Laboratory of Clinical Pathology, Department of Experimental, Diagnostic and Specialty Medicine (DIMES), University of Bologna, Bologna, Italy,* [2]*IRCCS Azienda Ospedaliero Universitaria di Bologna, Bologna, Italy*

Extensive evidence indicates an association of air pollution exposure with an increased risk of cardiovascular disease (CVD) development. Fine particulate matter (PM) represents one of the main components of urban pollution, but the mechanisms by which it exerts adverse effects on cardiovascular system remain partially unknown and under investigation. The alteration of endothelial functions and inflammation are among the earliest pathophysiological impacts of environmental exposure on the cardiovascular system and represent critical mediators of PM-induced injury. In this context, endothelial stem/progenitor cells (EPCs) play an important role in vascular homeostasis, endothelial reparative capacity, and vasomotor functionality modulation. Several studies indicate the impairment of EPCs' vascular reparative capacity due to PM exposure. Since a central source of EPCs is bone marrow (BM), their number and function could be related to the population and functional status of stem cells (SCs) of this district. In this review, we provide an overview of the potential mechanisms by which PM exposure hinders vascular repair by the alteration of progenitor and stem cells' functionality.

Keywords: air pollution, particulate matter, cardiovascular disease, vascular injury, endothelial repair, endothelial progenitor cells (EPCs)

OPEN ACCESS

Edited by:
Valerie Kouskoff,
The University of Manchester, United Kingdom

Reviewed by:
Timothy O'Toole,
University of Louisville, United States
Zhenguo Liu,
University of Missouri System, United States

***Correspondence:**
Gianandrea Pasquinelli
gianandr.pasquinelli@unibo.it

Specialty section:
This article was submitted to Stem Cell Research, a section of the journal Frontiers in Cell and Developmental Biology

Received: *16 March 2022*
Accepted: *20 April 2022*
Published: *27 May 2022*

Citation:
Costa A and Pasquinelli G (2022) Air Pollution Exposure Induces Vascular Injury and Hampers Endothelial Repair by Altering Progenitor and Stem Cells Functionality. Front. Cell Dev. Biol. 10:897831. doi: 10.3389/fcell.2022.897831

INTRODUCTION

The World Health Organization (WHO) estimates seven million premature deaths worldwide every year due to ambient air pollution (World health statistics, 2021). Extensive epidemiological evidence indicates that not only the respiratory system but almost every organ of the body is affected by polluted air exposure. Indeed, smaller pollutants that arise in the lungs can penetrate the bloodstream reaching the entire body, thus inducing cardiovascular injury, metabolic disorders, systemic inflammation, and carcinogenicity (Franchini and Mannucci, 2011; Rao, 2018). Recent evidence also indicates that air pollution aggravates coronaviruses' epidemics, such as SARS and COVID-19, with greatest effects in urban areas, where emission levels are highest (Hutter et al., 2020; Cascetta et al., 2021; Salgado et al., 2021).

The outdoor air pollution—especially by $PM_{2.5}$—is deemed to be responsible for about 3.3 million premature deaths (Lelieveld et al., 2015), with accumulating evidence to indicate that the greatest number is related to cardiovascular diseases (CVDs) (Tofler and Muller, 2006; Brook et al., 2010). In

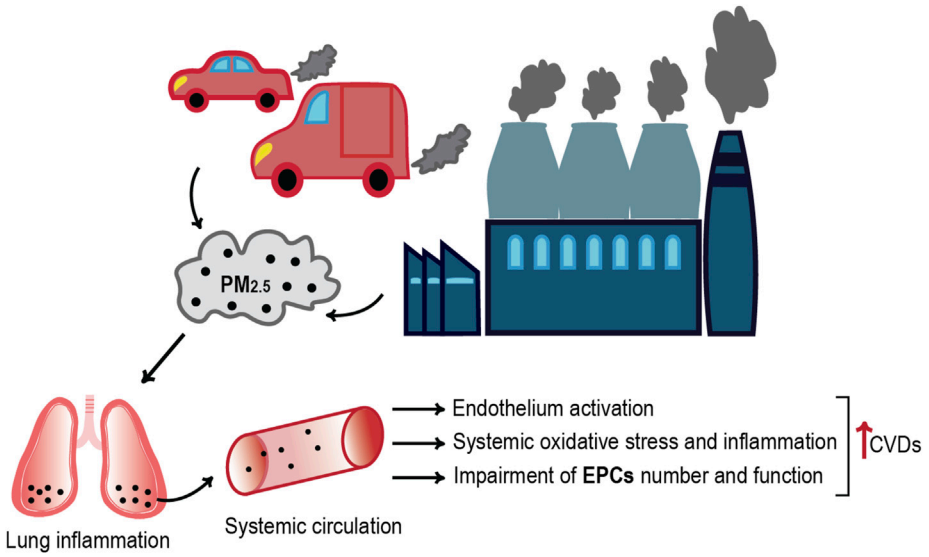

GRAPHICAL ABSTRACT |

Europe, the 45% of the mortality rate is caused by CVDs, which accounts for the 37% within the 28 countries of the European Union (Lelieveld et al., 2015; Wilkins et al., 2017). Furthermore, long-term $PM_{2.5}$ inhalation might result in endothelial injury, vascular homeostasis dysregulation and inflammation, increased coagulation-thrombosis risk, atherosclerosis, and hypertension, effects that could accelerate cardiovascular disease or generate negative cardiovascular events (Cui et al., 2016; Chen et al., 2018; Haberzettl et al., 2018).

In this context of endothelial dysfunction or injury, the endothelial progenitor cells (EPCs) play an essential role, as central regulators of vascular regeneration, angiogenesis, and reendothelialization, which facilitate to vascular repair (Jian et al., 2018; Bayraktutan, 2019). Since the exposure to ambient fine particles leads to cardiovascular injury and, at the same time, defects in vascular repair and regeneration (Chen et al., 2018), it is of common interest to understand how $PM_{2.5}$ affects the number and the functionality of EPCs.

In this review, we summarize the mechanisms by which PM exposure alters EPCs health and how it affects vascular repair following exposure-related cardiovascular injury.

GENERAL INFORMATION ON $PM_{2.5}$ AIR POLLUTION

In relation to particle size, environmental particulate matter is generally classified in PM_{10} coarse, $PM_{2.5}$, and ultrafine particles (UFPs), characterized by an aerodynamic diameter of 10–2.5 μm, <2.5 μm, and <0.1 μm, respectively (Brook et al., 2010). Urban PM has a varied and complex composition, displaying elemental and organic carbon species (PAHs, nitro-PAHs, alkenes, etc.), especially from a major part of combustion-derived PM. Another important component is the non-carbon one, represented by various minerals' dusts, sea salt, ammonium, nitrates, and sulfates. Additionally, the surface of PM may accumulate small amounts of biological materials (i.e., endotoxins), which are likely to be involved in airway inflammation and other aspects of the pathophysiological response (Miller and Newby, 2020).

In terms of toxicity, smaller size particles are considered of particular importance for health since they exert the greater effects due to their large reactive surface area and the ability to be inhaled deeply in the alveoli of the lungs (Ohlwein et al., 2019). Among the common fine particle air pollutants, $PM_{2.5}$, containing redox-active transition metals, quinones, and secondary organic aerosols, are mostly generated by the human combustion of fossil fuels (from industry processes, vehicle-exhaust emissions, and power generation) and display the longest atmospheric lifetime (Brook et al., 2010; Lakey et al., 2016). Since not filtered by the respiratory tract, these particles have been proposed to affect the cardiovascular system by reaching the terminal bronchioles via inhalation, entering alveoli, penetrating biological membranes, and inducing an inflammatory response in the lung, with the release of inflammatory mediators that enter the bloodstream (Miller and Newby, 2020).

TABLE 1 | Annual mean concentration of fine particulate matter $PM_{2.5}$ by region, population-weighted (Indicator 11.6.2), for the year 2016 (World Health Organization, 2021).

Region	*μg/m³*
South-East Asia	54
Eastern Mediterranean	51
Africa	39
Western Pacific	39
Europe	13
Americas	12

Among the World's population, the 91% lives in places where air pollution levels exceed the WHO guidelines limits, set at 5 μg/m^3 for fine particulate matter $PM_{2.5}$ annual mean (**Table 1**). The World Health Organization attributes the 58% of outdoor air pollution-related premature deaths to stroke and ischemic heart disease, the 18% due to respiratory disease, and the 6% due to lung cancer (World health statistics, 2021).

$PM_{2.5}$ Impact on Cardiovascular Risk

Several toxicological studies suggest that $PM_{2.5}$ are key mediators of endothelial dysfunction; therefore, this fraction of particulate matter is associated with increased cardiovascular mortality (Brook et al., 2010; O'Toole et al., 2010). Richard B Hayes et al. investigated the relationship between $PM_{2.5}$ exposure and cause-specific cardiovascular disease mortality in 565,477 people, aged 50–70 years, from the National Institutes of Health-AARP Diet and Health Study. They observed an association of 10 μg/m^3 $PM_{2.5}$ with a 16% and a 14% increase in mortality from ischemic heart disease and stroke, respectively. Moreover, CVD risks were increased with respect to $PM_{2.5}$ exposures in the range of 8–12 μg/m^3, 12–20 μg/m^3, and >20 μg/m^3 (Hayes et al., 2020). Conversely, a study conducted by McGuinn et al. on a cardiac characterization cohort in North Carolina showed no significant effects of $PM_{2.5}$ exposure on biomarkers of cardiovascular risk, but they observed a strong association between these two factors in individuals affected by metabolic syndrome, as hypertension, diabetes, and obesity. Since in the United States the prevalence of the metabolic syndrome is estimated at >30% further studies should not only investigate the $PM_{2.5}$ impact in CVD risk induction but should also consider the effects on those people with pre-existing cardiovascular risk factors (McGuinn et al., 2019).

As already mentioned, a small proportion of particles directly reach the systemic circulation (Brook et al., 2010; Miller and Newby, 2020), where high levels of $PM_{2.5}$ have been correlated with an important decrease in the function of vascular endothelial cells (VECs) that cover the internal surface of blood vessels and are fundamental for the homeostasis of physiological processes (Cao, 2018). Accordingly, endothelial injury increases the release of inflammatory cytokines, leading to blood monocyte recruitment on the activated endothelial monolayer and their infiltration into the sub-endothelial space, essential in the development of atherosclerotic plaques (Lau and Baldus, 2006; Miller and Newby, 2020; Liang et al., 2021).

Several data indicate that PM exposure leads to an increased reactive oxygen species (ROS) production and oxidative stress in the epithelial lining fluid of the human respiratory tracts (Cui et al., 2015a; Lakey et al., 2016). Accordingly, inflammation and vascular-insulin resistance that derived from the increased pulmonary oxidative stress favor cardiovascular disease even with short-term $PM_{2.5}$ exposure (Haberzettl et al., 2018). It is well established that the oxidative stress, pivotal in the pathophysiology of varied CVDs, contributes to endothelial cell activation, which represents an early step in vascular dysfunction development (Horstman et al., 2004; Daiber et al., 2017). In addition, the increased concentration of $PM_{2.5}$ is responsible for VEC induced death, as a result of oxidative stress injury, inflammation, and endoplasmic reticulum stress (Xie et al., 2021). A study conducted by Li et al. on HUVECs (human umbilical vein vascular endothelial cells) exposed to $PM_{2.5}$ revealed an increased ROS generation that resulted in a significant decreased cell viability. Likewise, fine particles' exposure leads to the reduced activity of superoxide dismutase (SOD) and glutathione peroxidase (GPx), which in turn cause an imbalance in the pro-oxidant/antioxidant homeostasis of HUVECs (Li et al., 2016). In this context, the endothelium inflammation is an inexorable consequence. The study of Montiel-Dávalos et al. on $PM_{2.5}$ toxic effects on HUVECs also reports that the fine particles induce cell activation, followed by monocytic adhesion, through promoting the expression of varied adhesion molecules (E-selectin, P-selectin, ICAM-1) (Montiel-Dávalos et al., 2007), one of the initial events by activated endothelium. In addition, Rui et al. proved that the $PM_{2.5}$-related oxidative stress leads to the expression of ICAM-1 (intercellular adhesion molecule 1) and VCAM-1 (vascular cell adhesion molecule 1) on the cell surface, via the activation of ERK/AKT/NF-kB signaling pathway, thus promoting monocyte adhesion to VECs (Rui et al., 2016). Some evidences also suggest that $PM_{2.5}$-stimulated cytotoxicity in HUVECs accelerates proinflammatory cytokines' secretion (e.g., CRP, TNF-α, IL-6, and IL-8), leading to endothelial activation through the JAK1/STAT3 signaling pathway stimulation (Hu et al., 2016). In addition, some data showed that $PM_{2.5}$ is responsible for endothelial vasomotor function impairment by increasing the circulating levels of AngII, activating the AT1R (AngII/AngII type 1 receptor) axis, and activating the phospholipase C (PLC) and protein kinase C (PKC) in HUVECs. Accordingly, the biosynthesis of endothelin-1 (ET-1), a protein involved in the cell proliferation and vascular tone regulation, is promoted (Liang et al., 2020). It has also been demonstrated that, in an Ang II-induced abdominal aortic aneurysm (AAA) model, $PM_{2.5}$ promotes AAA formation and induces an increase of AAA-related pathological changes, MMP2 and MCP-1 expression in human aortic smooth muscle cells (HASMCs), as the potential result of $PM_{2.5}$-induced senescence and ROS accumulation (Jun et al., 2018).

Furthermore, the *in vivo* study of Chen et al. proved the anti-oxidant and anti-inflammatory effects of probucol, a drug commonly used to lower LDL and HDL cholesterol, in the preservation of the endothelial function by reducing the amount of endogenous nitric oxide (NO) synthase inhibitors. By this way, probucol inhibits the expression of various adhesion molecules, thus promoting the proliferation of endothelial cells, while preventing the apoptosis of the endothelial cells due to oxidative injury (Chen et al., 2018).

THE REGENERATIVE POTENTIAL OF ENDOTHELIAL PROGENITOR CELLS IN VASCULAR REPAIR

Endothelial Progenitor Cells (EPCs) derive from the bone marrow, which are retained via adhesion molecules (i.e., CXCR4) or through interactions between α4β1-integrin

and VCAM-1. EPCs originate from a primitive, undifferentiated hematopoietic and vascular cell precursor, circulate in the peripheral blood, and are implicated in neo-angiogenesis (Werner et al., 2005; Singh et al., 2021).

Despite EPCs exact phenotypic identity, origin, and location are debated (Fadini et al., 2012), flow cytometry and immunohistochemistry are the most commonly used techniques for their identification. However, it is difficult to accurately isolate EPCs based on cell surface markers they express because most of them are co-expressed by other endothelial or hematopoietic cells. Thus, the best option for EPCs detection seems the employment of a panel of antibodies targeting markers for hematopoietic cells, immaturity, stemness, and endothelial maturity (CD45, CD133, CD34, and KDR, respectively). In this way, it is possible to better discriminate between endothelial-committed EPCs (CD34 + CD133 + KDR + $CD45^-$, CD34 + KDR + $CD45^-$, and CD133 + KDR + $CD45^-$) and undifferentiated EPCs (CD34 + CD133 + $CD45^-$, $CD34^+$,CD45-, and CD133 + $CD45^-$) (Bayraktutan, 2019).

Consequent to vascular injury, EPCs cells mobilize from the bone marrow into peripheral blood, in response to biochemical stimuli (VEGF, SDF-1α), for example, in the case of ischemic injury (Bayraktutan, 2019; Singh et al., 2021). EPCs are also stimulated to migrate into the circulation upon hypoxic conditions by interactions between CXCR4 and its antagonist SDF-1a or upon matrix metalloproteinase-9 (MMP-9)-mediated release of the soluble c-Kit ligand (Heissig et al., 2002; Petit et al., 2007; Singh et al., 2021). After leaving the bone marrow, EPCs reach the site of endothelial injury where they attach and promote angiogenesis and revascularization by differentiating into mature, functional endothelial cells, or by paracrine stimulation of the existing endothelium to proliferate and migrate (Asahara et al., 1997; Singh et al., 2021). In brief, the EPCs' mobilization to the vascular injury is influenced by physical factors, such as vascular structure and density, and flow rate, and, also, the expression of cell surface adhesion molecules, in particular VCAM-1 and ICAM-1. Moreover, the increased availability of cytokines, such as IL-6 and GM-CSF (granulocyte-macrophage colony-stimulating factor), contributes to the regulation of EPCs' counts and behavior, for example, after ischemic injury (Orlic et al., 2001; Fan et al., 2008).

Unsurprisingly, the presence of immature circulating cells in the peripheral blood is considered a marker of organism's regenerative capacity; therefore, several clinical trials have been designed to increase EPCs' number at the site of tissue damage (Assmus et al., 2002; Wollert et al., 2004). The EPC-based therapies attract a lot of interest because of the peculiar ability of these cells to detect and repair endothelial damage and to differentiate into other cell lines to promote vasculogenesis, angiogenesis, and neurogenesis after stroke injury (Sekiguchi et al., 2009).

Werner et al. demonstrated the predictive role of CD34 + KDR + circulating EPCs in the occurrence of cardiovascular events and death from cardiovascular causes. They proved that a single measurement of CD34 + KDR + EPCs may help to identify patients with increased cardiovascular risk, predicting cardiovascular outcomes in patients with coronary artery disease. A strongly higher incidence of cardiovascular causes-related death was observed in patients with low baseline levels of EPCs during an observational period of 12 months (Werner et al., 2005).

Several experimental and clinical studies have also shown the EPCs' involvement in improving revascularization in ischemia models (i.e., hindlimb ischemia and myocardial ischemia), in promoting endothelial health in restenosis and renal failure, and play a role in the pathogenesis of coronary disease, despite in this context their exact role remains to be determined (Werner et al., 2005; Thum et al., 2006; Groleau et al., 2010).

PM-Exposure Effects on EPCs

Several studies have been performed to evaluate whether and how different factors can influence EPCs' homeostasis and function. From those studies emerged that EPCs changes are associated with cardiovascular risk factors (diabetes, aging, dyslipidemia, hypertension, atherosclerotic disease, etc.), but also with environmental conditions, such as the exposure to air pollution (Chen et al., 2016; Arcangeli et al., 2017; Singh et al., 2021). In particular, some evidence has indicated that the number and function of EPCs significantly decrease in animals after $PM_{2.5}$ exposure, principally due to the increase of reactive oxygen species (ROS) levels and inflammation (Cui et al., 2016). The study of Cui et al. on C57BL/6 mice exposed to PM for 1 month demonstrated a strong decrease of circulating EPCs due to increased apoptosis via ROS production. Indeed, they observed the high amount of intracellular ROS in circulating EPCs in mice exposed to PM compared to the control group, as the major cause of increased apoptosis of EPCs (Cui et al., 2015b). The findings of variations in EPC number due to air pollution's redox-active constituents suggest that PM exposure influences EPC levels by inducing oxidative stress.

Another study conducted on both human and mice by O'Toole et al. revealed that high $PM_{2.5}$ level exposure causes a reversible vascular injury, attested by the suppression of EPCs' number (O'Toole et al., 2010). The same research group also performed a second study in which mice were exposed for nine consecutive days to concentrated ambient $PM_{2.5}$ (CAP), reporting a decrease in the number of circulating EPCs, VEGF-stimulated aortic Akt phosphorylation, and plasma NO levels in *wild-type* mice but not in those overexpressing extracellular superoxide dismutase (ecSOD-Tg). The study also indicates that EPCs from CAP-exposed ecSOD-Tg mice were able to restore hindlimb ischemia when injected post-hindlimb perfusion (Haberzettl et al., 2018). All these findings suggest that $PM_{2.5}$ impairs the vascular endothelial damage repair by altering the abundance and function of EPCs (Liang et al., 2020).

Furthermore, it has been observed that PM exposure not only affects circulating EPCs but also significantly decreases the population of bone marrow stem cells (BMSCs) (Abplanalp et al., 2019), causing a decreased proliferation of these cells via ROS-mediated mechanism in association with Akt pathway inhibition (Cui et al., 2015a). Thus, PM exposure, leading to a decreased number and function of BMSCs, could partially result in an impaired EPCs' number and function. However, it appears that different EPC subpopulations are differentially affected by PM exposure. Diverse effects based on particles size have been

TABLE 2 | Effects of air pollutants on different EPC populations.

Air Pollutants	*Effects*	Source
Ni-$PM_{0,1}$	↓ number and function of bone marrow-resident CD34 + KDR + cells	Ref. (Liberda et al., 2010)
Ni-$PM_{0,1}$	↑ number of bone marrow and circulating Sca-1+KDR + $CD45^-$ cells	Ref. (Liberda et al., 2014)
CAP	↓ number of circulating Sca-1+KDR + cells	Ref. (Haberzettl et al., 2018)
	↑ number of bone marrow-resident Sca-1+KDR + cells	
$PM_{2.5}$	↓ number of circulating CD31 + CD34 + CD45 + CD133 + cells	Ref. (O'Toole et al., 2010)
	↑ number of bone marrow Sca-1+KDR + cells	Ref. (Haberzettl et al., 2012)
	↓ number of circulating CD34 + KDR+, CD34 + KDR + $CD45^-$, CD34 + KDR + CD133 + cells	Ref. (Niu et al., 2013)
Outdoor $PM_{2.5}$ and $PM_{0.1}$	↑ number of circulating CD34 + CD133+ and CD31 + CD133 + cells	Ref. (DeJarnett et al., 2015)
Indoor $PM_{2.5}$ and $PM_{0.1}$	↑ number of circulating CD34 + CD133 + KDR + cells	Ref. (Jantzen et al., 2016)
	↓ number of circulating CD34 + KDR + cells	
PM_{10}	↑ number of circulating CD34 + CD133 + cells	Ref. (Brook et al., 2013)

Ni-PM0.1 = nickel nanoparticles; CAP, concentrated ambient $PM_{2.5}$.

reported in various studies (**Table 2**), all indicating that EPCs are early, sensitive, and direct targets of air pollution exposure (Liberda et al., 2010; O'Toole et al., 2010; Haberzettl et al., 2012; Niu et al., 2013; Brook et al., 2013; Liberda et al., 2014; DeJarnett et al., 2015; Jantzen et al., 2016; Haberzettl et al., 2018; Li et al., 2021).

Interestingly, sex differences seem to occur in EPC population changes after PM exposure, as demonstrated by Liu et al. in two studies performed on male and female C57BL/6 PM-exposed mice. They observed that PM exposure leads to a decrease of circulating EPCs' number in male via increased oxidative stress, without affecting the circulating EPCs' population in females independent of estrogen (Liu et al., 2021). Indeed, PM exposure-induced reduction of circulating and bone marrow's EPC populations, ascribable to the significant increase of ROS production observed in male, not female, mice, may be due to the decreased expression of SOD1 in male mice (Liu et al., 2022).

Li et al. performed a transcriptomic analysis of cells isolated from CAP-exposed mice, with the aim to identify $PM_{2.5}$-dependent mRNA and miRNA expression changes associated with reduced levels of circulating EPCs and in their proliferation and angiogenic potential defects. They identified, in EPCs derived from CAP-exposed mice, 55 upregulated and 53 downregulated miRNA involved in cell movement, cell death and survival, cellular development, and cell growth and proliferation. In the same group, they also found 122 upregulated and 44 downregulated genes, principally implicated in the regulation of cell movement, cell and tissue development, and cellular assembly and organization. For instance, CXCR3, the receptor for multiple CXC chemokines that promote the mobilization and migration of EPCs, was downregulated in CAP-exposed mice, thus limiting the availability of these cells for the repair of distal tissue damage. Likewise, the downregulation of angiopoietin receptor Tek (Tie2) implies an inefficient EPC maturation in exposed mice. Among the other genes, the proto-oncogene Myc was upregulated, in accordance with the idea that $PM_{2.5}$ may hamper EPC differentiation. Likewise, the upregulation of the pro-inflammatory cytokine Ccl5 suggests a mechanism by which $PM_{2.5}$-exposed EPCs remain in an early, immature state, and thus inefficient in promoting vascular repair. All these results suggest that $PM_{2.5}$-induced changes in gene expression may contribute to EPC dysfunction and such changes may contribute to the adverse cardiovascular outcomes of air pollution exposure (Li et al., 2021).

CONCLUSION

Several epidemiological studies positively associate air pollutants exposure with CVDs' development risk. In particular, the urban $PM_{2.5}$ have been attributed vascular endothelial dysfunction and increased inflammation, which partially promote coagulation-thrombosis and ischemic risk, atherosclerosis, and hypertension, thus promoting and/or accelerating cardiovascular events. $PM_{2.5}$ prevalently exert their effects via oxidative stress and inflammation, and their ability to easily translocate to the blood circulation could account for the widespread effects of these particles around the body; however, the mechanisms remain not completely understood. $PM_{2.5}$ induce VECs' toxicity and affect their physiological functions, also regulating a set of endothelium-related biomarkers including EPCs. Taken together, the reviewed studies demonstrate that $PM_{2.5}$ exposure leads to EPCs' dysfunction and altered homeostasis, which in turn contribute to the increased CVDs' risk. Thus, EPCs' level and functionality may represent a sensitive biomarker of endothelial injury caused by PM exposure. Furthermore, circulating EPC responses to PM exposure, as well as the responsible mechanistic pathways, may differ between acute and chronic exposures. Indeed, long-term air pollution exposure has been associated with lower levels of EPCs, as a result of cumulative damage to the bone marrow or circulating EPCs, impaired EPCs' release, and/or decrease of bioavailable EPCs because of their continuous mobilization and subsequent exhaustion. On the contrary, short-term exposure to high doses of PM more likely seems to resemble the biological responses associated with acute EPC levels increase (as myocardial ischemia, exercise, etc.), reflecting the natural mobilization of these cells for endothelial damage repair after PM exposure (Brook et al., 2013). Despite the link between air pollution and EPCs' dysfunctions is clearly established, the mechanisms whereby different exposure times (long/short-term) could have opposite effects on EPCs' number and function remain to be fully elucidated. In addition, the possibility that different EPC subpopulations may be differentially affected by PM exposure should be further investigated.

In conclusion, the association between the long-term exposure to ambient fine particles and the risk of cardiovascular disease development implies the need to improve the air pollution abatement for CVD prevention. On the other hand, in addition to good habits (i.e., healthy nutrition, healthy sleeping, and exercise (Kampfrath et al., 2011; Lui et al., 2013; Souza et al., 2020)), new strategies of intervention and prevention are required to improve EPCs' number and function in order to mitigate the adverse effects of polluted air on human health.

AUTHOR CONTRIBUTIONS

GP: conceptualization and manuscript revision; AC: text writing and bibliography.

REFERENCES

Abplanalp, W., Haberzettl, P., Bhatnagar, A., Conklin, D. J., and O'Toole, T. E. (2019). Carnosine Supplementation Mitigates the Deleterious Effects of Particulate Matter Exposure in Mice. *J. Am. Heart Assoc.* 8 (13), e013041. doi:10.1161/JAHA.119.013041

Arcangeli, A., Lastraioli, E., Piccini, B., D'Amico, M., Lenzi, L., Pillozzi, S., et al. (2017). Circulating Endothelial Progenitor Cells in Type 1 Diabetic Patients: Relation with Patients' Age and Disease Duration. *Front. Endocrinol. (Lausanne)* 8 (OCT), 278. doi:10.3389/fendo.2017.00278

Asahara, T., Murohara, T., Sullivan, A., Silver, M., Van Der Zee, R., Li, T., et al. (1997). Isolation of Putative Progenitor Endothelial Cells for Angiogenesis. *Science* 275 (5302), 964–967. doi:10.1126/science.275.5302.964

Assmus, B., Schächinger, V., Teupe, C., Britten, M., Lehmann, R., Döbert, N., et al. (2002). Transplantation of Progenitor Cells and Regeneration Enhancement in Acute Myocardial Infarction (TOPCARE-AMI). *Circulation* 106 (24), 3009–3017. doi:10.1161/01.cir.0000043246.74879.cd

Bayraktutan, U. (2019). Endothelial Progenitor Cells: Potential Novel Therapeutics for Ischaemic Stroke. *Pharmacol. Res.* 144 (January), 181–191. Available from. doi:10.1016/j.phrs.2019.04.017

Brook, R. D., Bard, R. L., Kaplan, M. J., Yalavarthi, S., Morishita, M., Dvonch, J. T., et al. (2013). The Effect of Acute Exposure to Coarse Particulate Matter Air Pollution in a Rural Location on Circulating Endothelial Progenitor Cells: Results from a Randomized Controlled Study. *Inhal. Toxicol.* 25 (10), 587–592. doi:10.3109/08958378.2013.814733

Brook, R. D., Rajagopalan, S., Pope, C. A., Brook, J. R., Bhatnagar, A., Diez-Roux, A. V., et al. (2010). Particulate Matter Air Pollution and Cardiovascular Disease. *Circulation* 121 (21), 2331–2378. doi:10.1161/cir.0b013e3181dbece1

Cao, Y. (2018). The Toxicity of Nanoparticles to Human Endothelial Cells. *Adv. Exp. Med. Biol.* 1048, 59–69. doi:10.1007/978-3-319-72041-8_4

Cascetta, E., Henke, I., and Di Francesco, L. (2021). The Effects of Air Pollution, Sea Exposure and Altitude on Covid-19 Hospitalization Rates in italy. *Int. J. Environ. Res. Public Health* 18 (2), 1–11. doi:10.3390/ijerph18020452

Chen, L., Ding, M.-L., Wu, F., He, W., Li, J., Zhang, X.-Y., et al. (2016). Impaired Endothelial Repair Capacity of Early Endothelial Progenitor Cells in Hypertensive Patients with Primary Hyperaldosteronemia. *Hypertension* 67 (2), 430–439. doi:10.1161/hypertensionaha.115.06597

Chen, Y., Hu, K., Bu, H., Si, Z., Sun, H., Chen, L., et al. (2018). Probucol Protects Circulating Endothelial Progenitor Cells from Ambient pm2.5 Damage via Inhibition of Reactive Oxygen Species and Inflammatory Cytokine Production *In Vivo*. *Exp. Ther. Med.* 16 (6), 4322–4328. doi:10.3892/etm.2018.6791

Cui, Y., Jia, F., He, J., Xie, X., Li, Z., Fu, M., et al. (2015). Ambient Fine Particulate Matter Suppresses *In Vivo* Proliferation of Bone Marrow Stem Cells through Reactive Oxygen Species Formation. *PLoS One* 10 (6), 1–14. doi:10.1371/journal.pone.0127309

Cui, Y., Sun, Q., and Liu, Z. (2016). Ambient Particulate Matter Exposure and Cardiovascular Diseases: A Focus on Progenitor and Stem Cells. *J. Cell. Mol. Med.* 20 (5), 782–793. doi:10.1111/jcmm.12822

Cui, Y., Xie, X., Jia, F., He, J., Li, Z., Fu, M., et al. (2015). Ambient Fine Particulate Matter Induces Apoptosis of Endothelial Progenitor Cells through Reactive Oxygen Species Formation. *Cell. Physiol. Biochem.* 35 (1), 353–363. doi:10.1159/000369701

Daiber, A., Steven, S., Weber, A., Shuvaev, V. V., Muzykantov, V. R., Laher, I., et al. (2017). Targeting Vascular (Endothelial) Dysfunction. *Br. J. Pharmacol.* 174 (12), 1591–1619. doi:10.1111/bph.13517

DeJarnett, N., Yeager, R., Conklin, D. J., Lee, J., O'Toole, T. E., McCracken, J., et al. (2015). Residential Proximity to Major Roadways Is Associated with Increased Levels of AC133 + Circulating Angiogenic Cells. *Atvb* 35 (11), 2468–2477. doi:10.1161/atvbaha.115.305724

Fadini, G. P., Losordo, D., and Dimmeler, S. (2012). Critical Reevaluation of Endothelial Progenitor Cell Phenotypes for Therapeutic and Diagnostic Use. *Circ. Res.* 110 (4), 624–637. doi:10.1161/circresaha.111.243386

Fan, Y., Ye, J., Shen, F., Zhu, Y., Yeghiazarians, Y., Zhu, W., et al. (2008). Interleukin-6 Stimulates Circulating Blood-Derived Endothelial Progenitor Cell Angiogenesis *In Vitro*. *J. Cereb. Blood Flow. Metab.* 28 (1), 90–98. doi:10.1038/sj.jcbfm.9600509

Franchini, M., and Mannucci, P. M. (2011). Thrombogenicity and Cardiovascular Effects of Ambient Air Pollution. *Blood [Internet]* 118 (9), 2405–2412. Available from. doi:10.1182/blood-2011-04-343111

Groleau, J., Dussault, S., Haddad, P., Turgeon, J., Me´nard, C., Chan, J. S., et al. (2010). Essential Role of Copper-Zinc Superoxide Dismutase for Ischemia-Induced Neovascularization via Modulation of Bone Marrow-Derived Endothelial Progenitor Cells. *Atvb* 30 (11), 2173–2181. doi:10.1161/atvbaha.110.212530

Haberzettl, P., Conklin, D. J., Abplanalp, W. T., Bhatnagar, A., and O'Toole, T. E. (2018). Inhalation of Fine Particulate Matter Impairs Endothelial Progenitor Cell Function via Pulmonary Oxidative Stress. *Atvb* 38 (1), 131–142. doi:10.1161/atvbaha.117.309971

Haberzettl, P., Lee, J., Duggineni, D., McCracken, J., Bolanowski, D., O'Toole, T. E., et al. (2012). Exposure to Ambient Air Fine Particulate Matter Prevents VEGF-Induced Mobilization of Endothelial Progenitor Cells from the Bone Marrow. *Environ. Health Perspect.* 120 (6), 848–856. doi:10.1289/ehp.1104206

Hayes, R. B., Lim, C., Zhang, Y., Cromar, K., Shao, Y., Reynolds, H. R., et al. (2020). PM2.5 Air Pollution and Cause-specific Cardiovascular Disease Mortality. *Int. J. Epidemiol.* 49 (1), 25–35. doi:10.1093/ije/dyz114

Heissig, B., Hattori, K., Dias, S., Friedrich, M., Ferris, B., Hackett, N. R., et al. (2002). Recruitment of Stem and Progenitor Cells from the Bone Marrow Niche Requires MMP-9 Mediated Release of Kit-Ligand. *Cell* 109 (5), 625–637. doi:10.1016/s0092-8674(02)00754-7

Horstman, L. L., Jy, W., Jimenez, J. J., and Ahn, Y. S. (2004). Endothelial Microparticles as Markers of Endothelial Dysfunction. *Front. Biosci.* 9, 1118–1135. doi:10.2741/1270

Hu, H., Wu, J., Li, Q., Asweto, C., Feng, L., Yang, X., et al. (2016). Fine Particulate Matter Induces Vascular Endothelial Activation via IL-6 Dependent JAK1/STAT3 Signaling Pathway. *Toxicol. Res.* 5 (3), 946–953. doi:10.1039/c5tx00351b

Hutter, H. P., Poteser, M., Moshammer, H., Lemmerer, K., Mayer, M., Weitensfelder, L., et al. (2020). Air Pollution Is Associated with Covid-19 Incidence and Mortality in Vienna, Austria. *Int. J. Environ. Res. Public Health* 17 (24), 1–11. doi:10.3390/ijerph17249275

Jantzen, K., Møller, P., Karottki, D. G., Olsen, Y., Bekö, G., Clausen, G., et al. (2016). Exposure to Ultrafine Particles, Intracellular Production of Reactive Oxygen Species in Leukocytes and Altered Levels of Endothelial Progenitor Cells. *Toxicology* 359-360, 11–18. Available from. doi:10.1016/j.tox.2016.06.007

Jian, D., Wang, W., Zhou, X., Jia, Z., Wang, J., Yang, M., et al. (2018). Interferon-induced Protein 35 Inhibits Endothelial Cell Proliferation, Migration and Re-endothelialization of Injured Arteries by Inhibiting the Nuclear Factor-Kappa B Pathway. *Acta Physiol.* 223 (3), e13037. doi:10.1111/apha.13037

Jun, X., Jin, G., Fu, C., Jinxuan, Z., Xueling, L., Jiaxin, H., et al. (2018). PM2.5 Promotes Abdominal Aortic Aneurysm Formation in Angiotensin Ⅱ-infused Apoe-/- Mkice. *Biomed. Pharmacother.* 104 (December 2017), 550–557. Available from. doi:10.1016/j.biopha.2018.04.107

Kampfrath, T., Maiseyeu, A., Ying, Z., Shah, Z., Deiuliis, J. A., Xu, X., et al. (2011). Chronic Fine Particulate Matter Exposure Induces Systemic Vascular Dysfunction via NADPH Oxidase and TLR4 Pathways. *Circ. Res.* 108 (6), 716–726. doi:10.1161/circresaha.110.237560

Lakey, P. S. J., Berkemeier, T., Tong, H., Arangio, A. M., Lucas, K., Pöschl, U., et al. (2016). Chemical Exposure-Response Relationship between Air Pollutants and Reactive Oxygen Species in the Human Respiratory Tract. *Sci. Rep.* 6 (August), 1–6. Available from. doi:10.1038/srep32916

Lau, D., and Baldus, S. (2006). Myeloperoxidase and its Contributory Role in Inflammatory Vascular Disease. *Pharmacol. Ther.* 111 (1), 16–26. doi:10.1016/j.pharmthera.2005.06.023

Lelieveld, J., Evans, J. S., Fnais, M., Giannadaki, D., and Pozzer, A. (2015). The Contribution of Outdoor Air Pollution Sources to Premature Mortality on a Global Scale. *Nature* 525 (7569), 367–371. doi:10.1038/nature15371

Li, L. Z., Yuan, X. Y., Wang, Y. M., Zhou, W., Zhao, J., and Peng, S. Q. (2016). PM2.5 Induces Oxidative Damage and Affects Nuclear Factor-Erythroid 2 Related Factor 2 Pathway in Human Umbilical Vein Endothelial Cells. *Zhonghua Yu Fang. Yi Xue Za Zhi* 50 (8), 710–715. doi:10.3760/cma.j.issn.0253-9624.2016.08.008

Li, X., Haberzettl, P., Conklin, D. J., Bhatnagar, A., Rouchka, E. C., Zhang, M., et al. (2021). Exposure to Fine Particulate Matter Air Pollution Alters Mrna and Mirna Expression in Bone Marrow-Derived Endothelial Progenitor Cells from Mice. *Genes. (Basel).* 12 (7), 1058. doi:10.3390/genes12071058

Liang, S., Zhang, J., Ning, R., Du, Z., Liu, J., Batibawa, J. W., et al. (2020). The Critical Role of Endothelial Function in Fine Particulate Matter-Induced Atherosclerosis. *Part Fibre Toxicol.* 17 (1), 61. doi:10.1186/s12989-020-00391-x

Liang, S., Zhao, T., Xu, Q., Duan, J., and Sun, Z. (2021). Evaluation of Fine Particulate Matter on Vascular Endothelial Function *In Vivo* and *In Vitro*. *Ecotoxicol. Environ. Saf.* 222, 112485. Available from:. doi:10.1016/j.ecoenv.2021.112485

Liberda, E. N., Cuevas, A. K., Gillespie, P. A., Grunig, G., Qu, Q., and Chen, L. C. (2010). Exposure to Inhaled Nickel Nanoparticles Causes a Reduction in Number and Function of Bone Marrow Endothelial Progenitor Cells. *Inhal. Toxicol.* 22 (Suppl. 2), 95–99. doi:10.3109/08958378.2010.515269

Liberda, E. N., Cuevas, A. K., Qu, Q., and Chen, L. C. (2014). The Acute Exposure Effects of Inhaled Nickel Nanoparticles on Murine Endothelial Progenitor Cells. *Inhal. Toxicol.* 26 (10), 588–597. doi:10.3109/08958378.2014.937882

Liu, X., Wang, A., Chen, Z., Cui, Y., Hao, H., Domeier, T. L., et al. (2022). Tempol Preserves Endothelial Progenitor Cells in Male Mice with Ambient Fine Particulate Matter Exposure. *Biomedicines* 10 (2), 1–11. doi:10.3390/biomedicines10020327

Liu, X., Xiao, Y., Zhu, Q., Cui, Y., Hao, H., Wang, M., et al. (2021). Circulating Endothelial Progenitor Cells Are Preserved in Female Mice Exposed to Ambient Fine Particulate Matter Independent of Estrogen. *Int. J. Mol. Sci.* 22 (13), 7200. doi:10.3390/ijms22137200

Lui, M. M.-S., Tse, H.-F., Mak, J. C.-W., Lam, J. C.-M., Lam, D. C.-L., Tan, K. C. B., et al. (2013). Altered Profile of Circulating Endothelial Progenitor Cells in Obstructive Sleep Apnea. *Sleep. Breath.* 17 (3), 937–942. doi:10.1007/s11325-012-0781-4

McGuinn, L. A., Schneider, A., McGarrah, R. W., Ward-Caviness, C., Neas, L. M., Di, Q., et al. (2019). Association of Long-Term PM2.5 Exposure with Traditional and Novel Lipid Measures Related to Cardiovascular Disease Risk. *Environ. Int.* 122, 193–200. doi:10.1016/j.envint.2018.11.001

Miller, M. R., and Newby, D. E. (2020). Air Pollution and Cardiovascular Disease: Car Sick. *Cardiovasc Res.* 116 (2), 279–294. doi:10.1093/cvr/cvz228

Montiel-Dávalos, A., Alfaro-Moreno, E., and López-Marure, R. (2007). PM2.5 and PM10 Induce the Expression of Adhesion Molecules and the Adhesion of Monocytic Cells to Human Umbilical Vein Endothelial Cells. *Inhal. Toxicol.* 19 (Suppl. 1), 91–98. doi:10.1080/08958370701495212

Niu, J., Liberda, E. N., Qu, S., Guo, X., Li, X., Zhang, J., et al. (2013). The Role of Metal Components in the Cardiovascular Effects of PM2.5. *PLoS One* 8 (12), e83782. doi:10.1371/journal.pone.0083782

O'Toole, T. E., Hellmann, J., Wheat, L., Haberzettl, P., Lee, J., Conklin, D. J., et al. (2010). Episodic Exposure to Fine Particulate Air Pollution Decreases Circulating Levels of Endothelial Progenitor Cells. *Circ. Res.* 107 (2), 200–203. doi:10.1161/CIRCRESAHA.110.222679

Ohlwein, S., Kappeler, R., Kutlar Joss, M., Künzli, N., and Hoffmann, B. (2019). Health Effects of Ultrafine Particles: A Systematic Literature Review Update of Epidemiological Evidence. *Int. J. Public Health* 64 (4), 547–559. doi:10.1007/s00038-019-01202-7

Orlic, D., Kajstura, J., Chimenti, S., Limana, F., Jakoniuk, I., Quaini, F., et al. (2001). Mobilized Bone Marrow Cells Repair the Infarcted Heart, Improving Function and Survival. *Proc. Natl. Acad. Sci. U.S.A.* 98 (18), 10344–10349. doi:10.1073/pnas.181177898

Petit, I., Jin, D., and Rafii, S. (2007). The SDF-1-CXCR4 Signaling Pathway: A Molecular Hub Modulating Neo-Angiogenesis. *Trends Immunol.* 28 (7), 299–307. doi:10.1016/j.it.2007.05.007

Rao, G. H. (2018). Cardiometabolic Diseases: A Global Perspective. *J. Cardiol. Cardiovasc Ther.* 12 (2), 1–6. doi:10.19080/jocct.2018.12.555834

Rui, W., Guan, L., Zhang, F., Zhang, W., and Ding, W. (2016). PM2.5-induced Oxidative Stress Increases Adhesion Molecules Expression in Human Endothelial Cells through the ERK/AKT/NF-κB-dependent Pathway. *J. Appl. Toxicol.* 36 (1), 48–59. doi:10.1002/jat.3143

Salgado, M. V., Smith, P., Opazo, M. A., and Huneeus, N. (2021). Long-term Exposure to Fine and Coarse Particulate Matter and Covid-19 Incidence and Mortality Rate in chile during 2020. *Int. J. Environ. Res. Public Health* 18 (14), 7409. doi:10.3390/ijerph18147409

Sekiguchi, H., Ii, M., and Losordo, D. W. (2009). The Relative Potency and Safety of Endothelial Progenitor Cells and Unselected Mononuclear Cells for Recovery from Myocardial Infarction and Ischemia. *J. Cell. Physiol.* 219 (2), 235–242. doi:10.1002/jcp.21672

Singh, P., O'Toole, T. E., Conklin, D. J., Hill, B. G., and Haberzettl, P. (2021). Endothelial Progenitor Cells as Critical Mediators of Environmental Air Pollution-Induced Cardiovascular Toxicity. *Am. J. Physiology-Heart Circulatory Physiology* 320 (4), H1440–H1455. doi:10.1152/ajpheart.00804.2020

Souza, L. V., De Meneck, F., Fernandes, T., Oliveira, E. M., and Franco, M. d. C. (2020). Physical Activity Intervention Improved the Number and Functionality of Endothelial Progenitor Cells in Low Birth Weight Children. *Nutr. Metabolism Cardiovasc. Dis.* 30 (1), 60–70. Available from. doi:10.1016/j.numecd.2019.08.011

Thum, T., Fraccarollo, D., Galuppo, P., Tsikas, D., Frantz, S., Ertl, G., et al. (2006). Bone Marrow Molecular Alterations after Myocardial Infarction: Impact on Endothelial Progenitor Cells. *Cardiovasc. Res.* 70 (1), 50–60. doi:10.1016/j.cardiores.2006.01.002

Tofler, G. H., and Muller, J. E. (2006). Triggering of Acute Cardiovascular Disease and Potential Preventive Strategies. *Circulation* 114 (17), 1863–1872. doi:10.1161/circulationaha.105.596189

Werner, N., Kosiol, S., Schiegl, T., Ahlers, P., Walenta, K., Link, A., et al. (2005). Circulating Endothelial Progenitor Cells and Cardiovascular Outcomes. *N. Engl. J. Med.* 353 (10), 999–1007. doi:10.1056/nejmoa043814

Wilkins, E., Wilson, L., Wickramasinghe, K., Bhatnagar, P., Leal, J., Luengo-Fernandez, R., et al. (2017). European Cardiovascular Disease Statistics 2017, European Heart Network, Brussels. *Eur. Cardiovasc Dis. Stat.* 34 (39), 3028–3034. Available at: http://www.ehnheart.org/images/CVD-statistics-report-August-2017.pdf

Wollert, K. C., Meyer, G. P., Lotz, J., Ringes Lichtenberg, S., Lippolt, P., Breidenbach, C., et al. (2004). Intracoronary Autologous Bone-Marrow Cell Transfer after Myocardial Infarction: The BOOST Randomised Controlled Clinical Trial. *Lancet* 364, 141–148. doi:10.1016/s0140-6736(04)16626-9

World health statistics (2021). *Monitoring health for the SDGs, sustainable development goals*. Geneva: World Health Organization.

Xie, W., You, J., Zhi, C., and Li, L. (2021). The Toxicity of Ambient Fine Particulate Matter (PM2.5) to Vascular Endothelial Cells. *J. Appl. Toxicol.* 41 (5), 713–723. doi:10.1002/jat.4138

Conflict of Interest: The authors declare that the research was conducted in the absence of any commercial or financial relationships that could be construed as a potential conflict of interest.

Publisher's Note: All claims expressed in this article are solely those of the authors and do not necessarily represent those of their affiliated organizations, or those of the publisher, the editors, and the reviewers. Any product that may be evaluated in this article, or claim that may be made by its manufacturer, is not guaranteed or endorsed by the publisher.

frontiers | Frontiers in Cell and Developmental Biology

ORIGINAL RESEARCH
published: 30 May 2022
doi: 10.3389/fcell.2022.886879

Mature Myotubes Generated From Human-Induced Pluripotent Stem Cells Without Forced Gene Expression

*Kei Fujiwara[1], Risa Yamamoto[2], Tomoya Kubota[2], Atsutoshi Tazumi[3], Tomoka Sabuta[1], Masanori P. Takahashi[2] and Hidetoshi Sakurai[1]**

[1]Center for iPS Cell Research and Application (CiRA), Kyoto University, Kyoto, Japan, [2]Clinical Neurophysiology, Department of Clinical Laboratory and Biomedical Sciences, Division of Health Sciences, Osaka University Graduate School of Medicine, Osaka, Japan, [3]Laboratory for Pharmacology, Pharmaceutical Research Center, Asahi Kasei Pharma Corporation, Shizuoka, Japan

Human-induced pluripotent stem cells (hiPSCs) are a promising tool for disease modeling and drug screening. To apply them to skeletal muscle disorders, it is necessary to establish mature myotubes because the onset of many skeletal muscle disorders is after birth. However, to make mature myotubes, the forced expression of specific genes should be avoided, as otherwise dysregulation of the intracellular networks may occur. Here, we achieved this goal by purifying hiPSC-derived muscle stem cells (iMuSC) by Pax7-fluorescence monitoring and antibody sorting. The resulting myotubes displayed spontaneous self-contraction, aligned sarcomeres, and a triad structure. Notably, the phenotype of sodium channels was changed to the mature type in the course of the differentiation, and a characteristic current pattern was observed. Moreover, the protocol resulted in highly efficient differentiation and high homogeneity and is applicable to drug screening.

Keywords: myogenic differentiation, mature myotube, human iPS cell, transgene free, screening tools

OPEN ACCESS

Edited by:
Atsushi Asakura,
University of Minnesota Twin Cities, United States

Reviewed by:
Yuko Miyagoe-Suzuki,
National Center of Neurology and Psychiatry, Japan
Eiji Wada,
Tokyo Medical University, Japan

****Correspondence:***
Hidetoshi Sakurai
hsakurai@cira.kyoto-u.ac.jp

Specialty section:
This article was submitted to Stem Cell Research, a section of the journal Frontiers in Cell and Developmental Biology

Received: *01 March 2022*
Accepted: *11 April 2022*
Published: *30 May 2022*

Citation:
Fujiwara K, Yamamoto R, Kubota T, Tazumi A, Sabuta T, Takahashi MP and Sakurai H (2022) Mature Myotubes Generated From Human-Induced Pluripotent Stem Cells Without Forced Gene Expression. Front. Cell Dev. Biol. 10:886879. doi: 10.3389/fcell.2022.886879

INTRODUCTION

Many congenital and late-onset myopathies are characterized by the malformation of intracellular structures, such as the triad structure, which is composed of t-tubules and the sarcoplasmic reticulum (SR) (Buj-Bello et al., 2008; Al-Qusairi et al., 2009; Cowling et al., 2014), sarcomeric structures (Li et al., 2020), and nuclei morphology (Davidson and Lammerding, 2014). To investigate the pathophysiology of these disorders *in vitro*, it is necessary to generate mature myotubes with intramuscular structures that form in the late-stage development.

Human-induced pluripotent stem cells (hiPSCs) are a powerful tool for analyzing the pathophysiology of various disorders. In the field of skeletal muscle biology, efficient and stable differentiation methods for the generation of myotubes from hiPSCs have been reported. We generated myotubes by driving the transcription factor *MyoD*, a myogenic gene, exogenously (Tanaka et al., 2013). In this method, myotubes are differentiated directly from hiPSCs for 6–7 days with high purity and efficiency. Using this method, we have successfully established disease models of muscular diseases such as dysferlinopathy (Tanaka et al., 2013), Duchenne muscular dystrophy (Shoji et al., 2015), Pompe disease (Yoshida et al., 2017), and myotonic dystrophy (Ueki et al., 2017). Following the model for dysferlinopathy, a drug screening system was established (Uchimura et al., 2017), and an effective chemical for treatment (Nocodazole) was found (Kokubu et al., 2019). However, these *MyoD*-mediated myotubes are immature and show neither the sarcomeric structure nor the triad structure, making them unsuitable for studying skeletal muscle diseases that occur with late-stage development. Another transcription factor commonly expressed exogenously is

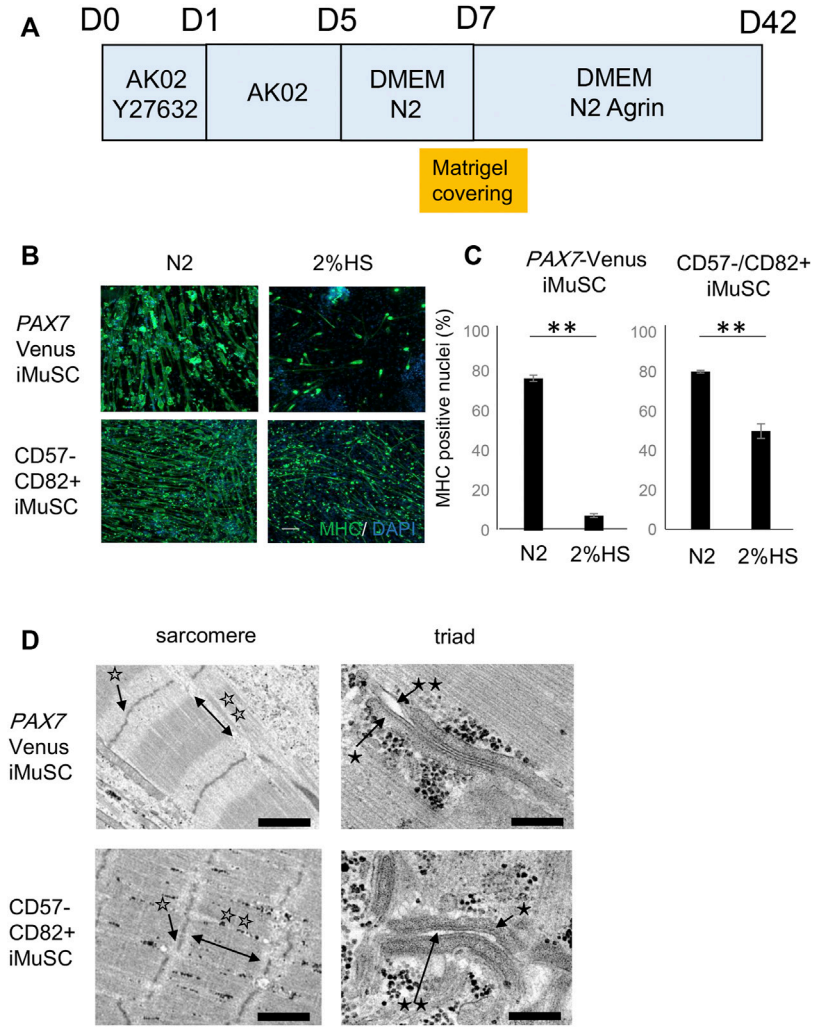

FIGURE 1 | Generation of mature myotubes from iMuSCs *in vitro*. **(A)** Schematic of the myotube differentiation schedule. The proliferation phase of iMuSCs is from days **(D)** 0 to 5. D5 is when the medium is switched to the differentiation medium. D7 is when the 3D Matrigel covering is done. **(B)** Representative images of myotubes (anti-MHC green) in 2% HS and N2 supplement at D14. Scale bar, 1,000 μm. **(C)** Ratio of nuclei of MyHC-positive myotubes to total nuclei in 2% HS and N2 supplement at D14. The ratio was higher in the N2 medium compared with that in the HS medium for both Pax7-Venus iMuSC-derived myotubes (left) and CD57^{-}–CD82^{+} iMuSC-derived myotubes (right). Data are represented as the mean ± SEM. $^{**}p < 0.01$, unpaired two-tailed Student's t-test. **(D)** Representative electron microscopic images of myotubes in m-condition (Matrigel embedding) at D42. Well-aligned sarcomeric structures and triad structures are seen in Pax7-Venus iMuSC-derived myotubes (upper panel) and CD57^{-}–CD82^{+} iMuSC-derived myotubes (lower panel). The white single star (☆) indicates the Z-line, white double stars (☆☆) indicate the A-line, the black single star (*) indicates the sarcoplasmic reticulum, and black double stars (**) indicate t-tubules. Scale bars, 250 nm (PAX7-Venus sarcomere), 200 nm (PAX7-Venus triad), 1,000 nm (CD57^{-}–CD82 $^{+}$ sarcomere), and 200 nm (CD57^{-}–CD82 $^{+}$ triad).

Pax7 (Darabi et al., 2012). Using muscle stem cells obtained by lentiviral-expressed *Pax7*, several groups have produced mature myotubes (Rao et al., 2018; Selvaraj et al., 2019). However, the exogenous expression may disrupt intracellular gene networks.

Skeletal muscles are huge organs with electrical excitability, which is precisely organized by several ion channels and transporters. Among them, the voltage-gated sodium channel (Nav) plays an essential role as the generator of action potentials (Ahern et al., 2016). In the mature skeletal muscle, Nav1.4, which is encoded by *SCN4A* gene, is expressed dominantly, whereas the immature skeletal myotube is known to express a significant amount of Nav1.5, which is encoded by *SCN5A* gene, which is primarily expressed in cardiac myotubes (Yang et al., 1991) (Martínez-Mármol et al., 2007). A well-known difference between them is sensitivity for tetrodotoxin (TTX); Nav1.4 is a TTX-sensitive Nav channel (IC_{50} = 25 nM), whereas Nav1.5 is TTX-resistant (IC_{50} > 1 μM) (Chanine et al., 1994). In addition, electrophysiological experiments using the heterologous expression system have shown that the voltage dependence of Nav1.5 is shifted in the hyperpolarized direction compared to that of Nav1.4; Nav1.5 activates at a lower voltage than Nav1.4 (Sheets and Hanck, 1999; Vilin et al., 2012). These properties influence the physiological excitability of skeletal muscles so that electrophysiological assessments are also important to evaluate the maturity of myotubes from hiPSCs.

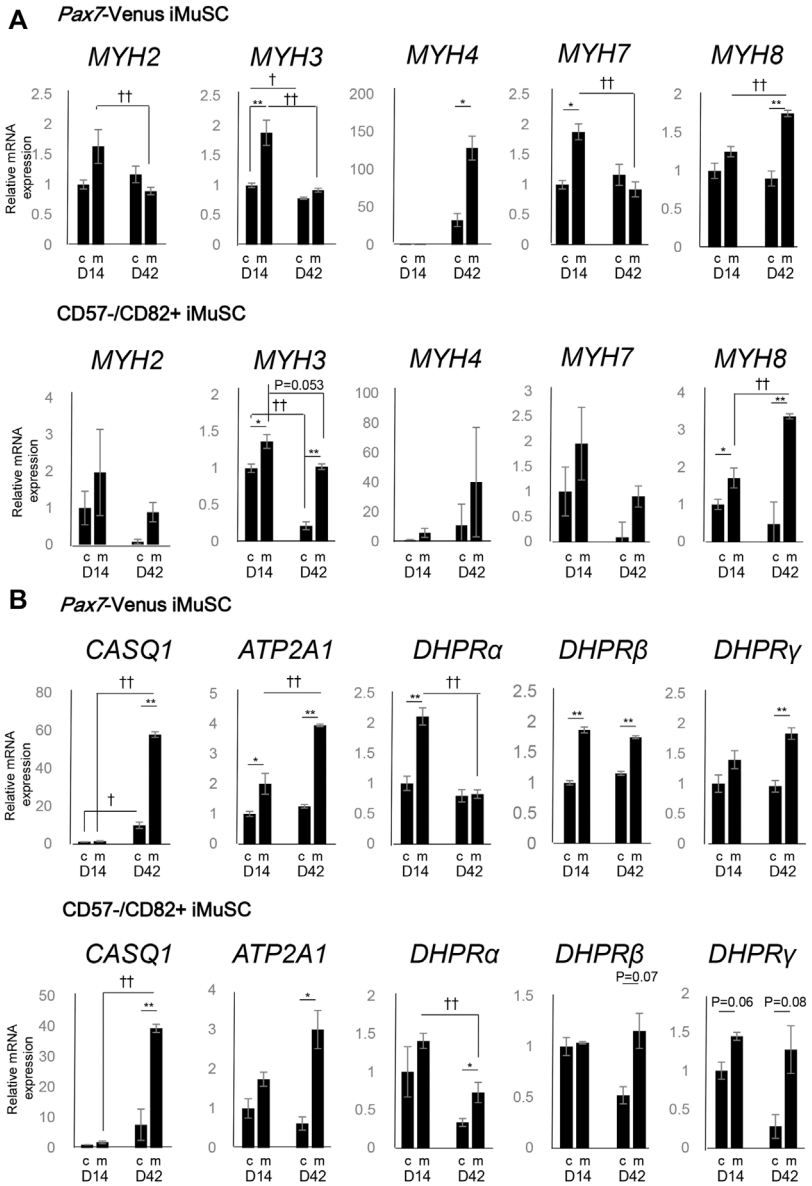

FIGURE 2 | Myosin heavy chain (MYH) subtypes and triad-associated genes display characteristic expression patterns. **(A)** The mRNA expression of the myosin heavy chain family (MYH2, MYH3, MYH4, MYH7, and MYH8) was quantified by real-time PCR. The expression levels of the MYH genes in PAX7-Venus iMuSC-derived myotubes (upper) and in $CD57^{-}$–$CD82^{+}$ iMuSC-derived myotubes (lower) on days 14 and 42 in c-condition (no Matrigel embedding) and m-condition (Matrigel embedding) are shown. **(B)** The mRNA expression of SR-related genes (Casq1 and Atp2a1) and t-tubule-related genes (DHPRα, DHPRβ, and DHPRγ) was quantified by real-time PCR. The expression levels of MYH genes in PAX7-Venus iMuSC-derived myotubes (upper) and in $CD57^{-}$–$CD82^{+}$ iMuSC-derived myotubes (lower) on days 14 and 42 in c-condition and m-condition are shown. The vertical axis of the graph shows the relative expression level normalized by 18S rRNA, the housekeeping gene. The expression level is standardized by the expression level (=1) on day 5. $^{*}p < 0.05$, $^{**}p < 0.01$; c-condition vs. m-condition. †$p < 0.05$, ††$p < 0.01$; day 14 vs. day 42 (unpaired two-tailed Student's t-test). Error bars indicate the standard error of mean (SEM). In each group (day 14c, day 14m, day 42c, and day 42m), three independent samples were used for the analysis.

Recently, we established a protocol to prepare hiPSC-derived muscle stem cells (iMuSCs) using small molecules without driving transcription factors exogenously (Zhao et al., 2020). Using these iMuSCs, here we developed a novel method to produce mature myotubes with well-aligned sarcomeric structures and triad structures *in vitro*. These myotubes displayed mature skeletal muscle characteristics not only in gene expression patterns but also in electrical excitability. Additionally, we differentiated iMuSCs to myotubes with high efficiency and homogeneity in 96 multi-well plates. These findings enable disease modeling and

drug screening of congenital and late-onset myopathies using disease-specific hiPSCs.

RESULTS

Preparation of hiPSC-Derived Muscle Stem Cells (iMuSCs) by Fluorescence Monitoring and Antibody Selection

An illustration of our previous method to generate fetal iMuSCs is shown in **Supplementary Figure S1A** (Zhao et al., 2020). To isolate these iMuSCs, hiPSCs carrying a *PAX7* (satellite cell marker)-Venus reporter was used (Nalbandian et al., 2021). After approximately 80 days of culture, Venus-positive cells appeared in the differentiation culture (**Supplementary Figure S1B**) and were purified by flow cytometry (**Supplementary Figure S1C**). To replace the *PAX7*-Venus reporter hiPSCs, we developed a purification method using antibodies for surface markers. Although several surface markers are reported, we utilized CD82, a marker of progenitor cells in human skeletal muscles (Alexander et al., 2016; Uezumi, A. et al., 2016), as a positive selection marker, and CD57 (also known as HNK-1), a marker of neural crest cells, as a negative selection marker for iMuSCs (Borchin et al., 2013). After staining day-80 differentiated cells with CD82 and CD57 antibodies (see *Methods*), the differentiated cells were separated into four fractions: $CD57^{+}CD82^{+}$, $CD57^{-}$–$CD82^{+}$, $CD57^{+}CD82^{-}$, and $CD57^{-}$–$CD82^{-}$ (**Supplementary Figure S2A**). A gene expression analysis revealed that the $CD57^{-}$–$CD82^{+}$ fraction showed the highest expression level for several muscle stem/progenitor markers including *PAX7, MYF5,* and *MYOD* among the four fractions (**Supplementary Figure S2B**). An immunocytochemical analysis demonstrated that more than 80% of $CD57^{-}$–$CD82^{+}$ cells expressed *PAX7* (**Supplementary Figure S2C**). Together, these results suggest that cell sorting the $CD57^{-}$–$CD82^{+}$ fraction efficiently purifies iMuSCs from non-reporter hiPSCs. Thus, we could obtain iMuSCs by *PAX7*-Venus fluorescence monitoring and by $CD57^{-}$–$CD82^{+}$ antibody selection.

Optimization of Myotube Differentiation From Purified iMuSCs

We then optimized the *in vitro* myotube differentiation of the purified iMuSCs. **Figure 1A** shows a simple scheme of the *in vitro* myotube differentiation protocol. iMuSCs were proliferated to 100% confluence by AK02 media for 5 days (**Supplementary Figure S3A**), at which time we examined the component of differentiation media that affected the myotube differentiation efficiency. N2 supplement was found to promote the induction of myosin heavy chain (MHC)-positive myotubes, which is a hallmark of myogenic differentiation efficiency compared with 2% horse serum (HS) supplement (**Figures 1B,C**).

Generation of Mature Myotubes With Sarcomere and Triad Structures

After switching to differentiation media with N2 supplement, iMuSCs displayed a spindle-like morphology at day 7 of the culture (**Supplementary Figure S3B**). Generally, myotubes are surrounded by connective tissues, such as extracellular matrix, *in vivo*. To imitate this environment, we developed a novel method to embed a high concentration of Matrigel to the culture dish *in vitro* (**Supplementary Figure S4A**) by referring to a previous report (Falcone, S. et al., 2014) that demonstrated murine primary satellite cell maturation *in vitro*. After embedding the Matrigel, iMuSC-derived myotubes began to fuse to each other and displayed spontaneous self-contractions at day 14 of the culture (**Supplementary Figure S3C** and **Supplementary Movie S1**). This feature was more obvious at day 42 of the culture (**Supplementary Figure S3D**).

Mature skeletal muscle is equipped with structures for contraction, such as the sarcomere and triad structures, which is composed of t-tubules and the SR. At day 42 of the culture, the intramuscular structure was evaluated by electron microscopy (**Figure 1D**). Well-aligned sarcomere and triad structures were visible, suggesting that the myotubes were considerably mature.

Finally, we evaluated the effect of Matrigel embedding by comparing the condition with Matrigel embedding (m-condition) to without Matrigel embedding (c-condition) (**Supplementary Figure S4B**). The size of the myotubes was measured between two conditions at day 42 of the culture to assess the maturation level of myotubes. m-condition increased the myotube diameter by 16.5% ($p < 0.013$) if using *PAX7*-Venus iMuSCs and by 19.8% if using $CD57^{-}$–$CD82^{+}$ iMuSCs ($p < 0.009$) (**Supplementary Figures S4C,D**).

Expression of Genes Involved in *MYH* Subtypes and Calcium Homeostasis is Characteristic of Myotube Maturation

To assess the maturity of differentiated myotubes, the expression of *MYH* genes was investigated between c-condition and m-condition at days 14 and 42 using *PAX7*-Venus and $CD57^{-}$–$CD82^{+}$ iMuSC-derived myotubes. The expression of *MYH3* (embryonic subtype) was decreased from day 14 to day 42 in both iMuSC-derived myotube types (**Figure 2A**). This pattern of expression, which indicates a shift from developmental to adult myosin, is consistent with the findings during native muscle development (Schiaffino et al., 2015) and differentiation (Brown et al., 2012). Moreover, the expression of *MYH3* itself was higher in m-condition than in c-condition.

On day 14, the expression of four different *MYH* subtypes associated with postnatal to adult development (*MYH2,4,7,8*) was elevated. Especially on day 42, the expression of *MYH4* was elevated in m-condition compared with that in c-condition in *PAX7*-Venus iMuSC-derived myotubes (**Figure 2A**).

Moreover, the expression of genes related to SR and t-tubules was investigated. On day 42, the expression of SR-related markers (*CASQ1* and *ATP2A1*) was notably elevated in m-condition compared with that in c-condition in *PAX7*-Venus and $CD57^{-}$–$CD82^{+}$ iMuSC-derived myotubes (**Figure 2B**). Also on day 42, the expression of t-tubule-related genes (*DHPRβ* and *DHPRγ*) was elevated in m-condition in both myotube types (**Figure 2B**). Altogether, these results suggest that m-condition promotes mature myotubes *in vitro* more than c-condition.

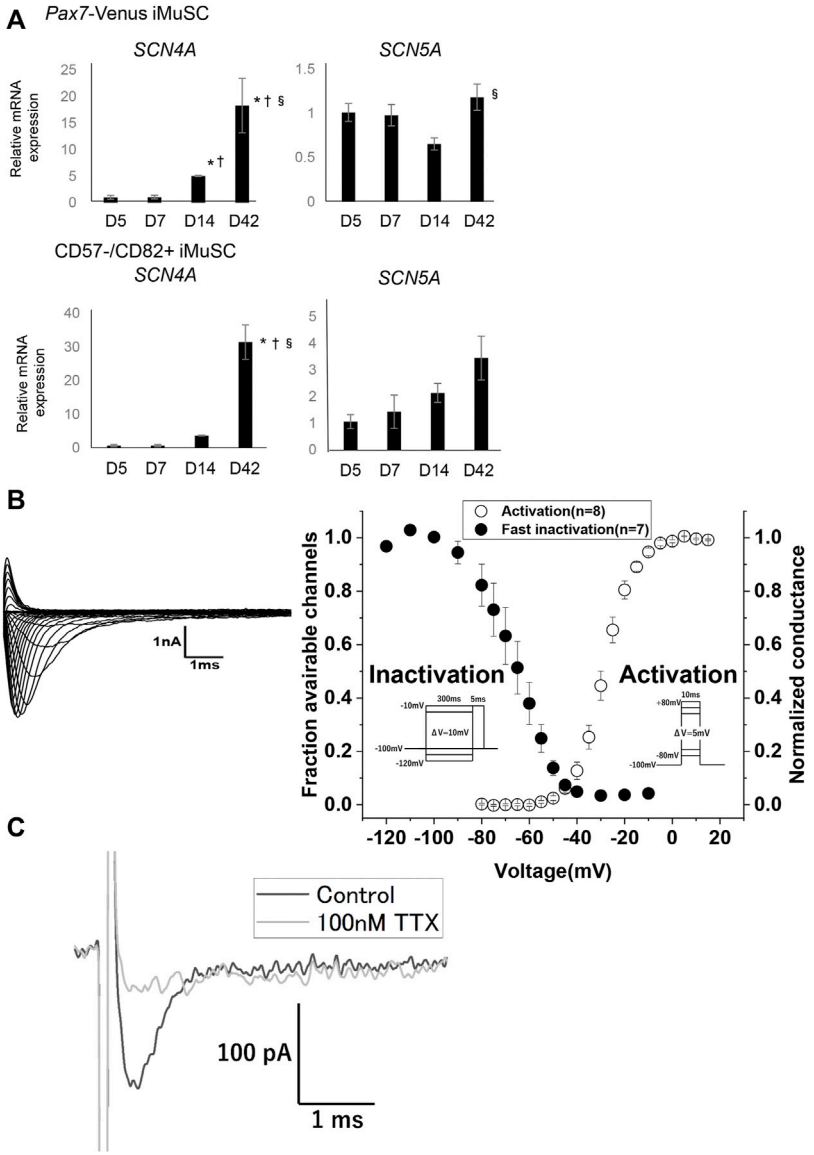

FIGURE 3 | Myotubes have voltage-dependent Na⁺channels, most likely Nav1.4. **(A)** The mRNA expressions of SCN4A, which codes Nav1.4, and SCN5A, which codes Nav1.5, were quantified by real-time PCR. The expression levels of SCN4A and SCN5A in PAX7-Venus iMuSC- and CD57^{-}–CD82^{+} iMuSC-derived myotubes on days 5, 7, 14, and 42 are shown. The vertical axis shows the relative expression level normalized by 18S rRNA, the housekeeping gene. The expression of SCN4A gradually elevated with time. Error bars indicate the standard error of mean (SEM). In each group (days 5, 7, 14, 42), three independent samples were used for the analysis. *$p < 0.05$; vs. day 5. †$p < 0.05$; vs. day 7. §$p < 0.05$; vs. day 14. **(B)** Representative current traces elicited by the activation protocol in PAX7-Venus iMuSCs around day 7 of the culture (left). Voltage dependence of activation (right, open circles) and steady-state fast inactivation (left, filled circles) (right). **(C)** Representative current obtained by the out-side-out patch clamp technique. The black trace indicated the Na + current without TTX elicited by -10 mV test pulse from −100 mV of holding potential. The gray trace indicated the Na + current from the identical cell in the presence of 100 nM TTX elicited by the same test pulse.

Finally, the expression of *MYH*, t-tubules, and SR related genes was investigated in m-condition with or without Agrin to clarify the effect of Agrin for myotube differentiation. The expression of most genes was comparable between with and without Agrin except a slight difference of *MYH3* and *DHPRβ* at day 42. These data indicate that Agrin itself does not have significant effect on the expression of myogenic markers (**Supplementary Figure S5**). However, the triad structure was observed only in the presence of Agrin (**Figure 1D**) and never detected without Agrin condition (data not shown), suggesting that Agrin might have an important role for forming the triad structure.

Myotubes Display Characteristic Electric Properties Related to Sodium Channels

Next, to assess physical maturity, the electrical properties of the myotubes derived from iMuSC were investigated. The gene expressions of *SCN4A* and *SCN5A* were investigated in both

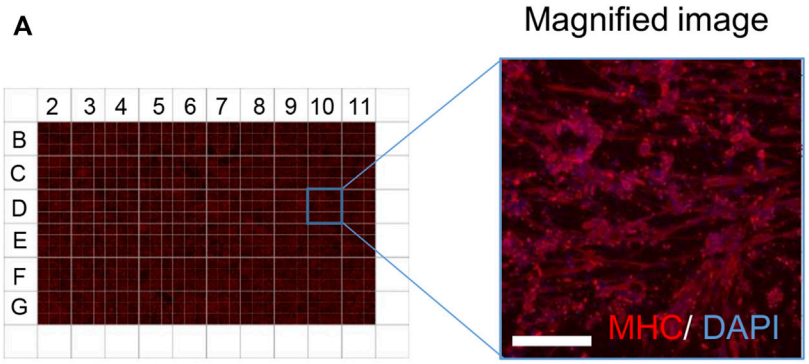

B

	1	2	3	4	5	6	7	8	9	10	11	12
A												
B		69.3	81.6	72.1	79.1	82.8	78	75.2	76.8	76.3	77.3	
C		81.1	79	77.2	78.1	81.1	82.4	80.6	79.8	75	77.4	
D		81.2	81.5	77.8	79.4	77.8	82.1	81.3	80.8	79.7	80.3	
E		79.4	78.6	79	79.7	77	78.2	82.7	81.6	79.1	76.7	
F		80	78.4	82.2	80.6	80	78.9	79.7	79.7	79	77.4	
G		79.3	82.5	77.8	81.7	80	81.6	78	77.7	75.4	76.9	
H												

AVERAGE (%)	79.00767
CV (%)	3.176013

FIGURE 4 | Effective and homogeneous differentiation system in a 96-well plate. **(A)** An image of MHC-stained myotubes (red) in a 96-well plate. A magnified image is also shown. Scale bar, 100 μm. **(B)** Schematic of the 96-well plate used in the screening. (Upper) Numbers in every well indicate the ratio of MHC-positive nuclei to total nuclei (%). (Lower) A bar graph of the ratio of MHC-positive nuclei in the 96-well plate. The average ratio of MHC-positive nuclei and the coefficient of variation (CV) are shown.

PAX7-Venus and $CD57^{-}$–$CD82^{+}$ iMuSC-derived myotubes (**Figure 3A**). Interestingly, *SCN4A* expression both in *PAX7*-Venus and in $CD57^{-}$–$CD82^{+}$ iMuSC-derived myotubes was increased dramatically in a time-dependent manner with the culture. The expression of *SCN5A* was increased in $CD57^{-}$–$CD82^{+}$ iMuSC-derived myotubes as the cells matured but was relatively stable in *PAX7*-Venus iMuSC-derived myotubes. These results suggest that Nav1.4 is dominant in both *PAX7*-Venus and $CD57^{-}$–$CD82^{+}$ iMuSC-derived myotubes.

Additionally, voltage-dependent sodium currents were measured in *PAX7*-Venus iMuSC-derived myotubes using the whole-cell patch-clamp technique. Representative raw traces of sodium currents recorded from cultured cells around day 7 of the culture are shown (**Figure 3B** left). Transient currents were elicited in a voltage-dependent manner, suggesting that currents were derived from Nav channels. To characterize the sodium currents, the kinetics of the channel gating was examined. The voltage dependence of the activation (**Figure 3B**, right, open circles) and the steady-state fast inactivation (**Figure 3B**, filled circles) are shown. The estimated parameters for the intermediate potentials ($V_{1/2}$) and slope factors (k) are listed in **Supplementary Table S2**. Next, we investigated the TTX sensitivity of the Na^{+} current by the out-side-out patch clamp technique, which enables us to expose the membrane to TTX without physical prevention by the Matrigel. In the membrane excised from the myotube around day 11, approximately 140 pA of Na^{+} current was recorded in the conventional bath solution without TTX (**Figure 3C**, black). After exposure of 100 nM TTX, the current was blocked nearly completely (**Figure 3C**, gray), suggesting that the excitability of *PAX7*-Venus iMuSC-derived myotubes relies on the expression of Nav1.4 rather than Nav1.5.

iMuSCs can be Utilized for Multi-Well Screening

hiPSC-based phenotype screening can be used to develop novel drugs (Yamashita, A et al., 2014). To use our myotubes as a resource for drug discovery, iMuSCs were differentiated to

myotubes in a 96-well plate to model a multi-well drug screening system. Only the internal 60 wells in the plate were used because external margins of the plate are not always suitable due to instability of the cell culture (Lundholt, BK et al., 2003). At 28 days of culture, iMuSCs in each of the 60 wells were differentiated to myotubes with high homogeneity and positive for MHC (**Figure 4A**). The average differentiation efficiency was over 79%, and the coefficient of variation number (CV number) was under 3.3% (**Figure 4B**), suggesting that this model satisfied criteria for a multi-well drug screening system.

DISCUSSION

In this article, we succeeded in generating mature myotubes in a transgene-free condition with high efficiency using hiPSC-derived iMuSCs. Because this method does not require unique devices, it is relatively easy to reproduce myotube differentiation. Mature myotubes were generated using commercially available items such as Matrigel, growth factors, and 96-well cell culture plates. Therefore, this multi-well differentiation system is applicable to disease modeling and drug screening.

In the field of skeletal muscle biology, hiPSCs are a promising tool for disease modeling and phenotypic screening (Ortiz-Vitali and Darabi, 2019). However, at present, it is difficult to make mature, physiological myotubes from hiPSCs that are reliable for phenotypic screening. Although our colleague demonstrated that screening applicable mature myocytes could be induced by the MyoD-mediated differentiation method, a contractile stimulation by electric field stimulation is still necessary to induce the sarcomeric structure (Uchimura et al., 2021). Therefore, we aim to develop a more simple method to generate screening applicable mature myotubes from hiPSCs in this study.

Recently, some groups succeeded in making mature myotubes from hiPSCs characterized by the formation of the triad structure by exogenously driving the *PAX7* gene (Rao et al., 2018; Selvaraj et al., 2019). However, this approach may result in abnormal transcriptional networks, which could have adverse effects on the pathophysiological analysis of various muscular diseases. Myotubes generated using growth factors or nutrient factors without exogenous gene expression could solve this problem (Caron et al., 2016; Swartz et al., 2016). However, myotubes generated by chemical compounds lack properties characteristic of mature myotubes, such as the triad structure and elevated *SCN4A* gene expression. Another way to generate mature myotubes is to use specific devices. For example, silicone posts providing continuous tension promote the maturation of hiPSC-derived myotubes (Mafioletti et al., 2018). However, such devices are not suitable for phenotype screening because their material is not easily transferable to such systems. On the other hand, the present study realized mature myotubes that are applicable to phenotype screening.

Several reports have suggested that myotube culture with hydrogel covering promotes differentiation and maturation (Maffioletti et al., 2018; Jensen et al., 2020; Urciuolo et al., 2020). In these reports, Matrigel diluted in the differentiation medium was used as the hydrogel material, and the myotubes indicated maturation by the expression change of various *MYH* gene subtypes. In an environment of Matrigel embedding, myotubes are fully covered with extracellular matrix from all directions, mimicking the environment observed *in vivo*. This condition is likely more suitable for the differentiation of mature myotubes because laminin, entactin, and collagen IV, which are all major components of Matrigel, play important roles in muscle differentiation and maturation (Lee et al., 2015; Penton et al., 2016).

In mature skeletal muscle, Nav1.4 is dominantly expressed, whereas the expression of Nav1.5 is predominant in immature and denervated skeletal muscle (Kallen et al., 1990) (Yang et al., 1991). A previous report showed that Nav1.4 activates at the more depolarized voltage compared with Nav1.5 (Sheets and Hanck, 1999) (Vilin et al., 2012). In addition, the expression ratio of Nav1.4 and Nav1.5 can influence the excitability of the skeletal muscle, such as its sensitivity to pH (Vilin et al., 2012) and intracellular calcium (Ben-Johny et al., 2014). Transient Na^+ currents recorded from *Pax7*-Venus iMuSC-derived myotubes in this study showed that the voltage dependence of activation was more depolarized than that from hiPSC-derived cardiac myotubes (Selga et al., 2018). Moreover, our out-side-out patch clamp recording showed that the Na^+ currents are TTX-sensitive, indicating the existence of a large amount of Nav1.4. These results supported that *Pax7*-Venus iMuSC-derived myotubes implement physiological excitability comparable to the normal skeletal muscle.

A major advancement of hiPSC applications is the detection of therapeutic chemicals by large-scale screening (Ortiz-Vitali and Darabi, 2019). To apply our method accordingly, it is necessary to establish a multi-well system with homogeneous differentiation capacity. CV is an index that measures the variation in each well, and previous reports suggest that a CV<15% is desirable for drug screening (Lariosa-Willingham, K. D. et al., 2016), which is a criterion that our system achieved.

To conclude, we generated mature myotubes without driving exogenous genes. The myotubes displayed a mature character with regard to morphology, gene expression patterns, and sodium channel properties. Thus, our differentiation method for myotubes may be a novel approach to study disease pathophysiologies and to identify therapeutic chemicals for skeletal muscle disorders.

EXPERIMENTAL MODEL AND SUBJECT DETAILS

Human iPSC Lines and Maintenance

Experiments using hiPSCs were approved by the Ethics Committee at the Graduate School and Faculty of Medicine Kyoto University (approval numbers #E1762, #G567, and #Rinsho71). This study was performed conforming to the guidelines of the Declaration of Helsinki and was conducted after obtaining written informed consent.

The hiPSC line 201B7 was generated from purchased fibroblasts of a healthy donor by retroviral transduction (Takahashi et al., 2007). Ff-WJ14s516 (an HLA-homozygous hiPSC line with the most frequent haplotype in Japan; abbreviated as S516 in this manuscript) was established from

cord blood cells by an episomal vector system (Okita et al., 2013) at the Facility for iPS cell Therapy, CiRA, Kyoto University. HiPSCs were cultured in StemFit media (AK02N; Ajinomoto) and passaged once a week. At the passage, the cells were completely detached from a 3.5-cm well in a dish by incubating in 500 µl of Accutase (Nacalai Tesque) for 10 min followed by neutralization with 2 ml of Stemfit media. After pipetting gently, 3×10^5 hiPSCs were seeded on the dish in Stemfit media containing a Rock inhibitor, 10 µM Y-27632 (Nacalai Tesque). The medium was replaced with 1.5 ml of StemFit media without the Rock inhibitor 2, 4, 5, and 6 days after passage. The maximum passage number was 30.

METHOD DETAILS

Purification of iMuSCs

The myogenic differentiation of hiPSCs was performed following a previous protocol (Zhao M. et al., 2020). Cell populations including fetal iMuSCs were obtained at days 80–100. The purification of iMuSCs was performed by FACS sorting (BD FACS aria 650110J1). For the 201B7-*Pax7* Venus line (Nalbandian et al., 2021), the iMuSCs were purified by Venus fluorescence. For non-reporter lines, iMuSCs were purified as the $CD57^-$–$CD82^+$ population. Allophycocyanin-conjugated CD82 antibody (Biolegend 342108) was used at a final concentration of 1:100. Phycoerythrin-conjugated CD57 antibody (BD Pharmingen 560844) was used at a final concentration of 1:200. The cells were stained with the antibodies for 30 min, followed by washing with HBSS buffer once.

Expansion and Differentiation of iMuSCs

Purified iMuSCs were plated onto a 1:100 Matrigel growth factor reduced (Corning 354230) in a StemFit media-coated 96-well microplate (IWAKI 3860–096). The microplate was pre-coated with Matrigel diluted by StemFit media at 1:100 for 1 h at 37°C. Then, 5,000 purified iMuSCs were seeded onto the plate and cultured in StemFit media containing 10 µM Y-27632 for expansion.

iMuSCs started to proliferate and reach confluency after approximately 5 days of culture. In this process, the medium was changed every day until day 5. After the day of seeding, the medium was replaced to Stemfit media without Y-27632. Differentiation was induced by switching to differentiation media composed of DMEM (Invitrogen 11885084) supplemented with 1% N2 supplement (Gibco 17502048) or 2% HS (Sigma H1138). Recombinant rat Agrin (R&D Systems 550-AG) was used for better differentiation.

Matrigel Covering and Agrin Addition

At day 7 of the culture, 3D Matrigel covering was performed. A Matrigel mixture composed of cold DMEM media (40 µl) and Matrigel (20 µl) was prepared. First, the differentiation media was completely removed from the well, and myotubes were covered with the Matrigel mixture as previously described (Falcone S. et al., 2014). Afterward, the culture dish was incubated at 37°C for 30 min. As a result, myotubes were covered with a high concentration of Matrigel mixture. Next, the differentiation medium containing Agrin at a final concentration of 80 µg/ml was gently added on the 3D Matrigel. Finally, the culture dish was moved to a 37°C incubator, and the medium was changed every 2 days. After the Matrigel coating, Agrin-containing DMEM/N2 media was used as the differentiation media.

RNA Isolation and Quantitative Polymerase Chain Reaction (qPCR)

Total RNA was isolated using a ReliaPrep RNA cell Miniprep Kit (Promega Z6012) according to the manufacturer's instructions. Reverse transcription was performed by ReveTra Ace qPCR RT Mater Mix with gDNA remover (TOYOBO FSQ-301). SYBR Green reagent (Applied Biosystems) was used to detect the target sequences. qPCR was performed using StepOnePlus. (Applied Biosystems) The list of primers used in this study is shown in **Supplementary Table S1**.

Immunostaining

Myotubes were fixed with PBS containing 2% (w/v) paraformaldehyde for 10 min at 4°C. Samples were washed with PBS twice, followed by blocking with Blocking One (Nacalai Tesque) for 60 min at 4 °C and incubated overnight at 4 °C with primary antibodies diluted in 10% (v/v) Blocking One in PBS-T (PBS with 0.2% (v/v) Triton X-100 solution (Nacalai Tesque). The samples were then washed 3 times with PBS-T and incubated for 1 h at room temperature with secondary antibodies diluted in 10% (v/v) Blocking One in PBS-T. Finally, the samples were incubated with DAPI for 5 min to visualize cellular nuclei, followed by washing with PBS twice.

Analysis of Myosin Heavy Chain-Positive Cells

An analysis of myosin heavy chain (MHC)-positive cells was performed using Arrayscan High-Content Systems (Thermofisher). After immunostaining of the myotubes with MHC antibody, the ratio of nuclei with the surrounding MHC fluorescence to total nuclei was calculated. The threshold was changed depending on the background signal.

Electron Microscopy

The samples were fixed with 2% paraformaldehyde (PFA) and 2% glutaraldehyde (GA) in 0.1 M phosphate buffer (PB), pH 7.4, at the incubation temperature (37°C) and then put into a refrigerator for 30 min to lower the temperature to 4°C. Thereafter, they were fixed with 2% GA in 0.1 M PB at 4°C overnight. After the fixation, the samples were washed 3 times with 0.1 M PB at 4°C for 1 h. The samples were dehydrated in graded ethanol solutions (50%, 70%, 90%, 100%) as follows: 50% and 70% for 5 min each at 4°C, 90% for 5 min at room temperature, and three changes of 100% for 5 min each at room temperature. Then, the samples were transferred to a resin (Quetol-812; Nissin EM Co., Tokyo, Japan) and polymerized at 60°C for 48 h. The polymerized resins were ultra-thin-sectioned at 70 nm with a diamond knife using an ultramicrotome (Ultracut UCT; Leica, Vienna, Austria) and

mounted on copper grids. They were stained with 2% uranyl acetate at room temperature for 15 min and then washed with distilled water, followed by secondary staining with Lead stain solution (Sigma-Aldrich Co., Tokyo, Japan) at room temperature for 3 min. The grids were observed by a transmission electron microscope (JEM-1400Plus; JEOL Ltd., Tokyo, Japan) at an acceleration voltage of 100 kV. Digital images (3,296 × 2,472 pixels) were taken with a CCD camera (EM-14830RUBY2; JEOL Ltd., Tokyo, Japan). Samples were analyzed by Tokai Electron Microscopy, Inc. (Nagoya, Japan).

Cell Preparation for Current Measurements

To measure sodium currents, a modified culture protocol was used to easily access the patch electrode to an isolated cell. Briefly, 12-mm round glass coverslips (Warner Instruments, Holliston, MA) were used with Matrigel the day before seeding. The cells were harvested on the Matrigel-coated coverslips without overlaying the Matrigel mixture. The myotubes were cultured in the differentiation medium until the patch-clamp experiment.

Whole-Cell and Out-Side-Out Patch Clamp Recording

Sodium currents were measured using a patch-clamp electrode and the whole-cell recording technique. Recordings were made using an Axopatch 200B amplifier (Molecular Devices, San Jose, CA), and data acquisition was done using a Digidata 1440A (Molecular Devices, San Jose, CA). pCLAMP10.7 software was used (Molecular Devices, San Jose, CA) for the data collection and analysis. Patch electrodes were fabricated from borosilicate glass tubes (Sutter, Novato, CA) using a P-97 Flaming/Brown Micropipette Puller (Sutter, Novato, CA). The electrode's tip was heat-polished with a final resistance of 1.5–2.3 MΩ in the bath solution. Series resistance was compensated at 80–85% by the analog circuitry of the amplifier. All recordings were conducted at room temperature (25°C). The pipette internal solution contained (in mM) 105 CsF, 35 NaCl, 10 ethylene glycol tetraacetic acid (EGTA), and 10 Cs-HEPES (pH 7.4). The bath solution contained (in mM) 140 NaCl, 4 KCl, 2 $CaCl_2$, 1 $MgCl_2$, 5 glucose, and 10 Na-HEPES (pH 7.4).

Before starting a measurement, the membrane potential was held at −100 mV for about 5 min to ensure a recovery from slow inactivation. The activation of Na currents was measured by applying a 10 ms depolarizing step pulse from −80 to +80 mV at 5 mV increments. Any cells with peak currents <1 or >10 nA on a step depolarization from −120 mV to −10 mV were excluded. The voltage dependence of the steady-state fast inactivation was measured as peak inward currents elicited by a −10 mV test pulse after a 300 ms conditioning potential of −120 mV to −10 mV. For out-side-out configuration, we prepared electrodes with a final resistance of 1.5 MΩ. A control current without TTX was obtained by a −10 mV test pulse from −120 mV, Then, the current in the presence of 100 nM TTX was obtained by the identical test pulse.

Validation of Screening System

For the validation of screening system, myotubes differentiated at 28 days with Matrigel covering the *in vitro* culture were used. The myotubes were stained with MHC antibody (Santacruz sc-20641) followed by analysis using a high-content screening instrument (Thermo Scientific Arrayscan System).

QUANTIFICATION AND STATISTICAL ANALYSIS

Data Analysis of Electric Currents

Curve fitting was manually performed using Origin (OriginLab Northampton, MA). Conductance was calculated using the following equation:

$$G(V) = I_{peak} \Big/ (V - E_{rev})$$

The reversal potential, E_{rev}, was measured experimentally for each cell. The voltage dependence of activation was calculated from the following Boltzmann equation:

$$G(V) = G_{max} \Big/ \left[1 + exp\left(-\left(V - V_{1/2}\right)/k\right)\right]$$

Steady-state fast inactivation was fitted to the Boltzmann function calculated from the following equation, where $V_{1/2}$ is the half-maximum voltage, and k is the slope factor:

$$I/I_{max} = 1 \Big/ \left[1 + exp\left(\left(V - V_{1/2}\right)/k\right)\right]$$

I_{max} was calculated as the average of the three I values before and after the potential, where I shows the maximum point.

Statistical Analysis

Medium components, myofiber diameter, and qPCR (*MYH*, *SCN*, SR-related, and t-tubule-related genes) were analyzed using an unpaired two-tailed Student's *t*-test. The expressions of Pax7, MyoD, and Myf5 were analyzed using a *t*-test with Bonferroni correction. The expressions of SCN4A and SCN5A were analyzed using Tukey's test. Data are presented as means ± SEM. $p < 0.05$ was considered statistically significant.

DATA AVAILABILITY STATEMENT

The raw data supporting the conclusion of this article will be made available by the authors without undue reservation.

ETHICS STATEMENT

The studies involving human participants were reviewed and approved by the Ethics Committee at the Graduate School and Faculty of Medicine Kyoto University. The patients/participants provided their written informed consent to participate in this study.

AUTHOR CONTRIBUTIONS

KF, HS, and AT designed the experiments. KF conducted experiments for the cell differentiation and FLATTEST. RY,

TK, and MT conducted measurements of the electric current. AT conducted the flow cytometry by antibodies. KF and TS performed the qPCR experiments. KF, AT, and RY generated figures. KF, TK, and HS wrote the manuscript.

FUNDING

This work was mainly supported by a grant from The Acceleration Program for Intractable Diseases Research utilizing Disease-specific iPS cells (JP21bm0804005) and partially by a grant from The Core Center for iPS Cell Research (JP21bm0104001), both of which are programs in the Research Center Network for Realization of Regenerative Medicine, Japan Agency for Medical Research and Development (AMED, to HS).

ACKNOWLEDGMENTS

The authors thank Hiromitsu Fuse, Yohei Nishi, and Akira Ohta for technical advice on the cell culture and establishment of the drug screening system. We also thank Mr. Itsuki Mori and Mr. Tasuku Ohso for their technical help.

SUPPLEMENTARY MATERIAL

The Supplementary Material for this article can be found online at: https://www.frontiersin.org/articles/10.3389/fcell.2022.886879/full#supplementary-material

Supplementary Figure S1 | Purification of iMuSCs from the mesoderm cell population by flow cytometry using *PAX7*-Venus fluorescence. **(A)** Schematic of the iMuSC differentiation protocol. **(B)** Representative images of Venus-fluorescent-positive iMuSCs. Scale bars, 200 μm. **(C)** Arrow indicates Venus-positive fraction (P5) in the flow cytometry map.

Supplementary Figure S2 | Purification of iMuSCs from the mesoderm cell population by flow cytometry using CD57 and CD82 antibodies. **(A)** Schematic of the flow cytometry data. CD57-negative and CD82-positive cells are located in the P5 fraction as purple dots. **(B)** The mRNA expressions of Pax7, MyoD, and Myf5 were quantified by real-time qPCR in every fraction (CD57- CD82+, CD57+ CD82+, CD57- CD82-, CD57+ CD82-) purified by flow cytometry. The expression level of these three genes in unsorted samples was set as the control. The vertical axis of the graph shows the relative expression level normalized by b-actin, the housekeeping gene. The expression level in each fraction was standardized by the expression level of the unsorted (unsort) sample. (The relative expression of Pax7 in the unsorted sample is 1.) Pax7, MyoD, and Myf5 were abundantly expressed in the CD57–CD82+ fraction compared with the unsorted sample. **(C)** The protein expression of Pax7 in every fraction by immunocytochemistry. (Left) Pax7-positive cells were abundant in the CD57–CD82+ fraction compared with those in the other fractions (CD57+ CD82+, CD57- CD82-, CD57+ CD82-). *<0.05 **<0.01, unpaired two-tailed Student's t-test.

Supplementary Figure S3 | Representative images of myotubes on days 5 **(A)**, 7 **(B)**, 14 **(C),** and 42 **(D)** of the culture. Right panels are magnified images. Scale bars, 100 μm (left) and 100 μm (right).

Supplementary Figure S4 | (A) Schematic of the 3D Matrigel covering. Blue (myotube), beige (differentiation medium; DM), and red (Matrigel mixture). **(B)** Schematic of the two conditions (m-condition and c-condition) for the differentiation. **(C,D)** Representative images of myotubes (anti-MHC, green) in c-condition and m-condition. There was a significant increase in the size of *PAX7*-Venus and CD57-CD82+ iMuSC-derived myotubes at day 42 of the culture (n=45 and n=46 myotubes from control and Matrigel samples, respectively). Scale bar, 100 μm.

Supplementary Figure S5 | The mRNA expression of the myosin heavy chain family (*MYH2, MYH3, MYH4, MYH7, and MYH8*) , SR-related genes (*Casq1* and *Atp2a1*) , and t-tubule-related genes (*DHPRα, DHPRβ,* and *DHPRγ*) was quantified by real-time PCR. The expression level of each gene in *PAX7*-Venus iMuSC-derived myotubes on days 14 and 42 between with and without Agrin was shown. Matrigel embedding was performed in both with and without Agrin conditions. The vertical axis of the graph shows the relative expression level normalized by 18S rRNA, the housekeeping gene. The expression level is standardized by the expression level (=1) on day 5. *$p < 0.05$, **$p < 0.01$ (unpaired two-tailed Student's t-test). Error bars indicate the standard error of mean (SEM). In each group (day 14; Agrin+ Agrin-, day 42; Agrin+ Agrin-), three independent samples were used for the analysis.

Supplementary Video S1 | Twitching myotubes in m-condition at day 28 of culture.

REFERENCES

Ahern, C. A., Payandeh, J., Bosmans, F., and Chanda, B. (2016). The Hitchhiker's Guide to the Voltage-Gated Sodium Channel Galaxy. *J. Gen. Physiol.* 147 (1), 1–24. doi:10.1085/jgp.201511492

Al-Qusairi, L., Weiss, N., Toussaint, A., Berbey, C., Messaddeq, N., Kretz, C., et al. (2009). T-tubule Disorganization and Defective Excitation-Contraction Coupling in Muscle Fibers Lacking Myotubularin Lipid Phosphatase. *Proc. Natl. Acad. Sci. U.S.A.* 106 (44), 18763–18768. doi:10.1073/pnas.0900705106

Alexander, M. S., Rozkalne, A., Colletta, A., Spinazzola, J. M., Johnson, S., Rahimov, F., et al. (2016). CD82 Is a Marker for Prospective Isolation of Human Muscle Satellite Cells and Is Linked to Muscular Dystrophies. *Cell Stem Cell* 19 (6), 800–807. doi:10.1016/j.stem.2016.08.006

Ben-Johny, M., Yang, P. S., Niu, J., Yang, W., Joshi-Mukherjee, R., and Yue, D. T. (2014). Conservation of Ca2+/calmodulin Regulation across Na and Ca2+ Channels. *Cell* 157 (7), 1657–1670. doi:10.1016/j.cell.2014.04.035

Borchin, B., Chen, J., and Barberi, T. (2013). Derivation and FACS-Mediated Purification of PAX3+/PAX7+ Skeletal Muscle Precursors from Human Pluripotent Stem Cells. *Stem Cel Rep.* 1 (6), 620–631. doi:10.1016/j.stemcr.2013.10.007

Brown, D. M., Parr, T., and Brameld, J. M. (2012). Myosin Heavy Chain mRNA Isoforms Are Expressed in Two Distinct Cohorts during C2C12 Myogenesis. *J. Muscle Res. Cel Motil* 32 (6), 383–390. doi:10.1007/s10974-011-9267-4

Buj-Bello, A., Fougerousse, F., Schwab, Y., Messaddeq, N., Spehner, D., Pierson, C. R., et al. (2008). AAV-mediated Intramuscular Delivery of Myotubularin Corrects the Myotubular Myopathy Phenotype in Targeted Murine Muscle and Suggests a Function in Plasma Membrane Homeostasis. *Hum. Mol. Genet.* 17 (14), 2132–2143. doi:10.1093/hmg/ddn112

Caron, L., Kher, D., Lee, K. L., McKernan, R., Dumevska, B., Hidalgo, A., et al. (2016). A Human Pluripotent Stem Cell Model of Facioscapulohumeral Muscular Dystrophy-Affected Skeletal Muscles. *Stem Cells Transl. Med.* 5 (9), 1145–1161. doi:10.5966/sctm.2015-0224

Chahine, M., Bennett, P. B., George, A. L., Jr, and Horn, R. (1994). Functional Expression and Properties of the Human Skeletal Muscle Sodium Channel. *Pflugers Arch.* 427 (1-2), 136–142. doi:10.1007/BF00585952

Cowling, B. S., Chevremont, T., Prokic, I., Kretz, C., Ferry, A., Coirault, C., et al. (2014). Reducing Dynamin 2 Expression Rescues X-Linked Centronuclear Myopathy. *J. Clin. Invest.* 124 (3), 1350–1363. doi:10.1172/jci71206

Darabi, R., Arpke, R. W., Irion, S., Dimos, J. T., Grskovic, M., Kyba, M., et al. (2012). Human ES- and iPS-Derived Myogenic Progenitors Restore DYSTROPHIN and Improve Contractility Upon Transplantation in Dystrophic Mice. *Cell Stem Cell* 10 (5), 610–619. doi:10.1016/j.stem.2012.02.015

Davidson, P. M., and Lammerding, J. (2014). Broken Nuclei - Lamins, Nuclear Mechanics, and Disease. *Trends Cel Biol.* 24 (4), 247–256. doi:10.1016/j.tcb.2013.11.004

Falcone, S., Roman, W., Hnia, K., Gache, V., Didier, N., Lainé, J., et al. (2014). N-WASP Is Required for Amphiphysin-2/BIN 1-dependent Nuclear Positioning and Triad Organization in Skeletal Muscle and Is Involved in the Pathophysiology of Centronuclear Myopathy. *EMBO Mol. Med.* 6 (11), 1455–1475. doi:10.15252/emmm.201404436

Jensen, J. H., Cakal, S. D., Li, J., Pless, C. J., Radeke, C., Jepsen, M. L., et al. (2020). Large-scale Spontaneous Self-Organization and Maturation of Skeletal Muscle

Tissues on Ultra-compliant Gelatin Hydrogel Substrates. *Sci. Rep.* 10 (1), 13305. doi:10.1038/s41598-020-69936-6

Kallen, R. G., Sheng, Z.-H., Yang, J., Chen, L., Rogart, R. B., and Barchi, R. L. (1990). Primary Structure and Expression of a Sodium Channel Characteristic of Denervated and Immature Rat Skeletal Muscle. *Neuron* 4 (2), 233–242. doi:10.1016/0896-6273(90)90098-z

Kokubu, Y., Nagino, T., Sasa, K., Oikawa, T., Miyake, K., Kume, A., et al. (2019). Phenotypic Drug Screening for Dysferlinopathy Using Patient-Derived Induced Pluripotent Stem Cells. *Stem Cell Transl Med* 8 (10), 1017–1029. doi:10.1002/sctm.18-0280

Lariosa-Willingham, K. D., Rosler, E. S., Tung, J. S., Dugas, J. C., Collins, T. L., and Leonoudakis, D. (2016). Development of a High Throughput Drug Screening Assay to Identify Compounds that Protect Oligodendrocyte Viability and Differentiation under Inflammatory Conditions. *BMC Res. Notes* 9 (1), 444. doi:10.1186/s13104-016-2219-8

Lee, E. A., Jung, G., Im, S. G., and Hwang, N. S. (2015). Extracellular Matrix-Immobilized Nanotopographical Substrates for Enhanced Myogenic Differentiation. *J. Biomed. Mater. Res.* 103 (6), 1258–1266. doi:10.1002/jbm.b.33308

Li, F., Kolb, J., Crudele, J., Tonino, P., Hourani, Z., Smith, J. E., 3rd, et al. (2020). Expressing a Z-Disk Nebulin Fragment in Nebulin-Deficient Mouse Muscle: Effects on Muscle Structure and Function. *Skeletal Muscle* 10 (1), 2. doi:10.1186/s13395-019-0219-9

Lundholt, B. K., Scudder, K. M., and Pagliaro, L. (2003). A Simple Technique for Reducing Edge Effect in Cell-Based Assays. *J. Biomol. Screen.* 8 (5), 566–570. doi:10.1177/1087057103256465

Maffioletti, S. M., Sarcar, S., Henderson, A. B. H., Mannhardt, I., Pinton, L., Moyle, L. A., et al. (2018). Three-Dimensional Human iPSC-Derived Artificial Skeletal Muscles Model Muscular Dystrophies and Enable Multilineage Tissue Engineering. *Cel Rep.* 23 (3), 899–908. doi:10.1016/j.celrep.2018.03.091

Martínez-Mármol, R., David, M., Sanches, R., Roura-Ferrer, M., Villalonga, N., Sorianello, E., et al. (2007). Voltage-dependent Na+ Channel Phenotype Changes in Myoblasts. Consequences for Cardiac Repair. *Cardiovasc. Res.* 76 (3), 430–441. doi:10.1016/j.cardiores.2007.08.009

Nalbandian, M., Zhao, M., Sasaki-Honda, M., Jonouchi, T., Lucena-Cacace, A., Mizusawa, T., et al. (2021). Characterization of hiPSC-Derived Muscle Progenitors Reveals Distinctive Markers for Myogenic Cell Purification toward Cell Therapy. *Stem Cel Rep.* 16 (4), 883–898. doi:10.1016/j.stemcr.2021.03.004

Okita, K., Yamakawa, T., Matsumura, Y., Sato, Y., Amano, N., Watanabe, A., et al. (2013). An Efficient Nonviral Method to Generate Integration-free Human-Induced Pluripotent Stem Cells from Cord Blood and Peripheral Blood Cells. *Stem Cells* 31 (3), 458–466. doi:10.1002/stem.1293

Ortiz-Vitali, J. L., and Darabi, R. (2019). iPSCs as a Platform for Disease Modeling, Drug Screening, and Personalized Therapy in Muscular Dystrophies. *Cells* 8 (1). doi:10.3390/cells8010020

Penton, C. M., Badarinarayana, V., Prisco, J., Powers, E., Pincus, M., Allen, R. E., et al. (2016). Laminin 521 Maintains Differentiation Potential of Mouse and Human Satellite Cell-Derived Myoblasts during Long-Term Culture Expansion. *Skeletal Muscle* 6 (1), 44. doi:10.1186/s13395-016-0116-4

Rao, L., Qian, Y., Khodabukus, A., Ribar, T., and Bursac, N. (2018). Engineering Human Pluripotent Stem Cells into a Functional Skeletal Muscle Tissue. *Nat. Commun.* 9 (1), 126. doi:10.1038/s41467-017-02636-4

Schiaffino, S., Rossi, A. C., Smerdu, V., Leinwand, L. A., and Reggiani, C. (2015). Developmental Myosins: Expression Patterns and Functional Significance. *Skeletal Muscle* 5, 22. doi:10.1186/s13395-015-0046-6

Selga, E., Sendfeld, F., Martinez-Moreno, R., Medine, C. N., Tura-Ceide, O., Wilmut, S. I., et al. (2018). Sodium Channel Current Loss of Function in Induced Pluripotent Stem Cell-Derived Cardiomyocytes from a Brugada Syndrome Patient. *J. Mol. Cell Cardiol.* 114, 10–19. doi:10.1016/j.yjmcc.2017.10.002

Selvaraj, S., Mondragon-Gonzalez, R., Xu, B., Magli, A., Kim, H., Lainé, J., et al. (2019). Screening Identifies Small Molecules that Enhance the Maturation of Human Pluripotent Stem Cell-Derived Myotubes. *Elife* 8. doi:10.7554/eLife.47970

Sheets, M. F., and Hanck, D. A. (1999). Gating of Skeletal and Cardiac Muscle Sodium Channels in Mammalian Cells. *J. Physiol.* 514 (Pt 2), 425–436. doi:10.1111/j.1469-7793.1999.425ae.x

Shoji, E., Sakurai, H., Nishino, T., Nakahata, T., Heike, T., Awaya, T., et al. (2015). Early Pathogenesis of Duchenne Muscular Dystrophy Modelled in Patient-Derived Human Induced Pluripotent Stem Cells. *Sci. Rep.* 5, 12831. doi:10.1038/srep12831

Swartz, E. W., Baek, J., Pribadi, M., Wojta, K. J., Almeida, S., Karydas, A., et al. (2016). A Novel Protocol for Directed Differentiation of C9orf72-Associated Human Induced Pluripotent Stem Cells into Contractile Skeletal Myotubes. *Stem Cells Transl. Med.* 5 (11), 1461–1472. doi:10.5966/sctm.2015-0340

Takahashi, K., Tanabe, K., Ohnuki, M., Narita, M., Ichisaka, T., Tomoda, K., et al. (2007). Induction of Pluripotent Stem Cells from Adult Human Fibroblasts by Defined Factors. *Cell* 131 (5), 861–872. doi:10.1016/j.cell.2007.11.019

Tanaka, A., Woltjen, K., Miyake, K., Hotta, A., Ikeya, M., Yamamoto, T., et al. (2013). Efficient and Reproducible Myogenic Differentiation from Human iPS Cells: Prospects for Modeling Miyoshi Myopathy *In Vitro*. *PLoS One* 8 (4), e61540. doi:10.1371/journal.pone.0061540

Uchimura, T., Asano, T., Nakata, T., Hotta, A., and Sakurai, H. (2021). A Muscle Fatigue-like Contractile Decline Was Recapitulated Using Skeletal Myotubes from Duchenne Muscular Dystrophy Patient-Derived iPSCs. *Cel Rep. Med.* 2 (6), 100298. doi:10.1016/j.xcrm.2021.100298

Uchimura, T., Otomo, J., Sato, M., and Sakurai, H. (2017). A Human iPS Cell Myogenic Differentiation System Permitting High-Throughput Drug Screening. *Stem Cel Res.* 25, 98–106. doi:10.1016/j.scr.2017.10.023

Ueki, J., Nakamori, M., Nakamura, M., Nishikawa, M., Yoshida, Y., Tanaka, A., et al. (2017). Myotonic Dystrophy Type 1 Patient-Derived iPSCs for the Investigation of CTG Repeat Instability. *Sci. Rep.* 7, 42522. doi:10.1038/srep42522

Uezumi, A., Nakatani, M., Ikemoto-Uezumi, M., Yamamoto, N., Morita, M., Yamaguchi, A., et al. (2016). Cell-Surface Protein Profiling Identifies Distinctive Markers of Progenitor Cells in Human Skeletal Muscle. *Stem Cel Rep.* 7 (2), 263–278. doi:10.1016/j.stemcr.2016.07.004

Urciuolo, A., Serena, E., Ghua, R., Zatti, S., Giomo, M., Mattei, N., et al. (2020). Engineering a 3D *In Vitro* Model of Human Skeletal Muscle at the Single Fiber Scale. *PLoS One* 15 (5), e0232081. doi:10.1371/journal.pone.0232081

Vilin, Y. Y., Peters, C. H., and Ruben, P. C. (2012). Acidosis Differentially Modulates Inactivation in NaV1.2, NaV1.4, and NaV1.5 Channels. *Front. Pharmacol.* 3, 109. doi:10.3389/fphar.2012.00109

Yamashita, A., Morioka, M., Kishi, H., Kimura, T., Yahara, Y., Okada, M., et al. (2014). Statin Treatment Rescues FGFR3 Skeletal Dysplasia Phenotypes. *Nature* 513 (7519), 507–511. doi:10.1038/nature13775

Yang, J. S., Sladky, J. T., Kallen, R. G., and Barchi, R. L. (1991). TTX-sensitive and TTX-Insensitive Sodium Channel mRNA Transcripts Are Independently Regulated in Adult Skeletal Muscle after Denervation. *Neuron* 7 (3), 421–427. doi:10.1016/0896-6273(91)90294-a

Yoshida, T., Awaya, T., Jonouchi, T., Kimura, R., Kimura, S., Era, T., et al. (2017). A Skeletal Muscle Model of Infantile-Onset Pompe Disease with Patient-specific iPS Cells. *Sci. Rep.* 7 (1), 13473. doi:10.1038/s41598-017-14063-y

Zhao, M., Tazumi, A., Takayama, S., Takenaka-Ninagawa, N., Nalbandian, M., Nagai, M., et al. (2020). Induced Fetal Human Muscle Stem Cells with High Therapeutic Potential in a Mouse Muscular Dystrophy Model. *Stem Cel Rep.* 15 (1), 80–94. doi:10.1016/j.stemcr.2020.06.004

Conflict of Interest: The author AT was employed by Asahi Kasei Pharma Corporation.

The remaining authors declare that the research was conducted in the absence of any commercial or financial relationships that could be construed as a potential conflict of interest.

Publisher's Note: All claims expressed in this article are solely those of the authors and do not necessarily represent those of their affiliated organizations, or those of the publisher, the editors, and the reviewers. Any product that may be evaluated in this article, or claim that may be made by its manufacturer, is not guaranteed or endorsed by the publisher.

Advantages of publishing in Frontiers

OPEN ACCESS
Articles are free to read for greatest visibility and readership

FAST PUBLICATION
Around 90 days from submission to decision

HIGH QUALITY PEER-REVIEW
Rigorous, collaborative, and constructive peer-review

TRANSPARENT PEER-REVIEW
Editors and reviewers acknowledged by name on published articles

Frontiers
Avenue du Tribunal-Fédéral 34
1005 Lausanne | Switzerland

Visit us: www.frontiersin.org
Contact us: frontiersin.org/about/contact

REPRODUCIBILITY OF RESEARCH
Support open data and methods to enhance research reproducibility

DIGITAL PUBLISHING
Articles designed for optimal readership across devices

FOLLOW US
@frontiersin

IMPACT METRICS
Advanced article metrics track visibility across digital media

EXTENSIVE PROMOTION
Marketing and promotion of impactful research

LOOP RESEARCH NETWORK
Our network increases your article's readership